Investigation of the hydrogen electrode reactions on Ni electrocatalysts in alkaline medium

Alexandr Oshchepkov

UNIVERSITÉ DE STRASBOURG

ÉCOLE DOCTORALE SCIENCES CHIMIQUES

Institut de Chimie de Strasbourg (IC)
Institut de Chimie et Procédés pour l'Energie, l'Environnement et la Santé (ICPEES)

THÈSE

présentée par :

Alexandr OSHCHEPKOV

soutenue le : **22 novembre 2017**

pour obtenir le grade de : **Docteur de l'université de Strasbourg**

Discipline/ Spécialité : Chimie / Chimie Physique

co-tutelle

Étude des réactions d'électrodes de l'hydrogène sur des électrocatalyseurs de Ni en milieu alcalin

Investigation of the hydrogen electrode reactions on Ni electrocatalysts in alkaline medium

THÈSE dirigée par :
M. BONNEFONT Antoine — Maître de Conférences, Université de Strasbourg

THÈSE co-dirigée par :
Mme. SAVINOVA Elena — Professeur, Université de Strasbourg
M. PARMON Valentin — Professeur, Institut de Catalyse Boreskov (RU)

RAPPORTEURS :
M. MAILLARD Frederic — Chargé de recherches, CNRS-Université de Grenoble Alpes
Mme. TSIRLINA Galina — Professeur, L'université d'État Lomonossov de Moscou (RU)

AUTRES MEMBRES DU JURY :
M. MASLII Alexander — Professeur, Institut de la Chimie et de la Mécanochimie des Etats Solides (RU)

Alexandr OSHCHEPKOV

Étude des réactions d'électrodes de l'hydrogène sur des électrocatalyseurs de Ni en milieu alcalin

Résumé

La thèse présentée traite principalement de l'influence de la composition et de l'état de surface d'électrodes à base de Ni sur la cinétique et le mécanisme des réactions d'oxydation/dégagement de l'hydrogène (HOR/HER) en milieu alcalin. En combinant les résultats de mesures électrochimiques avec une modélisation microcinétique, il a pu être montré que l'activité spécifique du Ni pour l'HOR/HER augmente jusqu'à 10 fois en présence à la fois d'oxydes de Ni et de Ni métallique à la surface de l'électrode. En outre, l'influence de l'addition d'un second métal aux électrocatalyseurs à base Ni sur leurs activités pour l'HOR/HER a été étudiée dans le cas des systèmes NiMo/C et NiCu/C. Dans les deux cas, une augmentation de l'activité spécifique a été observée par rapport à l'échantillon Ni/C de référence et a été attribuée à une diminution de l'énergie d'adsorption de l'hydrogène adsorbé sur Ni, espèce intermédiaire de l'HOR/HER.

DE MOTS-CLÉS : Nickel, Électrocatalyseurs, Réaction d'oxydation de l'hydrogène, Réaction de d'évolution de l'hydrogène, Milieu alcalin, Modèle cinétique, Pile à combustible

Résumé en anglais

The present thesis is mainly focused on the influence of the surface state of Ni electrodes on the kinetics and the mechanism of the hydrogen oxidation/evolution reactions (HOR/HER) in alkaline medium. By combining the results of electrochemical measurements with microkinetic modeling, it was shown that specific activity of Ni in the HOR/HER increases up to 10 times if along with metallic Ni, Ni oxide species are present on the electrode surface. In addition, the effect of the addition of a second metal to Ni electrocatalysts on their activity in the HOR/HER was investigated for NiMo/C and NiCu/C systems. In both cases an enhancement of specific activity was observed in comparison with the reference Ni/C sample, which was assigned to a decrease of the adsorption energy of the hydrogen intermediate on Ni participating in the HOR/HER.

KEYWORDS : Nickel, Electrocatalysts, Hydrogen oxidation reaction, Hydrogen evolution reaction, Alkaline media, Kinetic modeling, Fuel cell

Acknowledgement

Taking the opportunity, I would like to thanks all the people and organizations without whom this PhD work would not be possible.

First and foremost, I wish to express my deepest gratitude to my advisors: Professor **Elena Savinova**, for her passion, patience, motivation and great help in the understanding where to go; Dr. **Antoine Bonnefont** for his enthusiasm, encouragement and for teaching me in the kinetic modeling; Professor **Valentin Parmon** for his guidance, which helped me to choose the right direction in the scientific life and for supporting all of my initiatives. I am proud to work with you and had the opportunity to learn many things from you during the PhD study. Thank you very much!

I am very grateful to the **University of Strasbourg** (Doctoral School "Sciences Chimiques"), **Institut de Chimie de Strasbourg** (IC), **Institut de Chimie des Procédés pour l'Energie, l'Environnement et la Santé** (ICPEES) in Cronenbourg and **Boreskov Institute of Catalysis** in Novosibirsk (RU) for providing the possibility to perform all the required experiments. I also would like to thanks the **French Ministry of Foreign Affairs and International Development** for attributing me the Eiffel and Vernadski PhD fellowships as well as **CNRS** and **RFBR** organizations for the financial support of the research projects.

I wish to express my warmest gratitude to my dissertation committee members, Professor **Galina Tsirlina**, Professor **Alexander Maslii** and Dr. **Frederic Maillard** for their time, insightful comments and questions on the PhD study. It is a great honor for me, that you accepted to be a part of the jury of this thesis.

Many thanks to all the people who helped me with materials preparation and characterization: Dr. **Olga Cherstiouk**, Dr. **Sergey Pronkin** and Dr. **Alexandr Simonov** for the help with performance of some electrocatalytic measurements; Dr. **Pavel Simonov** for the synthesis of Ni/C and NiCu/C electrocatalysts; Dr. **Alexey Serov** and Dr. **Katerina Artyushkova** for the preparation of NiMo/C electrocatalyst and its characterization by TEM, XRD and XPS; Dr. **Corinne Ulhaq-Bouillet** and Dr.

Vladimir Zaikovskii for TEM, HRTEM and STEM analysis; Dr. **Vasiliki Papaefthimiou**, Dr. **Spiros Zafeiratos**, Dr. **Ren Kvon** and **Viktoriia Saveleva** for XPS analysis; Dr. **Thierry Dintzer**, Dr. **Nina Rudina** for SEM analysis; Dr. **Tatyana Kardash** and Dr. **Alexander Shmakov** for XRD analysis; Dr. **Anne Boss** for ICP-AES analysis.

Thanks also to **Veronique Verkruysse** and **Francine Jacky** for the vast administrative staff they realized.

I would like to thank **Sebastien**, **Gwénaëlle**, **Anya**, **Pierre-Alex**, **Wen**, **Thomas**, **Ivan**, **Denis** and **Pablo** with whom I shared most free time of laboratory life in France and all the nice people I met during my PhD. Thank you for creating a warm and kindly atmosphere in the lab.

A great thanks to **European Doctoral College** and, in particularly, the educational director of PDI program **Christopher Mueller** for having given me the opportunity to be a part of this community. Many thanks also to **Virginie Herbasch**, **Joëlle Hubé**, **Christine Fromholtz**, **Laurence Barondeau** and all the members of PDI program and **StrasAIR** for making the PhD life more interesting and filling it with lots of remarkable events.

Last but certainly not least, I would like to thanks **my parents**, **my brother** and especially **my darling wife** who always believe in me and support me allowing to stay motivated for hard working. Thanks also to **my friends** for their patience and warm welcoming every times I came back to Russia.

Table of contents

List of abbreviations

List of abbreviations

AMFC	Alkaline Membrane Fuel Cell
Ch activated	Chemically activated
CV	Cyclic voltammogram
DFT	Density Functional Theory
EC activated	Electrochemically activated
ED	Electrodeposited
EDX	Energy-Dispersive X-Ray Spectroscopy
FC	Fuel Cell
GC	Glassy carbon
HER	Hydrogen Evolution Reaction
HOR	Hydrogen Oxidation Reaction
HR-TEM	High Resolution Transmission Electron Microscopy
ICP-AES	Inductively Coupled Plasma – Atomic Emission Spectrometry
KB	KetjenBlack, carbon support
MSE	Mercury Sulfate Electrode
PEMFC	Proton Exchange Membrane Fuel Cell
PGM	Platinum-Group Metals
RHE	Reversible Hydrogen Electrode
SEM	Scanning Electron Microscopy
SERS	Surface Enhanced Raman Spectroscopy
STEM	Scanning Transmission Electron Microscopic
TEM	Transmission Electron Microscopy
XC-72	Vulcan XC-72, carbon support
XPS	X-Ray Photoelectron Spectroscopy
XRD	X-Ray Diffraction

Table of symbols

Symbol	Meaning	Dimension
S_{EC}	Electrochemical surface area	cm^2
S_{CO}	Surface area determined by CO-chemisorption	cm^2
S_{geom}	Geometric surface area of the electrode	cm^2
j_0	Exchange current density after normalization on S_{EC} or S_{CO}	$\mu A \cdot cm^{-2}_{Ni}$
	Exchange current density after normalization on S_{geom}	$\mu A \cdot cm^{-2}_{geom}$
i_0	Exchange current density normalized to the mass of metal	$A \cdot g^{-1}_{Ni}$ $A \cdot g^{-1}_{Me}$
j_k	Kinetic current density normalized to the surface of Ni	$\mu A \cdot cm^{-2}_{Ni}$
i_k	Kinetic current density normalized to the mass of Ni	$A \cdot g^{-1}_{Ni}$
C_{dl}	Double layer capacity	$\mu F \cdot cm^{-2}$
$\Delta_{ad}G^0_H$	Gibbs energy of adsorbed hydrogen intermediate	eV
H_{ad}	Adsorbed (index '$_{ad}$') hydrogen atoms	
E	Potential	V
η	Overpotential ($E - E_{eq}$)	V
I	Current	A
j	Current density normalized to the surface	$\mu A \cdot cm^{-2}$
i	Current density normalized to the mass of metal	$A \cdot g^{-1}$
m	Mass	g
M	Molar concentration	$mol \cdot l^{-1}$
α	Charge transfer coefficient	
β	Symmetry factor for the adsorption/desorption of H_{ad}	
E_a	Activation energy	$kJ \cdot mol^{-1}$
k_i	Reaction rate constant	
θ	Surface coverage	
T	Temperature	K, °C
P	Pressure	Pa
F	Faraday constant	96485 $kJ \cdot mol^{-1}$
R	Gas constant	8.314 $J \cdot mol^{-1}\ K^{-1}$

General Introduction

Increasing energy demand and diminishing of fossil fuel resources have largely stimulated development of renewable and non-traditional energy sources during the past decades. Hydrogen is perceived as one of the most promising energy carriers, because of its high (per unit mass) energy density (ca. 3 times higher compared to gasoline). By use of fuel cell (FC) technology, the chemical energy stored in H_2 can be electrochemically converted to electric energy with high efficiency and zero emissions (the only product of hydrogen oxidation being water). It is essential that hydrogen can be produced from renewable energy sources such as solar or wind (through the water splitting process). Besides, conversion of surplus electricity in the form of chemical energy of a fuel (e.g. hydrogen) allows to mitigate the intermittent nature of renewable power sources. Among hydrogen-fed FCs, the technology of the proton exchange membrane fuel cell (PEMFC) has had the most progress until now. Significant decrease of the total content of platinum-group metals (PGMs) in the PEMFC stacks has been achieved during the past decades. However despite of this, the necessity to use the PGMs still remains one of the reasons for the high price of PEMFC, which is hindering their wide commercialization. One of the promising approaches to reduce the cost of FCs, intensively developed during the past decade, is based on the transition from acidic to alkaline media. The latter is achieved by the replacement of proton exchange membrane by anion exchange membrane and the development of alkaline membrane fuel cell (AMFC). The main advantage of the FC with alkaline electrolyte is the possibility to use non-noble metal (thus widely available and cheaper) catalysts, which would be unstable in acidic media.

Among non-noble metals, Ni is perceived as one of the most promising electrocatalysts for the anodes of AMFCs. It has low price, shows good corrosion stability in alkaline environments and possesses fair activity in the hydrogen evolution reaction (HER, i.e. the reverse reaction of the hydrogen oxidation (HOR), occurring at the anode of a FC). Due to utilization of Ni at the cathodes of alkaline water electrolyzers, the HER on Ni has been widely investigated. However the values of electrocatalytic activity of Ni reported in the literature may differ by nearly two orders of magnitude. There are two likely reasons for this inconsistency. First, in many studies, the activity is normalized to the geometric surface area of the electrode, while

its real surface area could be significantly different from the geometric one. Second, the kinetics of the HER might depend on the methodologies used for preconditioning of the Ni electrode surface prior to measurements, which differ in these studies. Meanwhile, Ni is prone to the formation of hydrides upon cathodic polarization and surface oxide species after anodic polarization and/or contact with the oxygen from air. The influence of Ni hydrides, formed at the cathode during water electrolysis, has been investigated in detail. On the contrary, even if some authors have pointed to a noticeable influence of surface oxidation on the activity of Ni electrodes in the HOR/HER, there have been no systematic studies of this effect yet.

Activity of Ni in the HOR/HER, being high compared to other non-noble metals, is, however, significantly lower with respect to the activity of Pt. It is known from the literature, that addition of a second metal (for example, Co, Zn, Fe, Cu, Mo, Cr, etc.) results in a noticeable increase of the activity of Ni electrocatalysts in the HER. Recently several works devoted to the study of bi- and polymetallic catalysts in the HOR have also appeared. However the values of electrocatalytic activity reported by different authors are often contradictory (which could either be assigned to the above mentioned difficulties in the determination of the real surface area of the electrode or obtaining a reproducible surface state). Besides, the reasons for the observed activity increase are still not clearly understood and remain the subject of discussions.

In summary, we note that the literature data concerning electrocatalysis of the HER on Ni are often contradictory, thus complicating comparison of the results obtained in different laboratories. Moreover, there are only a few studies devoted to the investigation of the HOR on Ni and Ni-based electrodes, or the influence of their composition and surface state on the activity. Meanwhile, understanding of these phenomena is essential for disclosing the origins of the catalytic enhancement in bimetallic Ni-based systems as well as the development of more efficient AMFC anodes.

The **objectives of the present work** were to unveil the key factors, which determine electrocatalytic activity of Ni in the HOR, and to develop efficient mono- and bimetallic Ni-based electrocatalysts for this process.

These objectives were achieved by solving the following **problems**:

1. Determination of specific electrocatalytic activity of polycrystalline Ni in the HOR/HER in alkaline medium, and understanding its dependence on the temperature;
2. Uncovering the dependence of specific electrocatalytic activity of Ni in the HOR/HER on the extend of its surface oxidation;
3. Developing a mathematical microkinetic model allowing to describe in a semi-quantitative way the influence of the main parameters affecting the kinetics of the HOR/HER on mono- and bimetallic Ni-based electrocatalysts, including the influence of surface oxide species;
4. Synthesis and physicochemical characterization of nanostructured Ni electrocatalysts supported on porous carbon and determination of their specific activity in the HOR/HER in dependence of the surface state;
5. Determination of specific electrocatalytic activity of NiMo/C and NiCu/C electrocatalysts in the HOR/HER, defining an optimal composition of the NiCu/C electrocatalysts, and unveiling the influence of the second metal on physicochemical properties of Ni.

The structure of the thesis

The thesis comprises 205 pages and contains 5 chapters, 61 figures, 11 tables, 3 appendixes and 299 references.

Chapter 1 is the literature review. It provides an overview of the HOR/HER kinetics and mechanism, including the dependence of the activity on the type of metal as well as the electrolyte pH. It also summarizes the data on the electrochemical properties of Ni electrodes in alkaline media and their electrocatalytic activity in the HOR/HER.

Chapter 2 describes the materials and methods used in this work to study the Ni-based electrocatalysts.

Chapter 3 is devoted to the study of model polycrystalline Ni electrodes. By combining electrochemical measurements with microkinetic modeling, the influence of the surface state of Ni electrodes on the kinetics of the HOR/HER is discussed.

Chapter 4 is focused on the synthesis of nanostructured Ni electrocatalysts immobilized on either a flat surface of glassy carbon or a porous carbon support with the aim to get high metal loading at relatively small particle sizes. An influence of the surface state on the activity of these electrodes in the HOR/HER is discussed as well.

Chapter 5 is dedicated to the study of carbon supported bimetallic NiCu/C and NiMo/C catalysts and understanding how their composition influences the activity of Ni in the HOR/HER.

Finally, the **General conclusions and the Outlook** of the work are presented.

At the end of the thesis, supplementary information can be found in the **Appendix** section.

Chapter 1:
Literature Review

1.1. Hydrogen electrode reactions

Hydrogen electrode reactions, which include the processes of cathodic evolution and anodic oxidation of hydrogen, are among the best-understood electrocatalytic processes up to now [1,2]. Relative simplicity of their mechanism has allowed to use the HOR/HER as model reactions in electrochemistry. Already in 1905 Tafel established the famous phenomenological equation relating the currents to the electrode potential [3]. Later in 1930, Volmer and Erdey-Gruz for the first time pointed out the retarded electrochemical step of the discharge of hydrogen ions during the HER [4,5], while Kobosev and Nekrasova demonstrated the influence of the adsorption energy of H_{ad} atoms on the kinetics of this process [6]. It was the study of the HER, which inspired Kobosev and Monblanova to invent the term "electrocatalysis" for the description of the catalytic effect of the electrode material on the kinetics of electrode reactions. Whereas development of polarography by Heyrovsky [7–9] as well as development of the thermodynamic theory of surface processes across the metal/solution interface and theory of the double layer structure by Frumkin [10–12] provided great impact to further progress in electrochemical kinetics.

1.1.1. Kinetics of the HOR/HER

The overall reactions of anodic oxidation (forward direction) and cathodic evolution (backward direction) of hydrogen in acidic or alkaline media can be expressed as follows:

$H_2 \rightleftarrows 2H^+ + 2e^-$ (in acidic media) (eq. 1.1)

$H_2 + 2OH^- \rightleftarrows 2H_2O + 2e^-$ (in alkaline media) (eq. 1.2)

Notwithstanding their simplicity, compared to the outer-sphere electrode reactions the HOR/HER are complicated by the adsorption with the formation of adsorbed H_{ad} atoms as surface intermediate. The HOR/HER usually proceed according to either Heyrovsky-Volmer or Tafel-Volmer mechanism. The corresponding reaction steps can be written in acidic media as

$H_2 \rightleftarrows 2H_{ad}$ (Tafel step) (eq. 1.3)

$H_2 \rightleftarrows H_{ad} + H^+ + e^-$ (Heyrovsky step) (eq. 1.4)

$H_{ad} \rightleftarrows H^+ + e^-$ (Volmer step) (eq. 1.5)

or in alkaline media as

$H_2 \rightleftarrows 2H_{ad}$ (Tafel step) (eq. 1.6)

$H_2 + OH^- \rightleftarrows H_{ad} + H_2O + e^-$ (Heyrovsky step) (eq. 1.7)

$H_{ad} + OH^- \rightleftarrows H_2O + e^-$ (Volmer step) (eq. 1.8)

In contrast to catalysis, in electrocatalysis the reaction rate depends on the electrode potential. For simplicity, let us first discuss the influence of the potential on the rate of a one-electron outer-sphere electrode reaction, which is non-complicated by adsorption:

$R \rightleftarrows O + e^-$ (eq. 1.9)

Here both oxidized (O) and reduced (R) species are present in the solution. The reaction rate can be written as follows [2]:

$$v = \vec{k} C_R^s - \overleftarrow{k} C_O^s \quad \text{(eq. 1.10)}$$

where $\vec{k}$ and $\overleftarrow{k}$ are heterogeneous rate constants (in cm s^{-1}) of the anodic and cathodic reactions, respectively; C_O and C_R are the concentrations (in mol cm^{-3}) of the reacting species close to the metal/solution interface (superscript 's').

The observed overall currents (in amperes (A)) can be then written as

$$I = \vec{I} - \overleftarrow{I} = vFA = \vec{k} FAC_R^s - \overleftarrow{k} FAC_O^s \quad \text{(eq. 1.11)}$$

where F is Faraday constant (in C mol^{-1}), A is the electrode surface area (in cm^2).

According to the theory of activated complex the rate constant k depends exponentially on the standard free energy of activation ($\Delta G^{\#}$) as

$$k = k' \exp\left(\frac{-\Delta G^{\#}}{RT}\right) \quad \text{(eq. 1.12)}$$

In electrochemical reactions, $\Delta G^{\#}$ for the cathodic ($\Delta \vec{G}^{\#}$) and anodic ($\Delta \vec{G}^{\#}$) reactions depends on the electrode potential E as follows [2]:

$$\Delta \vec{G}^{\#} = \Delta \vec{G}^{\#,0} - (1-\alpha)F(E - E^{0\prime}) \qquad \text{(eq. 1.13a)}$$

$$\Delta \overleftarrow{G}^{\#} = \Delta \overleftarrow{G}^{\#,0} + \alpha F(E - E^{0\prime}) \qquad \text{(eq. 1.13b)}$$

where $E^{0\prime}$ is the formal electrode potential and α is the charge-transfer coefficient.

By inserting eq. 1.12 and 1.13 into eq. 1.11 and introducing the standard rate constant k^0, which corresponds to the case of equal bulk concentrations of oxidized and reduced species ($C_{\mathrm{O}}^{\mathrm{b}} = C_{\mathrm{R}}^{\mathrm{b}}$), one would obtain the following equation for the overall current density:

$$i = \frac{I}{A} = C_{\mathrm{R}}^{\mathrm{s}} F k^0 \exp\left(\frac{(1-\alpha)F(E-E^{0\prime})}{RT}\right) - C_{\mathrm{O}}^{\mathrm{s}} F k^0 \exp\left(\frac{-\alpha F(E-E^{0\prime})}{RT}\right) \qquad \text{(eq. 1.14)}$$

At equilibrium (i = 0), the partial anodic and cathodic current densities have the same absolute value, which is denoted as the exchange current density (i_0). Taking into account that surface and bulk concentrations under equilibrium conditions are also equal ($C^s = C^b$), i_0 can be written as:

$$i_0 = F k^0 C_O^{b\,(1-\alpha)} C_R^{b\,\alpha} \qquad \text{(eq. 1.15)}$$

Finally, by assuming rapid mass transport (i.e. when the reaction is controlled only by kinetics of the process) at equal bulk concentrations of oxidized and reduced species and introducing the overpotential ($\eta = E - E_{\mathrm{eq}}$, where E_{eq} is the electrode potential at equilibrium conditions) instead of E, we obtain the well-known Butler-Volmer equation [2]:

$$i = i_0 \left\{\exp\left(\frac{(1-\alpha)F\eta}{RT}\right) - \exp\left(\frac{-\alpha F\eta}{RT}\right)\right\} \qquad \text{(eq. 1.16)}$$

The eq. 1.16 can be simplified at "low" ($\eta < \frac{RT}{\alpha F}$) or "high" ($\eta \gg \frac{RT}{\alpha F}$) values of overpotential. In the first case, in the so-called micropolarization region ($|\eta| \leq 10$ mV at T = 298 K) the exponents in the eq. 1.16 can be expended in a Taylor series, leading to a linear relation between current density and overpotential:

$$i = \frac{i_0 F}{RT}\eta \qquad \text{(eq. 1.17)}$$

At large enough values of η ($|\eta| \geq 50$ mV at $T = 298$ K), one of the exponents in the eq. 1.16 becomes much smaller compared to the other and can be neglected, resulting in the equations 1.18a and b for large negative and large positive η, respectively:

$$|i| = i_0 \exp\left(\frac{-\alpha F \eta}{RT}\right) \qquad \text{(eq. 1.18a)}$$

$$|i| = i_0 \exp\left(\frac{(1-\alpha) F \eta}{RT}\right) \qquad \text{(eq. 1.18b)}$$

These equations yield a straight line, if we plot them in semi-logarithmic scale, also known as Tafel plots [3]:

$$\eta = a + b \cdot \ln|i| \qquad \text{(eq. 1.19)}$$

where a and b are called Tafel constants. Evaluation of the slope b allows to estimate α, while extrapolation of the linear segment of $\ln|i|/\eta$ curve up to the equilibrium potential (η = 0) yields i_0. The Tafel plots are very useful tool for discussing kinetics of the electrode processes.

It should be noted that in contrast with outer-sphere electrode reactions the description of the kinetics of electrocatalytic processes is complicated by the formation of adsorbed intermediates. In particular, the surface coverages by these species, which generally also depend on the electrode potential, should be included in the Butler-Volmer equation (see Section 2.4). The latter complicates interpretation of the Tafel slopes in such electrocatalytic reactions as the HER (at negative η) or the HOR (at positive η).

Depending on the rate determining step, theory predicts at 25 °C a different value for the Tafel slope in the potential region of the HER [13,14], i.e. 120 mV for the limiting Volmer reaction, 30 mV – for the Tafel reaction and 40 mV – for the Heyrovsky reaction. However, for the majority of materials the Tafel slope of 120 mV is usually observed at practical current densities, due to either a slow discharge of hydrogen ions, or a slow electrochemical desorption of H_{ad} atoms from the electrode surface [13,14]. A low Tafel slope of 30 mV is mostly observed for expensive

precious metals and only in acidic media, when the Volmer reaction is extremely rapid (being one of the most rapid elementary reactions). In particular, on Pt electrodes at pH close to 0 its rate is calculated to be ca. 0.42 A cm^{-2} [15]. The situation when various steps proceed with comparable rates has also been suggested [16,17]. In this case analysis of the Tafel slope becomes questionable. Besides, activated adsorption following Temkin's isotherm (instead of Langmuir isotherm usually used for the description of adsorption) has been postulated in order to explain the Tafel slope of ca. 60 mV observed in some studies [13].

Activities of different electrodes in the HOR/HER can be compared by estimation of corresponding exchange current densities, i_0, at equal operating conditions and normalizing them by either surface area or mass of the active component. However, one should also consider the value of the Tafel slope. If it significantly differs for different electrodes, then an inverse order of their activities might be obtained depending on the desired range of η [2].

1.1.2. Electrocatalysts for the HOR/HER

Studying different metal electrodes in the HOR/HER has shown that the values of electrocatalytic activities might differ up to six orders of magnitude depending on the electrode composition. Many researchers have tried to make a link between physicochemical properties of the electrodes and their activities in the HOR/HER [18]. Among possible correlations the dependence of the HOR/HER exchange current density on the value of Gibbs energy ($\Delta_{ad}G_H$) of adsorption of the hydrogen intermediate (H_{ad}) on the catalyst surface (or on the value of M-H_{ad} binding energy) is the most commonly used now. This is mainly due to the fact that adsorbed H_{ad} atoms are the key intermediate of the HOR/HER, according to the equations 1.3 – 1.8. The observed dependence shows volcano-type behavior (Fig. 1.1) in accordance with the Sabatier principle proposed in the early 1900s, and well-known in heterogeneous catalysis. The Sabatier principle states that the most active catalyst should adsorb reactive intermediates neither too weakly, nor too strongly [19,20]. As can be seen from the Fig. 1.1 the highest HER activity is observed for PGMs (Pt, Pd, Ir, Rh) with $\Delta_{ad}G_H$ close to zero, being in agreement with the prediction of Parson [21]. Some

differences between the dependences plotted by different authors mainly arose from the utilization of different approaches for the determination of $\Delta_{ad}G_H$ value. They are based on measuring the M-H_{ad} binding energy in corresponding metal hydrides (in early works, Fig. 1.1a) or DFT calculations (in modern works, Figs. 1.1b, c) [18,22,23]. Despite the observed correlations, the volcano-plots of the HOR/HER have been subject of justified criticism due to neglecting possible difference in the mechanisms of the hydrogen oxidation and evolution reactions on the same catalyst as well as a possible existence of several types of hydrogen adsorbates with different adsorption energy [24,25]. Besides, the presence of oxide species on the surface of non-noble metals further complicates the utilization of volcano-plots, being one of the likely reasons of existing inconsistencies in the values of M-H_{ad} binding energy and exchange currents in the HOR/HER [26]. Notwithstanding some limitations, there have been a number of successful attempts to use volcano-plots for creating bimetallic systems with enhanced electrocatalytic activity in the HOR/HER by combination of metals located on the opposite branches of the curve [27,28]. Along with the use of adsorption energy $\Delta_{ad}G_H$, some other descriptors, such as electron work functions, melting points, etc. have also been proposed to correlate with the activity of catalysts in the HOR/HER [14,25,29–31]

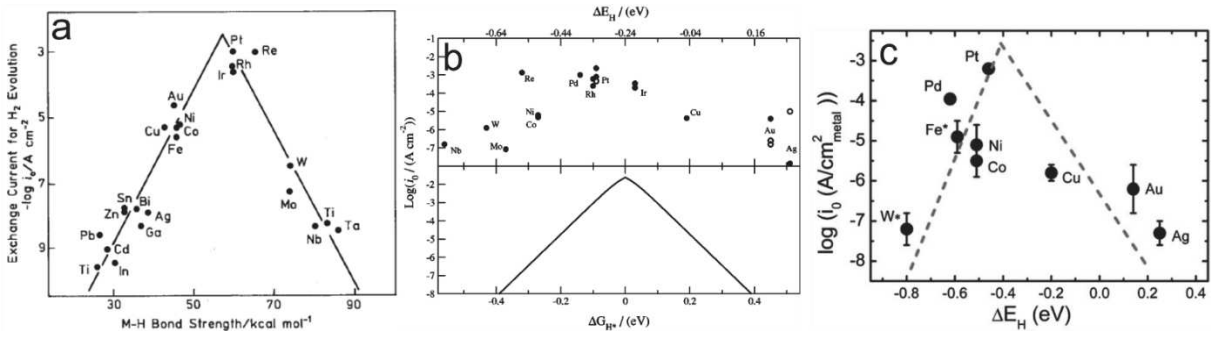

Fig. 1.1 *Exchange current density of the HER (in acidic (a, b) and alkaline (c) medium) plotted as a function of M-H_{ad} binding energy (a, given from the Ref. [18]) or free energy of adsorption of H_{ad} atoms on the catalyst (b and c, given from the Refs. [22,23]).*

Comparison of the HOR/HER in acidic and alkaline medium

As it has been already pointed out, the catalytic activity of Pt in the HOR/HER is extremely high in acidic media [32–34] and even little amount of the catalyst is enough for the reactions to occur. However, the HOR/HER activity of PGMs decreases by almost two orders of magnitude in alkaline media [33], being in the range of 0.55 – 0.69 mA cm^{-2} for polycrystalline Pt and Pt/C catalysts in diluted alkaline electrolytes [32,35]. The fact that the activity of Pt, Pd and Ir changes by a similar factor prompted Durst et al. [33] to propose that adsorption energy of H_{ad} is the only factor which affects the HOR/HER activity on various catalysts and determines the differences in the activity values depending on the pH [33]. This assumption is in agreement with observations of Zheng et al., who reported close to linear dependence between the values of M-H_{ad} binding energy (estimated from the potential of H_{upd}[a] desorption peak in cyclic voltammograms (CV)) and pH [36]. Notably, similar slopes of the dependence were obtained for supported Pt/C, Pd/C, Ir/C and Rh/C catalysts. Moreover, log(i_0) was found to decrease linearly with increase of pH and M-H_{ad} binding energy [36]. Sheng at al. [37] reached the same conclusion while studying polycrystalline Pt disk electrode at various pH and assuming that the position of the H_{upd} desorption peaks is determined by the binding energy of Pt-H_{ad}. However, Koper et al. have recently shown that the potential of these peaks also depends on the adsorption potential of oxygenated species on the surface of Pt [38].

Markovic et al. have proposed that along with the adsorption energy of H_{ad} atoms two other descriptors, namely the nature of the proton source (H_3O^+ or H_2O) and the presence of surface spectators are required to understand the role of pH in the HOR/HER [39]. The authors suggested a hypothesis according to which in alkaline media the HOR/HER require two types of sites on the electrode surface for the adsorption of H_{ad} as well as OH_{ad} (formed by the reaction $OH^- \leftrightarrow OH_{ad} + e^-$) species, while in acidic media H_{ad} is the only important intermediate [39,40]. Following the

[a] H_{upd} corresponds to the hydrogen adsorption/desorption in the potential region above an equilibrium potential of reversible hydrogen electrode

hypothesis, higher (compared to Au (111) and Pt (111)) activity of Ir (111) in the HER in alkaline medium was assigned by Markovic et al. to larger strength of OH_{ad} adsorption on the surface of Ir [39,40]. However, this conclusion was based on the analysis of the very first anodic scan of corresponding CVs, while comparison of the steady-state curves, performed by Durst et al. [33], indicates that the HOR/HER activity decreases in the order of Pt/C > Ir/C > Pd/C. Bi-functional mechanism was also suggested by Markovic et al. to explain a promotion effect of Ru on the activity of Pt, according to which the adsorption of OH_{ad} and H_{ad} takes place on Ru and Pt atoms respectively [39]. However, the enhancement of the activity in PtRu systems has been later shown to be mostly due to the weakening of Pt-H_{ad} bond in the presence of Ru [41]. In addition, the adsorption of OH_{ad} was found to occur on PGMs at lower potentials when the pH is increased [36,42,43]. It means that if the OH_{ad} would be the intermediate of the HOR in alkaline media, then the rate of this reaction should increase at higher pH, while in fact an opposite tendency is observed [36].

Besides the above mentioned reaction between adsorbed H_{ad} and OH_{ad}, Markovic et al. also proposed that presence of low-coordinated metal sites or transition metal hydroxides on the surface of noble metals should promote the Volmer step of water dissociation, which is often assumed to be the rate-determining step of the HOR [39,40,44–46]. Another explanation for the promoting effect of $Ni(OH)_2$ on the HOR/HER activity of Pt has been recently suggested by Koper et al., according to which the presence of $Ni(OH)_2$ on the Pt surface lowers the energetic barrier for the reorganization of water molecules in the double layer, thus facilitating transfer of OH^- [47]. The authors proposed that in acidic media, in the case of transfer of H^+ protons, the energetic barrier is insignificant, but increases in alkaline solution, what might be the reason for a decrease of the HOR/HER activity with an increase of pH [47]. According to Wang et al., the addition of a more oxophilic metal (such as Ru or Ni) to Pt could also shift the onset potential of OH_{ad} adsorption on the Pt surface to more positive values, thus enhancing the overall HOR/HER activity [41].

On the basis of the above analysis, we conclude that activity of PGMs in the HOR/HER at various pH is mainly determined by the value of M-H_{ad} binding energy,

while the presence of surface spectators (for example, transition metal hydroxides) might change the strength of the H_{ad} adsorption as well as affect the adsorption of water molecules, thus influencing the rate of the Volmer step.

1.2. Electrochemical properties of Ni-based electrocatalysts

Non-noble metals have been used for many years as cathode catalyst of the HER in alkaline water electrolysis. Iron utilized at the beginning was later replaced by steel, while recently the interest has been shifted towards application of Ni-based catalysts. The latter is mainly caused by higher corrosion stability of Ni in alkaline solutions compared to steel, even if its activity is slightly lower [48].

Electrochemistry of metallic Ni electrodes has been studied for almost 100 years, starting, likely, from the works of Emelianova [49], Frumkin et al. [50,51], Legran and Levina [52], Conway et al. [53–60], Breiter et al. [61,62], Bockris and Potter [63] as well as many others. The most significant results, obtained in alkaline media, have been recently summarized by Hall et al. [64,65] and Jerkiewicz et al. [66–68], who paid special attention to the discussion of various processes, which take place on the surface of Ni electrodes depending on the applied potential. However some questions, for example, an influence of the degree of surface oxidation were barely discussed. In addition, there are still several controversial issues that require more detailed study.

1.2.1. Electrochemical behavior of Ni in alkaline medium

Typical cyclic voltammograms obtained on a freshly polished polycrystalline Ni disk in an alkaline electrolyte are presented in the Fig. 1.2 [68]. In order to facilitate the discussion about characteristic features of the CV of the Ni electrode, we marked out two potential regions, namely the "low-potential region" at $E \leq 0.5$ V[b] and the "high-potential region" at $0.5 < E < 1.6$ V.

[b] If not otherwise stated, the potential is referred to the reversible hydrogen electrode (RHE).

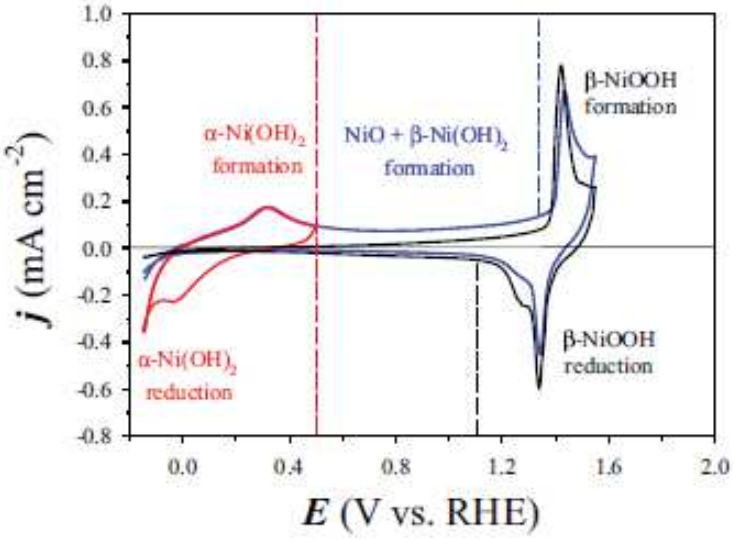

Fig. 1.2 *CVs obtained for a polycrystalline Ni electrode in 0.5 M KOH at a sweep rate v = 100 mV·s^{-1} and T = 293 K. The first CV (red curve) covers the potential range of [–0.15 – 0.50 V], while two other CVs (first scan – blue curve and tenth scan – black curve) cover the potential range of [–0.15 – 1.55 V]. Given from the Ref. [68].*

In *the low-potential region* anodic and cathodic peaks are generally assigned with the formation and reduction of surface α-Ni(OH)$_2$, respectively [64,66,69–71]. Anodic dissolution and cathodic redeposition of Ni, predicted on the basis of the Pourbaix diagram [72] and observed in acidic media, were shown (based on electrochemical quartz crystal microbalance measurements and experiments with rotating Ni disk electrode) to be insignificant in alkaline electrolytes [71,73]. Several models have been suggested for the mechanism of low-potential Ni oxidation, among which the nucleation and growth model and the place exchange model have the best agreement with experimental observations [66]. The latter model was proposed by Conway et al. [74] and later improved by Jerkiewicz et al. [66] by adding the influence of applied potential on the structure and physical properties of the surface hydroxides. According to that model, the formation of nickel hydroxide proceeds through the following mechanism:

$$Ni + OH^- \rightarrow Ni\text{-}OH_{ad} + e^- \text{ (fast)}$$

$$Ni\text{-}OH_{ad} \rightarrow (OH\text{-}Ni)_{\text{quasi-3D lattice}} \text{ (rate determining step)}$$

$$(OH\text{-}Ni)_{\text{quasi-3D lattice}} + OH^- \rightarrow Ni(OH)_{2,ad} + e^- \text{ (fast)}$$

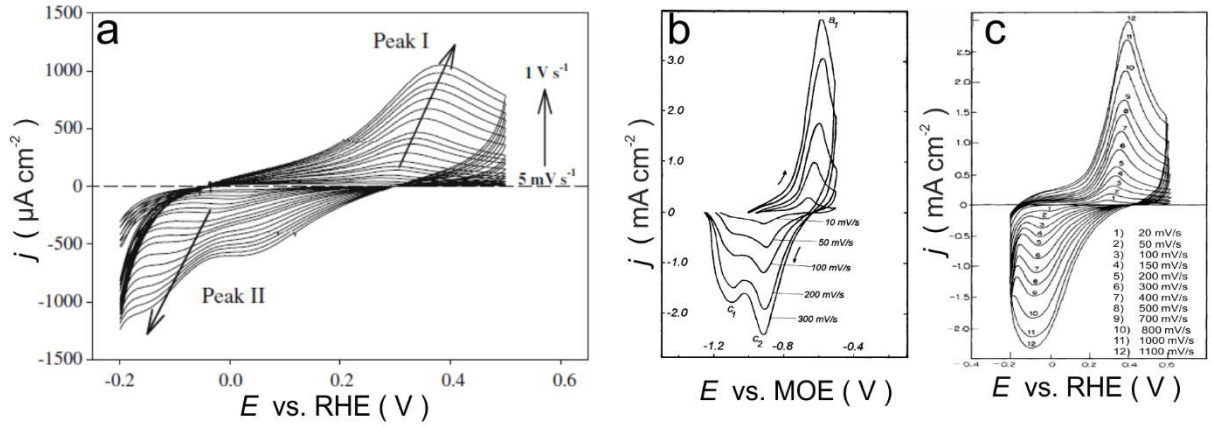

Fig. 1.3 *CVs obtained for polycrystalline Ni electrode at various sweep rates in (a) 0.5 M KOH (given from the Ref. [66]), (b) 1.0 M NaOH (after subtraction of the currents corresponding to the HER, given from the Ref. [75]) and (c) 0.5 M NaOH electrolyte (given from the Ref [76]).*

Existence of intermediate Ni-OH_{ad} species was proposed on the basis of CVs obtained at various sweep rates (v), when two cathodic peaks were observed at high v (Fig. 1.3a). However, two cathodic peaks (even at relatively low v) were also noticed by D'Alkaine and Santanna [75], who assigned the one at more negative potentials to the reduction of an oxide film formed on the electrode surface during its preparation to the experiment (Fig. 1.3b). On the contrary, only one cathodic peak was observed by Conway et al. [76] independent of the sweep rate (Fig. 1.3c), which makes the question about the nature of the second cathodic peak disputable. It should be noted that the presence of highly mobile adsorbed OH_{ad} species, characterized by low binding energy with the Ni surface, was detected by *in situ* scanning tunneling microscopy at potentials around 0.1 V, i.e. before the formation of α-$Ni(OH)_2$ [77]. Meanwhile the place exchange model is not able to explain some observed phenomena. In particular, in spite of widely accepted in literature belief that in *the low-potential region* the surface of Ni is covered by a monolayer of surface $Ni(OH)_2$ (see, for example, [64,66,78]), experiments carried out with the use of *in situ* scanning tunneling microscopy [79,80] as well as analysis of the CVs obtained at low temperatures (< 263 K) [71] predict a formation of 3D islands of $Ni(OH)_2$ before full coverage of the electrode surface (Fig. 1.4). The latter likely explains the common use

of the term 'α-$Ni(OH)_2$' for the oxide species formed on Ni electrode surface in *the low-potential region*.

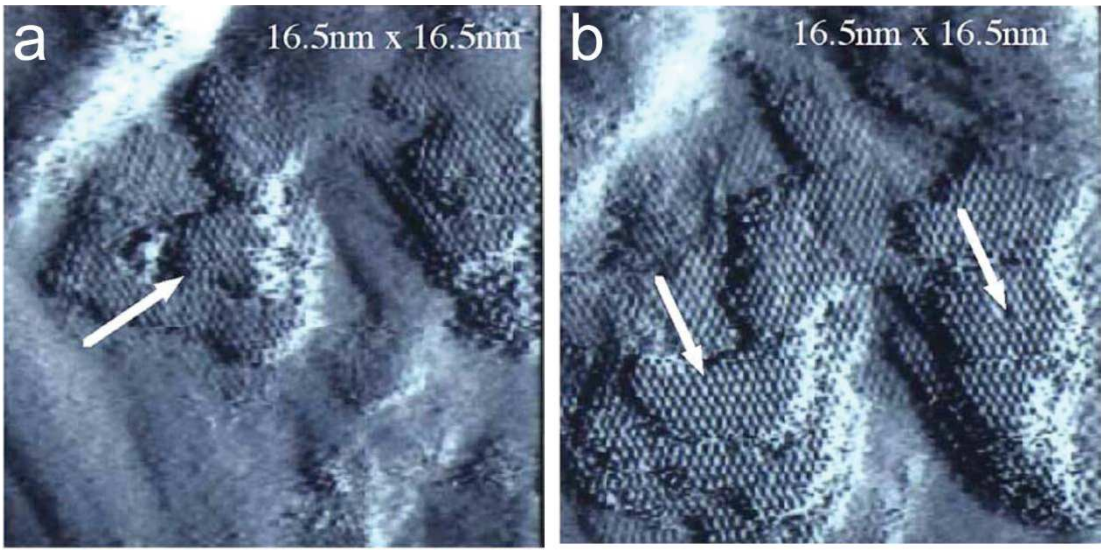

Fig. 1.4 *Sequence of STM images for the formation of $Ni(OH)_2$ film (shown by arrows) on Ni (111) at 150 mV vs SHE in 0.05 M Na_2SO_4: (a) immediately after stepping the potential from -300 to 150 mV vs SHE; (b) 3 min after (a) (given from the Ref. [79]).*

In some works the formation of NiO was proposed to occur after oxidation of Ni at $E < 0.5$ V instead of α-$Ni(OH)_2$ [73,81]. However, *in situ* experiments with the use of Raman [70] or IR spectroscopy [82] as well as X-ray photoelectron spectroscopy (XPS) [83] have shown that the amount of NiO on the surface of Ni in *the low-potential region* is insignificant (or NiO is completely absent). Besides, several authors stated that along with the oxidation of Ni surface the oxidation of a**d**sorbed on the surface and/or a**b**sorbed in the Ni metal hydrogen contributes to the anodic peak at $E < 0.5$ V [64,66,73,84–86]. Ni hydrides are known to be produced at high cathodic overpotentials (see below). It was shown that contribution of the oxidation of a**b**sorbed hydrogen and/or Ni hydrides to the anodic peak currents increases in the case of long cathodic polarization or cycling up to high negative potentials [85]. At the same time recording of CVs in a narrow potential range results in insignificant contribution of these processes [71,73,87]. Note however that the contribution of the oxidation of a**d**sorbed hydrogen to the anodic peak currents have to be considered. Based on electrochemical quartz crystal microbalance measurements Grden et al.

concluded, that oxidation of a**d**sorbed hydrogen is occurring just before the low-potential Ni oxidation [73]. More detailed discussion about the influence of cathodic polarization on the CV shape of Ni electrode can be found in the works [64,66] and references therein.

In *the high-potential region* increase of the applied potential leads to transformation of α-$Ni(OH)_2$ into β-$Ni(OH)_2$ with decrease of the degree of hydration as schematically shown in Fig. 1.5a, along with the thickening of NiO layer [64,65,67,68,70,77,88,89]. Oxidation of Ni electrode at more positive potentials than 0.5 V results in a shift of the cathodic peak in *the low-potential region* towards negative values, suggesting formation of more stable Ni oxide species on the electrode surface [66,75,90]. Moreover, cycling up to $E > \sim 0.9$ V (at $v = 100$ mV·s^{-1}) leads to disappearance of the cathodic peak due to irreversible character of β-$Ni(OH)_2$ formation (unlike α-$Ni(OH)_2$), what can be clearly seen in Fig. 1.2 [64,91,92]. Note that partial reduction of β-$Ni(OH)_2$ is possible upon application of high cathodic overpotentials. The first identification of two pseudopolymorphs of $Ni(OH)_2$ was done by Bode et al. [93], who also suggested a scheme, describing the processes of Ni oxidation in *the high-potential region* (Fig. 1.5b). According to that scheme increase of the applied potential leads to further oxidation of both α- and β-$Ni(OH)_2$ with the formation of Ni oxyhydroxide [68,93–96]. The anodic peak corresponding to this process is located at potentials around 1.4 V (Fig. 1.2), while reduction of Ni oxyhydroxide ($NiOOH \rightarrow Ni(OH)_2$) occurs in the potential interval of 1.2 – 1.4 V with appearance of, usually, two cathodic peaks, whose exact position depends on the involved phases of NiOOH (β or γ) as well as $Ni(OH)_2$ (α or β) [96,97]. Besides, two anodic peaks can also be visible at low sweep rates ($v \leq 10$ mV·s^{-1}), while temperature and oxide film thickness affect the position of both anodic and cathodic peaks in *the high-potential region* [85,96,98]. Above ca. 1.5 V the oxygen evolution reaction begins, where, according to *in situ* Raman experiments [88,99–102] and XPS measurements [83,103], the surface of Ni electrode is covered by NiOOH and NiO.

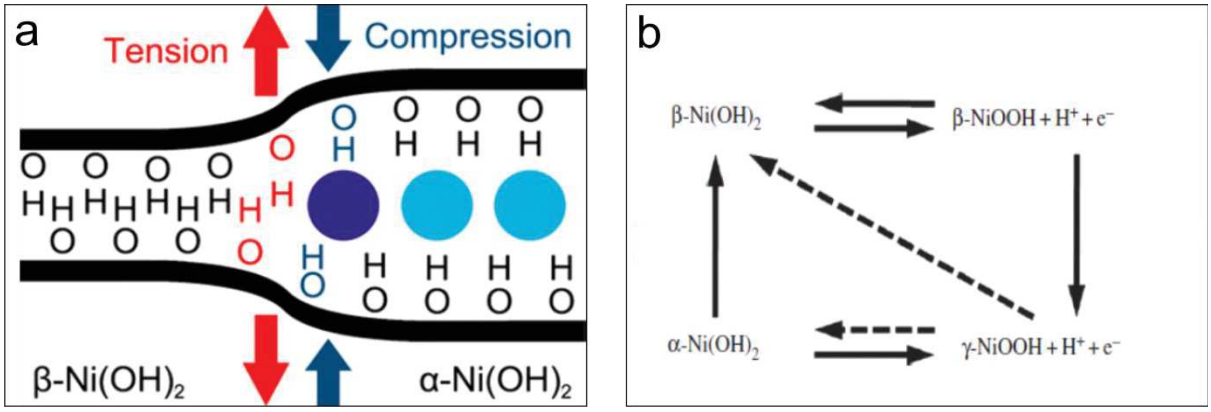

Fig. 1.5 *(a) Schematic representation of the α/β-phase transition. Blue circles represent water molecules located between the NiOH layers in α-Ni(OH)₂. Given from the Ref. [104]; (b) A general scheme of the chemical and electrochemical processes that occur on the surface of Ni electrode in the high-potential region. Given from the Ref. [65].*

At negative applied potentials the HER and hydrogen a**b**sorption into Ni metal lattice (with further formation of Ni hydrides) proceed along with the reduction of Ni surface oxide species. At present, two bulk phases, namely α and β, are known for Ni hydrides, similarly to these for Pd hydrides [64,105]. The lattice parameters of α-NiH and β-NiH are ca. 1 % and ca. 6 %, respectively, greater compared to Ni metal [106–108]. According to Ref. [64], the equilibrium potentials for the formation of α-NiH and β-NiH may be estimated as -0.075 – -0.095 V and -0.12 – -0.13 V, respectively. As shown by Hall et al. [64] and Soares et al. [109], undisputed existence of bulk α- or β-NiH is observed (by XRD) only for the electrodes treated galvanostatically at currents above $I < -0.3$ A cm^{-2}. Meanwhile one cannot exclude the presence of small amounts of absorbed hydrogen or α-NiH even at potentials close to 0 V vs RHE.

Influence of the oxidation of the Ni electrode surface on its electrochemical behavior

Oxidation of Ni is well known to occur rapidly after its exposure to oxygen-containing atmosphere even at room temperature. According to the ‘‘island-growth’’ model proposed by Holloway and Hudson, this process proceeds in three stages: (i) oxygen chemisorption; (ii) nucleation and lateral growth of nickel oxide islands; (iii) slow thickening of the oxide layer up to ca. 2 – 4 atomic layers of NiO [110]. If the oxidation takes place in the presence of water (under humid air or oxygen

atmosphere), then three-layered structure consisting of $Ni(OH)_2$ upper layer and NiO layer between the metal substrate and $Ni(OH)_2$ is formed [89,111–113]. After immersion of the air-formed oxide into an alkaline solution, Ni hydroxide layer becomes thicker, while overall three-layered $Ni/NiO/Ni(OH)_2$ structure generally remains the same [89,112].

It should be noted that unlike chemical oxidation in air, which at room temperature is stopped at ca. 1-2 nm thickness of the oxide layer, electrochemical oxidation by anodic polarization results in much thicker oxide with larger crystalline domains [85,89,111,112,114].

It has been observed that in CVs, obtained after either chemical (under contact with air or concentrated acid solutions) or electrochemical (for example, after cycling up to the potentials above 0.8 V) oxidation, a second anodic peak appears at around $E \approx 0.10$ V (Fig. 1.6) [62,78,81,84,85,91,92,115–117]. The amplitude and the position of that peak significantly depend on the values of anodic and cathodic potential limits of the CV [85,92]. There is no common view concerning the origin of the peaks observed in CVs of oxidized Ni electrodes in the potential interval of [0 – 0.15 V]. Several processes have been suggested in different works, such as (i) adsorption of hydroxide-ions with the formation of $Ni–OH_{ad}$ [115], (ii) oxygen adsorption [92], (iii) dissolution of Ni with the formation of $HNiO_2^-$ [75], (iv) oxidation of a**d**sorbed hydrogen [62,116–118], (v) oxidation of a**b**sorbed hydrogen and/or Ni hydrides [62,78,84,91,115]. The impact of each of these processes, likely, depends on the methodology used for preconditioning of the electrode surface as well as the measurement protocol. In particular, utilization of a highly passivated electrode subjected to prolonged cathodic polarization at high overpotentials results in significant contribution of the process (v) [84,91]. On the contrary, oxygen adsorption (ii) is unlikely if under experiments are performed in an inert atmosphere. The same conclusion is valid for the dissolution and further redeposition of Ni in alkaline media (iii) especially if the concentration of hydroxide-ions is higher than 0.1 M, as it was shown in Refs. [71,73].

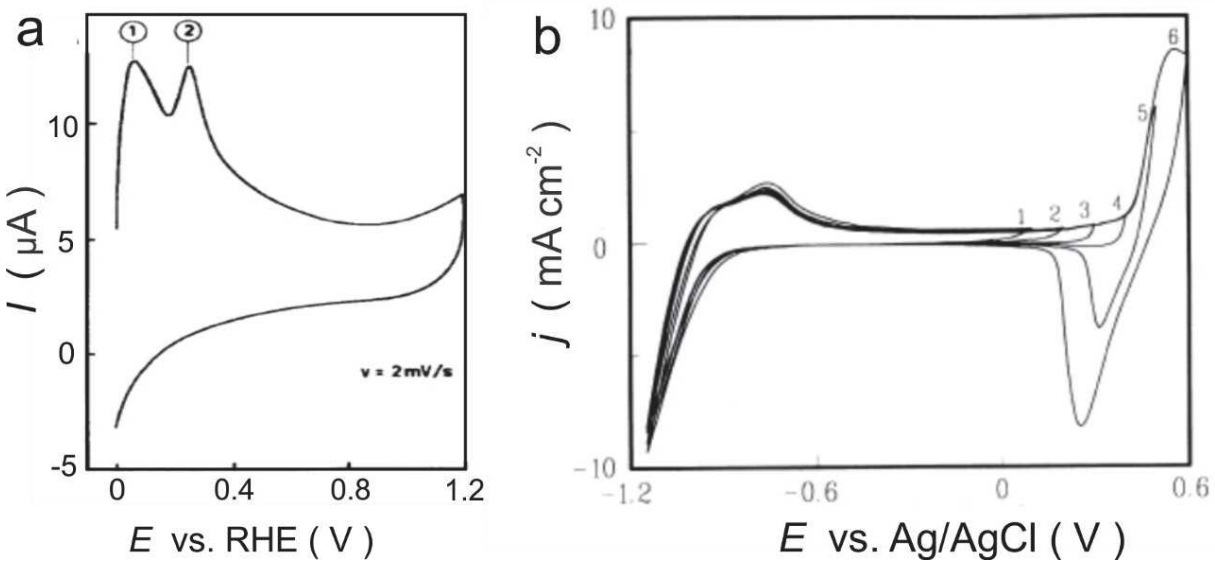

Fig. 1.6 *(a) CVs, obtained for polycrystalline Ni in 0.1 M KOH after registration of 11 potential sweeps from -0.8 to 1.2 V at v = 2 mV·s^{-1}. Given from the Ref. [84]; (b) CVs, obtained for Ni/C electrode in 0.2 M NaOH at v = 20 mV·s^{-1} and various anodic limits. Given from the Ref. [116]*

Influence of the structure of Ni electrode surface on its electrochemical behavior

The influence of crystallographic orientation of the Ni surface on its electrochemical behavior has been studied in several works both in acid and in alkaline media [61,62,77,115,119–121]. The shape of the CVs (at $v \geq 50$ mV·s^{-1}) was found to be similar for low-index Ni planes (111), (110), (100), but the potential of the anodic peak corresponding to α-$Ni(OH)_2$ formation shifts following the order (110) < (100) < (111) [61,115,120]. This observation confirms structure-sensitive adsorption of hydroxide ions on Ni surface. Meanwhile the potential of the cathodic peak is similar for three Ni single crystals.

An additional anodic peak in the potential interval of [0.1 – 0.2 V] was observed in CVs, obtained at low sweep rates ($v \leq 5$ mV·s^{-1}) (Fig. 1.7a) [115]. The position of that peak depends on the crystallographic orientation of Ni surfaces. In particular, the peak maximum is located around 0.07 V on Ni (110) plane, being as high as the main peak of α-$Ni(OH)_2$ formation. The same peak on Ni (100) plane is observed at more positive potentials (around 0.12 V), while on Ni (111) plane its contribution is less

visible (Fig. 1.7a). The dependence of the processes of Ni oxidation in *the high-potential region* on the crystallographic orientation of its surface was noticed only for first three scans of CVs (Fig. 1.7b). Meanwhile continuous cycling leads to the structure disordering and, as a result, similar shape of CVs for three types of Ni planes (Fig. 1.7b) [61,120].

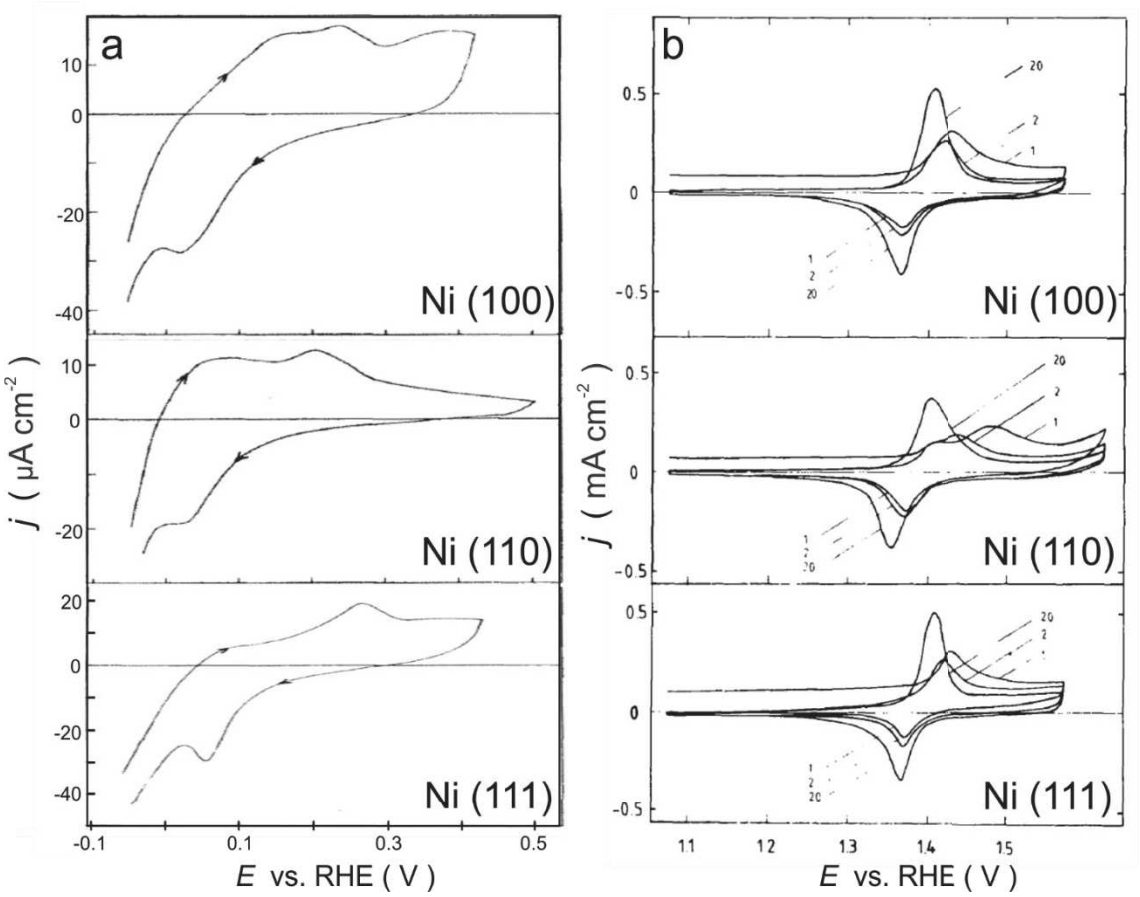

Fig. 1.7 *CVs, obtained for Ni (100), Ni (110), Ni (111) single crystals in deaerated 0.1 M NaOH at T = 25 °C in (a) the low-potential region at v = 5 mV·s^{-1} (given from the Ref. [115]) and (b) the high-potential region at v = 50 mV·s^{-1} (given from the Ref. [120]).*

1.2.2. Determination of the electrochemical surface area of Ni

Estimation of the electrochemical surface area (S_{EC}) of the electrode is one of the key stages for determination of its specific electrocatalytic activity and comparison of several materials between each other. At present, the most widely used approach for the determination of S_{EC} is described in the work of Machado and Avaca [78], who suggested to use the charge under the peak of α-$Ni(OH)_2$ formation and the

corresponding conversion coefficient of 514 μC cm^{-2}. This is an average value determined from the measurements performed using low-index Ni single crystals [120]. Note that there is no strong theoretical background of this value unlike the values used in the case of noble metals [122]. Transfer of 2 electrons is usually assumed in the calculations [78]. However, since one cannot exclude a possible impact of the electrochemical hydrogen desorption in the measured anodic charge, then it is better to consider a number of involved electrons between 2 and 3. In some works the charge of the cathodic peak of α-$Ni(OH)_2$ reduction (after subtraction of the currents corresponding to the HER) is used instead of the charge under the anodic peak [123,124]. Despite its wide use, the S_{EC} values obtained by this method should be considered as approximate due to the used assumptions. First, as discussed above, along with the Ni/α-$Ni(OH)_2$ redox transition other processes may occur in *the low-potential region*, giving an indefinite contribution to the charge obtained by integration. Therefore, in order to minimize an impact of 'side' processes the potential limits should be chosen in such a way that, on the one hand, provide complete reduction of α-$Ni(OH)_2$ formed during the anodic scan, while avoiding formation of irreducible β-$Ni(OH)_2$ and, on the other hand, minimize the formation of a**b**sorbed hydrogen and Ni hydrides, whose oxidation contributes to the anodic charge. Second, although a monolayer coverage of Ni surface by α-$Ni(OH)_2$ during its oxidation is suggested, in fact the thickness of the surface oxide layer is unknown. Moreover its thickness may vary depending on the structure and the composition of the electrode surface. Finally, as it has been shown above, the way of pretreatment of the surface of the Ni electrode may significantly influence its voltammetric behavior in *the low-potential region*. Therefore it is not clear which charge should be used for the estimation of S_{EC}.

In addition to the method, suggested by Machado and Avaca, in some works, mostly related to the study of Ni-based alloys, the value of S_{EC} was recalculated from the value of the electrochemical double layer capacitance (C_{dl}), obtained using electrochemical impedance spectroscopy [124–128]. However, analysis of the literature points out that the value of C_{dl} depends on the surface state of Ni electrode leading to the variation of specific capacitance from 20 to 60 μF·cm^{-2} [62,124–

126,129,130]. Therefore, in the majority of works authors preferred to record impedance spectra in the HER region, where contribution of the oxide phases is believed to be insignificant. However an increased probability of the formation of Ni hydrides in this case can also affect the measured values.

The value of S_{EC} can also be determined in *the high-potential region*. In this case, the value of C_{dl} is usually estimated either by electrochemical impedance spectroscopy under the assumption that the surface of Ni electrode is covered by Ni(II)/Ni(III) oxide species or on the basis of CVs recorded at various sweep rates in the double layer potential region (with typically 0.1 V potential window) [131,132]. In the latter case plotting of the current values measured at a certain potential as a function of sweep rate gives a straight line with the slope equal to C_{dl}. Along with the use of the C_{dl} value, the charge of monolayer formation of NiOOH was suggested to be used for an estimation of S_{EC} as well. Corresponding measurements should be performed in the following way. First, anodic currents are applied in order to form NiOOH. Second, after interruption of the charging currents cathodic current transients are recorded [130,133]. Then, if one would plot the estimated total transient charge (Q_{cath}) against the overpotential of the anodic charging step (η_{an}), at sufficiently high values of η_{an}, Q_{cath} will reach a plateau, which corresponds to a monolayer coverage by NiOOH. Theoretically derived conversion coefficient of 420 μC cm^{-2} is proposed by authors as an "universal accepted standard" for approximate estimation of S_{EC}. However, a possible formation of β- and γ-NiOOH, whose unit cell parameters and symmetries are somewhat different, may result in slightly different values of S_{EC} [65,94].

A yet another method has been proposed by Hall et al. [134], who suggested to use an oxalate salt to limit the thickness of surface $Ni(OH)_2$ by a single layer. Sharp and narrow peaks for the Ni(II)/Ni(III) oxidation-reduction processes were observed in CVs in the presence of oxalate, giving constant cathodic charge at $v \geq 150$ mV·s^{-1} (analysis of the anodic charge is complicated by the involvement of the oxygen evolution reaction). The authors then assumed a Coulombic charge of 195 μC cm^{-2} estimated from the lattice parameters of α-$Ni(OH)_2$ (for β-$Ni(OH)_2$ the difference is

only around 3%) and obtained the roughness factor for mechanically polished Ni electrode equal to 1.78.

It should be noted that all the methods for S_{EC} determination, which require cycling of Ni electrode up to high positive potentials (> 0.5 V), lead to the formation of irreducible oxide species on the surface and in some cases may even change the surface roughness [64,65,67,68,70,77,88,89]. Therefore, it is reasonable to determine the value of S_{EC} from *the high-potential region* only when studying processes, taking place at high anodic potentials, for example, anodic oxygen evolution/reduction reactions.

1.3. Electrocatalytic properties of Ni-based electrocatalysts in the HOR/HER

1.3.1. Analysis of adsorption energies of the HOR/HER intermediates on Ni

According to Sabatier principle, one of the main parameters, which determines the activity of electrocatalysts, is the adsorption energy of reactive compounds (educts, intermediates and products) on the electrode surface, which depends on its nature [2,19,20]. It is generally assumed (and experimentally observed in many cases), that the strength of adsorption decreases going from more open planes to the close-packed ones, which for face-centered cubic lattice of Ni would mean the order of Ni (110) > Ni (100) > Ni (111) (corresponding coordination numbers of surface atoms are 7, 8 and 9, respectively). In this section we analyze adsorption energies, which were obtained using DFT calculations for the main species involved in the HOR/HER in base, namely: molecular and atomic hydrogen (H_2, H_{ad}), water molecules (H_2O_{ad}), hydroxo-species (OH_{ad}) and, given the tendency of nickel towards oxidation, atomic oxygen (O_{ad}). These compounds can adsorb on metal surface in various positions, such as *on top*, *bridge*, and *hollow*, being coordinated by one, two, and three surface atoms, respectively.

Hydrogen molecules were found to adsorb on the surface of low-index Ni planes in the *on top* position [135–138] with their further dissociation. The lowest energy barrier for dissociation was obtained for Ni (110) [139–142]. Adsorbed H_2O_{ad} molecules occupy the same position, binding with the surface through the oxygen atom, while adsorbed H_{ad}, OH_{ad} and O_{ad} species occupy *hollow* sites [135,136,143,144]. DFT calculations predict that adsorption energies for H_2O_{ad} and OH_{ad} on different Ni planes decrease following the order Ni (110) > Ni (100) > Ni (111) [135,144–147], while for the adsorption energies of H_{ad} and O_{ad} atoms the observed order is Ni (100) > Ni (111) > Ni (110) [135,141,144,146–148]. Note, however, that the difference between the adsorption energies of H_{ad} atoms on Ni (111) and Ni (100) can be considered insignificant and in some studies a bit larger values were obtained for Ni (111) compared to Ni(100) [141,149]. It was also found that adsorption of H_{ad} on stepped surfaces (210) and (531) is characterized by just a little higher energy compared to the adsorption on low-index Ni planes [141]. Besides, it was concluded that surface diffusion of H_{ad} atoms between different surface sites is facile, while their diffusion into subsurface sites (necessary for the formation of Ni hydrides) is expected only after occupation of all available surface sites [136].

Adsorption of water molecules H_2O_{ad}, which along with H_{ad} atoms participate in the HOR/HER through the Volmer and Heyrovsky steps (eq. 1.7, 1.8), can also significantly affect the kinetics of the HOR/HER. According to the DFT calculations, adsorption energy of H_2O_{ad} molecules is significantly lower compared to the other intermediates of the processes [135,143,144,150]. In particular, Mohsenzadeh at al. obtained the values of -4.98, -3.44, -2.51 and -0.39 eV for the adsorption of O_{ad}, OH_{ad}, H_{ad} and H_2O_{ad} on Ni (110) plane, respectively [144]. Besides, an energetic barrier for water splitting was found to be significant in the case of Ni (111) surface [151,152], but is decreasing for more open Ni (100) and Ni (110) planes as well as stepped or other low-coordinated surfaces, due to an increase of the adsorption energy of H_2O_{ad} molecules [144,150,153]. The latter may stimulate the Heyrovsky step and, as a result, lead to an increase of the activity in the HER. It is worth to note, that pre-adsorption of strongly bonded species on Ni surface significantly affects subsequent adsorption of water molecules. It was found that existence of H_{ad} atoms on Ni surface leads to the

formation of multilayer islands of water, surrounded by chains of adsorbed H_{ad} atoms already at small surface coverage [151,154]. On the contrary, pre-covering of Ni surface with O_{ad} atoms increases the binding energy of Ni-OH_2 due to the formation of hydrogen bonds between adsorbed water molecule and nearby O_{ad} atom [135,150,155]. The latter also facilitates water splitting with the formation of two OH_{ad} molecules, which was observed on Ni (111) surface in the combined XPS-TPD (TPD – temperature programmed desorption) experiments [156].

DFT calculations also showed that the binding energies of both Ni-H_{ad} and Ni-OH_{ad} decrease at the vicinity of pre-adsorbed O_{ad} atoms [142,155,157–159]. It was found that the adsorption of H_{ad} atoms occurs only at a considerable distance from the adsorbed O_{ad} atoms [157]. A repulsive interaction, although to a much lesser extent, was also observed for the adsorption of OH_{ad} nearby O_{ad} atoms [159].

1.3.2. Activity of monometallic Ni electrocatalysts in the HOR/HER

Owing to the use of alkaline water electrolysis at the industrial level, studies of Ni-based electrocatalysts in the HOR/HER have been primarily carried out in the potential region of the HER, while the interest to the HOR has been quite small until recently. Early studies were largely dedicated to Raney Ni electrodes, while during the past decades the interest has shifted to bimetallic Ni-based catalysts [28,160–165]. However, even without influence of a second metal the exchange current densities of Ni electrodes reported in the literature may differ by nearly two orders of magnitude [62,63,126,166–168]. As it was mentioned in *the Introduction*, this diversity can be caused by the use of various methods for pretreatment of Ni electrodes before carrying out electrocatalytic measurements. In this section we present a short analysis of published works, which allows one to observe the influence of the structure and the composition of the surface of Ni electrodes on their activity in the HOR/HER.

Influence of Ni structure on its activity in the HOR/HER

Very few works were devoted to the study of the HOR/HER on Ni depending on the crystallographic orientation of its surface [62,115,121]. Weininger et al. and Zoltowski et al. [62,121] observed very small or even no effect of the crystallographic orientation of the surface, because of, likely, poor quality of used single crystals or

chosen experimental procedure, during which the electrodes lost their initial surface structure after oxidation in alkaline electrolyte (see Section 1.2.1, Fig. 1.7). On the contrary, Floner et al. observed significant difference in the shape of CVs, obtained for low-index Ni planes as well as polycrystalline Ni disk electrode in *the low-potential region* [115]. It was found, that electrocatalytic activity of Ni (in terms of exchange current densities) in the HOR decreases following the order Ni (110) > Ni (100) > Ni (111) >> Ni_{poly} (Fig. 1.8). To explain the observed differences, the authors proposed a hypothesis that the onset potential of hydrogen oxidation on Ni is determined by the strength of the adsorption of water molecules, which hinder the adsorption of H_{ad} atoms on a particular surface. However, according to the analysis of theoretical studies (see Section 1.3.1), adsorption energy of H_{ad} and OH_{ad} species is much higher compared to the one for H_2O_{ad} molecules [135,143,144,150]. Therefore blockage of the active sites on the Ni surface by H_2O_{ad} molecules seems to be unlikely. At the same time, analysis of the DFT calculations allows to suggest that the activity of Ni single crystals in the HOR/HER is mainly determined by the strength of Ni-H_{ad} bond, which is decreased in the order Ni (111) > Ni (100) > Ni (110) [115,135,141,144,149]. The latter correlates with the observed by Floner et al. dependence of Ni activity on the crystallographic orientation of its surface. The presence of adsorbed hydrogen atoms at E < ~0.15 V is in agreement with the observation of p-nitroaniline hydrogenation currents in this potential interval[116]. From the control experiments on Pt the authors showed that this process is occurring in the region of underpotential deposition of hydrogen [116]. Besides, Hu and Wen showed that full oxidation of Ni electrode surface at T = 400 °C leads to complete suppression of p-nitroaniline hydrogenation, due to the absence of adsorbed hydrogen on the surface [116]. Comparison of Figs. 1.7 and 1.8 clearly shows that Ni oxidation overlaps with the HOR in a wide potential range [115,169]. This results in a rapid decrease of the HOR currents and complete suppression of HOR at E > ~0.3 V due to the blockage of the electrode surface by Ni hydroxide (Fig. 1.8). On the reverse sweep (cathodic direction), the HOR begins with the onset of $Ni(OH)_2$ reduction [115].

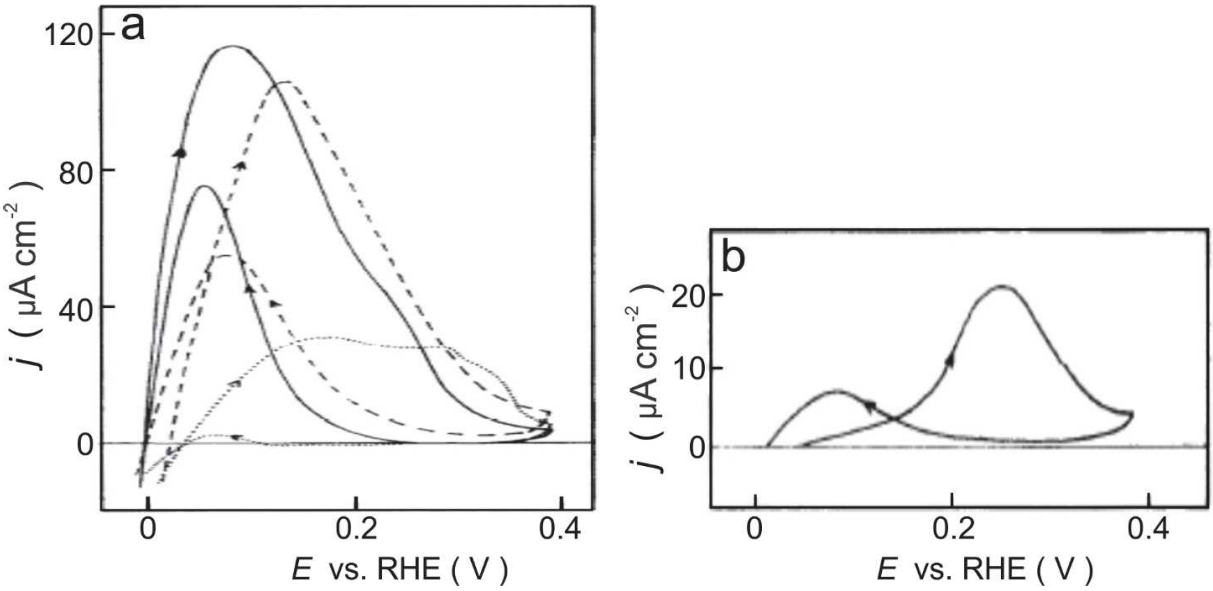

Fig. 1.8 *CVs, obtained for (a) Ni single crystals (Ni (110) – solid line, Ni (100) – dashed line, Ni (111) – dotted line) and (b) polycrystalline Ni in H_2-saturated 0.1 M NaOH at v = 1 mV·s^{-1} and T = 25 °C. Given from the Ref. [115].*

The influence of the Ni structure on its activity in the HOR/HER can be further considered on the basis of works devoted to the study of such materials as porous Ni films [170–172], nanowires [173,174], dendrites [168,175], nanosheets [176] and nanospikes [177]. It was found that normalizing HER currents to the geometric surface area results in much higher activity for these materials with respect to a polycrystalline Ni electrode. However, the enhanced apparent catalytic activity is mainly due to an increase of the number of active sites on the electrode surface (i. e. an increase of the roughness factor), while the specific activity attributed to the S_{EC} was found to be almost the same, for example, for a Ni nanospike array, electrodeposited Ni and Ni plate [177] or Ni particles, electrodeposited Ni film and commercial Ni foil [168]. Meanwhile a bit higher specific activity, normalized to the S_{EC}, in the HER was observed for Ni dendrites compared to Ni particles [168].

Recently, Zhuang et al. have shown that the HOR activity of Ni can be significantly enhanced after doping of the carbon nanotube (CNT) support with nitrogen (from 9.2 to 28 μA cm^{-2} for Ni/CNT and Ni/N-CNT, respectively) [123]. On the basis of DFT calculations, the enhanced activity of Ni was assigned by the authors to a decrease of Ni-H_{ad} bond strength in the vicinity of nitrogen atoms.

Influence of the oxidation of Ni surface on its activity in the HOR/HER

Despite the fact that systematic study of the influence of Ni surface oxidation on its activity in the HOR/HER has not been performed yet, in some works the authors observed a decrease of the Tafel slope and the HER overpotential after electrochemical oxidation (by cycling up to $E > 1.0$ V) of the surface of Ni disk [62,84,126,169,170,178,179]. In particular, Lasia et al. reported about an increase of the exchange current density of Ni in the HER from 1.4 to 29 μA cm^{-2}_{geom} after cycling of the electrode in the potential region of [-0.35 – 1.6 V] at $v = 50$ mV·s^{-1} [126]. Noticeably, the roughness factor of the electrode is believed to remain unaffected by such treatment [62]. On the contrary, prolonged anodic polarization leads to a decrease of the HER activity of Ni, likely, due to the formation of irreversible β-$Ni(OH)_2$ which strongly passivates the surface of the electrode, decreasing its fractional coverage by hydrogen [166]. It is known, that bulk Ni oxide and hydroxide are inactive in the HER due to the low adsorption energies of hydrogen atoms on their surfaces [180]. Therefore, an enhanced activity compared to that of the reduced electrode surface can be observed only if Ni oxide species coexist on the electrode surface with metallic Ni sites (necessary for hydrogen adsorption) [181].

Danilovic et al. have shown, that the activity of Ni in the HER increases by a factor of four after modification of its surface by deposited $Ni(OH)_2$ [182]. The authors proposed that $Ni(OH)_2$ serves to enhance the water dissociation step by weakening the H-OH bond of the adsorbed water, while H_{ad} adsorption takes place on nearby metallic Ni sites [182]. The same approach but with the use of NiO instead of $Ni(OH)_2$ allowed Gong et al. to obtain NiO/Ni-CNT sample, which outperforms two reference Ni/CNT and, especially, NiO/CNT samples [183–185]. The synergistic effect was also proposed to explain the high activity of Ni/NiO/$CoSe_2$ hybrid [186], Ni/NiO nanosheets [187] and single-crystalline Ni nanosheet arrays subjected to partial oxidation [176]. Besides, DFT calculations performed by Kuang et al. revealed that desorption of H_2 possesses a lower energy barrier on the Ni/NiO (111) surface than on pure Ni (111) surface (3.228 and 3.763 eV, respectively) [176].

1.3.3. Activity of bimetallic Ni-based electrocatalysts in the HOR/HER

To date several reviews have been published summarizing the studies of bimetallic NiM systems, as well as compounds of Ni with various non-metals (selenides, phosphides, carbides, nitrides, sulfides) in the HER [14,48,131,160,185,188–191]. Considering the fact that the description of all the systems studied is too large for the current review, in this section we mainly focus on the evaluation of the activity enhancement factor after an addition of a second metal to Ni catalyst as well as the possible causes of the observed changes. Most of the works reviewed in this section are related to the study of the HER on Ni-based electrocatalysts, while some recent works devoted to the HOR are also considered.

The first example of Ni-based catalysts is Raney Ni, which can be produced by leaching of Al (or Zn) from Ni-Al(Zn) precursor alloys in concentrated alkaline solution at elevated temperatures, thus providing high porosity and large surface area of Ni [129,192–194]. However, the second metal may partly remain in the material after leaching and, therefore, influence the catalyst properties. This can be a likely reason for an enhanced activity in the HER usually observed for Raney Ni with respect to pure Ni [48,129,192,194,195]. Later, especially during the past 20 years, many other bi- and polymetallic Ni-based systems have been studied, among which NiAg [196], NiBi [197], NiCo [128,198–200], NiCu [201–203], NiFe [127,204,205], NiMo [205–220], NiMn [132,221,222], NiRu [223], NiSn [224], NiTi [225–227], NiV [228,229], NiCr [164,184,230] and NiW [127,212,220,228,231,232]. In addition, modification of Raney Ni by an addition of other transition metals has been also investigated [161,162,192,195,233–235]. Absolute majority of these samples were prepared in the form of thick deposits by electrodeposition techniques. Although such methods as dip pyrolysis [206], high energy alloying [208], melting [210,211], wet impregnation [164] and some other were also employed for the catalyst preparation.

It should be noticed that direct comparison of the HER activity of various NiM electrocatalysts is almost impossible due to a lack of information about the real Ni surface area S_{EC}, which is necessary for estimation of specific catalytic activity. Comparison of the activity values, normalized by geometric surface area, for porous

samples, is incorrect since an enhancement of an apparent activity can be due to an increase of the real metal surface area [14,129,198,205,219,224,225]. Besides determination of the S_{EC} of Ni by different methods further complicates the comparison of results obtained in different laboratories. Therefore, comparison of several NiM electrocatalysts studied in the same work (thus, using the same methods) seems to be more reliable. In particular, Raj et al. [165] reported that the HER activity decreases in the row Ni-Mo > Ni-Zn > Ni-Co > Ni-W > Ni-Fe > Ni-Cr > Ni-plated steel, which agrees with the observation of Navarro-Flores et al. [127], who compared NiMo, NiW, NiFe and pure Ni. However Bates et al. have recently reported that activity of NiCr/C exceeds the values measured for NiMo/C and NiFe/C [164]. This discrepancy, likely, originates from an ignorance of possible difference in the values of S_{EC} of Ni, while comparing different systems. Meanwhile, careful analysis of the works in which bimetallic NiM catalysts were studied taking into account an estimation of the real surface area, allowed us to determine the systems for which an increase of the specific electrocatalytic activity of Ni in the HER is the most reliable. These systems can be divided into two groups depending on the enhancement effect caused be second metal: (i) the activity increases less than 3 times for NiCo [128], NiCu [201–203], NiFe [205], NiTi [227], NiAg [196]; (ii) the activity increases up to two orders of magnitude for NiMo [211,212,214,216,217,220], NiMn [132,221,222], NiW [220,231] and NiCr [164,184]. Significant decrease of the HER overpotential was also observed after simple addition of Mo ions (MoO_4^{2-}) to the alkaline electrolyte and was attributed to the adsorption of Mo on the electrode surface with the formation of Ni-Co-Mo [236] or Ni-Mo [237,238]. Ternary alloys on the basis of NiMo, namely NiMoCo [28] and NiMoZn [239], have also shown high activity in the HOR/HER.

In order to explain synergistic effect of an increase of the HOR/HER activity observed for bimetallic NiM electrocatalysts, the well-known Sabatier principle and based on it volcano dependence of the HOR/HER exchange current density on the hydrogen adsorption energy $\Delta_{ad}G_H$ are usually used (see Section 1.1.2). Despite some limitations, it allows one to predict an increase of the activity, in particular, for the alloys of Ni, strongly adsorbing hydrogen, with metals, which adsorb hydrogen

weakly (for example, Ag or Cu). In the case of transition metals such as Mn, Mo, Ti, Cr, W, utilization of volcano-plots is, however, complicated by the tendency of these metals to form oxides under operating conditions (which exclude the possibility to use $\Delta_{ad}G_H$ calculated for pure metals). To explain an enhancement of the specific activity observed for these systems, some authors suggested to use the Brewer-Engel valence bond theory [29,240]. According to this theory the electrons of the metal with more filled d-bands are shared with the metal with less filled or empty d-orbitals, while the highest activity is observed for systems with nearly filled d-orbital [31,212]. In particular, addition of Mo or W was shown to decrease the d-band vacancy of Ni, which becomes nearly zero at about 11 and 8 at.% content of Mo and W, respectively, being in good agreement with the observed optimum surface composition of NiMo and NiW catalysts, possessing the highest activity in the HER [210,212,228]. Modification of the electronic structure of Ni by the second metal presumably leads to a decrease of $\Delta_{ad}G_H$ value on Ni and, as a result, to an increase of its activity in the HOR/HER [28,213]. Besides, the presence of transition metal oxides (Mn, Cr, Mo, Ti) on the electrode surface is believed to facilitate the coordination of water molecules and, as a result, accelerate the Volmer step, which in some cases is the rate-determining step for the HOR/HER [132,211,221,227].

1.3.4. Stability of Ni-based electrocatalysts in the HOR/HER

Due to the fact that Ni-based catalysts have been primarily studied in the region of the cathodic hydrogen evolution, their stability can be discussed only with regard to this process. It was found, that during prolonged use of Ni catalysts in alkaline water electrolysis, the value of the cathodic overpotential, which must be applied to the electrode to achieve a given current density, increases [175,241]. Taking into consideration the works, where an increase of the HER activity of Ni was observed in the presence of a small amount of Ni oxide, one can assume that the first overpotential decay is caused by the reduction of these surface oxide species [50,170,179,185]. In addition, some phase separation between NiO and Ni may occur, likely, due to high resistance in a thick oxide layer [185], which leads to a decrease of the active surface area. Further decrease in the HER activity is believed to be due to the formation of Ni

hydrides [78,109,242–245], the presence of which after prolonged cathodic polarization was confirmed by XRD [64,109]. It is worth to note, that Conway et al. suggested a promoting role of Ni hydrides in the HER instead, which may serve as protectors of Ni-based cathodes from oxidation [246]. Meanwhile, this conclusion is, likely, valid only for metastable α-NiH_x, while the formation of β-phase has negative effect [243,247]. Soares et al. proposed that formation of Ni hydrides decreases the HER activity due to the modification of the density of states at the Fermi level [109].

Along with an enhancement of the activity of Ni in the HER, addition of a second metal was found to increase the stability of the catalyst during long-term operation of the electrolyzer (Cu-[248], Mn3O4-[132], Mo-[206,228], doped Raney Ni - [233,234]) as well as shutdown cycles [228,249]. It is believed that addition of a second metal prevents formation of β-NiH_x [204] as well as deep oxidation of Ni [230,249]. Recently, after discovering of the positive synergetic effect in the Ni-NiO system on the HER activity and considering instability of Ni oxide species during water electrolysis, it was proposed that the oxide of the second metal may act as a stabilizing agent for the Ni-NiO system [164,184,185]. In particular, Gong et al. reported about an increase of the stability of Ni/NiO composites in the HER after an addition of Cr_2O_3 [184,185].

1.3.5. Mechanism of the HOR/HER on the surface of Ni electrocatalysts

The study of the mechanism of the HOR/HER is an important stage in the study of the kinetics of these processes on various electrocatalysts. Along with the fundamental significance, unveiling of the reaction mechanism and discovering the rate-determining step allow one to propose possible ways for the enhancement of the catalytic activity. The mechanism of the HER on Ni electrodes has been studied since the beginning of the XX^{th} century, but there is still no consensus concerning either the contribution of individual steps of the process (Tafel-Volmer vs Heyrovsky-Volmer mechanism) or the rate-determining step in the literature. These discrepancies are largely due to differences in the experimental protocols and the methodologies used

for preconditioning of the Ni electrode surface prior to the experiment, i.e. the same factors which affect the activity of Ni in the HOR/HER.

The first significant studies of the HOR/HER kinetics on the surface of Ni electrode were, likely, carried out by Tafel [3], Frumkin et al. [50,51] and Bockris and Potter [63]. It is worth to note, that even at that time it was assumed that the presence of surface oxides may significantly affect the kinetics of the HOR/HER. Therefore experiments were performed in such a way as to minimize their formation. In particular, Frumkin et al. annealed Ni electrode at 400 – 420 °C in H_2 atmosphere inside of specially constructed electrochemical cell just before filling it with alkaline electrolyte [50]. Bockris et al. used Ni electrodes, which were preliminarily annealed in H_2 atmosphere and sealed in fragile glass bulbs in the absence of oxygen [63,250]. Later the kinetics of the HER on Ni has been widely investigated by many others [17,62,78,126,166,241,244,251–257], while the kinetics of the HOR on Ni was considered in only few cases [50,115,258].

Based on the methods used for preconditioning of Ni electrode surface prior to the investigation of the HOR/HER kinetics, the published works can be divided into two groups. The first group contains studies in which the surface of Ni electrodes was subjected to cathodic polarization with the purpose to remove possible traces of Ni oxide species. As was shown by Conway et al. [246,256,259] as well as Machado and Avaca [78] such treatment may result in the formation of Ni hydrides, therefore the catalyst composition can be labeled as Ni/NiH_x (Table 1.1). Note also, that the formation of Ni hydrides under application of cathodic overpotentials is facilitated if Ni electrode was first subjected to anodic polarization for a short time [84,91]. The second group contains studies in which the surface of Ni electrodes was either subjected to continuous cycling between high anodic and high cathodic potential limits or cleaned by its contact with acid solutions [166,251–253]. Such preconditioning, likely, results in the formation of surface oxide species NiO_x, which may coexist with metallic Ni sites even at negative overpotentials (at least for a short period of time), while the corresponding catalyst composition can be labeled as Ni/NiO_x (Table 1.1).

A careful analysis of the published works in accordance with the current level of understanding of the electrochemical behavior of Ni in alkaline medium (see Section 1.2) allows one to suggest that the HER usually follows the Volmer-Heyrovsky mechanism on metallic Ni electrodes even in the presence of Ni hydrides (Ni/NiH_x, Table 1.1) [50,78,126,255–257]. On the contrary, for systems where existence of NiO_x species on the surface of Ni electrodes is expected from either the pretreatment procedure employed or utilization of high anodic potentials (E > 0.9 V) during the measurements, the reported mechanism of the HER was usually attributed to the Vomer-Tafel mechanism (Ni/NiO_x, Table 1.1) [166,251–253,260]. Besides, Krstajic et al. shown that the mechanism of the HER can switch from the Volmer-Tafel at -0.2 < η < 0 V to the Volmer-Heyrovsky at η < -0.2 V [257,261]. Changing of the Tafel slope at different overpotentials was also reported by Kibria et al. [254] and Conway et al. [246,256] and most likely reflects the changes in the surface composition of the Ni electrode at different hydrogen overpotentials.

Table 1.1 Kinetic parameters and the mechanism of the HER (* denotes the rate-determining step), depending on the pre-treatment of the surface of nickel electrodes

Methodology of Ni electrode pretreatment	Possible surface state	T, K	Electrolyte	Tafel slope, mV	j_0, μA cm$^{-2}_{geom}$	j_0, μA cm$^{-2}_{Ni}$	Proposed mechanism of the HER	Ref.
Ni rod was heated at 400-420 °C in H_2 atmosphere and then cooled down inside the cell before immersing in the electrolyte. Then it was cathodically polarized until stabilization of the potential.	Ni metal with possible traces of NiH_x	293	0.001 - 8.8 M NaOH	108-115	-	-	Volmer* – Heyrovsky	[50]
Ni wires were annealed in H_2 atmosphere and sealed in fragile glass bulbs. The latter were broken inside the electrolyte just before measurements.	Ni metal with possible traces of NiH_x	293	0.10 M NaOH	101	0.4	-	Volmer* – Tafel	[63]
Ni rod was scraped with grease-free blade to give a bright surface before measurements	Ni metal with possible traces of NiO_x	300	2 M NaOH	88	10	-	Volmer* – Tafel	[251]
Ni rod was cleaned in a mixture of conc. chromic and sulfuric acid, washed in boiling water and polarized cathodically for 5 min at j = 2 mA cm^{-2} (a); the electrode was additionally oxidized by cycling up to E > 1.0 V (b).	Ni/NiO_x	303	0.1 M NaOH	125 (a); 90 (b)	25 (a); 10 (b)	-	Volmer* – Tafel	[166]
Ni wires were annealed in H_2 atmosphere and sealed in fragile glass bulbs. The latter were broken inside the electrolyte just before measurements.	Ni metal with possible traces of NiH_x	298	0.2 M NaOH	120	10	-	Volmer – Heyrovsky*	[256]
Polished Ni foil was pulse polarized (5 cycles) by application of an anodic pulse to reach E = 1.6 V after 3 s and then the current direction was changed until the electrode reached E = -0.36 V.	Ni/NiH_x	296	1.3 M KOH	105-125	17±4	-	Volmer – Heyrovsky	[17]
Ni rod was cycled several times between potentials of hydrogen and oxygen evolution reactions.	Ni/NiO_x	303	1 M KOH	146±19	102±78	-	Volmer – Tafel	[252,253]
After polishing Ni wire was cathodically polarized at $E \approx$ -0.53 V for 1 h.	Ni/NiH_x	303	30 об.% KOH	115	35.5	-	Volmer – Heyrovsky	[244]
(a) Cathodic polarization of polished Ni disk at j = 1 mA cm^{-2} for 30 min (b) cycling 10 times in the potential interval of [-0.35 – 1.6 V] at v = 50 mV·s^{-1}.	Ni/NiH_x (a); Ni/NiO_x (b)	298	1 M NaOH	115±9 (a); 269±61 (b)	1.8±1.6 (a); 29±13 (b)	-	Volmer – Heyrovsky (a) - (б)	[126]
After polishing Ni disk electrode was introduced in the electrolyte at $E \approx$ 0.03 V and then either stabilized at $E \approx$ -0.87 V (a) or at $E \approx$ -0.37 V after first anodic polarization at $E \approx$ 1.33 V for 10 min (b)	Ni/NiH_x (a); Ni/NiO_x (b)	293-298	1 M NaOH	-	-	-	Volmer – Heyrovsky	[255]
Polished Ni foil was cathodically polarized at $E \approx$ -0.37 V for 5 min.	Ni/NiH_x	298	0.5 M NaOH	128	-	3.4	Volmer – Heyrovsky*	[78]
Polished Ni rod was cathodically polarized at E = -0.3 V for 1 h.	Ni/NiH_x	296	0.1 M NaOH	121±3	4.6±0.3	-	-	[167]
Ni wire was first oxidized at E = 1.4 V for 5s and then cathodically polarized for 1h at E = -0.6 V.	Ni/NiH_x	293	1 M NaOH	121	1.1	-	Volmer – Heyrovsky*	[257]
Ni electrodes were obtained by galvanostatic deposition, then washed by water, dried in air flow and immersed in the electrolyte.	Ni/NiO_x	303	2 M NaOH	122	-	-	Volmer – Heyrovsky – Tafel	[171]

1.4. Conclusions of Chapter 1

Analysis of the studies devoted to the investigation of Ni-based catalysts in the HOR/HER evidences considerable interest of the scientific community to this field during the past years. Due to an industrial use of Ni-based catalysts in alkaline water electrolysis, the researchers have been largely focused on the study of the HER and development of more active Ni-based catalysts for this process. However growing interest in AMFC has led to an increasing number of publications devoted to the study of the HOR on Ni-based catalysts in recent years.

It was found that electrochemical properties of Ni in alkaline electrolytes significantly depend on the methodology used for the pretreatment of the electrode surface, which can be seen, in particular, by the change of the CV shape. In addition, there is a serious discrepancy in the literature concerning the values of specific electrocatalytic activity of Ni in the HER, which originates from, first, utilization of the geometric surface area for normalization of the activity and, second, dependence of the activity on the state of Ni surface (for example, the degree of its oxidation). It should be noted that there is also no consensus in the literature concerning the mechanism of the HOR/HER on Ni electrodes (Heyrovsky-Volmer or Tafel-Volmer). Therefore, the first problems, which were solved within the frames of this work, were to obtain reproducible data of specific (normalized to the real surface area) electrocatalytic activity of Ni in the HOR/HER and to determine how and why the oxidation of the surface of Ni electrode affects its activity in the HOR/HER. The analysis of the works published in the literature also does not allow one to make an unambiguous conclusion about the influence of the microstructure of the nickel catalyst on its activity in the HOR/HER. To better understand this issue, in the current work we prepared nickel nanoparticles of various sizes and determined their specific (real surface-weighted) activities in the HOR/HER.

Finally, the analysis of the works devoted to the study of Ni-based bimetallic catalysts allows one to conclude that (i) these materials were investigated primarily in the potential range of the HER, while their activity in the HOR has been studied

insufficiently; (ii) normalization of the activity on the geometric surface area does not allow one to make unambiguous conclusions about the effect of a second metal on the specific electrocatalytic activity of Ni in the HOR/HER; (iii) most of the studied NiM electrocatalysts were in the form of either thick deposits or polycrystalline alloys, whereas for application in AMFC it is necessary to prepare nanoparticles of metals supported on high surface area (e.g. carbon) supports. Aiming to better understand the influence of a second metal on electrochemical and electrocatalytic properties of Ni in the HOR/HER in the current work we studied carbon supported NiCu/C and NiMo/C catalysts.

In addition to the experimental study we also performed kinetic modeling which allows us to further advance in understanding the effects of the state of Ni electrode surface as well as the presence of a second component on it on the kinetics and mechanism of the HOR/HER.

Chapter 2:
Materials and Methods

2.1. Preparation of electrocatalysts and electrodes

2.1.1. Polycrystalline Ni rod and foil

To inspect an influence of Ni surface state on its electrochemical and electrocatalytic (in the HOR/HER) properties in 0.10 M NaOH electrolyte, polycrystalline Ni rod (Ø5 mm, Mateck, 99.99 %) and Ni foil (10 x 10 mm, Mateck, 99.99 %) were employed. Prior to use the top flat surface of the Ni rod and both sides of the Ni foil were thoroughly polished with Al_2O_3 slurries (Alfa Aesar) from 1.0 down to either 0.3 or 0.05 μm, after that they were rinsed by ultrapure water produced by either Milli-Q system (Milli Pore, USA, 18.2 MΩ·cm, TOC < 5 ppb) or ELGA Ultra Analytic apparatus (18.2 MΩ·cm, TOC < 3 ppb). Ni foil was additionally sonicated in a jar of water for 2 min to remove the traces of Al_2O_3.

2.1.2. Synthesis of nanostructured Ni_{ED}/GC and Ni_{ED}/XC-72 electrocatalysts

Nanostructured nickel electrodes were prepared by potentiostatic electrodeposition of Ni from the bath containing 0.01 M $NiSO_4$ + 0.10 M $(NH_4)_2SO_4$ solution (performed from $NiSO_4 \cdot 6H_2O$ (99.99%, Aldrich) and $(NH_4)_2SO_4$ (99.0%, Aldrich) granules) at T = 298 K using either nonporous glassy carbon (GC) cylinder or porous Vulcan XC-72 carbon (Cabot; BET surface area 254 $m^2\ g^{-1}$, total pore volume 0.43 $cm^3\ g^{-1}$) as a catalyst support. In the latter case, a thin layer of carbon (ca. 100 μg cm^{-2}_{geom}) was first deposited from its suspension with isopropanol : water (3:2, vol.) mixture on a clean and dry surface of GC and then dried under N_2 flow for at least 60 min. Prior to the use, the top surface of GC cylinders was thoroughly polished with Al_2O_3 slurries (1.0 and 0.3 μm), after that they were thoroughly rinsed by water and consecutively sonicated in acetone, ethanol and water (10 min in each solvent). Finally, the GC cylinders were dried in the oven at $T \approx 80$ °C for ca. 1 h. and then cooled dawn at room temperature. The electrodeposition procedure will be discussed in detail in Chapter 4.

2.1.3. Synthesis of bimetallic NiCu/C electrocatalysts

Bimetallic nickel-copper catalysts with 25 wt.% total metal loading and Ni:Cu molar ratio from 0.50:0.50 to 0.95:0.05 were prepared by P. A. Simonov in the Boreskov Institute of Catalysis (BIC, Novosibirsk, Russia) by the incipient wetness impregnation of the support with aqueous solutions of $Ni(OAc)_2$ and $Cu(OAc)_2$ taken in a desired proportion. Commercial furnace black Vulcan XC-72 (Cabot; BET surface area 210 $m^2\ g^{-1}$, total pore volume 0.36 $cm^3\ g^{-1}$) was used as a catalyst support. Monometallic Ni/C was also synthesized for the comparison. After reaching the incipient wetness point the mixture was dried in vacuum (T =100 °C, $P \approx 2.7 \cdot 10^3$ Pa), then calcined in a He flow by increasing the temperature from 50 to 250 °C in a stepwise manner (50° steps, 15 min each) and further reduced with H_2 at 250 ºC for 1 h. After reduction, the reactor was cooled down in H_2 atmosphere, which was further replaced by helium. Before taking the reduced catalysts out, their surfaces were passivated by introducing short air pulses to the helium flow.

In addition, monometallic Ni/C and bimetallic NiCu/C catalysts with Ni:Cu molar ratio from 0.90:0.10 to 0.98:0.02 were prepared by the same method, but using freeze-drying (lyophilization) instead of drying in vacuum with the objective to obtain more homogeneous catalysts (it will be discussed in detail in Chapter 5).

2.1.4. Synthesis of bimetallic NiMo/C electrocatalysts

Bimetallic NiMo/C catalyst with 50 wt.% total metal loading and Ni:Mo atomic ratio close to 0.9:0.1 was synthesized by A. Serov (Center for Micro-Engineered Materials, University of New Mexico, Albuquerque, USA) by the incipient wetness impregnation of the support with aqueous solutions of $Ni(NO_3)_2$ and $(NH_4)_2MoO_4$. KetjenBlack-600 carbon (KB, AkzoNobel, BET surface area ~ 1200 $m^2\ g^{-1}$) with larger compared to XC-72 BET surface area was used as a support to increase total metal loading. After reaching the incipient wetness point the mixture was dried in oven at T = 85 °C and then dry composite was ground with mortar and pestle. The fine powder was reduced in a hydrogen atmosphere (flow rate of 100 ccm) at T = 550 °C for 1 h. Before exposing the catalyst to the ambient it was passivated in a He flow containing 2% of O_2 at room temperature for 8 h.

2.2. Physicochemical methods of the study of electrocatalysts

2.2.1. Transmission Electron Microscopy (TEM), Scanning Transmission Electron Microscopic (STEM) and Energy-Dispersive X-Ray Spectroscopy (EDX)

Nanostructured Ni_{ED}/GC and Ni_{ED}/XC-72 electrocatalysts

TEM (including high resolution (HR-TEM)) and STEM were used to characterize, respectively, the microstructure of Ni nanoparticles in Ni_{ED}/XC-72 catalyst and their distribution over the carbon support. To do this the catalyst layer was transferred from the GC surface to a copper grid. Analogously, Ni nanoparticles directly deposited on GC support (Ni_{ED}/GC) were carefully scrapped from its surface and their microstructure was analyzed using HR-TEM. Microscopic measurements were performed by C. Ulhaq-Bouillet in Institut de Physique et Chimie des Materiaux de Strasbourg (IPCMS, Strasbourg, France). STEM was performed with a LaB6-JEOL 2100 microscope operating at 200 kV with a point to point resolution of 0.1 nm. TEM and HR-TEM were carried out with JEOL 2100F instrument operating at 200kV with a 0.2 nm resolution.

Bimetallic NiCu/C and monometallic Ni/C electrocatalysts

High Angle Annular Dark Field STEM (HAADF-STEM) analysis, EDX spectroscopy, elemental mapping and conventional HR-TEM measurements of Ni/C and $Ni_{1-x}Cu_x$/C catalysts were undertaken using a JEM-2200FS (JEOL) microscope. The measurements were performed by V. I. Zaikovskii in the BIC (Novosibirsk, Russia). The elemental maps were obtained using Ni K (E = 7.471 keV) and Cu K (E = 8.040 keV) lines. Lattice spacing was calculated by Fast Fourier Transform (FFT) using DigMicrograph (GATAN) soft.

Bimetallic NiMo/C electrocatalyst

The structure of $Ni_{0.9}Mo_{0.1}$/C catalyst and the metal particles distribution over carbon support surface were studied by TEM using a JEOL 2010 microscope with an

accelerating voltage of 200 keV. The measurements were performed by A. Serov (UNM CMEM, Albuquerque, USA).

2.2.2. Scanning Electron Microscopy (SEM)

The morphology of Ni nanoparticles in Ni_{ED}/GC samples was studied by SEM using microscopes of either a JEOL JSM-6700F at accelerating voltage of 6 kV or a JEOL JSM-6490LV. The measurements were performed by T. Dintzer in Institut de Chimie et Procédés pour l'Energie, l'Environnement et la Santé (ICPEES, Strasbourg, France) or by N. A. Rudina in the BIC (Novosibirsk, Russia), respectively.

2.2.3. X-Ray Photoelectron Spectroscopy (XPS)

Polycrystalline Ni foil

Surface state of the Ni foil (subjected to various pretreatments) was analyzed using XPS in an ultra-high vacuum chamber (residual gas pressure $<5\cdot10^{-6}$ Pa) equipped with a Clam2 (VG Microtech) electron analyzer and a dual anode (Al and Mg Kα) X-ray source. The measurements and XP spectra characterization were performed by V. Papaefthimiou and V. A. Saveleva in ICPEES (Strasbourg, France).

After electrochemical treatment (see Section 2.3.4) the Ni foil was taken out from the electrolyte (0.10 M NaOH) and immediately fixed on the XPS sample holder with a drop of water completely covering the surface of Ni foil in order to minimize its contact with the ambient atmosphere. Then the holder was quickly (less than 5 min) placed into the entry chamber of the XP spectrometer, after that gazes were evacuated up to $P \approx 10^{-5}$ Pa (during this step a drop of water evaporates from the surface of the Ni foil) and only then the sample was transferred to the main chamber of the XP spectrometer. Survey and narrow scan Ni2p, O1s, C1s spectra were recorded using the excitation photon energy of 1486.6 eV. Characterization of the Ni foil was carried out by means of normal (0 degrees) and grazing (50 degrees) take-off angle measurements. The temperature was maintained constant throughout the experiment at 30°C. NiO produced by thermal oxidation of Ni foil in air at $T = 500$ ºC for 1 h., and pure metallic Ni foil (cleaned by several Ar^+ sputtering and annealing cycles) were used as reference samples.

In the spectra deconvolution procedure, the same peak parameters for Ni^0, NiO and $Ni(OH)_2$ components were employed for all processed samples after Shirley background subtraction. The charge effect arising in the process of photoemission of electrons was taken into account by correcting the spectra with respect to C1s of the carbon line (284.8 eV). Quantitative calculations were performed using normalized Ni2p, O1s, C1s peak areas, taking into account the atomic sensitivity factors of each element [262]. Spectra analysis and their deconvolution were performed using CasaXPS software.

Taking into account the overlapping of the Ni^0, NiO and $Ni(OH)_2$ peaks in a narrow interval of binding energies, a self-consistent fitting of Ni2p, C1s and O1s XP spectra was undertaken by assuming, according to the literature [64,89,110,263], that oxidation of Ni under its contact with air and/or alkaline electrolyte results in the formation of NiO and $Ni(OH)_2$. Ni2p spectra were fitted using constrained line shapes for NiO (three components at 853.6, 855.2 and 860.9 eV) and $Ni(OH)_2$ (three components at 856.1, 861.9 and 855.3 eV) developed by Biesinger et al. [264], while the shape of Ni^0 was taken from the reference sample without deconvolution. O1s spectra were fitted using four components: adsorbed water (533.2 eV), surface hydroxyl (531.4 eV), NiO lattice oxygen (529.6 eV) and alcohol group (531.7 eV) [265–267]. The C1s spectra were fitted using two components: carbon (284.8 eV) and alcohol group (286.7 eV) [266,267].

At the first stage of deconvolution the contribution of NiO was determined. Lattice oxygen peak of O1s spectra has the most noticeable and characteristic peak at low value of binding energy (529.6 eV), which is not overlapping with the other components and corresponds to NiO phase. On the basis of the intensity of this peak and the atomic ratio for nickel oxide (Ni:O=1:1), the intensity of the NiO component was adjusted and then followed by fitting of the other components (Ni^0, $Ni(OH)_2$) for Ni2p spectra. The inverse procedure was applied for fitting the hydroxyl contribution to the O1s spectra, recalculated from the previously fitted $Ni(OH)_2$ intensity and the atomic ratio Ni:O=1:2. It should be mentioned that the intensity of the Ni2p peak was

calculated from the $Ni2p_{3/2}$ value multiplied by 1.5. The O1s deconvolution correction was finalized by comparing the atomic ratios of C:O for alcohol group.

Nanostructured Ni_{ED}/XC-72 electrocatalysts

Surface state of Ni_{ED}/XC-72 electrocatalysts (deposited on GC cylinder) was also analyzed using XPS in an ultra-high vacuum chamber (residual gas pressure $<5 \cdot 10^{-6}$ Pa) equipped with a VSW Class WA hemispherical electron analyzer and a dual anode (Al and Mg Kα) X-ray source. The measurements and XP spectra characterization were performed by V. Papaefthimiou and V. A. Saveleva in the ICPEES (Strasbourg, France).

Survey and high resolution Ni2p, O1s, C1s spectra were recorded in constant pass energy mode (44 and 22 eV, respectively). The charge effect arising in the process of photoemission of electrons was taken into account by correcting the spectra with respect to C1s of the carbon line (284.8 eV). XP spectra were curve fitted after Shirley background subtraction, following the procedure described above for polycrystalline Ni foil. Spectra analysis and their deconvolution were performed using CasaXPS software.

Bimetallic NiCu/C and monometallic Ni/C electrocatalysts

Surface state of Ni/C and NiCu/C electrocatalysts was analyzed by XPS using a SPECS electron spectrometer equipped with a PHOIBOS-150 MCD-9 hemispherical energy analyzer and monochromatic Al Kα source (200 W) with no charge compensation. The measurements and XP spectra characterization were performed by R. I. Kvon in the BIC (Novosibirsk, Russia). Prior to the measurements, the spectrometer was calibrated against $Au4f_{7/2}$ (84.00 eV) and $Cu2p_{3/2}$ (932.67 eV) peaks. Catalyst powders (without additional grinding) were pressed tightly onto a double sided adhesive conducting tape (3MTM). Residual gas pressure during the spectra acquisition was lower than $5 \cdot 10^{-6}$ Pa. A self-consistent spectra deconvolution employing the same peak parameters for Ni^0, NiO and $Ni(OH)_2$ components was achieved for all processed samples. The values of binding energies and the areas of the peaks were determined after Shirley background subtraction. Spectral analysis and data processing were performed with XPS Peak 4.1 software package.

Bimetallic NiMo/C electrocatalyst

Surface state of NiMo/C electrocatalyst was analyzed by XPS using a Kratos Axis Ultra DLD XP spectrometer equipped with a monochromatic Al Kα (150 W) source with no charge compensation. The measurements and XP spectra characterization were performed by K. Artyushkova in the Center for Micro-Engineered Materials (CMEM UNM, Albuquerque, USA). Survey and Ni2p, Mo3d, C1s and O1s high-resolution spectra were acquired at pass energies of 80 eV and 20 eV, respectively. A linear background subtraction was used for quantification of C1s and O1s spectra, while a Shirley background was applied to Ni2p and Mo3d spectra. Sensitivity factors provided by the manufacturer were utilized. Ni2p spectrum was fitted using constrained line shapes for Ni metal, NiO and $Ni(OH)_2$ developed by Biesinger et al. [264] and peaks for $NiMoO_4$ reported in the literature [268,269]. Mo3d spectrum was fitted using reference positions for metallic Mo, various Mo oxides and $NiMoO_4$ reported in the literature [270,271]. Data analysis and quantification were performed using CasaXPS software.

2.2.4. X-Ray Diffraction (XRD)

Bimetallic NiCu/C and monometallic Ni/C electrocatalysts

XRD data for Ni/C and NiCu/C catalysts were recorded on a Bruker D8 New (Germany) diffractometer equipped with a multistrip LynxEye detector using Cu Kα radiation (λ = 0.15418 nm). The measurements were performed by T. Yu. Kardash in the Boreskov Institute of Catalysis (BIC, Novosibirsk, Russia). The data were collected in the 2θ range between 15 and 100° with a 0.05° step size and 2 s per step acquisition time. The phase composition was determined using Powder Diffraction File (PDF-2) ICDD and Inorganic Crystal Structure Database as well as Topas v. 4.3 (Bruker AXS, Karlsruhe, Germany) software. Average crystallite sizes were estimated from the coherent scattering region using Scherrer equation.

Bimetallic NiMo/C electrocatalyst

XRD pattern for NiMo/C catalyst was obtained using a Scintag PAD V diffractometer in Bragg-Brentano geometry with a Mo X-ray source ($\lambda_{K\alpha 1}$ = 0.7093

nm). The measurement was performed by A. Serov in the Center for Micro-Engineered Materials (CMEM UNM, Albuquerque, USA). The data were collected in the 2θ range between 3 and 60° with a 0.02° step size and 15 s per step acquisition time. Data were analyzed using MDI JADE software and the ICSD database. Average crystallite sizes were estimated from the coherent scattering region using Scherrer equation.

2.2.5. CO chemisorption measurements

CO chemisorption measurements were employed to estimate the dispersion of Ni particles in the Ni/C and NiCu/C electrocatalysts. The measurements were performed by P. A. Simonov in the Boreskov Institute of Catalysis (BIC, Novosibirsk, Russia). In order to ensure complete reduction of the metal surface the samples were calcined in H_2 flow at 250 °C immediately before the measurements. After that, the temperature was lowered to 20 °C and the sample was saturated with chemisorbed CO by introducing of 10% (vol.) CO + H_2 mixture in the gas flow in a short pulse. Dispersion of Ni (D_{Ni}), defining as a ratio of surface Ni atoms capable to chemisorb CO to the total number of metal atoms in the sample, was calculated from the amount of chemisorbed CO, assuming that one surface Ni atom binds one CO molecule [272]. The dispersion can be then recalculated to the surface area of Ni (S_{CO}, cm^2) following the equation: $S_{CO} = \frac{6 \cdot D_{Ni} m_{Ni}}{10.8 \cdot \rho_{Ni}}$. Dedicated experiments using pure Cu sample confirmed that Cu does not adsorb CO under the applied experimental conditions.

2.2.6. Inductively Coupled Plasma – Atomic Emission Spectrometry (ICP-AES)

Determination of the mass of Ni in the Ni_{ED}/XC-72 samples and estimation of the Faradaic efficiency of the electrodeposition were performed by ICP-AES technique for several samples using a Varian 720 spectrometer. The sample probe was obtained by dissolving the catalyst layer from the top surface of GC cylinder in 30% HNO_3 solution. For that the GC cylinder was immersed in glass jars containing 2 ml of 30% HNO_3 solution for 60 min at $T \approx 50$ °C. The mass of the jar was measured

before and after this procedure to avoid mistakes caused by evaporation of a part of the solution. The instrument was calibrated using standards (1000 $mg \cdot l^{-1}$, CPI).

2.3. Electrochemical techniques

2.3.1. Materials

For electrochemical experiments, all solutions were prepared using ultrapure water produced by either Milli-Q system or ELGA Ultra Analytic apparatus. 0.10 M NaOH electrolyte was prepared from either NaOH solution (50 wt.% in water, Premium quality, Aldrich), or NaOH pellets (99.99%, Aldrich). For cleaning of Teflon- and glassware H_2O_2 (35% in water, Acros Organics) and H_2SO_4 (95-98%, Aldrich) were used.

High-purity gases (Ar 99.998%, N_2 99.99%, H_2 99.99%) were used for the electrochemical measurements.

2.3.2. Setup for electrochemical measurements

Electrochemical experiments were carried out using either a Biologic SP-300 potentiostat or an Autolab PGSTAT 30 potentiostat equipped with an analog Scangen module to apply a linear potential ramp, and a rotating disk electrode Autolab Rotator. The temperature was controlled using laboratory thermostat/cryostat Julabo F25 (Julabo Labortechnik GMBH, Germany) within ± 0.1 °C accuracy.

Electrochemical measurements were performed in a standard three-electrode cell made either from Teflon or Pyrex glass (schematically shown on Fig. 2.1). The compartments of the reference and counter electrodes were connected with the working electrode chamber *via* a Luggin capillary and a glass (or Teflon) frit, respectively. Depending on the type of experiments, polycrystalline Ni rod, polycrystalline Ni foil or GC cylinder with catalyst thin layer on its top surface were employed as the working electrode. The counter electrode was a high surface area platinum. The type of the reference electrode – to which the applied potential was referred – was dependent on the type of experiments. In alkaline electrolyte either a Mercury-Mercury oxide electrode (Hg|HgO|0.10 M NaOH, IJ Cambria Scientific,

E = 0.928 V vs RHE at 25 °C) or Silver-Silver chloride electrode (Ag|AgCl|KCl(sat.), E = 0.954 V vs RHE at 25 °C) were utilized as the reference electrode, while electrodeposition of Ni from the solution of $NiSO_4$ was carried out using Mercury-Mercury sulfate ($Hg|Hg_2SO_4|K_2SO_4$(sat.), Schott, E = 0.960 V vs RHE at 25 °C) reference electrode. A salt bridge was introduced between the compartments of the working and the reference electrodes, while using Ag|AgCl|KCl(sat.) RE, to prevent eventual Cl^- contamination of the main compartment. If not otherwise stated, all electrode potentials in this work are referred to the RHE.

Prior to electrochemical measurements all Teflon- and glassware were filled by a solution containing H_2O_2(30 %) + H_2SO_4 (conc.) (1:1, vol.) for at least 12 h. and then multiply washed by ultrapure (Milli-Q or Elga) water.

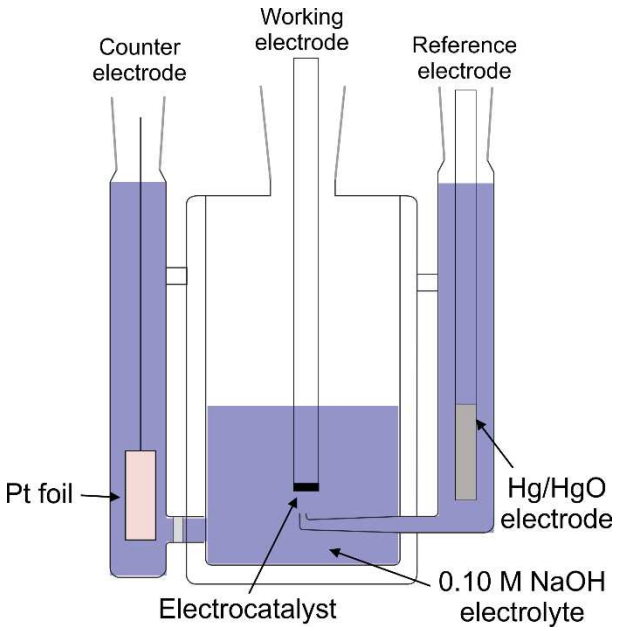

Fig. 2.1 *Schematic representation of three-electrode cell utilized in the work for performing of electrochemical measurements.*

The electrolyte resistance between the working and the reference electrode was determined by electrochemical impedance spectroscopy at constant potential around 0 V vs RHE in the frequency range from 100 kHz to 1 Hz using high-frequency component. The obtained values varied in the range between 10 and 35 Ω depending on the configuration of the cell and utilized sample holder. Considering the value of measured currents during electrochemical experiments, the Ohmic drop in most cases

was below 5 mV and therefore the iR-correction was not applied. However in the study of the Ni_{ED}/XC-72 electrocatalysts (see Section 4.3), the values of the measured currents were much larger compared to other experiments due to the much higher surface area of Ni. In that case the CVs were corrected by the Ohmic drop following the equation:

$$E = E_m - I_m \cdot R_u \qquad \text{(eq. 2.1.)}$$

where E_m and I_m correspond to the obtained experimental values of the current and the potential, while R_u is the resistance of the electrolyte between the working and the reference electrodes.

2.3.3. Electrode preparation

To perform electrochemical measurements either a Ni rod or a GC cylinder were fixed in a holder and their lateral surfaces were sealed with the Teflon tape so that only the flat top surface of the electrodes was accessible to the electrolyte. Ni foil, utilized for XPS measurements, was fully immersed in the electrolyte using thin Au wire as a current collector.

To study electrochemical properties of carbon supported catalysts (Ni/C, NiCu/C and NiMo/C) a thin film approach was utilized. First, the catalyst powder was ground with a pestle in a mortar to break down agglomerates and then a desired amount of the powder was mixed with isopropanol to get the suspension with the concentration of 1.0 mg ml^{-1}. Second, the suspension was sonicated in ultrasonic bath (Branson 1510 and Bandelin) for 30-60 min and just after that several aliquots (typically, 5 × 4 μl) of the suspension were pipetted on a clean surface of GC cylinder (the cleaning procedure is described in Section 2.1.2). The obtained on the GC surface catalyst layer was dried under gentle Ar or N_2 flow for 5-10 min between consecutive aliquots and for at least 60 min after final deposition.

2.3.4. Methodology of electrochemical measurements

2.3.4.1 Electrochemical pretreatment of the Ni electrodes

Polycrystalline Ni rod

To inspect an influence of the oxidation of Ni electrode surface on its electrochemical and electrocatalytic properties, the polycrystalline Ni rod was tested in 0.10 M NaOH electrolyte either immediately after polishing of its top surface (hereinafter, "non-activated Ni rod") or after a preliminary oxidation of it in air for ca. 48 h. (hereinafter, "Ch activated Ni rod"). In some cases, the surface of Ni rod was oxidized electrochemically (hereinafter, "EC activated Ni rod") by applying three potential cycles in N_2-saturated 0.10 M NaOH between -0.30 and 1.0 V at a sweep rate of 50 $mV \cdot s^{-1}$.

Before performing the main measurements, non-activated Ni rod was cycled in the potential region of [-0.20 – 0.30 V] at $v = 20$ $mV \cdot s^{-1}$ in order to remove oxide species formed on its surface during the transfer to the cell when the Ni rod was shortly exposed to the ambient. It should be noted that due to the tendency of Ni towards oxidation, each CV presented in Chapter 3 for the non-activated Ni rod (in both N_2 and H_2 atmosphere) was obtained in a separate experiment immediately after polishing of the electrode surface. Prior to the main electrochemical measurements, the surface of activated Ni rod was partially reduced by recording CVs in the potential range of [-0.06 – 0.40 V] at $v = 20$ $mV \cdot s^{-1}$ in order to obtain an active surface containing both metallic and an oxide sites (see Chapter 3).

Polycrystalline Ni foil for XPS measurements

Ni foil pretreated in two different ways was used to study the surface state of Ni by XPS. In the first case, the surface of a freshly polished Ni foil (see Section 2.1.1) was reduced in 0.10 M NaOH by applying cathodic polarization (E = -0.20 V) for 5 min, and then cycled once between -0.20 and 0.40 V and twice between -0.60 and 0.40 V at $v = 20$ $mV \cdot s^{-1}$ (hereinafter, "non-activated Ni foil"). In the second case, the surface of Ni foil was oxidized in air for ~48 h (producing a passive oxide film of ca. 2 nm thickness [110]) and then partially reduced by cycling several times between -

0.06 and 0.40 V at $v = 20$ mV·s^{-1} (hereinafter, "Ch activated Ni foil"). The final scan in both cases was stopped at 0 V on the anodic (i.e. going from negative to positive values) sweep of the CV. Immediately after that the electrodes were removed from the solution at open-circuit potential, rinsed with water and rapidly transferred to the XPS entry chamber as described in Section 2.2.3.

Nanostructured Ni_{ED}/GC and Ni_{ED}/XC-72 electrocatalysts

To study the influence of surface oxide species on electrochemical and electrocatalytic properties of nanostructured Ni_{ED}/GC and Ni_{ED}/XC-72, two states of their surfaces were considered. In the first case the experiments were performed immediately after the preparation of the sample and quick rinsing of the electrode by water (to remove the Ni salt left on the surface). Such electrodes in what follows are named "non-activated Ni_{ED}/GC and Ni_{ED}/XC-72". In the second case before conducting the measurements Ni_{ED}/GC and Ni_{ED}/XC-72 electrodes were rinsed by water, dried under N_2 flow and oxidized under the contact with air for ~24 h (this time was enough to reach similar to polycrystalline Ni degree of oxidation). These electrodes in what fallows are named "Ch activated Ni_{ED}/GC and Ni_{ED}/XC-72". After immersion of the electrodes in 0.10 M NaOH electrolyte they were conditioned by applying the same procedure as for non-activated and Ch activated Ni rod.

Supported Ni/C, NiCu/C and NiMo/C electrocatalysts

Prior to study of electrochemical and electrocatalytic properties of carbon supported Ni/C, NiCu/C and NiMo/C electrocatalysts in 0.10 M NaOH, their surface was reduced by cycling in inert atmosphere in the potential interval of [-0.30 – 0.40 V] for Ni/C and NiCu/C or [-0.20 – 0.40 V] for NiMo/C and at $v = 20$ mV·s^{-1} until a stable voltammetric response was attained.

2.3.4.2 Determination of electrochemical surface area of Ni

As discussed in the literature review (see Section 1.2.2), several methods have been proposed in the literature for determination of the electrochemically active surface area of Ni electrodes (S_{EC}). These include (i) analysis of the anodic and cathodic peaks in *the low-potential region*, which correspond to the formation and/or

reduction of α-$Ni(OH)_2$; (ii) utilization of C_{dl} values, estimated either by using electrochemical impedance spectroscopy or from CVs obtained at various sweep rates in the double layer potential interval; (iii) analysis of the anodic and cathodic peaks in *the high-potential region*, which correspond to the Ni(II)/Ni(III) oxidation-reduction processes.

We have chosen the first method, proposed in the work of Machado and Avaca [78], since it allows one, on the one hand, to avoid irreversible oxidation of the surface of Ni electrodes (which occurs in the case of the electrode cycling in *the high-potential region*) and, on the other hand, to use the same conversion coefficient (0.514 mC cm^{-2}) independently of the surface state of the electrodes (the value of C_{dl} can change after oxidation, as shown in Section 1.2.2). However this approach also has some limitations. In particular, a possible contribution of the charge related to the oxidation of a**d**sorbed/a**b**sorbed hydrogen in the measured anodic currents should be considered. Besides, the specific surface area of Ni could be underestimated due to an incomplete reduction of α-$Ni(OH)_2$ formed on the surface. These will be discussed in more detail in the Chapter 3.

The charge required to form a surface α-$Ni(OH)_2$ was estimated by integrating CVs acquired in the potential interval of [-0.06 – 0.40 V] ([-0.02 – 0.40 V] for Ni/C and NiCu/C) in 0.10 M NaOH solution, saturated by N_2 or Ar, at v = 20 mV·s^{-1} as shown in Fig. 2.2. The potential limits were selected on the basis of the analysis presented in the Section 3.2.1.

Based on the value of S_{EC}, the roughness factor of the surface of Ni electrodes could be determined as:

$$R_f = \frac{S_{EC}}{S_{geom}} \qquad \text{(eq. 2.2)}$$

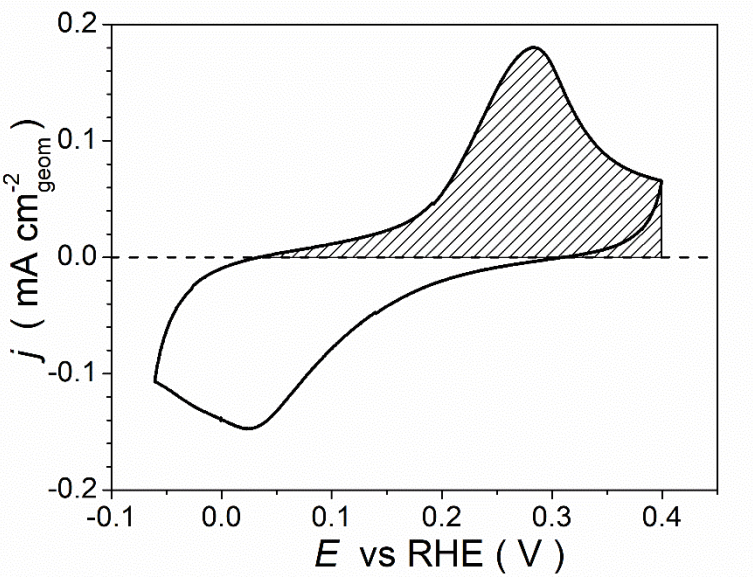

Fig. 2.2 *CVs obtained for non-activated Ni rod in N_2-saturated 0.10 M NaOH at $v = 20\ mV \cdot s^{-1}$ and T = 298 K. Patterned area was used for estimation of the surface area of the electrode.*

2.3.4.3 Determination of the electrocatalytic activity of Ni in the HOR/HER

Determination of the exchange current density

To compare the electrocatalytic activity of Ni electrodes in the HOR/HER, the values of the exchange currents were determined by analyzing the micropolarization region ($|\eta| \leq 10$ mV) of CVs (2nd scan) recorded in H_2-saturated electrolyte at a low sweep rate (5 or 2 $mV \cdot s^{-1}$), according to the eq. 1.17 (see Section 1.1.1). The use of potentiodynamic regime instead of potentiostatic measurements was motivated by the fact that it is better adapted for separation of the contributions of various surface processes, such as oxidation/reduction of hydrogen, formation of surface NiO_x, and formation of NiH_x. Typical potential interval of [-0.06 – 0.40 V] was used in most studies, except for the study of Ni/C and NiCu/C catalysts when the cathodic potential limit was extended up to -0.12 V. In the study of polycrystalline Ni rod at various temperatures, the cathodic potential limit was placed at -0.20 V in order to be able to analyze both the micropolarization region and the region of "high overpotentials". As a result, the exchange currents, the Tafel slopes and the apparent charge transfer coefficient α were determined by linearization of polarization curves plotted in Tafel

coordinates (eq. 1.19, see Section 1.1.1). The analysis was performed in the overpotential regions of $-0.20 < \eta < -0.07$ V and $0.06 < \eta < 0.12$ V for the HER and the HOR, respectively. From Fig. 2.3 one can see, that exchange current densities determined either using the Tafel equation or from the analysis of the micropolarization region are consistent with each other.

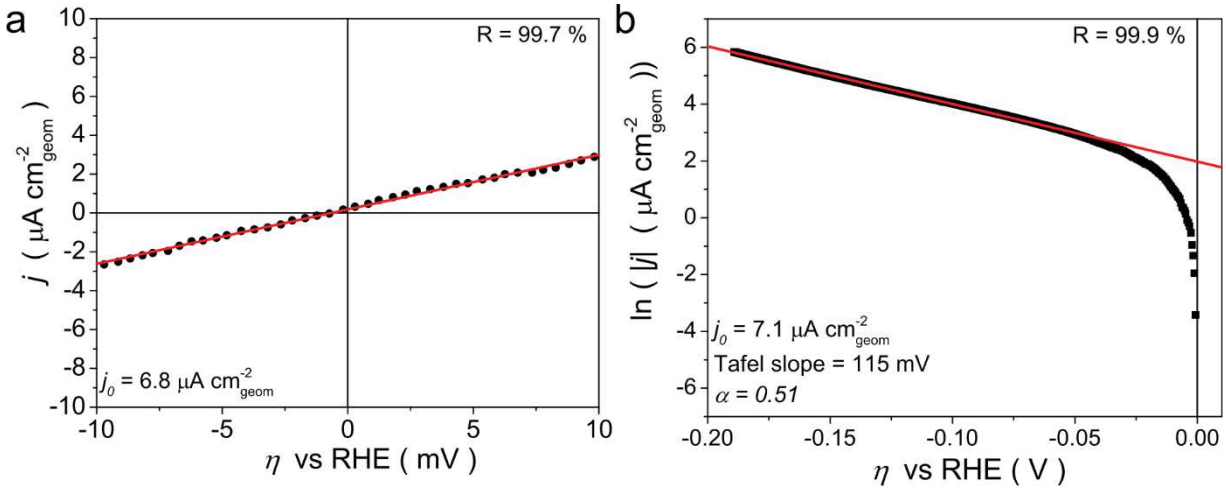

Fig. 2.3 *An example of analysis of (a) micropolarization region and (b) overpotential region of -0.20 < η < -0.07 V (where the Tafel equation is applicable) of CV obtained for non-activated Ni rod in H_2-saturated 0.10 M NaOH at v = 5 mV·s^{-1} at T = 298 K.*

Determination of the HOR kinetic current density – rotating disk electrode study

For a number of systems, where it was possible, the kinetics of the HOR was also investigated using the method of rotating disk electrode, the schematic cross view of which is shown in Fig. 2.4a [273,274]. Stirring of the electrolyte by rotation of the RDE accelerates the mass transport of reagents and products of a reaction, due to a decrease of the thickness of the diffusion layer (δ), defined as:

$$\delta = 1.61 \cdot D^{1/3} \nu^{1/6} \omega^{-1/2} \qquad \text{(eq. 2.3)}$$

where D is a diffusion coefficient, ν – kinematic viscosity of the electrolyte, ω – rotation rate.

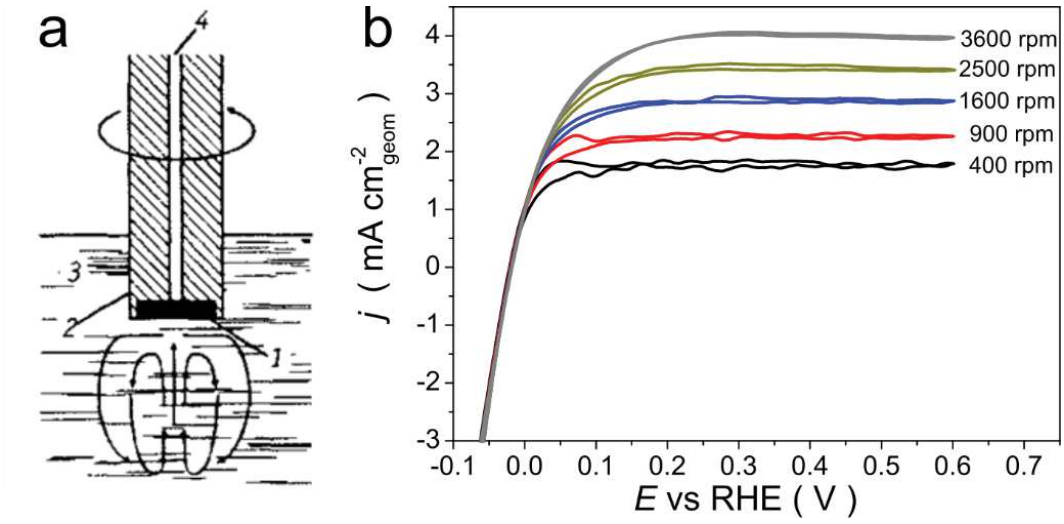

Fig. 2.4 *(a) Schematic cross view of a rotating disk electrode: 1 – working electrode; 2 – insulator; 3 – electrolyte; 4- current collector. Given from the Ref. [274]; (b) CVs obtained in H_2-saturated 0.10 M NaOH for Pt/C electrocatalyst at various rotation rates and v = 10 mV·s^{-1}.*

With an increase of overpotential and, as a consequence, acceleration of the charge transfer process, the reaction rate begins to be limited by the diffusion of reagents to the electrode surface. As a result, on CVs one can see stationary currents (Fig. 2.4b), which, according to Levich equation [273,274], can be written as follows:

$$I_D = 0.62 \cdot nD^{\frac{2}{3}}AFv^{-\frac{1}{6}}C_{H_2}\omega^{\frac{1}{2}} = B \cdot \omega^{\frac{1}{2}} \qquad \text{(eq. 2.4)}$$

where n is a number of involved electrons, A –geometric surface area of the electrode, F – Faraday constant, C_{H2} – the concentration of H_2 in saturated electrolyte and other parameters are the same as above. The corresponding parameters determined in 0.1 M NaOH at T = 298°K [275]: D_{H2} = 5.11·10^{-5} cm^2 s^{-1}, v = 0.010 cm^2 s^{-1}, C_{H2} = 7.8·10^{-7} mol cm^{-3}. Therefore, for Ni and GC rods used in the work (A = 0.196 cm^2, n = 2, F = 96485 C mol^{-1}) theoretical value of the curve slope B^{-1} equals to 11.16 mA^{-1} cm$^2_{disk}$ rpm.$^{0.5}$.

In the potential region, where both mass transport and charge transfer contribute to the rate of the reaction, the kinetic currents (I_k) can be calculated according to the Koutecky-Levich equation:

$$\frac{1}{I} = \frac{1}{I_k} + \frac{1}{I_D} = \frac{1}{I_k} + \frac{1}{B \cdot \omega^{0.5}} \qquad \text{(eq. 2.5)}$$

There are two main approaches to extract I_k. The first one is based on direct application of the eq. 2.5 at a given rotation rate provided that the value of I_D is known. The second method consists in plotting I^{-1} at selected potentials as a function of $\omega^{-1/2}$. According to the eq. 2.5, the obtained curve should be linear with a slope (B^{-1}) directly linked to the number of involved electrons, while the intercept gives the value of I_k^{-1}. The second approach was preferred in this work due to the fact that experimental values of the limiting diffusion currents may differ slightly from the theoretical one.

2.4. Kinetic modeling

Mean-field microkinetic modeling of the experimental current-potential curves obtained for several Ni electrodes (non-activated and activated Ni rod as well as NiMo/C electrocatalyst) was performed with the purpose to better understand the mechanism of the HOR/HER on the Ni surface as well as possible causes of the change of Ni activity in the HOR/HER. The modeling was carried out with a great help of Dr. A. Bonnefont from Institut de Chimie de Strasbourg (IC, Strasbourg, France).

The kinetics of the HOR/HER in an alkaline medium is described on the basis of the Tafel (eq. 2.6), the Heyrovsky (eq. 2.7) and the Volmer (eq. 2.8) steps incorporated into the mathematical model:

1) $H_2 + 2Ni \rightleftarrows 2\ Ni\text{-}H_{ad}$ (eq. 2.6)

2) $H_2 + OH^- + Ni \rightleftarrows Ni\text{-}H_{ad} + H_2O + e^-$ (eq. 2.7)

3) $Ni\text{-}H_{ad} + OH^- \rightleftarrows H_2O + e^- + Ni$ (eq. 2.8)

Here ‘Ni’ denotes a free nickel surface site.

In addition, in order to take into account the effect of nickel oxidation in the *low-potential region*, a two-step formation of surface $Ni\text{-}(OH)_{2,ad}$ was considered in the model (based on the Refs. [62,66,115]):

4) $OH^- + Ni \rightleftarrows Ni\text{-}OH_{ad} + e^-$ (eq. 2.9)

5) $Ni\text{-}OH_{ad} + OH^- \rightleftarrows Ni\text{-}(OH)_{2,ad} + e^-$ (eq. 2.10)

A Butler-Volmer dependence (eq. 1.16, see Section 1.1.1) on the electrode potential is assumed for the rate constants of charge transfer steps (eq. 2.7 – 2.10). Langmuir (the Frumkin interaction parameter γ = 0) or Frumkin (γ = 4) adsorption isotherms were used for the surface coverages of H_{ad}, OH_{ad} and $OH_{2,ad}$ on Ni or NiMo, respectively. This allowed us to obtain good agreement between the experimental and the simulated curves.

The rates of the reactions (1) – (5) in alkaline electrolyte can be expressed as:

$$v_1 = k_1^0 C_{H_2}(1 - \theta_H - \theta_{OH} - \theta_{(OH)_2})^2 - k_{-1}^0 {\theta_H}^2 \quad \text{(eq. 2.11)}$$

$$v_2 = k_2^0 \exp\left(\frac{(1-\alpha_2)FE}{RT}\right) C_{H_2} C_{OH^-}(1 - \theta_H - \theta_{OH} - \theta_{(OH)_2}) - k_{-2}^0 \exp\left(\frac{-\alpha_2 FE}{RT}\right) \theta_H \quad \text{(eq. 2.12)}$$

$$v_3 = k_3^0 \exp\left(\frac{(1-\alpha_3)FE}{RT}\right) C_{OH^-}\theta_H - k_{-3}^0 \exp\left(\frac{-\alpha_3 FE}{RT}\right)(1 - \theta_H - \theta_{OH} - \theta_{(OH)_2}) \quad \text{(eq. 2.13)}$$

$$v_4 = k_4^0 \exp\left(\frac{(1-\alpha_4)FE}{RT} - \frac{\gamma}{2}\theta_{OH}\right) C_{OH^-}\left(1 - \theta_H - \theta_{OH} - \theta_{(OH)_2}\right) - k_{-4}^0 \exp\left(\frac{-\alpha_4 FE}{RT} + \frac{\gamma}{2}\theta_{OH}\right)\theta_{OH} \quad \text{(eq. 2.13)}$$

$$v_5 = k_5^0 \exp\left(\frac{(1-\alpha_5)FE}{RT}\right) C_{OH^-}\theta_{OH} - k_{-5}^0 \exp\left(\frac{-\alpha_5 FE}{RT}\right)\theta_{(OH)_2} \quad \text{(eq. 2.14)}$$

Here C_{H2} and C_{OH^-} are the concentrations of H_2 and OH^- in the solution, which are assumed to be the same in the bulk of the electrolyte and near the electrode surface; θ_H, θ_{OH}, $\theta_{(OH)2}$ denote the surface coverage by the active intermediates Ni-H_{ad}, Ni-OH_{ad} and Ni-$(OH)_{2,ad}$, respectively; α_i is the charge transfer coefficient of the reaction 'i', while F, R, T are the Faraday constant, the ideal gas constant and the temperature, respectively.

When the potential E is scanned at a sweep rate v, the simulated current-potential curves can be obtained by solving the following set of differential equations:

$$\frac{d\theta_H}{dt} = 2v_1 + v_2 - v_3 \quad \text{(eq. 2.15)}$$

$$\frac{d\theta_{OH}}{dt} = v_4 - v_5 \quad \text{(eq. 2.16)}$$

$$\frac{d\theta_{(OH)_2}}{dt} = v_5 \quad \text{(eq. 2.17)}$$

$$\frac{dE}{dt} = v \quad \text{(eq. 2.18)}$$

The total Faradaic current density is due to the Heyrovsky and Volmer reactions and to the Ni hydroxide formation/reduction reactions:

$$j_F = \mathrm{F}S_t(\upsilon_2 + \upsilon_3 + \upsilon_4 + \upsilon_5) \quad \text{(eq. 2.19)}$$

Here S_t is the mole number of active Ni sites per electrode geometric surface area (in mol cm^{-2}).

As it has been discussed in the literature review, the H_{ad} adsorption free energy $\Delta_{ad}G^0_H$ is one of the key factors affecting the activity of the catalyst in the HOR/HER. As discussed by Bonnefont et al. [276], the rate constants of the Tafel, Heyrovsky and Volmer steps exponentially depend on the $\Delta_{ad}G^0_H$, if there is a linear relation between the value of $\Delta_{ad}G^0_H$ and the activation energies of the corresponding steps. An energy diagram for the non-activated Ni electrode is schematically shown in Fig. 2.5.

The value of $\Delta_{ad}G^0_H$ is directly related to the equilibrium potential of the Volmer step, and then to the ratio between the forward and backward rate constants of the Volmer step:

$$\Delta_{ad}G^0_H = RT \ln \frac{k^0_3 c_{OH^-}}{k^0_{-3}} \quad \text{(eq. 2.20)}$$

Furthermore, since the thermodynamic equilibrium potential of the H_2O/H_2 redox couple has to be kept at 0V vs. SHE, $\Delta_{ad}G^0_H$ is also related to the ratios between the forward and the backward rate constant of the Heyrovsky and Tafel steps by the expressions:

$$\Delta_{ad}G^0_H = RT \ln \frac{k^0_{-2}}{k^0_2 c_{OH^-} c_{H_2}} = \frac{1}{2} RT \ln \frac{k^0_{-1}}{k^0_1 c_{H_2}} \quad \text{(eq. 2.21)}$$

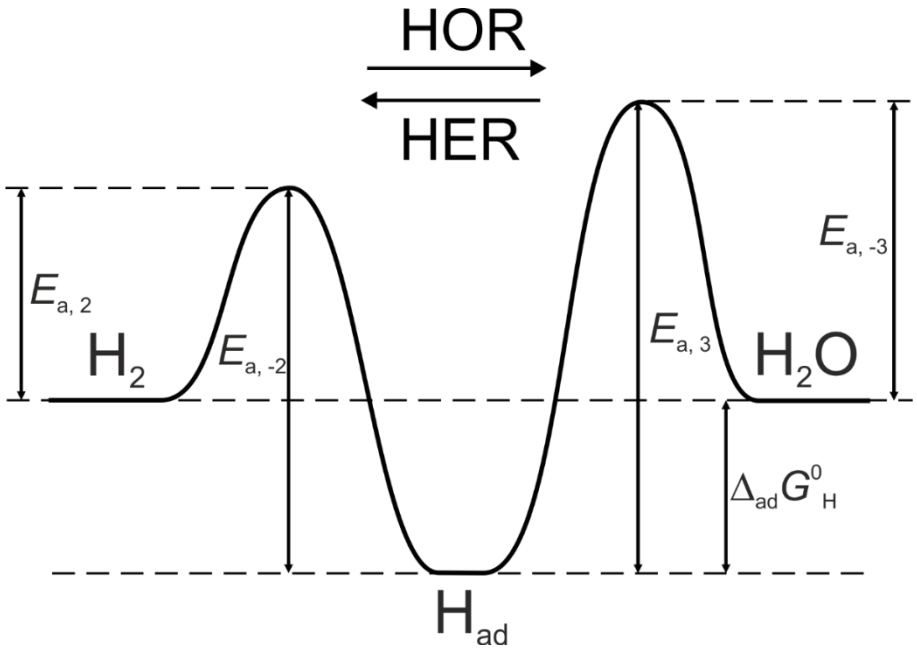

Fig. 2.5 *Schematic energy diagram for the HOR/HER on non-activated Ni electrode following the Heyrovsky-Volmer mechanism. $E_{a,i}$ correspond to the activation energies of the Heyrovsky and Volmer steps listed in the Table 3.4 (see Section 3.3.3).*

Chapter 3:
Polycrystalline Ni

3.1. Introduction

Analysis of the literature presented in Section 1.3 shows that Ni has been mainly studied in the potential region of the HER, whereas the interest to the HOR has appeared during the past decade, stimulated by the development of AMFCs. However, despite a considerable amount of works carried out since the beginning of the 20th century, some inconsistencies concerning the mechanism of the HOR/HER as well as the activity of Ni in this process still exist in the literature. This discrepancy is likely caused by the use of various procedures for pretreatment of the Ni electrode surface prior to the catalytic measurements, which results in different states of the electrode surface during investigation of the HOR/HER kinetics. It is known that the formation of Ni hydrides leads to a decrease of the activity of Ni in the HER. On the other hand, the effect of Ni surface oxidation on its electrocatalytic activity has not been studied in detail yet. However, the analysis of the literature suggests that significant discrepancy regarding the specific electrocatalytic activity of Ni in the HOR/HER is caused by uncontrolled formation of surface oxides and their effect on the kinetics of the HOR/HER.

In this chapter we have attempted to understand how the presence of stable Ni oxide species on the electrode surface affects the kinetics of the HOR/HER in alkaline media. For this, we used polycrystalline Ni rod, subjected to various surface treatments (see Section 2.3.4.1) in order to obtain two types of the surface: (i) preferentially metallic (hereinafter, “non-activated”), and (ii) partially oxidized (hereinafter, “Ch activated” or “EC activated” depending on the way of surface oxidation). As will be shown below, this terminology originates from the fact of significant enhancement of the activity of “Ch activated” and “EC activated” Ni samples in the HOR/HER compared to “non-activated” samples. Electrochemical and electrocatalytic measurements were carried out in the temperature range from 298 to 338 K on both types of Ni electrodes. In addition, the experimental study was complemented with kinetic modeling with the aim to better understand the kinetics of the HOR/HER depending on the surface state of Ni electrode. This allowed us to propose the mechanism of the HOR/HER, evaluate the contribution of individual

reaction steps (Heyrovsky, Volmer, Tafel) and put forward a hypothesis concerning the origin of the change of the activity of Ni in the HOR/HER in the presence of stable Ni oxide species on the surface of the electrode.

3.2. Surface properties of Ni electrodes

3.2.1. Establishing of potential limits for cycling of Ni electrodes in alkaline electrolyte

Fig. 3.1a shows the first CVs obtained for freshly polished Ni rod in N_2-purged 0.10 M NaOH just after immersion of the electrode in the electrolyte. As one may see, the cathodic peak (c_1) usually attributed to the reduction of α-$Ni(OH)_2$ [64,66,71,89] appears already on the first scan. This fact suggests formation of some amount of surface Ni oxide species during the transfer of the electrode to electrochemical cell, when it is shortly exposed to air, after polishing. Considering the value of an open-circuit potential (0.2 – 0.3 V), one may assume that formed surface oxides mostly consist of α-$Ni(OH)_2$. Meanwhile, cycling up to E = -0.2 V is sufficient for (almost) complete reduction of the electrode surface, as evidenced by the absence of any peaks on subsequently registered CV in the potential interval of [-0.2 – 0.2 V], i.e. when the anodic potential limit is placed before electrochemical oxidation of the surface of the Ni electrode (Fig. 3.1b). Further increase of the anodic potential limit leads to the appearance of an anodic (a_1) and cathodic (c_1) peaks, which, according to the literature [64,66,71,89], correspond to electrochemical formation and reduction of surface α-$Ni(OH)_2$, respectively. Note that setting the anodic potential limit close to the maximum of the peak a_1 leads to a splitting of cathodic peak c_1 into two components, which merge into one during potential cycling to $E \approx 0.4$ V (Fig. 3.1b). Since no cathodic peaks were detected in the CV registered in the potential interval of [-0.2 – 0.2 V], it is unlikely, that one of the two components of the peak c_1 originates from the reduction of Ni oxide species formed upon exposure of the electrode to air, as it was proposed by D'Alkaine and Santanna [75]. More plausible hypothesis was proposed by Jerkiewicz et al. [66], according to which two cathodic peaks are due to an existence of intermediate $NiOH_{ad}$ species before the formation of $Ni(OH)_2$. This

hypothesis will be used later in the development of the kinetic model. Nevertheless, it should be noted that *in situ* spectroscopic measurements are required for unambiguous assignment of the observed peaks.

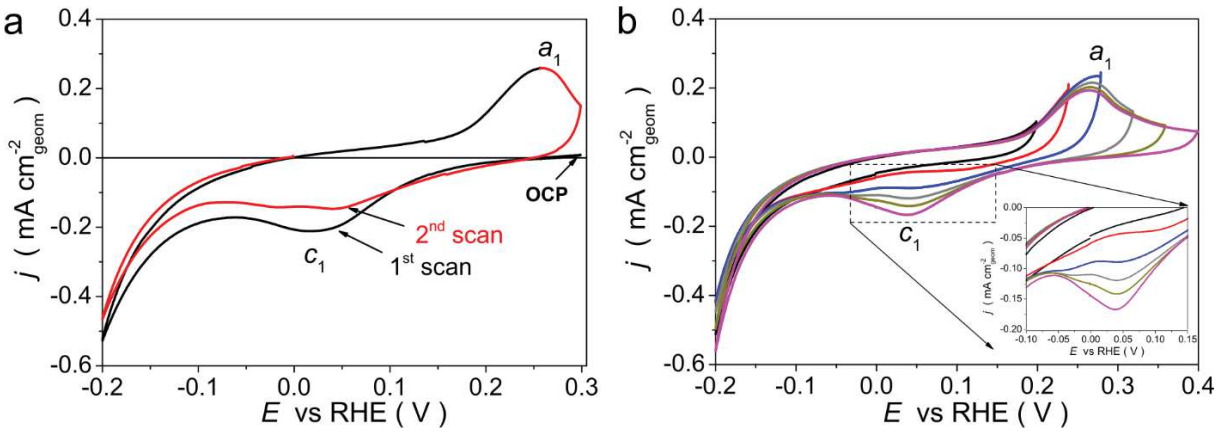

Fig. 3.1 *CVs obtained for non-activated Ni rod in N_2-saturated 0.10 M NaOH at v = 20 mV·s^{-1} (a) just after the polishing and (b) after reduction of air formed surface Ni oxide species. Inset on the panel (b) zoom in the potential interval of [-0.1 – 0.15 V].*

As noted in the literature review (see Section 1.2.1), an increase of the anodic potential limit to E > ~0.5 V leads to the formation of an electrochemically irreducible β-Ni(OH)$_2$ [64,66]. To avoid uncontrolled α to β-Ni(OH)$_2$ conversion and its influence on electrochemical properties of Ni, the anodic potential limit was set at 0.40 (at $v \leq 20$ mV·s^{-1}) or 0.50 V (at $v > 20$ mV·s^{-1}). To choose the cathodic potential limit (E_C), which is necessary for reducing the oxides formed at positive potentials, a series of CVs with varied cathodic limit (from -0.20 to -0.02 V) was obtained (Fig. 3.2a). For convenience, Fig. 3.2b shows the comparison of the absolute values of anodic (Q_A) and cathodic (Q_C) charges, determined at different cathodic limits of CV. The value of Q_C was calculated after subtraction of the anodic sweep at negative potentials, in order to minimize the contribution of the HER currents. One may notice that shifting the cathodic potential limit from -0.02 V to -0.20 V results in an increase of the absolute value of both the anodic and the cathodic charge, the latter growing to higher extent especially at E_C < -0.12 V. The difference between Q_A and Q_C observed in this case is likely caused by an increasing contribution of Ni hydrides, the formation of which is expected at E < -0.07 V [64], to the value of Q_C. At the same

time, increase of anodic currents at -0.20 < E_C < -0.12 V is believed to be due to the oxidation of hydrogen incorporated in the Ni metal [64]. Analysis of the obtained data suggests that setting the cathodic limit to -0.06 V is sufficient for the reduction of the Ni electrode surface after recording of an anode scan of the CV. Besides, this allows one to minimize possible contribution of Ni hydrides and, as a consequence, their effect on electrochemical and electrocatalytic properties of Ni electrodes.

On the basis of the above analysis, CVs were usually registered in the potential range of [-0.06 – 0.40 V] for the estimation of electrochemically active surface area of Ni electrodes as well as investigation of the kinetics of the hydrogen electrode reactions (mainly the HOR). For the study of the HOR/HER kinetics at elevated temperatures, this potential interval was extended up to [-0.2 – 0.4 V] in order to be able to analyze both the HER and the HOR, which was required for kinetic modeling.

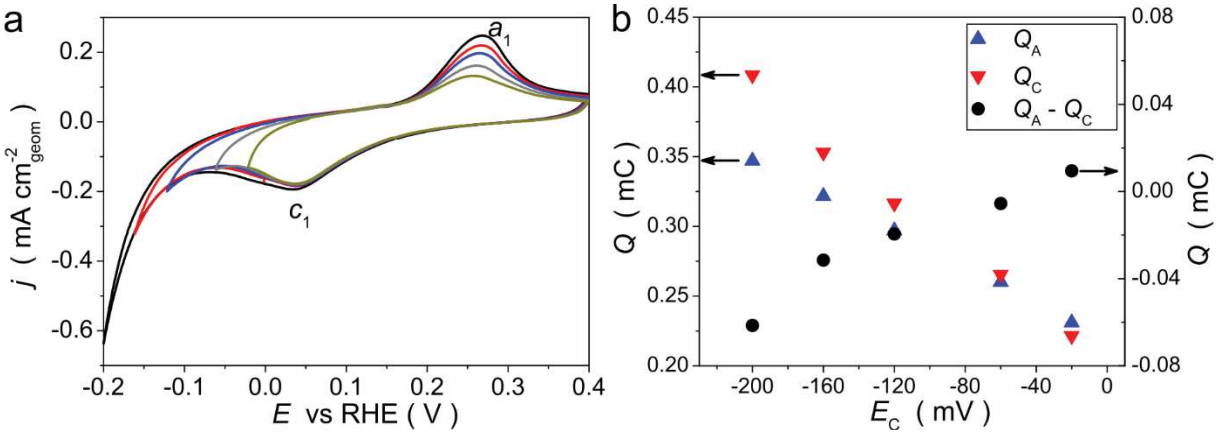

Fig. 3.2 *(a) CVs for non-activated Ni rod registered with various cathodic potential limits (EC = -0.20, -0.16, -0.12, -0.06, -0.02 V) in N_2-saturated 0.10 M NaOH at $v = 20\ mV \cdot s^{-1}$ and (b) corresponding to these curves absolute values of anodic (Q_A) and cathodic (Q_C) charges.*

3.2.2. Influence of surface Ni oxide species on the electrochemical behavior of Ni electrodes in alkaline media

As it has been discussed in the literature review (see Section 1.2.1), oxidation of Ni electrode surface results in changing the shape of CV and might be the reason for change of the HOR/HER activity as well as the mechanism of the reactions (see Sections 1.3.2). In order to further progress in understanding of this phenomenon, a part of experiments was carried out using a partially oxidized Ni electrode. Note that

the presence of metallic Ni sites on the electrode surface is an essential condition for the adsorption of H_{ad} atoms and the occurrence of the HOR/HER [181], while complete oxidation of the surface leads to deactivation of the Ni electrode, as will be shown later (see Section 3.3.1). Oxidation of the surface of Ni rod was performed in two ways: (i) under contact with oxygen from air for ~48 h. (Ch activated electrode), or (ii) by cycling to *the high-potential region* (EC activated electrode). After that, the electrode surface was partially reduced by conditioning in the potential interval of [-0.06 – 0.40 V]. Based on the literature data, such pretreatment is expected to result in the formation of three-layered structure Ni/NiO/$Ni(OH)_2$ on the surface of the electrode, with α-$Ni(OH)_2$ being on the top [89,110–113]. It was found that prolonged oxidation of Ni leads to, first, higher values of the open-circuit potential after immersion of the electrode in the electrolyte (between 0.4 and 0.55 V, i.e. ~0.2 V higher than in the case of freshly polished Ni rod) and, second, a change in the shape of CV, registered in the potential range of [-0.06 – 0.40 V] (Figs. 3.3a, b). Besides, the absence of a cathodic peak on the first scan of the CV indicates a difference in the nature of Ni oxide species initially present on the surface of non-activated and Ch activated Ni rod. Further cycling, however, leads to at least *partial* reduction of the surface of Ch activated electrode, which is accompanied by the growth of anodic and cathodic currents, appearance of the characteristic a_1 and c_1 peaks as well as an additional anodic peak a_2 in the potential range of [0 – 0.15 V] (Fig. 3.3b).

In order to be sure that the change of CV shape is caused by the *partial* oxidation of the Ni electrode surface and exclude a possible influence of some impurities, which might adsorb on the electrode surface during its storage under air, we then inspected the effect of electrochemical oxidation of the Ni rod. For that, freshly polished Ni rod (after removal of air formed Ni oxide species, as described in Section 3.2.1) was immersed in N_2-purged 0.1 M NaOH and then cycled three times in the potential region of [-0.30 – 1.0 V] at a sweep rate of 50 $mV \cdot s^{-1}$ (Fig. 3.3c). The final scan was stopped at 0 V during the anodic sweep of the CV. The positive potential limit for these CVs was chosen in such a way as to ensure oxidation of a part of the Ni surface with likely formation of NiO and β-$Ni(OH)_2$ (based on the literature data [64,66,99]), but avoiding full coverage of the electrode surface by electrochemically irreversible β-

$Ni(OH)_2$. On the CVs subsequently obtained in the typical potential interval [-0.06 – 0.40 V] (Figs. 3.3a, d) one can see two anodic (a_1, a_2) and one cathodic (c_1) peaks similarly to that observed for Ch activated Ni rod.

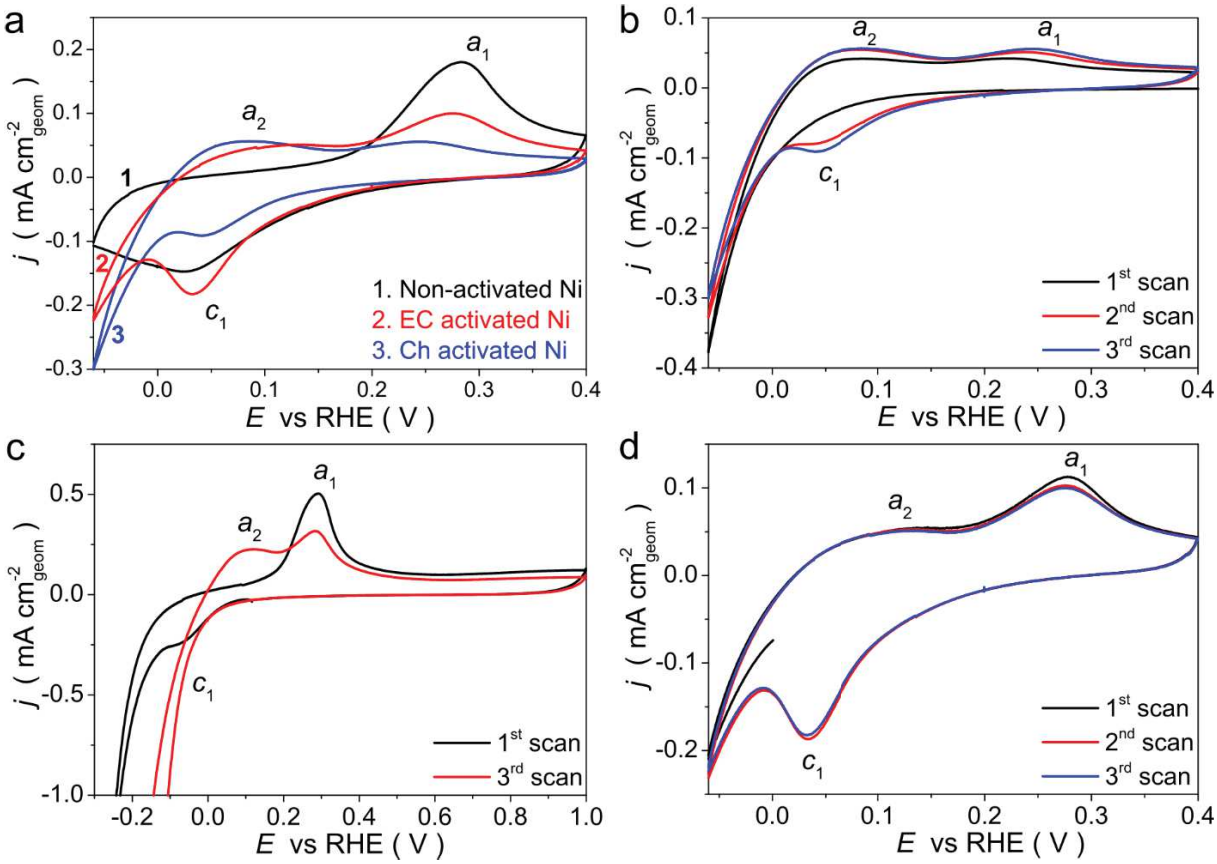

Fig. 3.3 *(a) Comparison of CVs obtained for non-activated (curve 1, black), EC activated (curve 2, red) and Ch activated (curve 3, blue) Ni rod in N_2-saturated 0.10 M NaOH for at $v = 20\ mV{\cdot}s^{-1}$; (c) CVs of Ni rod, obtained in the potential interval of [-0.30 – 1.00 V] at $v = 50\ mV{\cdot}s^{-1}$; Panels (b) and (d) shows evolution of the CVs, obtained in the potential interval of [-0.06 – 0.40 V] at v = 20 mV·s-1 for Ch activated and EC activated Ni rod, respectively.*

Finally, it was interesting to compare the values of S_{EC} of Ni calculated for the three types of electrodes (the method of determination is described in Section 2.3.4.2). The latter was found to decrease by a factor of ca. 1.2 and 1.5 for EC activated and Ch activated Ni rod, respectively, compared to non-activated Ni rod (Table 3.1, see Section 3.3.1). This confirms the assumption of blocking a part of the surface (~20 and ~33%, respectively) of the activated electrodes by stable (under experimental conditions) Ni oxide species.

3.2.3. Reversibility of Ni oxidation in the low-potential region

Influence of the sweep rate

As has been shown in the literature review (see Section 1.2.1), there is still no consensus regarding the nature of the processes, which occur in the potential region of the peaks a_1 and c_1. However, the main contribution in inert atmosphere is believed to be related to Ni/α-Ni(OH)$_2$ redox transition [64,66,78,89]. To inspect the reversibility of processes, contributing to peaks a_1 and c_1, a series of CVs was recorded for non-activated and Ch activated Ni rod at different potential sweep rates (Fig. 3.4). For clarity the curves in Fig. 3.4 are normalized by the sweep rate. One can see, that the maxima of the peaks a_1 and c_1, present in all CVs, shift toward more positive or more negative potentials, respectively, with an increase of the sweep rate. This behavior can be related to the slow (compared to the sweep rate) charge transfer [273,274]. The latter suggests that α-Ni(OH)$_2$ formation, even if chemically reversible, is an electrochemically irreversible surface process for both non-activated and activated surface state of Ni electrode. At the same time, the nature of the processes contributing to the peak a_2 (observed for activated electrodes) is more complicated and will be analyzed later after studying the behavior of the Ni electrodes in the presence of H$_2$ (see Section 3.3.1).

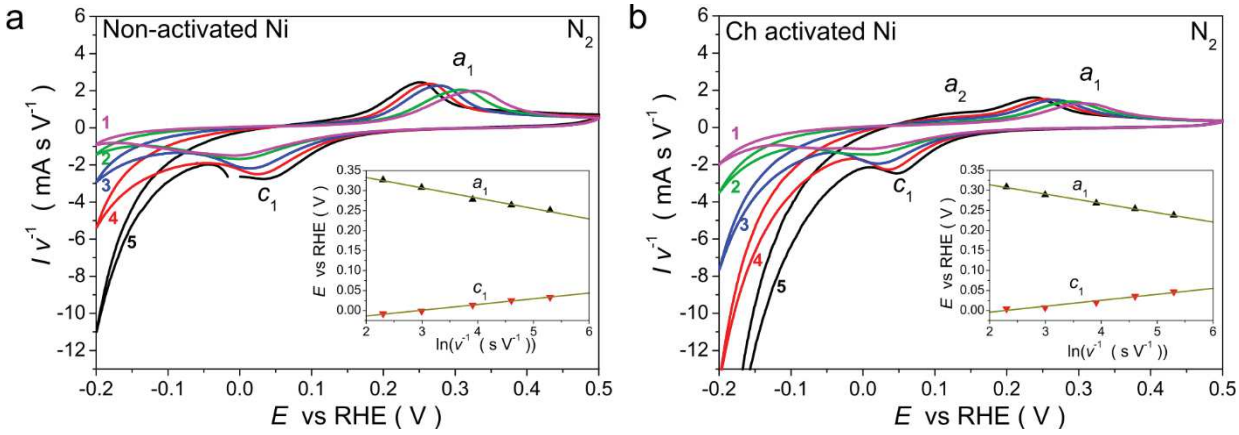

Fig. 3.4 *CVs obtained for non-activated (a) and Ch activated (b) Ni rod in N_2-saturated 0.10 M NaOH at various sweep rates v = 100 (curve 1, magenta), 50 (curve 2, green), 20 (curve 3, blue), 10 (curve 4, red), and 5 (curve 5, black) mV·s^{-1}. For convenience the currents were normalized by the sweep rates. Insets show the shift of peaks potential relative to the logarithm of the sweep rate.*

Influence of the temperature

In order to further advance in understanding of the processes occurring on the surface of a Ni electrode in the *low-potential region*, we inspected an influence of the temperature on the CV profile of both non-activated and EC activated Ni rod. If the anodic a_1 and the cathodic c_1 peaks correspond solely to the Ni/α-$Ni(OH)_2$ redox transition (as suggested in a number of publications [64,66,69–71]), then the peak positions are expected to shift toward more negative or more positive potentials, respectively, with an increase of the temperature (due to acceleration of the charge transfer reaction [273]). As can be seen from the Fig. 3.5, shifting of the maximum of the peak a_1 agrees with the expectation. At the same time, the maximum of the peak c_1 in the case of non-activated Ni rod remains almost unaffected by the temperature. Note that an increase of the temperature may lead to a deeper oxidation of the surface of the Ni rod during cycling. The latter may result in a shift of the cathodic peak c_1 toward more negative values [66,75,90] (i.e., in the opposite direction relative to the one expected with the temperature). To analyze a possible effect of this phenomenon a series of CVs was obtained at T = 298 K in such a way as to reproduce the difference between the anodic potential limit and the maximum of the peak a_1 observed in CVs obtained at various temperatures (Fig. 3.6). Inset in Fig. 3.5a shows that accounting of this factor allows one to observe a slight shift of the peak c_1 in the expected direction with the temperature. However, the magnitude of the shift is still significantly different from that observed for the peak a_1. Besides, it is interesting to note that in the case of EC activated Ni rod (see Fig. 3.5b), the peak a_1 shifts up with temperature to a larger extent compared to non-activated electrode.

Considering the above analysis and the value of the standard potential for the reaction $Ni(OH)_2 + 2e^- \rightleftarrows Ni + 2OH^-$ (~0.07 V vs RHE in 0.10 M NaOH [275]), it is reasonable to assume that there could be some other processes except of Ni/α-$Ni(OH)_2$ redox transition, which influence the position of the anodic peak a_1. More detailed analysis of this question will be presented in Section 3.3.3 with the help of kinetic modeling.

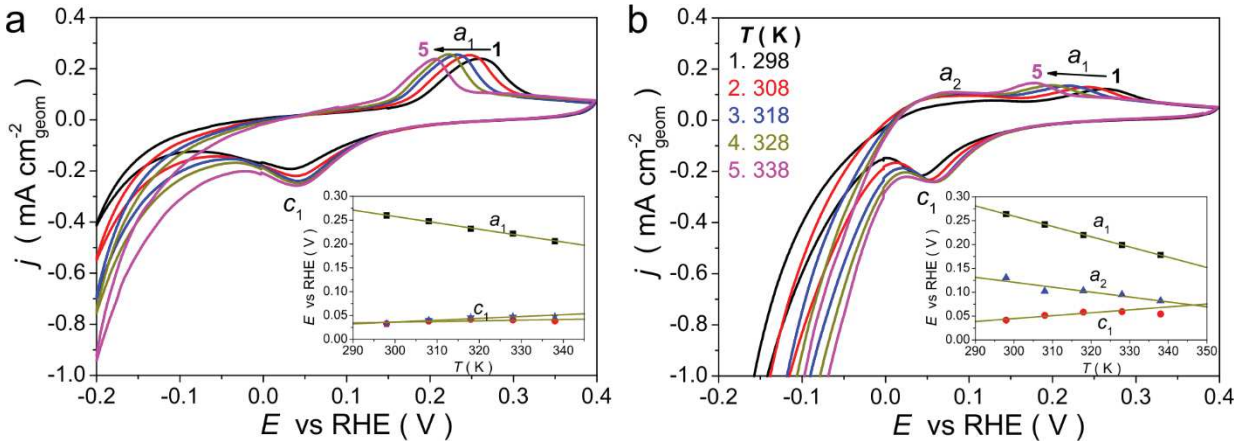

Fig. 3.5 *CVs for (a) non-activated and (b) EC activated Ni rod obtained in N_2-saturated 0.10 M NaOH at v = 20 mV·s^{-1} and various temperatures. Insets represent the shift of the potential of maximum of anodic (a_1 – black squares, a_2 – blue triangles) and cathodic (c_1 – red circles or blue stars (before and after correction, respectively, see the text for details)) peaks with temperature.*

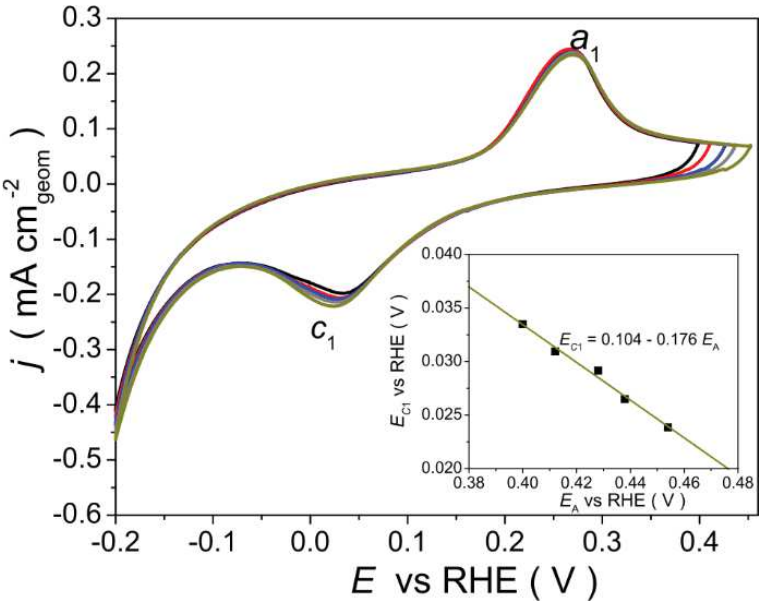

Fig. 3.6 *CVs for non-activated Ni rod obtained in N_2-saturated 0.10 M NaOH at v = 20 mV·s^{-1} and various positive potential limits (E_A). Inset shows the shift of the potential of cathodic peak c_1 with increase of the E_A.*

3.2.4. Investigation of the Ni electrode surface by physicochemical techniques

X-ray photoelectron spectroscopy (XPS)

In order to unveil the differences in the surface state of Ni samples, non-activated and Ch activated Ni foil (pre-treatment procedure is clarified in the Section 2.3.4.1) were characterized by XPS. Owing to the fact that we could only make *ex situ* analysis, the presence of surface oxides was expected, even if special care (protection of the electrode surface by a drop of water) was taken to minimize the contact of the electrode with air during its rapid (< 5 min) transferring to the XPS entry chamber. Therefore the purpose of the measurements was to check whether the oxide coverage and the type of detected oxide species change after subjecting the electrode to different pretreatment protocols.

Fig. 3.7 shows Ni2p XP spectra obtained for two types of Ni foil at different take-off angles. The deconvolution of the spectra into individual components (Ni^0, NiO and $Ni(OH)_2$) was done under the assumption that (according to the literature data [64,89,110,263]) oxidation of Ni in contact with oxygen and/or alkaline electrolyte mainly results in the formation of NiO and $Ni(OH)_2$. The curve-fitting procedure is described in Section 2.2.3.

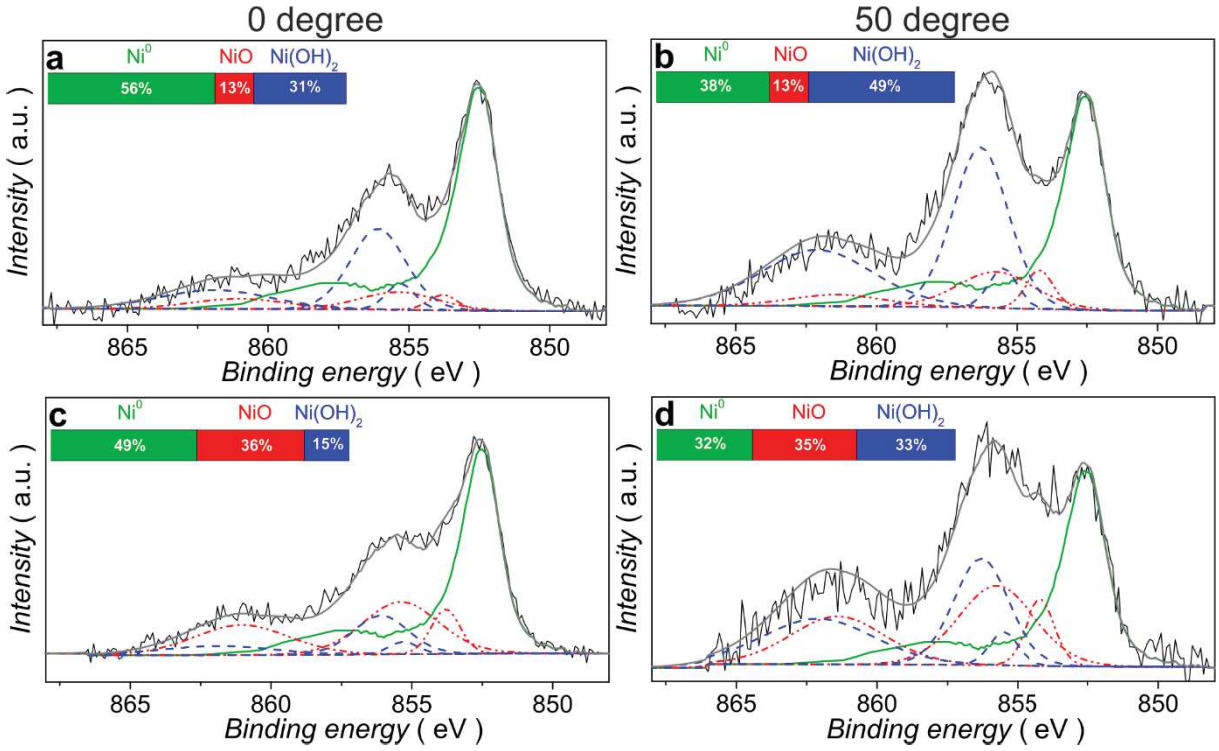

Fig. 3.7 *X-Ray photoelectron Ni $2p_{3/2}$ spectra for non-activated (a, b) and Ch activated (c, d) Ni foil at two take-off angles: (a, c) 0 and (b, d) 50 degrees. Spectra were curve-fitted with Ni^0 (solid line, green), NiO (dash-dotted line, red) and $Ni(OH)_2$ (dashed line, blue) components, their resulting atomic concentrations are indicated in the panels.*

According to the *ex situ* XPS characterization, surfaces of both samples contain Ni oxide and hydroxide species. While for the non-activated sample the surface is dominated by $Ni(OH)_2$, for the Ch activated one NiO prevails (see Figs. 3.7a, c). Therefore we assume that activation of the Ni surface under its contact with air results in the formation of surface NiO. Conditioning of the activated electrode in the potential interval of [-0.06 – 0.40 V] leads to only a *partial* reduction of the NiO layer. The existence of some amount of NiO on non-activated Ni foil is believed to be due to its incomplete removal during sample polishing and subsequent electrochemical treatment of the electrode (Fig. 3.8). Besides, one cannot exclude a possible formation of a small amount of NiO during the sample transfer to the XPS entry chamber through air. Meanwhile, the presence of $Ni(OH)_2$ on the electrode surfaces can be explained by its formation during the emersion of the electrode from 0.10 M NaOH at open-circuit potential (0.1 – 0.25 V) and its further transferring through air with a drop

of water. Taking into account the results of the experiments presented in Section 3.2.1 as well as the literature data [64–66,70,77], we tentatively attribute Ni hydroxide, observed on the Ni2p XP spectra, to the chemically reversible α-$Ni(OH)_2$. Considering the fact that α-$Ni(OH)_2$ is electrochemically reduced close to the equilibrium potential of the hydrogen electrode (Fig. 3.1), it is reasonable to assume that *in situ* the surface of non-activated electrode predominantly consists of metallic Ni^0.

Fig. 3.7 shows that the contributions of individual components to the XP spectra depend on the take-off angle (two take-off angles were utilized: 0 (sub-surface sensitive angle) and 50 degrees (surface sensitive angle)) in agreement with the Ni oxidation model described in the literature [89,110]. According to this model, a three-layer structure $Ni/NiO/Ni(OH)_2$ is formed with metallic Ni^0 located in the bulk of the sample, $Ni(OH)_2$ – in the upper layer and NiO – between them.

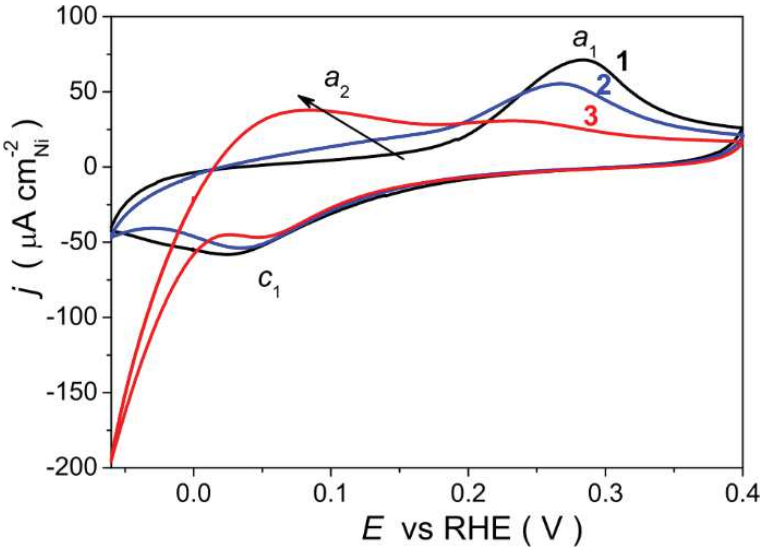

Fig. 3.8 *Comparison of CVs obtained for non-activated Ni rod (curve 1, black), non-activated Ni foil (curve 2, blue) and Ch activated Ni foil (curve 3, red) in N_2-saturated 0.10 M NaOH at v = 20 mV·s^{-1} and T = 298 K. The last two electrodes were utilized for the XPS measurements.*

It should be stressed that since the XPS analysis was performed *ex situ*, it allows only some tentative conclusions regarding the state of the Ni surface in electrolyte under the potential control.

X-ray photoelectron spectroscopy (in situ)

In order to reach unambiguous conclusions regarding the state of the Ni surface in electrolyte under the potential control, we have also tried to perform *in operando* measurements by the method of near ambient pressure XPS. For that a special facility mounted on SOLEIL (France) and BESSY II (Germany) synchrotron work stations was used. The measurements were carried out at pressures from 3 to 6 mbar. Membrane electrode assemblies were fabricated using alkaline polymer membrane Tokuyama A201 by the procedures described, for example, in [277,278]. Several types of Ni electrodes were tested. These include Ni film (obtained by vacuum deposition on the membrane), NiCu/C, NiMo/C and Ni_{ED}/C nanoparticles immobilized on the surface of the membrane in a mixture with anion-exchange ionomer in the form of a thin layer. Unfortunately, Ni oxide species, which are present on the surface of Ni electrodes taken from air, were found to be very stable preventing us from reduction of the electrode surface by applying any electrochemical treatment in the pressure interval of 3 – 6 mbar, even when the measurements were performed in gas/liquid cell (the cell device is described in [278]). Therefore the performed experiments did not allow us to obtain any reliable data regarding the surface state of the Ni electrode depending on the applied potential.

Surface-enhanced Raman spectroscopy (in situ)

Another technique for *in operando* study of the surface state is based on the use of surface-enhanced Raman spectroscopy (SERS) in liquid electrolyte simultaneously with electrochemical measurements in such a way as described in detail, for example, in the Refs. [99,279]. These experiments were done during one-week internship at the University of Leiden (The Netherland) under the guidance of Dr. Oscar Diaz-Morales and Prof. Marc T. M. Koper. Ni nanoparticles electrodeposited on Au substrate (Ni_{ED}/Au, the preparation procedure is similar to that described in Section 2.1.2 for Ni_{ED}/GC) were used as the working electrode. Comparison of the SER spectra of the Ni_{ED}/Au electrode, primarily held in air for 2 hours (i. e. chemically activated) and then immersed in the alkaline electrolyte at an open-circuit potential (~0.7 V vs RHE), confirms the formation of surface NiO in air (Fig. 3.9a) in agreement with the

literature data [99]. At higher potentials, the formation of β-$Ni(OH)_2$ (an appearance of the oscillations at a frequency of 450 cm^{-1} at $E = 0.9$ and 1.1 V) and NiOOH (an appearance of the oscillations at a frequency of 560 cm^{-1} at $E = 1.55$ V) can be observed as well. However, these characteristic oscillations disappear, when the potential is shifted to the region of [-0.06 – 0.40 V] (Figs. 3.9b, c). Similar obstacle also appeared when the electrode was studied immediately after immersing in the electrolyte, avoiding application of high anodic potentials. This observation is probably due to the fact that in *the low-potential region* the oxide film becomes very thin and, likely, disordered, which lead to a decrease in the intensity of the oscillations in the wavelength region from 400 to 700 cm^{-1} to the background level. Despite the fact that essential differences in the SER spectra of non-activated and Ch activated Ni_{ED}/Au electrodes were observed in the wavelength region of 1300 – 1700 cm^{-1} (Figs. 3.9b, c), the absence of any peaks in the interval between 400 and 600 cm^{-1} precludes us from unambiguous conclusions about the surface state of activated and non-activated Ni_{ED}/Au electrodes in the potential region of [-0.06 – 0.40 V].

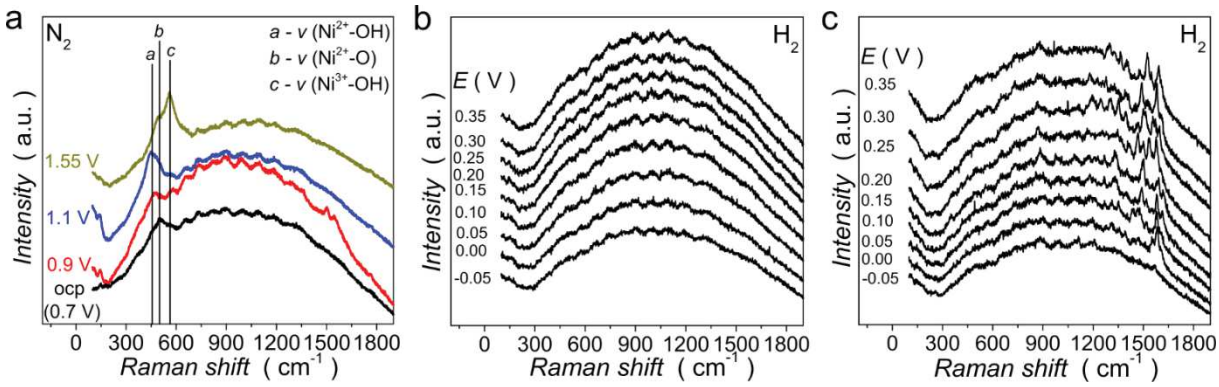

Fig. 3.9 *SER spectra recorded for Ch activated (a, c) and non-activated (b) Ni_{ED}/Au particles in (a) N_2- or (b, c) H_2-saturated 0.10 M NaOH. The electrochemical measurements were performed potentiostatically.*

3.3. Kinetics of the HOR/HER on Ni electrodes

3.3.1. Influence of the electrode pretreatment on the kinetics of the HOR/HER

Influence of Ni surface oxide species on the electrochemical behavior of Ni electrode in H_2 atmosphere

Fig. 3.10 compares CVs for a non-activated and Ch activated Ni rod registered in N_2- and H_2-saturated 0.10 M NaOH at $v = 20$ mV·s^{-1}. Characteristic anodic (a_1 and a_2) and cathodic (c_1) peaks observed under N_2 atmosphere may be also noticed in H_2 atmosphere (although the positions of these peaks are not exactly the same as under N_2). An increase of anodic currents in H_2 compared to N_2 atmosphere the occurrence of the HOR. This difference in currents is larger in the case of Ch activated electrode. Besides, it becomes more pronounced at lower sweep rates (comparison of Figs. 3.4 and 3.11). Moreover, the relative contribution of the a_2 peak was found to increase with a decrease of the sweep rate (Fig. 3.11b). Experiments performed at different rotation rates in the presence or absence of H_2 (Fig. 3.12) suggest that the HOR on polycrystalline Ni rod is kinetically rather than mass-transport (diffusion of H_2 to the electrode surface) controlled. It should be noticed, however, that increase of a number of active sites on the electrode surface (see Chapter 4, Section 4.3.4) allowed us to observe the rotation rate dependence for Ni_{ED}/C samples.

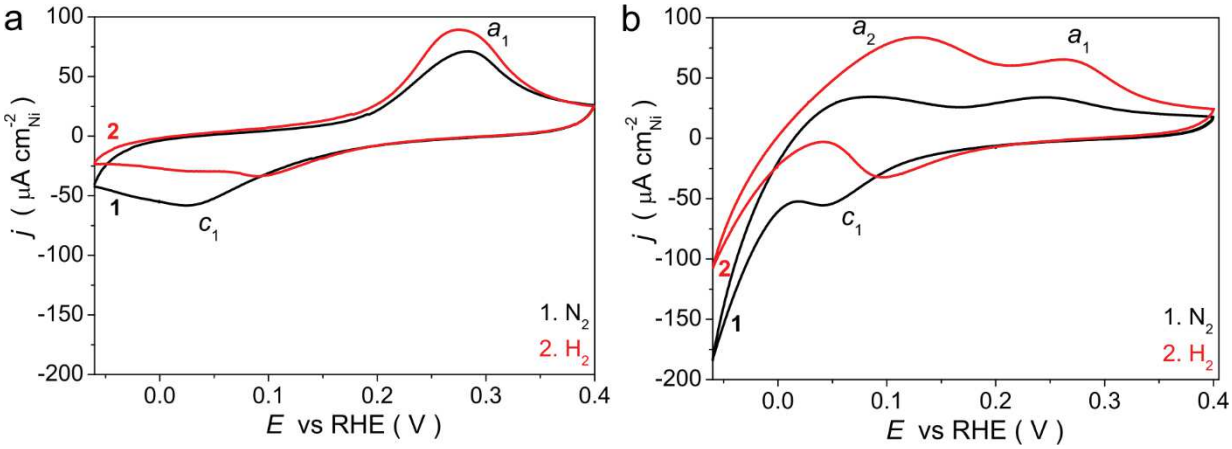

Fig. 3.10 *CVs for non-activated (curve 1, black) and Ch activated (curve 2, red) Ni rod obtained in (a) N_2- and (b) H_2-saturated 0.10 M NaOH at $v = 20$ mV·s^{-1}.*

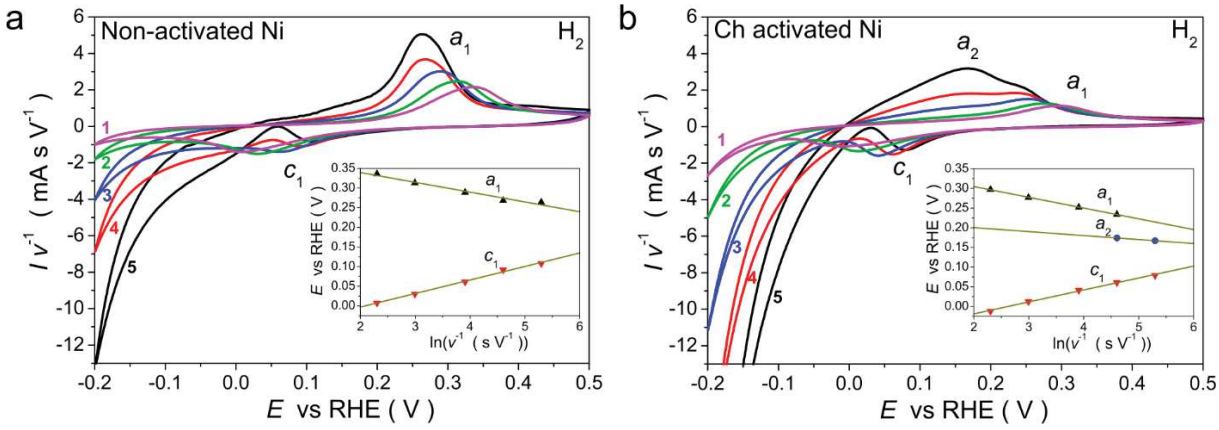

Fig. 3.11 *CVs for (a) non-activated and (b) Ch activated Ni rod obtained in H_2-saturated 0.10 M NaOH at various sweep rates v = 100 (curve 1, magenta), 50 (curve 2, green), 20 (curve 3, blue), 10 (curve 4, red), and 5 (curve 5, black) mV·s^{-1}. Insets shows the shift of the potential of the maximum of peaks a_1 and c_1 relative to the logarithm of the sweep rate.*

As noted in Section 1.2.1, various explanations have been proposed in the literature for the appearance of the peak a_2 in CVs in an inert atmosphere. Comparison of the experimental and literature data indicates that anodic currents under the peak a_2 observed in this work are likely due to the formation of Ni-OH_{ad} and/or oxidation of a**d**sorbed hydrogen [62,115–118]. Additional support for this will be presented later in the discussion of the results of kinetic modeling (see Section 3.3.3). Meanwhile, rotation rate independence of the currents in CVs obtained in an inert atmosphere (Fig. 3.12a) allows us to conclude that the peak a_2 cannot be associated with the oxidation of molecular hydrogen evolved during the electrode cycling at negative potentials. Besides, oxidation of a**b**sorbed hydrogen and/or Ni hydrides, which could be formed at potentials below ca. -0.07 V [78,84], also seems to be an unlikely reason for the appearance of the peak a_2 in CVs obtained in the potential interval of [–0.06 – 0.40 V] at relatively fast sweep rates v (20 mV·s^{-1}) (Figs. 3.3 and 3.10).

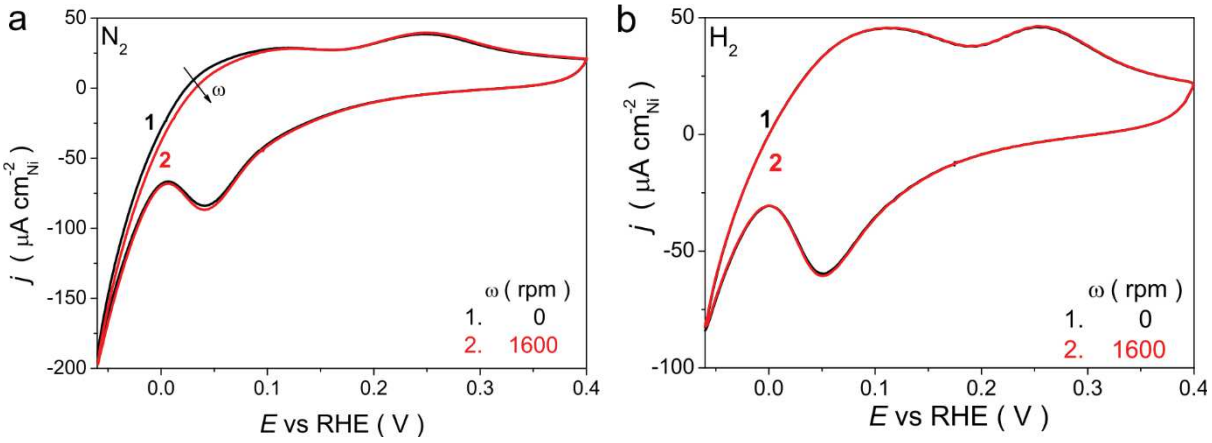

Fig. 3.12 *CVs for Ch activated Ni rod obtained in (a) N_2- and (b) H_2-saturated 0.10 M NaOH at the electrode rotation rate of 0 (curve 1, black) and 1600 (curve 2, red) rpm and $v = 20\ mV \cdot s^{-1}$.*

Electrocatalytic activity of Ni electrodes in the HOR/HER

Electrocatalytic activity of Ni electrodes in the HOR/HER was compared in terms of exchange current densities derived from the analysis of micropolarization region of CVs in H_2 atmosphere measured at a slow sweep rate. Only the anodic scan of the CV was used for the analysis because the HOR/HER in the cathodic scan is accompanied by the reduction of surface Ni oxide species, formed at positive potentials (Fig. 3.13a). The sweep rate of 5 $mV \cdot s^{-1}$ was used for the measurements, despite the fact that at lower values of v the hysteresis between the anodic and cathodic curves decreases (Fig. 3.13). Such a choice of the sweep rate was dictated by the necessity to reduce the time during which the electrode is subjected to either positive (might produce β-$Ni(OH)_2$) or negative (might produce Ni hydrides) potential limits. This allowed us to minimize uncontrolled influence of β-$Ni(OH)_2$ and/or NiH_x on the kinetics of the HOR/HER. Moreover, essentially similar (differed within 5%) HOR/HER activities could be calculated from the CVs registered at either 2 or 5 $mV \cdot s^{-1}$.

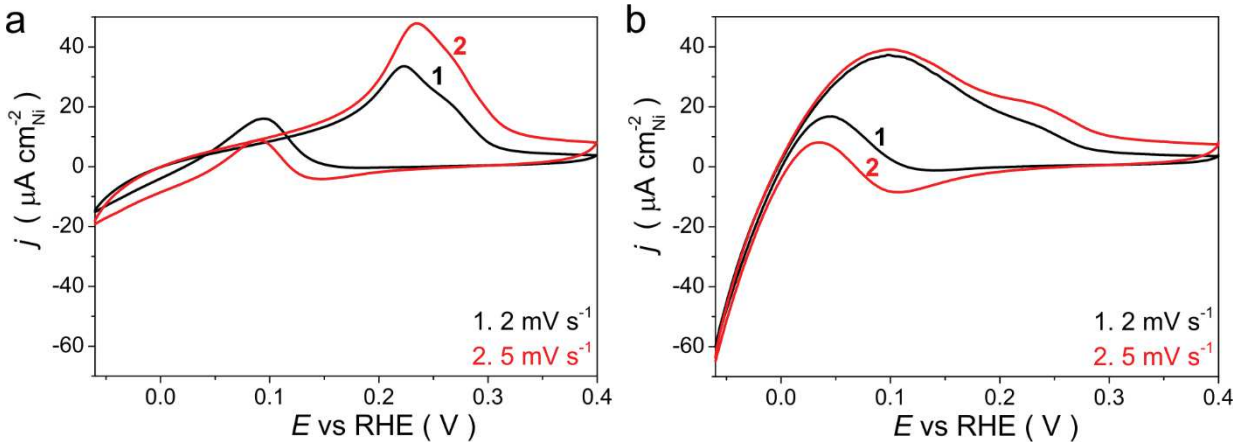

Fig. 3.13 *CVs for (a) non-activated and (b) Ch activated Ni rod obtained in H_2-saturated 0.10 M NaOH at v = 2 (curve 1, black) or 5 (curve 2, red) mV·s^{-1}.*

For the comparison of electrocatalytic activities of Ni electrodes in the HOR/HER the exchange currents were normalized to either electrochemical (μA·cm$^{-2}_{Ni}$) or geometric (μA·cm$^{-2}_{geom}$) surface area of polycrystalline Ni rod, as described in Section 2.3.4.3 (Table 3.1).

Fig. 3.14 shows typical CVs obtained in H_2 atmosphere for the Ni rod, whose surface was subjected to different pre-treatments. One can see that the HOR on non-activated Ni starts at relatively high anodic overpotentials (E > 0.15 V), which is due to the low activity of metallic Ni in the HOR/HER (2.3 ± 0.1 μA cm$^{-2}_{Ni}$). At the same time, on the activated Ni the HOR begins already at the thermodynamic equilibrium potential of the hydrogen electrode, reaching maximum current densities at 0.10 < E < 0.15 V. Analysis of the data in the Table 3.1 shows that the specific activity of Ch activated and EC activated Ni electrode is almost 9 and 7 times larger, respectively, than for non-activated Ni electrode. It should be stressed that the observed enhancement is not an artifact arising from the normalization to a smaller surface. Indeed, normalization of the activity to the geometric surface area of the Ni rod also shows more than 5 times enhancement for *partially* oxidized Ni electrode. Some differences in the activity values for Ch and EC activated Ni electrode are likely caused by the differences in their surface state.

Note, that only part of the surface of activated Ni electrodes is covered by oxide species (see Section 3.2.1), while full oxidation of their surface (achieved, for example, by cycling up to E = 1.6 V) results in blocking of the active Ni metal sites

necessary for the hydrogen adsorption [181] and, as a result, suppression of Ni activity in the anodic oxidation of hydrogen (Fig. 3.14b).

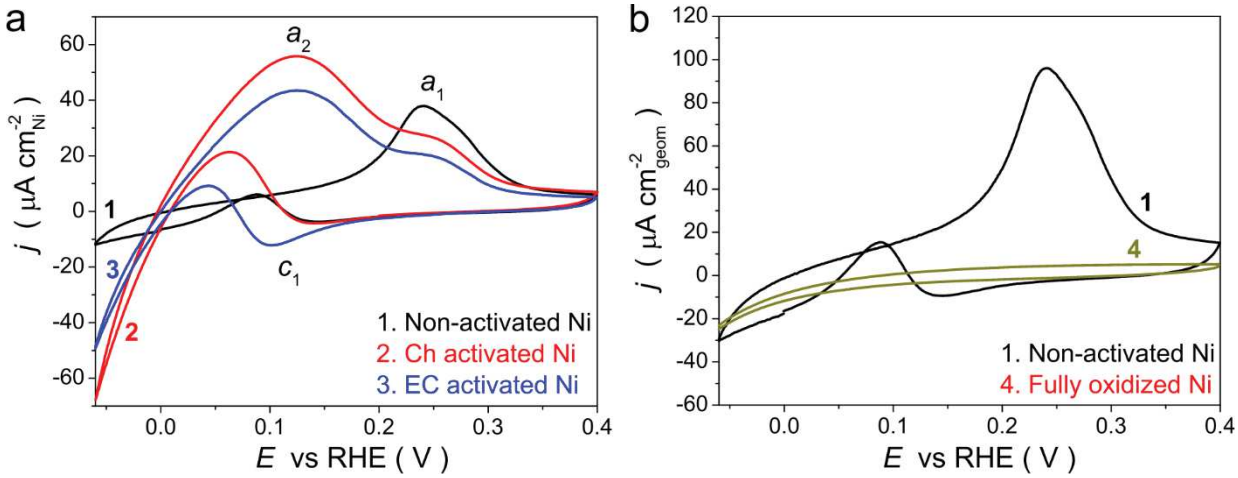

Fig. 3.14 *CVs for non-activated (curve 1, black), Ch activated (curve 2, red) and EC activated (curve 3, blue) Ni rod obtained in H_2-saturated 0.10 M NaOH at $v = 5$ mV·s^{-1}. CV for fully oxidized Ni rod (curve 4, dark yellow) is presented on the panel (b) for comparison. The currents are normalized by either (a) S_{EC} or (b) S_{geom}.*

Table 3.1 *The values of the exchange current densities in the HOR/HER obtained for polycrystalline Ni rod after various pre-treatments of its surface*

Catalyst	S_{EC}, cm^2	Exchange current density	
		j_0, μA·cm$^{-2}_{Ni}$	j_0, μA·cm$^{-2}_{geom}$
Non-activated Ni rod	0.52 ± 0.03	2.3 ± 0.1	6.0 ± 0.6
Ch activated Ni rod	0.35 ± 0.03	20 ± 2	33 ± 5
EC activated Ni rod	0.42 ± 0.04	14 ± 2	29 ± 3

As it has been noted in the experimental part, every single CV curve for non-activated Ni rod presented in this chapter was obtained in a separate experiment just after polishing of the electrode surface (see Section 2.3.4.1). This was found to be an essential condition to obtain a clean reproducible surface with minimum contribution of stable Ni surface oxides. It is thus interesting to see an evolution of the CV profile for non-activated and activated surface during recording of several subsequent scans at $v = 5$ mV·s^{-1} under H_2 atmosphere. Fig. 3.15a shows that in the case of non-activated Ni rod the HOR and the HER currents increase from one scan to the next, in particular, in the potential interval of the peak a_2. This increase in currents can be

presumably attributed to the formation of stable surface oxides, which are not reduced in the used potential region. Finally, a steady-state is established after ca. 10 scans, while the HOR/HER activity increases up to 1.5 times compared to the initial values for non-activated Ni rod. On the contrary, prolonged cycling of EC activated Ni rod leads to a decrease of its specific activity in the HOR/HER (Fig. 3.15b). The latter is accompanied by a decrease of the currents at potentials of the peak a_2 and is likely related to continuous reduction of surface Ni oxide species formed during the activation of the electrode. After 10 scans specific activity of EC activated Ni rod in the HOR/HER decreases by a factor of 1.5 in comparison with the initial value, while further drop of activity proceeds with a much lower rate.

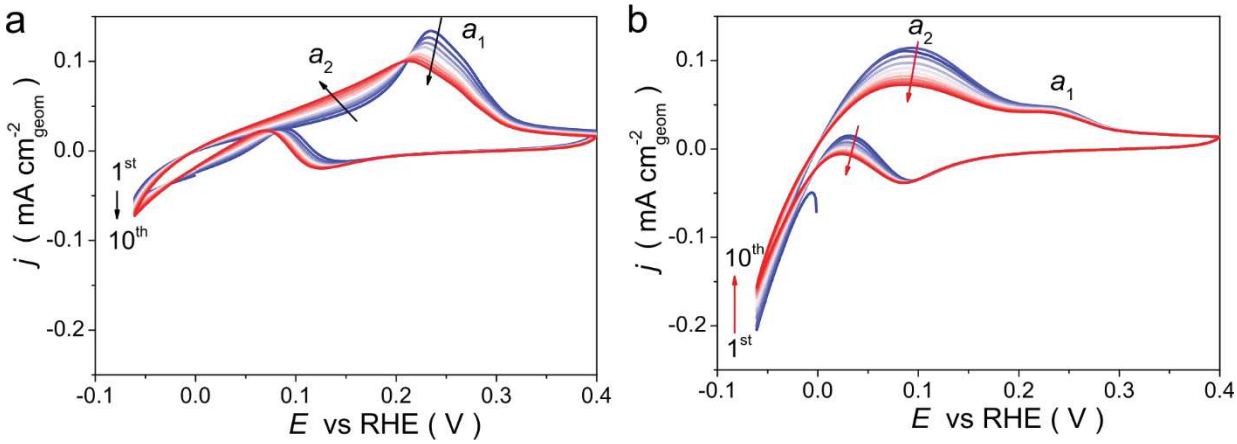

Fig. 3.15 *CVs obtained by recording of 10 consecutive scans for (a) non-activated and (b) EC activated Ni rod in H_2-saturated 0.10 M NaOH at v = 5 mV·s^{-1}.*

3.3.2. Influence of the temperature on the kinetics of the HOR/HER

For a more detailed study of the kinetics of the HOR/HER, including the effect of the surface state of Ni electrode, a series of experiments was performed at different temperatures. Comparison of CVs obtained in H_2 and N_2 atmosphere (Figs. 3.5 and 3.15) shows that with increase of temperature the HOR currents increase to a greater extent than the currents related to the oxidation of Ni electrode. Similarly, the HER currents also increase with temperature, confirming the results of earlier studies [78,241,244,254]. It is worth to note, that an abrupt increase in the currents (at $E < 0.15$ V) at the cathodic sweep of the CVs for non-activated Ni rod is also observed at elevated temperatures. Besides, the difference between the anodic and cathodic

currents increases with an increase of the temperature (Fig. 3.16a). On the contrary, almost the same slope was observed for anodic and cathodic sweeps of CVs obtained for EC activated Ni rod (Fig. 3.16b), the latter suggesting similar state of the electrode surface in both cases.

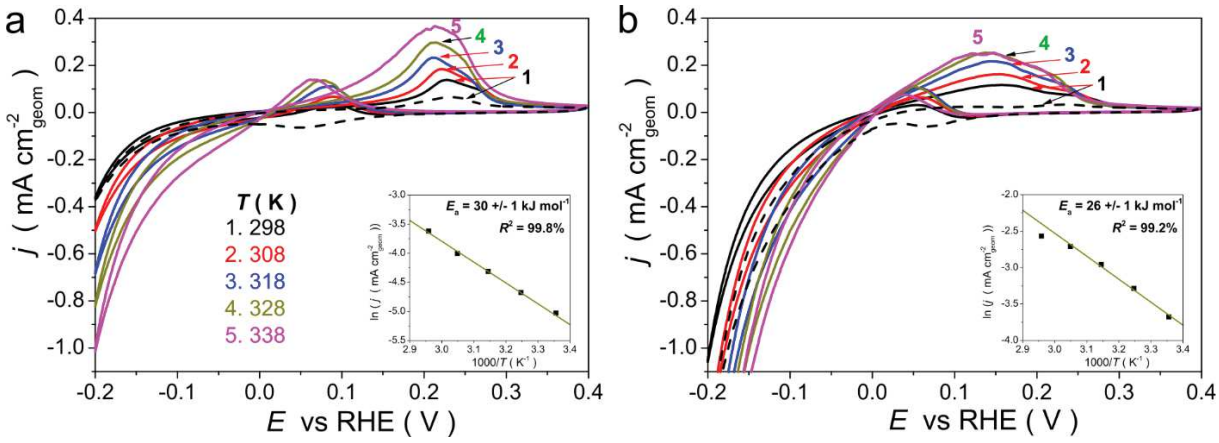

Fig. 3.16 *CVs for (a) non-activated and (b) EC activated Ni rod obtained in H_2-saturated 0.10 M NaOH at $v = 5$ mV·s^{-1} and 298 ≤ T ≤ 338 K; CVs obtained in N_2 atmosphere at $v = 5$ mV·s^{-1} and $T = 298$ K are presented for comparison by dashed curves. Insets represent Arrhenius plots of exchange current densities versus reciprocal temperature.*

Specific catalytic activities of non-activated and EC activated Ni rod in the HOR/HER normalized to the geometric surface area of the Ni rod are presented in Table 3.2. By plotting the activity values calculated from the anodic sweep of the CVs in Arrhenius coordinates (insets in Fig. 3.16), the apparent activation energy (E_a) was estimated to be 30 ± 1 and 26 ± 1 kJ mol^{-1} for non-activated and EC activated Ni rod, respectively. Deviation of the activity value j_0 for EC activated Ni rod at $T = 338$ K from the Arrhenius dependence correlates with the modification of the shape of the CVs presented in Fig. 3.16b and is likely caused by two factors: (i) stronger (probably excessive) oxidation of the electrode surface during its cycling up to $E = 1.0$ V and (ii) a possible limitation of the rate of the HOR/HER by slow H_2 mass-transport, rather than kinetics of the processes as in the case of lower values of j_0. The obtained values of E_a are comparable with those reported for the HER by Bockris and Potter (24 kJ mol^{-1} [63]), Kibria et al. (35 and 27 kJ mol^{-1}, at low and high cathodic overpotentials, respectively [254]) and Huot (21 kJ mol^{-1} [244]), while in some other studies much

higher values of E_a were obtained (58 kJ mol^{-1} [78], 60 kJ mol^{-1} [241], 60 and 73 kJ mol^{-1} [261]). The values of E_a determined for polycrystalline Ni rod are also close to the activation energies reported for Pt/C, Ir/C and Rh/C in alkaline media (29.6 ± 0.4, 32.8 ± 0.4, 26.6 ± 0.7 kJ mol^{-1}, respectively [36]), while being a bit smaller compared to the values reported for Pd/C (38.9 ± 3.0 [36]).

Table 3.2 *The values of the exchange current densities in the HOR/HER obtained for non-activated and EC activated Ni rod at various temperatures*

Temperature, K	**j_0, μA cm$^{-2}_{geom}$**					**E_a, kJ mol^{-1}**
	298	**308**	**318**	**328**	**338**	
Non-activated Ni	6.8	9.3	13.4	18.2	26.8	30 ± 1
EC-activated Ni	25.3	37.5	52.1	66.4	76.7	26 ± 1

Fig. 3.17 shows anodic sweeps of CVs plotted in Tafel coordinates and further used for the analysis of both anodic and cathodic potential intervals in accordance with the Tafel equation (eq. 1.18). It was found that the apparent Tafel slope calculated for non-activated Ni rod at low *cathodic overpotentials* (-0.20 < η < -0.07 V) changes in the range of 115 – 130 mV/decade, which essentially corresponds to a change in the RT/F term in the eq. 1.18 with temperature and agrees with the literature data [50,126,166,244,256,257] (Table 3.3). The apparent charge transfer coefficient α is almost constant and equal to 0.52 ± 0.01. In addition, the exchange current densities calculated by the use of eq. 1.18 are in line with the values calculated from the analysis of micropolarization region of CVs. On the contrary, analysis of the potential region of *anodic hydrogen oxidation* (0.06 < η < 0.12 V) clearly shows strong variation of the Tafel slope with temperature. This is likely due to significant impact of the currents related to the oxidation of Ni in a given potential region, especially at low temperatures. The latter follows from the comparison of CVs obtained in N_2 and H_2 atmosphere (Fig. 3.16a). At higher temperatures the HOR starts at more negative potentials and an impact of this process to the overall currents increases. As a result, the apparent Tafel slope of the HOR decreases with the temperature, tending to the values obtained in the interval of the HER (Table 3.3).

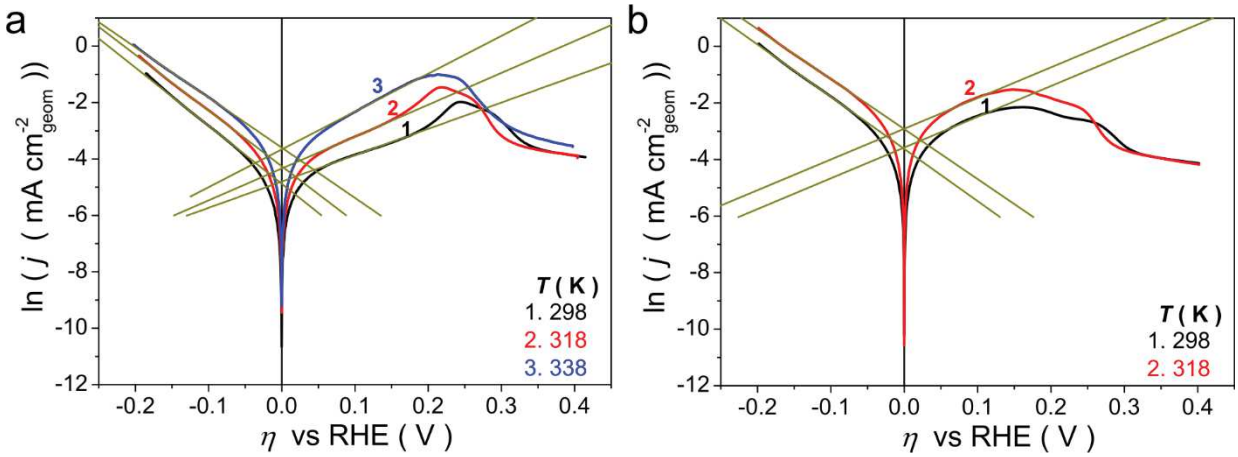

Fig. 3.17 *CVs for (a) non-activated and (b) EC activated Ni rod obtained in H_2-saturated 0.10 M NaOH at v = 5 mV·s^{-1} and various temperatures and plotted in Arrhenius coordinates.*

The behavior of the EC activated electrode (Fig. 3.17b) differs from that described above. The value of the apparent Tafel slope varies with the temperature in accordance with the change in the RT/F component for both the HER and the HOR, being in the range of 125 – 130 mV/decade and 210 – 220 mV/decade, respectively. The high values obtained at anodic overpotentials are likely related to the effect of the oxidation of Ni surface on the magnitude of the HOR currents, even at relatively low potentials [0.05 – 0.15 V].

Table 3.2 *The values of the apparent Tafel slope, determined (with an accuracy of ± 1 mV) at various temperatures*

	Potential interval	Tafel slope as a function of temperature, mV/decade				
		298 K	308 K	318 K	328 K	338 K
Non-activated Ni	-0.20 < η < - 0.07 V	115	116	116	123	129
	0.06 < η < 0.12 V	246	214	203	180	172
EC activated Ni	-0.20 < η < - 0.07 V	125	128	130	131	130
	0.06 < η < 0.12 V	211	214	212	219	218

3.3.3. Mean-field kinetic modeling of the HOR/HER

In the final part of this Chapter we present the analysis of the data of kinetic modeling performed with the aim to unveil the mechanism of the HOR/HER on metallic and partially oxidized Ni electrodes as well as understand the origin of the

HOR/HER kinetics enhancement in the presence of surface Ni oxides. The kinetic model was developed using the mean-field approximation, which *a priori* imposes certain limitations on the discussion of the obtained results. While the surface of the non-activated Ni rod can be considered relatively uniform, in the case of activated electrodes, *partial* reduction of the electrode surface may result in the formation of Ni oxide islands [79,280,281]. This can lead to the appearance of surface reaction centers with different properties and, as a consequence, different kinetics of the HOR/HER on them. Meanwhile, within the frame of the developed model, the surface was considered homogeneous even in the case of activated electrode. This approximation is dictated by the lack of *in situ* information about the state of the surface and the distribution of various centers on it, as well as the need to simplify the model.

Given the complexity of the electrochemical processes at Ni electrodes, the purpose of the model is not to accurately determine the rate constants of the reaction steps, but rather to propose a self-consistent interpretation of the experimental trends, which does not contradict the literature data regarding the HER kinetics [126,241,253,257].

Based on the results of XPS measurements we assumed that it is the presence of NiO (together with metallic Ni^0) on the surface of an activated Ni electrode, which is responsible for the changes of the CV in the supporting electrolyte, and an increase of the activity of Ni in the HOR/HER. The suggested hypothesis can be further supported by the analysis of computational studies devoted to the adsorption of various species (H_{ad}, OH_{ad}, O_{ad} and H_2O_{ad}) on the Ni surface [135,142–144,150,155,157–159], presented in Section 1.3.1. Confirming great tendency of Ni towards oxidation, DFT calculations have shown strong adsorption of O_{ad} and OH_{ad} on metallic Ni [135,150,155]. Besides, hydrogen is also strongly adsorbed on Ni, which may be considered as one of the likely reasons for its lower (compared to Pt) HOR/HER activity [27,135,136]. However, the binding energies of Ni-H_{ad} and Ni-OH_{ad} were shown by DFT calculations to decrease in the presence of adsorbed oxygen atoms [150,155]. In accordance with Sabatier principle, this effect should increase the activity of Ni towards the HOR/HER. In addition, DFT calculations showed that the

binding energy of H_2O_{ad}, which is weakly adsorbed on metallic Ni, is increased in the vicinity of adsorbed oxygen atoms [135,150,155]. This can affect the kinetics of the Volmer step, thus changing the activity of Ni in the HOR/HER.

Comparison of metallic and partially oxidized Ni electrodes

To describe the processes occurring on the surface of Ni electrodes in *the low-potential region*, the kinetic model was based on Tafel-Heyrovsky-Volmer mechanism (eq. 2.6 – 2.8) for the HOR/HER and the two-step Ni surface hydroxide formation (eq. 2.9 and 2.10). Assuming that the value of the Gibbs energy of adsorbed hydrogen intermediate ($\Delta_{ad}G^0_H$) differs on the surface of non-activated and activated Ni electrodes, two sets of rate constants (for the two types of the surface) were considered in this study, allowing us to reproduce the main characteristics of the corresponding CV curves (Appendix 2). The rate constants k_4^0, k_{-4}^0, k_5^0, k_{-5}^0 were adjusted to reproduce approximately the position of the Ni hydroxide formation and reduction peaks on the CVs of the Ni electrodes obtained in N_2 atmosphere. The values of k_1^0, k_2^0, and k_{-3}^0 were adjusted to reproduce the HOR/HER currents, whereas the choice of the rate constants for reverse reactions k_{-1}^0, k_{-2}^0, and k_3^0 must account for the values of $\Delta_{ad}G^0_H$ through the eq. 2.20 – 2.21 (see Section 2.4). To reproduce experimentally observed inhibition of the HOR at potentials higher than 0.15 V one has to assume relatively fast Ni-OH_{ad} and Ni-$(OH)_{2,ad}$ formation (k_4^0 and k_5^0) in comparison to the rate of the Volmer process (k_3^0). In order to minimize the number of adjustable parameters, the same values of k_4^0, k_{-4}^0, k_5^0, k_{-5}^0 were assumed for the activated and non-activated Ni electrode.

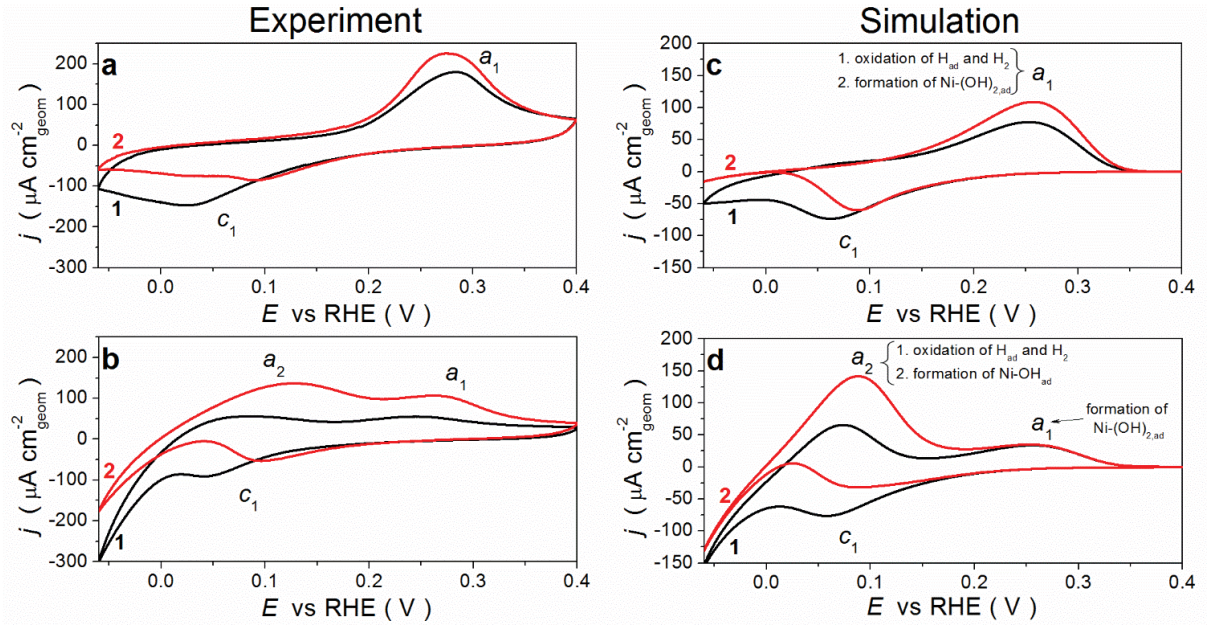

Fig. 3.18 *Comparison of the experimental (a, b) and simulated (c, d) CVs obtained for non-activated (a, c) and Ch activated (b, d) Ni rod in N_2- (curve 1, black) and H_2- (curve 2, red) saturated 0.10 M NaOH at v = 20 mV·s^{-1} and T = 298 K.*

Figs. 3.18a and c show the comparison of the simulated and experimental current-potential curves in N_2- and H_2-purged electrolytes for non-activated Ni. The essential experimental features, namely the presence of one anodic (a_1) and one cathodic (c_1) peaks in the CVs, under N_2 atmosphere, and the low HOR/HER activity could be qualitatively reproduced by assuming $\Delta_{ad}G^0$ = -0.10 eV (other parameters could be found in the Appendix 2). The low HOR/HER activity of non-activated Ni in the potential interval of [0 – 0.15 V] results from, on the one hand, the surface blocking by strongly adsorbed hydrogen and, on the other hand, the relatively slow Volmer step. The rate of electrocatalytic hydrogen oxidation increases with the potential and begins to appreciably exceed background currents at E > ~0.15 V, while at potentials E > ~0.25 V there is a drop in the HOR currents, which is caused by the formation of a monolayer of Ni hydroxide at the electrode surface. According to the developed model, in inert atmosphere the peak a_1 results from the contribution of both the electrochemical desorption of H_{ad} and the $Ni(OH)_{2,ad}$ formation (Fig. 3.18c), being in agreement with the conclusions of Hall et al. [64].

To explain the experimentally observed changes in the shape of CV and the HOR/HER activity enhancement upon oxidation of the Ni electrode, we assumed

weakening of the Ni-H_{ad} bond strength in the presence of surface NiO, and the ensuing increase of $\Delta_{ad}G^0_H$ by ca. 0.08 eV. This allowed us to reproduce the emergence of the peak a_2 (*cf* Figs. 3.17b and d) which is now attributed to the H_{ad} oxidation and Ni-OH_{ad} formation in agreement with the assumptions in some earlier studies [62,66,115]. At the same time, oxidation of $Ni(OH)_{ad}$ with the formation of $Ni(OH)_{2,ad}$ still occurs at the potentials of the peak a_1. Note however that to explain the strong HOR/HER activity enhancement for the Ch activated Ni the $\Delta_{ad}G^0_H$ increase alone was not sufficient (see Fig. 19), but also required an increase of the Volmer rate constant k_3^0. The latter implies that the presence of NiO on the surface results in changes in the double layer structure on the metal/electrolyte interface [47]. This is in agreement with the DFT calculations, which suggest that pre-adsorbed O_{ad} not only influences the binding energies of Ni-H_{ad} and Ni-OH_{ad}, but also the adsorption of water molecules on the Ni surface [150,155].

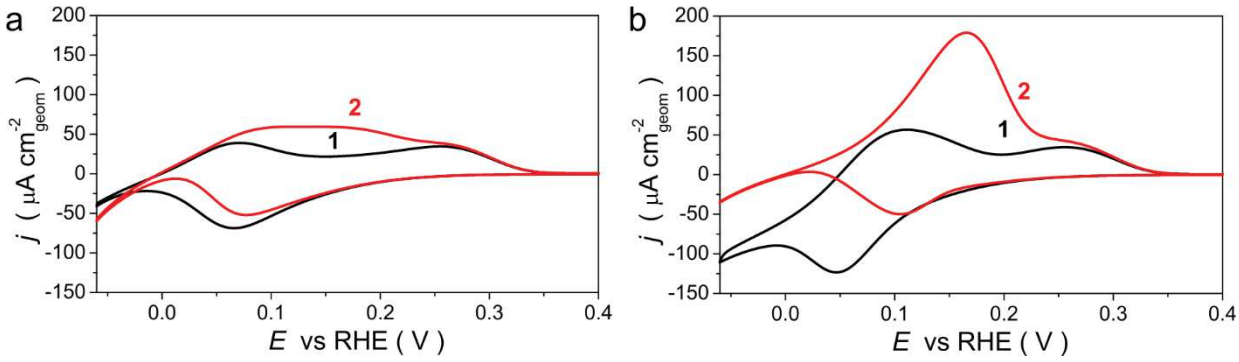

Fig. 3.19 *Simulated CVs obtained after either changing of $\Delta_{ad}G^0_H$ from -0.10 to -0.02 eV (a) or 10 times increase of k_3^0 (b) regarding the parameters determined for non-activated Ni in the absence (curve 1, black) or presence (curve 2, red) of H_2 at $v = 20\ mV{\cdot}s^{-1}$ and $T = 298\ K$.*

Influence of the temperature on the kinetics of the HOR/HER

To unveil the mechanism of the HOR/HER and to define kinetic parameters of individual reaction steps more precisely, the developed kinetic model was employed to describe the experimental CVs obtained at various temperatures for non-activated and activated Ni electrodes. The values of the rate constants of the Tafel, Heyrovsky and Volmer steps were adjusted in such a way as to describe the anodic sweep of the CVs recorded in H_2 atmosphere (Fig. 3.16). In addition, fitting of CVs obtained in

inert atmosphere (Fig. 3.5) was performed in order to extract the rate constants for Ni oxidation. As shown above, two processes occur in the potential region of the anodic peak a_1, namely the oxidation of strongly adsorbed H_{ad} and the formation of $Ni(OH)_2$. Taking into account this as well as stronger shift of the potential of the peak a_1 with temperature compared to that of the peak c_1 (Fig. 3.5), it is reasonable to assume that the position of the peak a_1 is mainly determined by the kinetics of electrochemical desorption of H_{ad}. Therefore, the rate constants for Ni oxidation and reduction were roughly adjusted from the position of the cathodic peak c_1 on the CVs obtained in inert atmosphere, allowing us at the same time to reproduce the abrupt decrease of the HOR current observed during the anodic sweep of CVs in H_2 atmosphere. As before, the same set of rate constants k_4^0, k_{-4}^0, k_5^0, k_{-5}^0 has been used for non-activated and EC activated Ni electrodes, with the aim to minimize the number of adjustable parameters (Appendix 3).

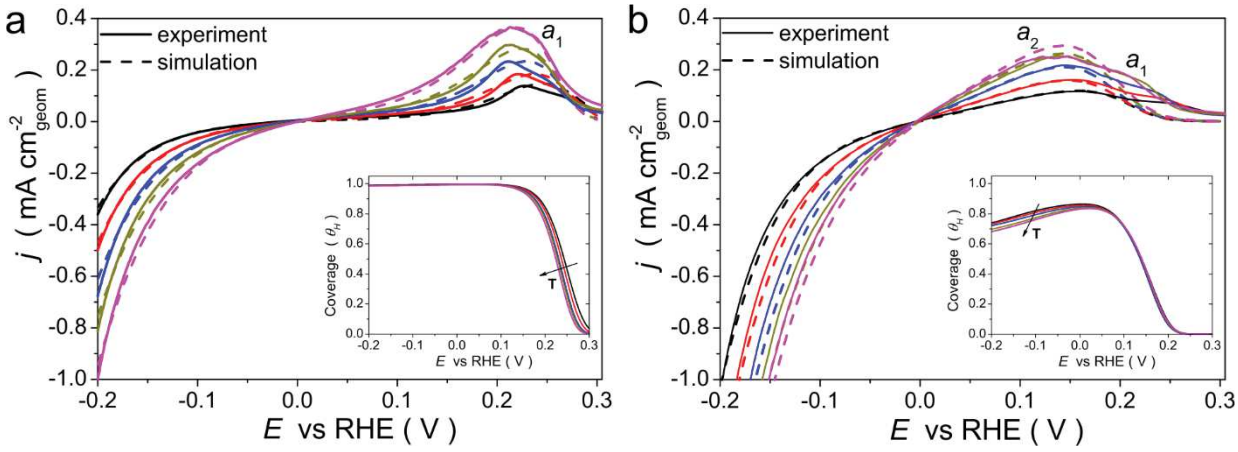

Fig. 3.20 *Comparison of the experimental (solid lines) and simulated (dashed lines) CVs for (a) non-activated and (b) EC activated Ni rod in H_2-saturated 0.10 M NaOH at $v = 5\ mV{\cdot}s^{-1}$ and $298 \leq T \leq 338$ K. Insets represent the coverage of Ni surface by adsorbed hydrogen depending on the applied potential.*

Fig. 3.20a compares simulated and experimental current-potential curves obtained in H_2-saturated 0.10 M NaOH for non-activated Ni rod. The developed model allows to reproduce well the experimental curves in all potential interval studied by assuming $\Delta_{ad}G^0_H = -0.15$ eV[c] and an increase of the rate constants for the

[c] The lower value of $\Delta_{ad}G^0_H$ in this case in comparison with the previously determined one (-0.10 eV) indicates an underestimation of the Ni-H_{ad} binding energy in previous experiments

Heyrovsky and Volmer steps with the temperature (Fig. 3.22a, Appendix 3), while the contribution of the Tafel step to the HOR/HER on metallic Ni was found to be negligible. Inset on Fig. 3.20a shows that a high coverage of Ni surface by strongly adsorbed H_{ad} is observed up to $E \approx 0.15$ V, being in agreement with previous findings. At higher potentials, the oxidation of the Ni surface begins along with oxidation of H_{ad}. This process reaches a maximum at $E \approx 0.3$ V, leading to a complete inhibition of the HOR (Fig. 3.21).

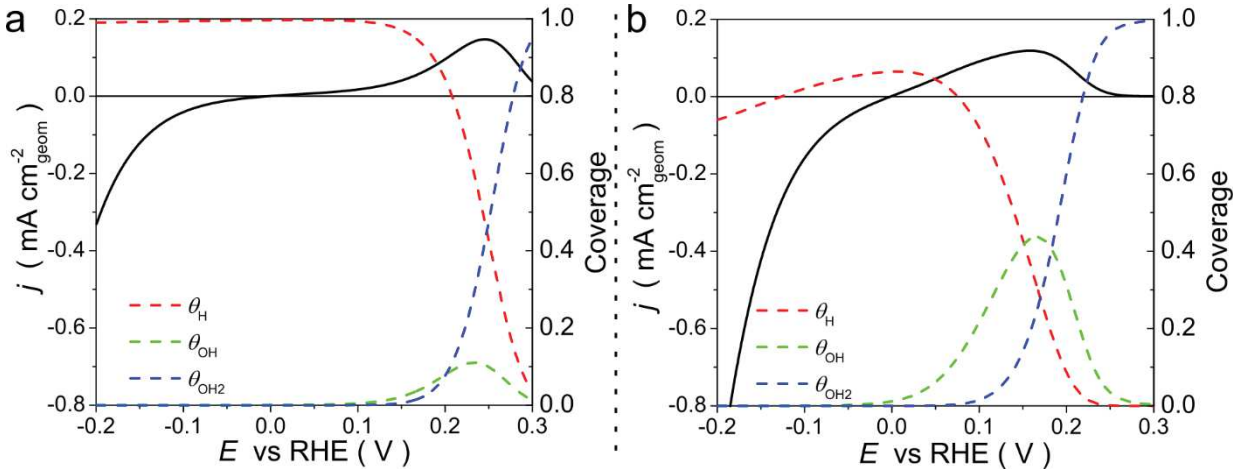

Fig. 3.21 *Simulated CVs for non-activated (a) and EC activated (b) Ni rod obtained in the presence of H_2 at $v = 5\ mV{\cdot}s^{-1}$ and $T = 298$ K. Dashed curves represent the coverage of the electrode surface by reactive intermediates.*

Careful analysis of calculated rate constants (Appendix 3, Fig. 3.22) allows to conclude that on the surface of non-activated Ni electrode the HOR/HER proceed according to the Heyrovsky-Volmer mechanism in agreement with several other studies, where authors assumed (almost) full coverage of Ni surface by adsorbed H_{ad} in the potential interval of the HER [78,253,257]. It should be noted that present work for the first time shows that the Heyrovsky-Volmer mechanism is valid not only for the HER but also for the HOR on metallic Ni. Besides, on the bases of data listed in Table 3.4 we conclude that the rate of the HER is determined by the backward Heyrovsky step (k_{-2}^0), while the rate of the HOR is controlled by the forward Volmer step (k_3^0). Remarkably, the calculated activation energy for the k_{-2}^0 is fairly close to the experimentally obtained value of E_a (ca. 32 and 30 kJ mol^{-1}, respectively,

Tables 3.2 and 3.4). In contrast, the calculated activation energy for the k_3^0, according to the modeling, was found to be much higher (ca. 42 kJ mol^{-1}, Table 3.4).

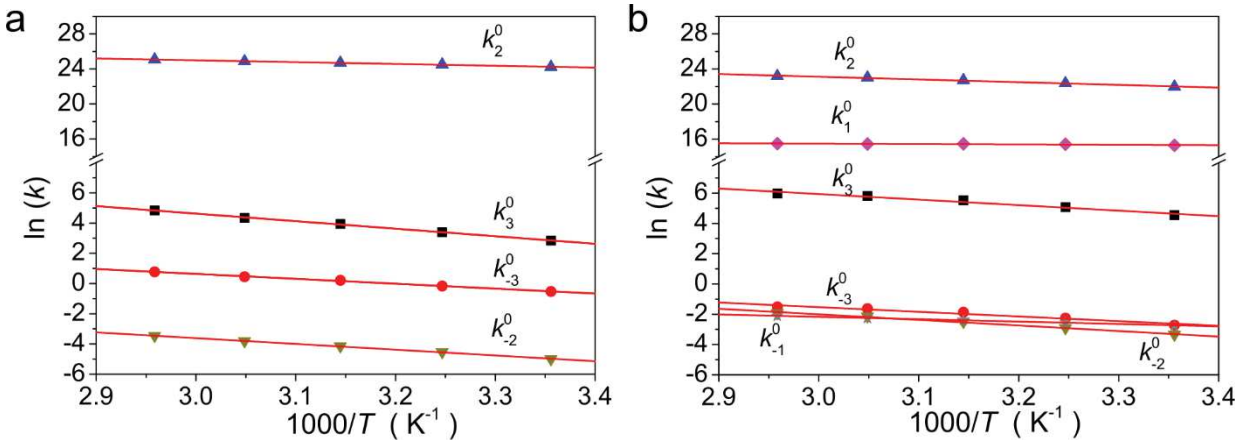

Fig. 3.22 *Arrhenius plots of the calculated rate constants for the Volmer ($k_{\pm 3}^0$), Heyrovsky ($k_{\pm 2}^0$) and Tafel ($k_{\pm 1}^0$) elementary steps versus reciprocal temperature for (a) non-activated and (b) EC activated Ni rod.*

In accordance with the analysis presented above, the HOR/HER activity enhancement on *partially* oxidized Ni electrode can be described by assuming an increase of the $\Delta_{ad}G^0_H$ in the presence of oxide species on the surface of the Ni electrode. Based on the analysis of CVs obtained at various temperatures, the change of $\Delta_{ad}G^0_H$ was found to be ca. 0.10 eV (from -0.15 to -0.05 eV). A reasonable fit of the experimental current-potential curves in the potential region of [-0.2 – ~0.2 V] was obtained for the activated Ni electrode (Fig. 3.20b). At the same time, deviations of the simulated curves from the experimental ones observed at $E > 0.2$ V are likely related to the approximations used in the development of the kinetic model. In reality the oxidation of Ni surface might be more complicated than that assumed in the model due to possible formation of multilayered islands of Ni hydroxide before full coverage of the Ni surface by $Ni(OH)_2$ is established [79,80]. Besides, the surface of partially oxidized Ni electrode likely contains several types of reactive Ni sites with different activity in the HOR, while in the mean-field approximation, it is considered to be homogeneous.

Despite some limitations of the model, a number of qualitative conclusions can be drawn from performed analysis. First, it was found that the HOR/HER on the surface of the activated Ni electrodes proceeds with the participation of all three

elementary steps, although with a greater contribution of the Heyrovsky and Volmer steps. Second, the backward Volmer (k_{-3}^0) and the backward Heyrovsky (k_{-2}^0) steps involved in the HER have similar rates in the case of EC activated Ni. The latter results in a decrease of the H_{ad} coverage of Ni surface compared to non-activated Ni electrode (inset on Fig. 3.20b). It should be noted that the coverage is related to the Ni surface sites initially free from stable Ni oxide species formed during the activation of the electrode. In contrast to the HER, the forward Volmer step (k_3^0) remains the rate determining one for the HOR. Finally, the activation energy determined for the forward Volmer process decreases from 42 on metallic Ni to 36 kJ mol^{-1} on *partially* oxidized Ni and becomes comparable with the values calculated for the forward Heyrovsky step (28 kJ mol^{-1}). Note that the experimentally obtained value of the apparent activation energy was even lower (ca. 26 kJ mol^{-1}) providing additional support for the involvement of the Tafel step in the mechanism of the HOR/HER on activated Ni.

Table 3.4 *The activation energies and the pre-exponential factors, determined for the rate constants of the Tafel ($k_{\pm 1}$), Heyrovsky ($k_{\pm 2}$) and Volmer ($k_{\pm 3}$) steps by the analysis of Fig. 3.22*

		k_1^0, cm^3 s^{-1} mol^{-1}	**k_{-1}^0, s^{-1}**	**k_2^0, cm^6 s^{-1} mol^{-2}**	**k_{-2}^0, s^{-1}**	**k_3^0, cm^3 s^{-1} mol^{-1}**	**k_{-3}^0, s^{-1}**
Non-activated Ni	E_a, kJ mol^{-1}	-	-	17±1	32±1	42±1	27±1
	A_i^0	-	-	$3.7\cdot10^{13}$	$2.5\cdot10^{3}$	$3.2\cdot10^{8}$	$3.2\cdot10^{4}$
EC activated Ni	E_a, kJ mol^{-1}	4±1[d]	13±1 *d*	28±1	33±1	34±2	30±2
	A_i^0	$2.2\cdot10^{7}$ *d*	12 *d*	$2.9\cdot10^{14}$	$2.1\cdot10^{4}$	$1.1\cdot10^{8}$	$1.1\cdot10^{4}$

[d] The values for the Tafel step are determined less precisely compared to all others

3.4. Conclusions of Chapter 3

Significant variations in the electrochemical and electrocatalytic properties of Ni in the hydrogen oxidation and hydrogen evolution reactions were observed depending on the pretreatment of the electrode surface. If electrochemical tests are performed shortly after polishing of the surface of Ni rod and care is taken to minimize its contact with air, then electrocatalytic activity of Ni in the HOR/HER is low and amounts to ca. 2 $\mu A\ cm^{-2}_{Ni}$ or ca. 6 $\mu A\ cm^{-2}_{geom}$ for the normalization by electrochemically active or geometric surface area, respectively. If, however, Ni electrode is "activated" by either its exposure to an ambient atmosphere or under controlled electrochemical conditions, then its activity in the HOR/HER increases up to ca. 20 $\mu A\ cm^{-2}_{Ni}$ (32 $\mu A\ cm^{-2}_{geom}$) or ca. 15 $\mu A\ cm^{-2}_{Ni}$ (29 $\mu A\ cm^{-2}_{geom}$), respectively. On the basis of *ex situ* angle-resolved XPS measurements this difference is tentatively explained by the presence of a significant amount of NiO on the surface of partially oxidized Ni.

By combining the experimental observations with microkinetic modeling we conclude that the enhancement of the electrocatalytic activity of Ni in the presence of surface Ni oxide species is due to a decrease of the adsorption energy of the hydrogen intermediate participating in the HOR/HER, along with an increase of the rate constant of the Volmer step. This conclusion agrees with the published results of DFT calculations suggesting decrease of the Ni-H_{ad} binding energy and an increase of the Ni-H_2O_{ad} binding energy in the presence of oxygen adsorbed on Ni surface. We infer that not only the rate of the HOR/HER, but also its mechanism is affected by the surface state of Ni electrode. On the surface of metallic Ni, the HOR/HER follow the Heyrovsky-Volmer mechanism with the forward Volmer step being the rate determining one for the HOR, while the rate of the HER is controlled by the backward Heyrovsky steps. On the surface of "activated" Ni electrode, where Ni metal sites co-exist with the "irreversible" surface oxide species, the contribution of the Tafel step in the mechanism of the reactions has to be taken into account. In this case the rates of the backward Volmer and Heyrovsky steps become comparable in the potential interval of the HER, while the HOR is still limited by the slow Volmer step.

The results of this study, among other things, allow one to reconcile the inconsistencies in the data reported in the literature regarding the electrocatalytic activity of Ni in the HOR/HER and the mechanism of this process (Heyrovsky-Volmer vs. Tafel-Volmer). The observed contradictions are attributed to differences in the surface state of Ni electrodes, which originate from the differences in the methodology used for the pretreatment of the surface of Ni electrode.

Chapter 4: Nanostructured Ni electrocatalysts

4.1. Introduction

For practical applications (e.g. at the anodes of AMFCs), carbon (or other conductive material) supported catalysts with high dispersion and loading of an active component are preferable. Such materials provide high specific surface area of the active component, which is necessary for preparation of compact and highly efficient FC systems. However, incorporation of Ni metal nanoparticles on carbon surface by traditional methods, such as, for example, wet impregnation or adsorption, usually results in formation of large agglomerates and, as a consequence, low Ni dispersion. An alternative method for preparation of supported catalysts is based on the method of electrodeposition, the main advantage of which is the possibility to tune the structure of the deposits and the particle size *via* modification of the deposition parameters, such as applied potential and the composition of the deposition bath. In addition, this method allows one to prepare nanostructured materials with high density of intergrain boundaries, which have proven to enhance the activity of metals in a number of catalytic [282,283] and electrocatalytic [284–289] processes.

Therefore the main tasks in the current chapter were formulated as follows:

(i) To develop an electrodeposition procedure allowing one to obtain Ni nanoparticles of relatively small size with a high density of them on the surface of carbon support;

(ii) To compare the electrochemical behavior of the obtained samples, as well as their electrocatalytic activity in the HOR/HER with the results of the study of polycrystalline Ni electrode;

(iii) To find out how the oxidative surface pre-treatment of the obtained electrodes affects their activity in the HOR/HER.

The synthesis of Ni particles was first performed using flat GC support, with the aim to determine the parameters of electrodeposition. After developing the procedure of electrodeposition and revealing the main characteristics of the obtained samples, a series of samples with a commercial carbon support Vulcan XC-72 was also obtained. This allowed us for the first time to prepare a supported catalyst with a high content (ca. 40 wt.%) of small Ni nanoparticles (ca. 10 nm).

4.2. Ni electrodeposited on flat GC support

4.2.1. Choice of electrodeposition parameters and investigation of the synthesized samples by physicochemical techniques

Synthesis of nanostructured catalysts was done by using the method of potentiostatic deposition from the electrolytic bath, containing 0.01 M $NiSO_4$ and 0.10 M $(NH_4)_2SO_4$. The range of Ni deposition potentials was determined on the basis of CVs obtained in an inert atmosphere at a sweep rate of 20 $mV \cdot s^{-1}$, and using GC rod as a working electrode (Fig. 4.1a). One can see that on the first scan (cathodic sweep) Ni deposition begins at potentials $E < -1.2$ V vs MSE[e], while at the anodic sweep of the CV a so-called "nucleation loop" is observed, which is typical for the processes of nucleation and growth. At the second scan, the deposition starts at more positive potentials, which is associated with the growth of previously formed Ni particles. It should be also noted that the deposition of Ni proceeds simultaneously with the HER.

Electrodeposition of Ni was performed in three steps using a pulse potentiostatic mode. The corresponding pulse potentials were chosen in such a way that nucleation of Ni nanoparticles occurs during the first applied potential (E_1 = -1.50 V vs. MSE), while their growth takes place mainly at the potential E_3 = -1.25 V vs. MSE. The second step (E_2 = -0.93 vs. MSE) was added with the aim to replenish the electrolyte layer in the vicinity of the electrode surface with Ni^{2+} ions.

[e] MSE = Mercury–Mercury Sulphate Electrode, E_{MSE} = 0.96 V vs RHE at T = 298 K, pH (0.01 M $NiSO_4$ + 0.10 M $(NH_4)_2SO_4$) ≈ 5.4

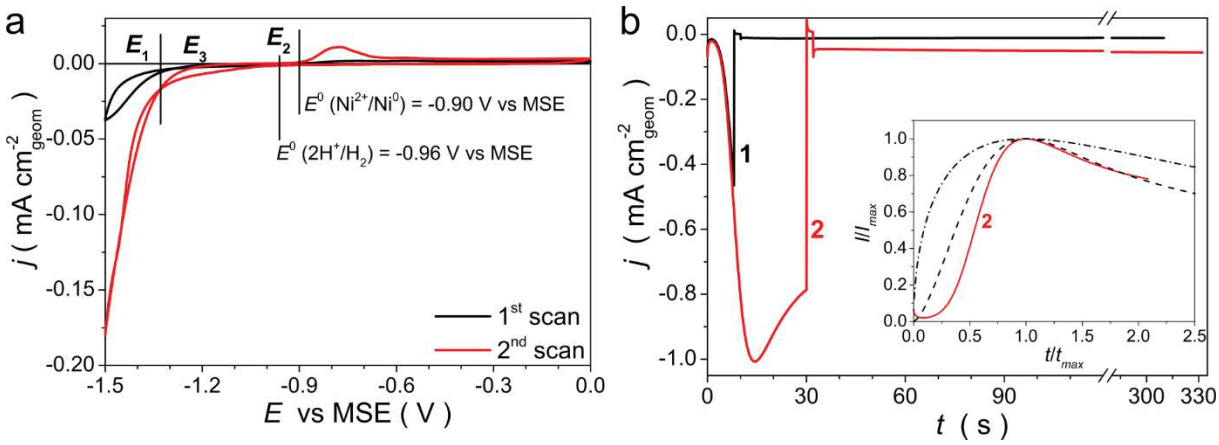

Fig. 4.1 *(a) CVs for GC electrode in N_2-saturated 0.01 M $NiSO_4$ + 0.10 M $(NH_4)_2SO_4$ solution at $v = 20\ mV \cdot s^{-1}$ and $T = 298$ K; (b) Ni deposition transients obtained for Ni_{ED}/GC-1 (curve 1, black) and Ni_{ED}/GC-2 (curve 2, red) (the parameters of deposition are listed in Table 4.1). Inset on the panel (b) shows reduced transients for Ni_{ED}/GC-2 along with model transients for instantaneous (dash dot line) and progressive (dashed line) nucleation.*

To inspect the influence of the electrodeposition parameters on the morphology of obtained Ni nanoparticles, a series of Ni_{ED}/GC samples with varied time of the nucleation step or concentration of Ni^{2+} ions in the electrolyte (Table 4.1) was obtained. Experimental transients for Ni deposition on GC support are shown in Fig. 4.1b. A well-defined current maximum (I_{max} achieved at t_{max}) was observed when the first deposition potential was applied for $t >$ ~20 s, allowing us to plot the I vs t dependence in dimensionless (i. e. normalized on I_{max} and t_{max}) coordinates. However the analysis of obtained transients and their comparison with model transients for instantaneous and progressive nucleation [290,291] is complicated by the concomitant hydrogen evolution. The low amount of Ni electrodeposited on GC support did not allow us to precisely determine its mass, thus preventing us from the estimation of the Faradaic efficiency of the electrodeposition. Meanwhile, as will be shown later for the electrodeposition of Ni on the Vulcan carbon support (see Section 4.3.1), the contribution of the HER currents is significant and cannot be ignored. This might explain significant deviation of the experimental transients from the model ones at $t < t_{max}$ (see the inset to Fig. 4.1b). Indeed, high contribution of the HER currents results in overestimation of the I_{max} value and thus underestimation of the value of I/I_{max}. Similarly, despite the fairly good agreement between experimental and model

transients for progressive nucleation at $t > t_{max}$, the impossibility of correct subtracting the contribution of the HER currents prevents us from making any unambiguous conclusions about the character of the nucleation and growth of Ni particles (see the inset in Fig. 4.1 b).

The microstructure and the morphology of the deposits were studied with the help of SEM. Typical images obtained for a number of samples (Fig. 4.2) indicate that an increase of the duration of the first deposition (potential E_1) step (Ni_{ED}/GC-2) or the concentration of Ni^{2+} ions in the electrolyte (Ni_{ED}/GC-3) lead to an increase of the Ni particle size.

Table 4.1 *Conditions of the electrodeposition of Ni particles on GC support. Modified parameters are marked in bold*

Sample	**Composition of the electrolytic bath**	**Deposition parameters (E_1 = -1.50 V, E_2 = -0.93 V, E_3 = -1.25 V vs. MSE)**	**Q_{total}, mC**	**d_{SEM}, nm**
Ni_{ED}/GC-1	0.01 M $NiSO_4$ + 0.1 M $(NH_4)_2SO_4$	t_1 = 8 s, t_2 = 2 s, t_3 = 300 s	1.0 ± 0.4	40 ± 10
Ni_{ED}/GC-2	0.01 M $NiSO_4$ + 0.1 M $(NH_4)_2SO_4$	t_1 = **30 s**, t_2 = 2 s, t_3 = 300 s	5.0 ± 1.2	80 ± 25
Ni_{ED}/GC-3	**0.10 M** $NiSO_4$ + 0.1 M $(NH_4)_2SO_4$	t_1 = 8 s, t_2 = 2 s, t_3 = 300 s	27.0 ± 4.0	~150
Ni_{ED}/GC-4[f]	0.01 M $NiSO_4$ + 0.1 M $(NH_4)_2SO_4$	t_1 = 8 s, t_2 = 2 s, t_3 = **120 s**	3.6 ± 1.8	25 ± 5

[f] Before electrodeposition the surface of GC cylinder was polished with 1.0 and 0.3 μm Al_2O_3 slurries for the Ni_{ED}/GC-4 sample, while in the case of Ni_{ED}/GC-1,2,3 samples, the GC surface was polished up to 0.05 μm Al_2O_3 slurry

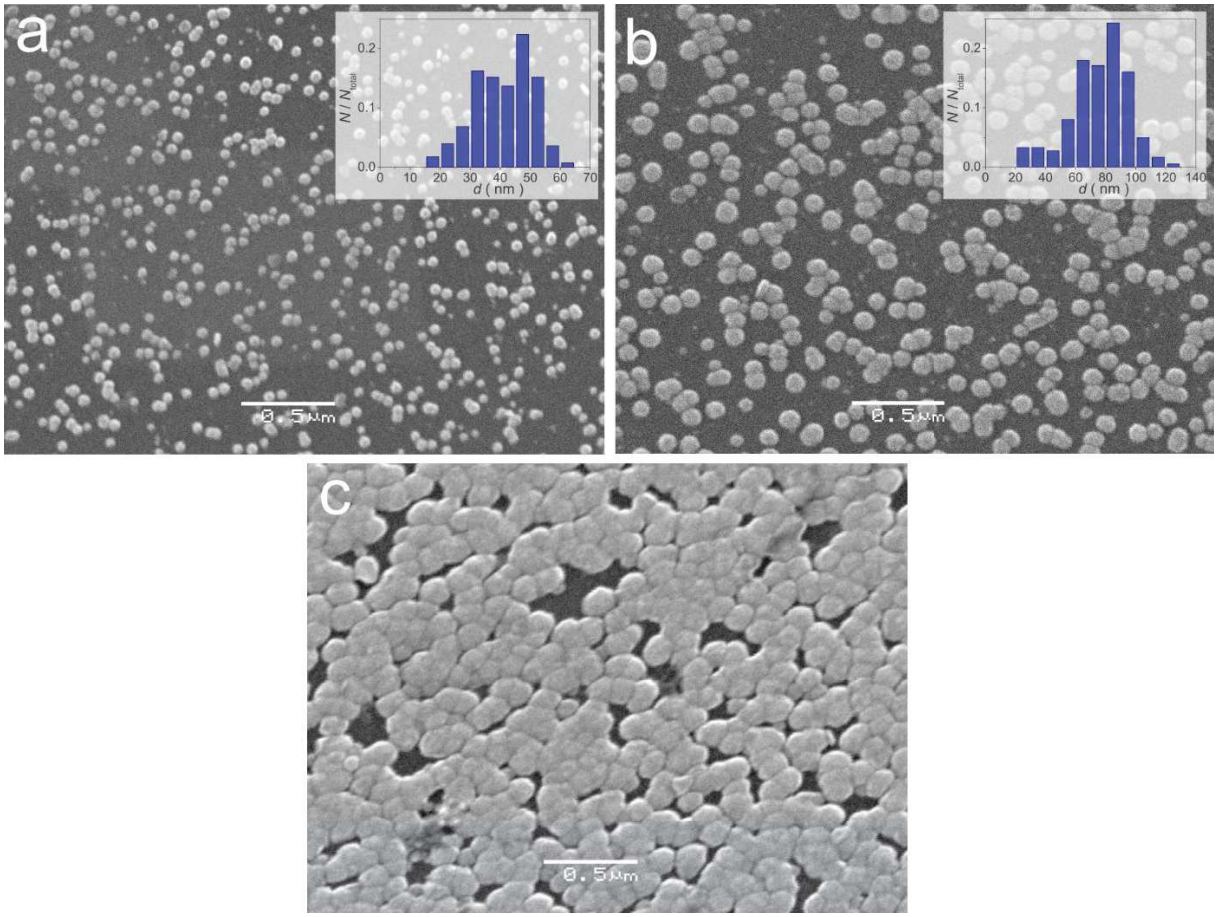

Fig. 4.2 *SEM images of Ni particles electrodeposited on GC support: Ni_{ED}/GC-1 (a), Ni_{ED}/GC-2 (b), Ni_{ED}/GC-3 (c), and corresponding size distribution of Ni globules.*

In order to obtain a narrower size distribution of Ni particles, the time of the first electrodeposition step in the synthesis of model Ni_{ED}/GC samples in what follows was set before reaching t_{max} (t_1 = 8 s). This allows one to reduce the contribution of the secondary nucleation and the growth of Ni particles when the potential E_1 is applied. In addition, with the aim to increase the density of sites accessible for the primary nucleation, the surface roughness factor of the GC support was increased. The latter was achieved by excluding the final polishing of the surface of GC support with 0.05 µm Al_2O_3 slurry (i. e. the GC rods were polished only with 1.0 and 0.3 µm Al_2O_3 slurries). Almost seven times increase of the number of particles per unit surface area was observed, if comparing the samples Ni_{ED}/GC-1 (ca. $7.7 \cdot 10^9$ particles/cm^2_{geom}) and Ni_{ED}/GC-4 (ca. $5.5 \cdot 10^{10}$ particles/cm^2_{geom}). In the latter case, with the aim to minimize agglomeration of the particles, the time for the third electrodeposition step was

decreased from 300 to 120 s, which resulted in a decrease of the surface mean diameter of Ni particles (Table 4.1, Fig. 4.3a).

It is well known, that electrodeposition often results in formation of nanostructured deposits due to the existence of secondary nucleation processes [284,287–289,291,292]. Analysis of the Ni_{ED}/GC-4 particles by TEM (after transferring the deposits from the GC surface to the copper mesh) evidences their nanostructured nature. The defect structure and the presence of intergrain boundaries can be observed in the HR-TEM image, shown in Fig. 4.3b. However particle mobility under the electron beam did not allow us to obtain the images at higher resolution, thus preventing us from their detailed analysis.

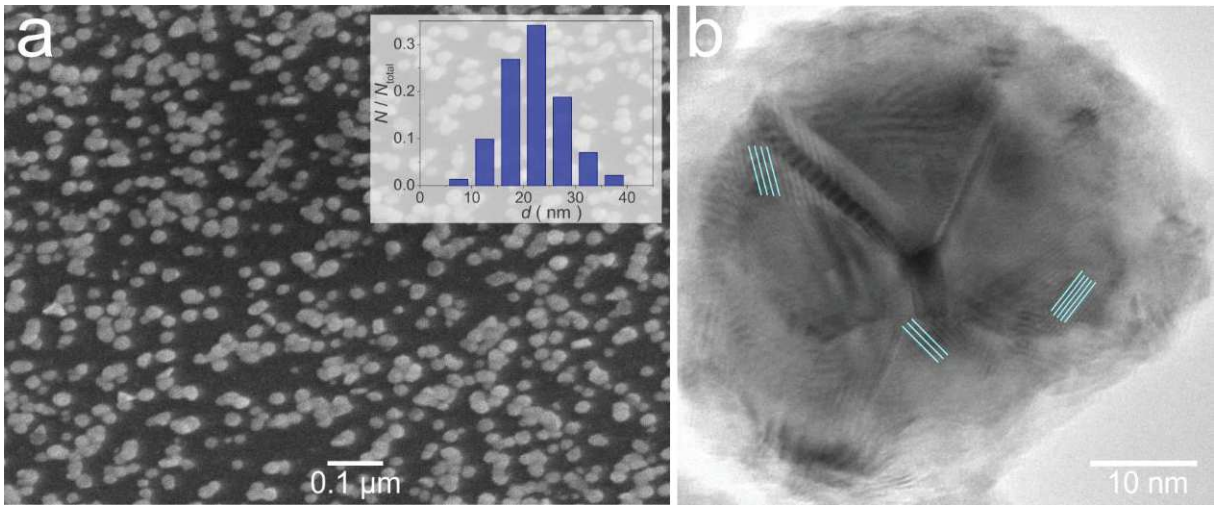

Fig. 4.3 *SEM and HR-TEM images of Ni_{ED}/GC-4 sample (the deposition parameters are listed in Table 4.1).*

Subsequently, for the electrochemical and electrocatalytic measurements, a series of Ni_{ED}/GC samples was obtained using the parameters listed in Table 4.1 for the Ni_{ED}/GC-4 sample.

4.2.2. Electrochemical properties of Ni_{ED}/GC electrocatalysts

Fig. 4.4a shows the CVs registered just after the immersion of freshly prepared Ni_{ED}/GC electrode in N_2-purged 0.10 M NaOH. As it has been noticed for non-activated Ni rod (see Section 3.2.1), the cathodic peak attributed to the reduction of Ni oxide species, which are formed on the electrode surface during its short exposure to the ambient, appears also on the first scan of the CV obtained for non-activated Ni_{ED}/GC electrode. However, this peak is broader compared to that observed for Ni rod and located at more negative potentials (ca. -0.08 and ca. 0.02 V for the non-activated Ni_{ED}/GC and Ni rod, respectively) (Figs. 4.4a and 3.1a). The latter is likely related to a stronger oxidation of the surface of Ni_{ED}/GC particles during the electrode transfer to the electrochemical cell with 0.1 M NaOH through air, even if this procedure was performed fast (less than 15 s). This assumption is in agreement with the fact that the value of the open-circuit potential measured for Ni_{ED}/GC just after its immersion of in the electrolyte was ca. 0.2 V more positive than that for the non-activated Ni rod (0.4 – 0.5 and 0.2 – 0.3 V, respectively). Notwithstanding this difference, already after the first scan of the CV, registered in the potential range of [-0.20 – 0.40 V], the air-formed Ni oxide species are believed to be reduced. As a result, the shape of the subsequent CVs becomes similar to that observed for a non-activated Ni rod (Fig. 4.4a) and discussed in Chapter 3.

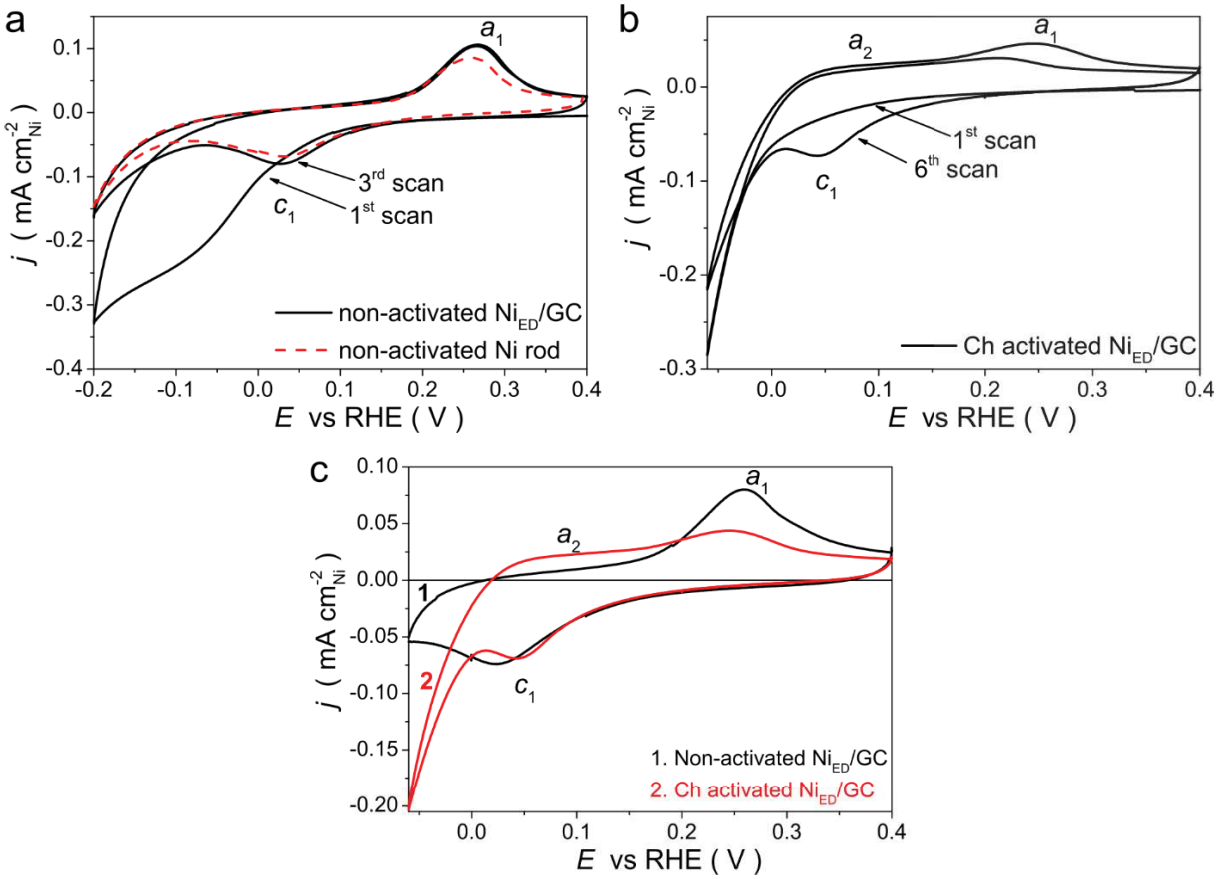

Fig. 4.4 *CVs obtained in N_2-saturated 0.10 M NaOH and v = 20 mV·s^{-1} for (a) non-activated and (b) Ch activated Ni_{ED}/GC just after an immersion of the electrodes in the electrolyte; (c) comparison of conditioned CVs obtained for non-activated (curve 1, black) and Ch activated (curve 2, red) Ni_{ED}/GC electrodes.*

In order to inspect whether the electrochemical and electrocatalytic properties of Ni_{ED}/GC nanoparticles change after their partial oxidation, as described in the previous chapter (see Chapter 3), the freshly prepared Ni_{ED}/GC electrode was dried under a N_2 flow and subjected to oxidation in air for quite a long time (typically 24 h.) ("Ch activated", see Section 2.3.4.1). The open-circuit potential, measured after the immersion of Ch activated Ni_{ED}/GC sample in 0.1 M NaOH, was found to be in the range of 0.55 – 0.70 V, which is ca. 0.15 V higher than the value measured for a Ch activated Ni rod (see Section 3.2.2). The latter likely indicates a deeper oxidation of Ni nanoparticles compared to a polycrystalline Ni rod. Similarly to Ch activated Ni rod, no cathodic peak was observed on the first scan of the CV recorded in the potential interval of [-0.06 – 0.40 V] (Figs. 4.4b and 3.3b), while partial reduction of the electrode surface resulted in an appearance of characteristic anodic (a_1) and

cathodic (c_1) peaks (Fig. 4.4b). The peak a_2 was less defined compared to the one observed for the Ch activated Ni rod, although its contribution to the anodic currents is visible if CVs registered for non-activated and Ch activated Ni_{ED}/GC are compared (Fig. 4.4c).

4.2.3. Kinetics of the HOR/HER on Ni_{ED}/GC electrocatalysts

Electrocatalytic activities of the Ni_{ED}/GC catalysts in the HOR/HER were estimated from the analysis of CVs registered in H_2-purged 0.10 M NaOH at $v = 5$ mV·s^{-1} (Fig. 4.5). Analysis of the data listed in the Table 4.2 shows that the activity of non-activated Ni_{ED}/GC is almost 3 times higher than the value measured for non-activated Ni rod (Table 3.1). However the observed difference is most likely due to the longer contact of the Ni_{ED}/GC sample with alkaline media during the measurements. Indeed, the CVs of non-activated Ni rod in H_2 atmosphere were obtained just after polishing of the electrode surface. On the contrary, before measuring the activity of non-activated Ni_{ED}/GC, CVs in N_2-saturated 0.1 M NaOH were registered (with the aim to determine the value of S_{EC}). To further confirm this assumption, the same experiments, namely consecutive measurements in, first, N_2 atmosphere and then in H_2 atmosphere, were carried out using freshly polished Ni rod (hereinafter, 'polished Ni rod'). It was found that the specific activities of non-activated Ni_{ED}/GC and polished Ni rod in the HOR/HER are essentially similar (Table 4.2), even if the shape of the corresponding CVs is not exactly the same (Fig. 4.5b).

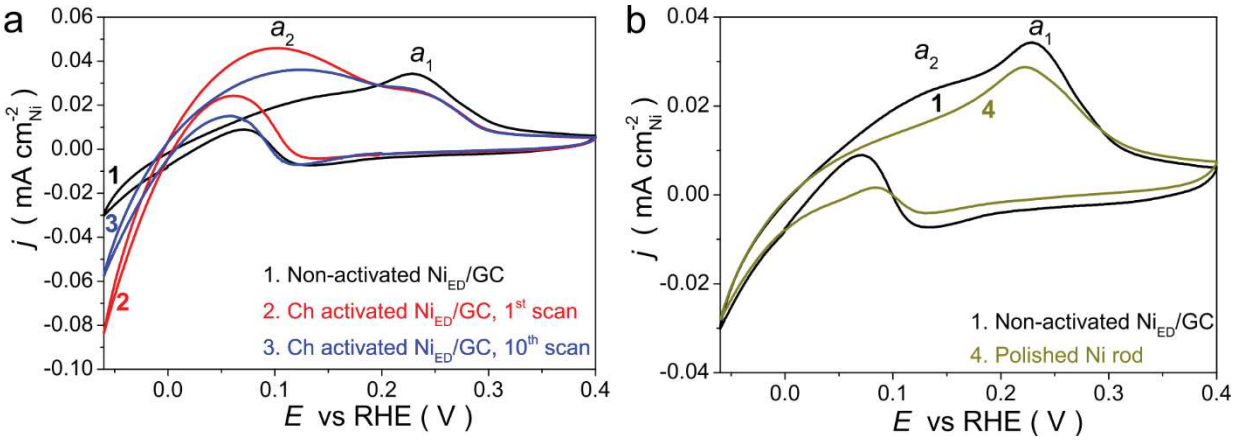

Fig. 4.5 *(a) CVs obtained in H_2-saturated 0.10 M NaOH at v = 5 mV·s^{-1} for non-activated (curve 1, black) and Ch activated (1st scan – curve 2, red and 10th scan –*

curve 3, blue) Ni_{ED}/GC; (b) Comparison of CVs obtained for non-activated Ni_{ED}/GC (curve 1, black) and polished Ni rod (curve 4, dark yellow).

The study of Ch activated Ni_{ED}/GC electrode in H_2 atmosphere showed that its specific activity in the HOR/HER is almost 4 times as high as the activity of non-activated Ni_{ED}/GC, while the value of S_{EC} decreases by less than 20% (Table 4.2) after partial oxidation of the surface of Ni_{ED}/GC particles. However, same as for the EC activated Ni rod (see Section 3.3.1), the activity of the Ch activated Ni_{ED}/GC sample decreases during prolonged cycling of the electrode in the potential region of [-0.06 – 0.4 V] (by about 30% for 10 scans). This is likely due to continuous reduction of the surface Ni oxide species (Fig. 4.5a).

Table 4.2 *The values of the exchange current densities in the HOR/HER obtained for Ni_{ED}/GC and polycrystalline Ni rod after various pre-treatment of their surface*

Catalyst	S_{EC} / cm^2_{Ni}	j_0 / µA cm^{-2}_{Ni}
Non-activated Ni_{ED}/GC	0.20 ± 0.09	6.4 ± 0.6
Ch activated Ni_{ED}/GC	0.17 ± 0.04	25 ± 3
Polished Ni rod	0.52 ± 0.03	6.0 ± 0.8

4.3. Ni electrodeposited on porous XC-72 carbon support

4.3.1. Choice of electrodeposition parameters and investigation of the synthesized samples by physicochemical techniques

To prepare electrocatalysts, which could be potentially applied at the anode of an AMFC, electrodeposition of Ni was also undertaken with the use of the high surface area Vulcan XC-72 carbon as a support. The latter was immobilized on the GC surface in the form of a thin layer (ca. 100 µg cm^{-2}_{geom}). The electrodeposition parameters were slightly modified in comparison with those described above. First, with the aim to obtain high metal loading on the porous carbon support, the time for the third deposition step (t_3) was increased from 120 to 210 s. Second, the rotation of

the electrode at a speed of 400 rpm was found to increase the currents of the deposition transients. The latter is probably due to the removal of hydrogen bubbles formed during electrodeposition from the electrode surface, as well as a decrease in the thickness of the diffusion layer. Fig. 4.6 compares the deposition transients registered for Ni electrodeposition on GC and on XC-72/GC surface. As one can see, a much larger amount of Ni is deposited in the latter case, most likely due to an increase in the surface area of the support and, as a consequence, an increase in the number of nucleation sites. The corresponding values of the total deposition charge (including the one related to the HER, which accompanies Ni deposition) were calculated to be 3.6 ± 1.8 and 140 ± 20 mC for GC and XC-72/GC supports, respectively.

An increase in the amount of Ni electrodeposited on a porous carbon support (compared to Ni_{ED}/GC) allowed us to measure the mass of the deposits for several Ni_{ED}/XC-72 samples using the ISP-AES technique (see Section 2.2.6). According to these measurements, faradaic efficiency (under the given conditions) of Ni electrodeposition was estimated to be ca. 35% (confirming the high contribution of the HER currents), while the typical metal loading was calculated to be 42 ± 3 wt.% (with respect to the total mass of the Ni_{ED}/XC-72 catalyst).

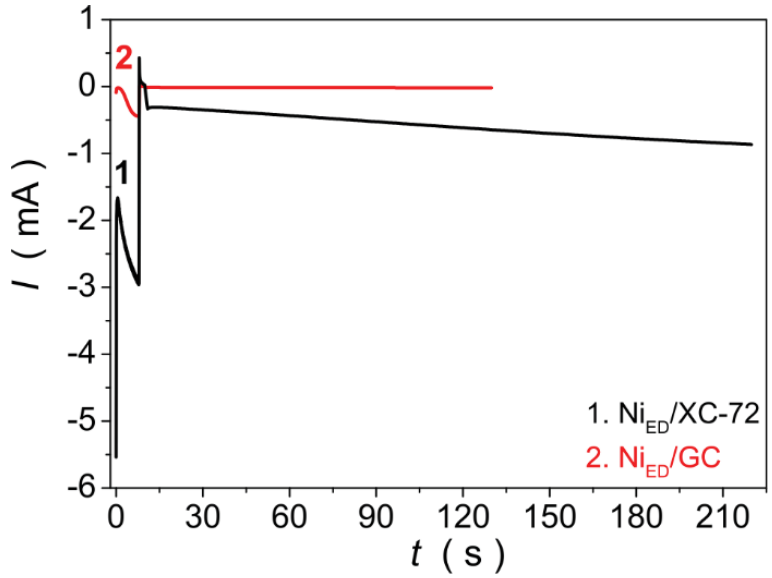

Fig. 4.6 *Nickel deposition transients obtained for Ni_{ED}/XC-72 (curve 1, black) and Ni_{ED}/GC (curve 2, red) electrodes in N_2-saturated 0.01 M $NiSO_4$ + 0.10 M $(NH_4)_2SO_4$ solution at T = 298 K.*

Investigation of the microstructure of Ni_{ED}/XC-72 samples

The microstructure of the metal particles in Ni_{ED}/XC-72 samples was investigated by TEM and STEM techniques. TEM survey images (Fig. 4.7a) revealed a fairly homogeneous distribution of Ni nanoparticles over the surface of XC-72 carbon support, while their surface mean diameter was estimated to be 10 ± 2 nm (under the assumption of the spherical particle shape). Moreover, the high resolution STEM images obtained in bright and dark fields (Figs. 4.7b, c) clearly show the nanostructured nature of Ni nanoparticles, which consist of crystallites of smaller size connected through the intergrain boundaries. The value of the interplanar spacing was calculated to be ca. 0.21 nm, which is consistent with the Ni (111) interplanar distances.

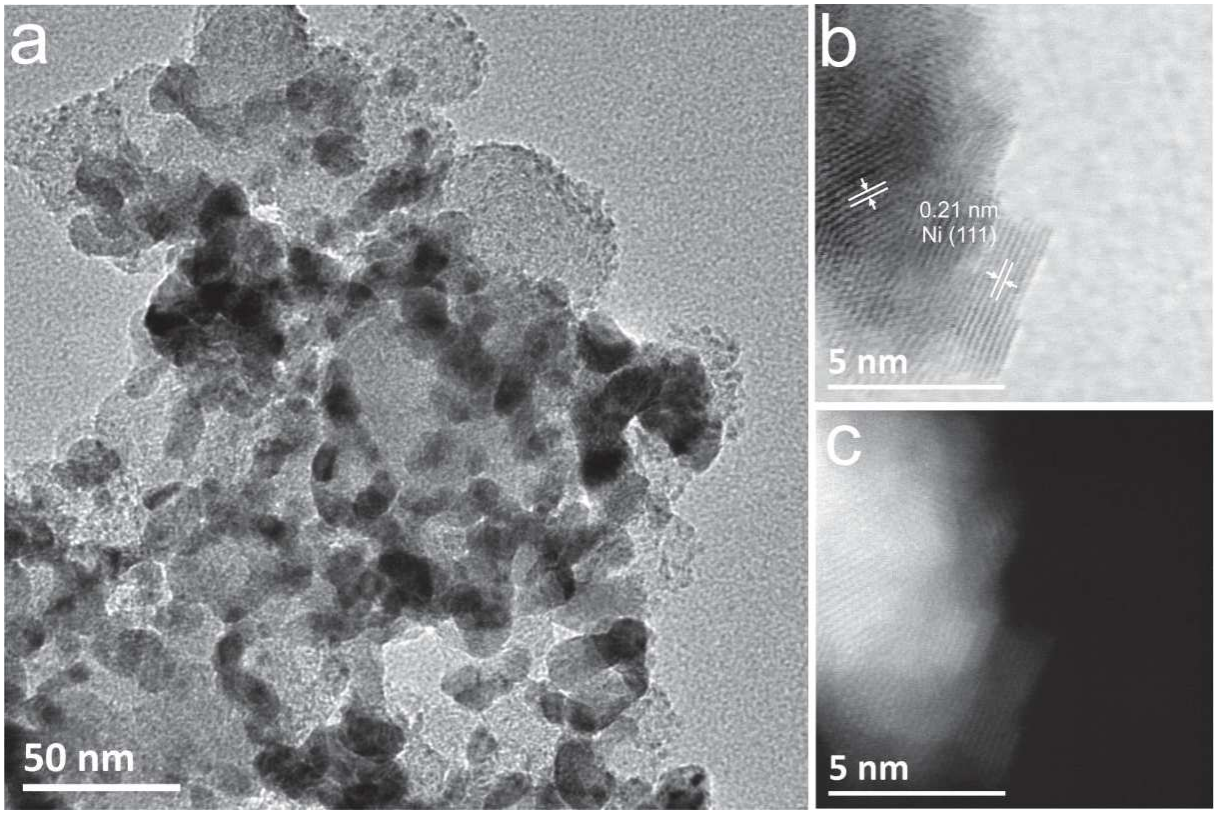

Fig. 4.7 *High resolution TEM (a) and STEM (bright (b) and dark (c) field) images of the Ni_{ED}/XC-72 electrocatalyst.*

Investigation of the surface state of Ni_{ED}/XC-72 samples

As will be shown later, prolonged cycling of the Ni_{ED}/XC-72 electrode in 0.10 M NaOH in the potential range of [-0.06 – 0.40 V] results in significant increase of its

activity in the HOR/HER (see Section 4.3.4). To explain the observed changes, the surface state of the Ni_{ED}/XC-72 electrocatalyst was investigated using XPS before and after such treatment. As it has been noticed in Section 3.2.5, due to *ex situ* character of the measurements, the presence of surface Ni oxides formed during the transfer of the electrodes to the XPS chamber through the air was expected. Because of this, the obtained XP spectra can be used only for comparative analysis of activated and non-activated samples.

The Ni 2p spectra (Fig. 4.8) obtained for Ni_{ED}/XC-72 samples were deconvoluted into three components, namely metallic Ni^0, NiO and $Ni(OH)_2$, using the procedure described for the experiments with the Ni foil (see Section 2.2.3). Analysis of the obtained XP spectra allows one to make several conclusions. First, we found that the surface of non-activated Ni_{ED}/XC-72 sample is oxidized to a higher extent compared to that of non-activated Ni foil. This is likely related to smaller size of Ni particles in Ni_{ED}/XC-72 sample and their defective structure, both known to facilitate adsorption of oxygen containing species [293]. Second, continuous cycling of the Ni_{ED}/XC-72 electrode in 0.10 M NaOH leads to a further decrease in the contribution of metallic Ni^0 component to the XP spectra (Fig. 4.8b). As for the Ni foil, the surface of the freshly prepared Ni_{ED}/XC-72 particles is predominantly covered with $Ni(OH)_2$, which can be presumably attributed to the α-form, given the possibility of its reduction under the conditions of electrochemical measurements (see Section 4.3.2). At the same time, an increase in the amount of $Ni(OH)_2$ on the electrode surface after prolonged cycling in the potential range of [-0.06 – 0.40 V] appears to be likely due to the formation of irreversible β-$Ni(OH)_2$. This is in agreement with a decrease of S_{EC} for the Ni_{ED}/XC-72 electrocatalyst (Table 4.3). The presence of NiO in the Ni2p spectra is likely associated with its formation during the transfer of the samples to the XPS entry chamber through the air. The available data are insufficient to unambiguously explain the greater contribution of the oxide to the XP spectrum of the non-activated sample.

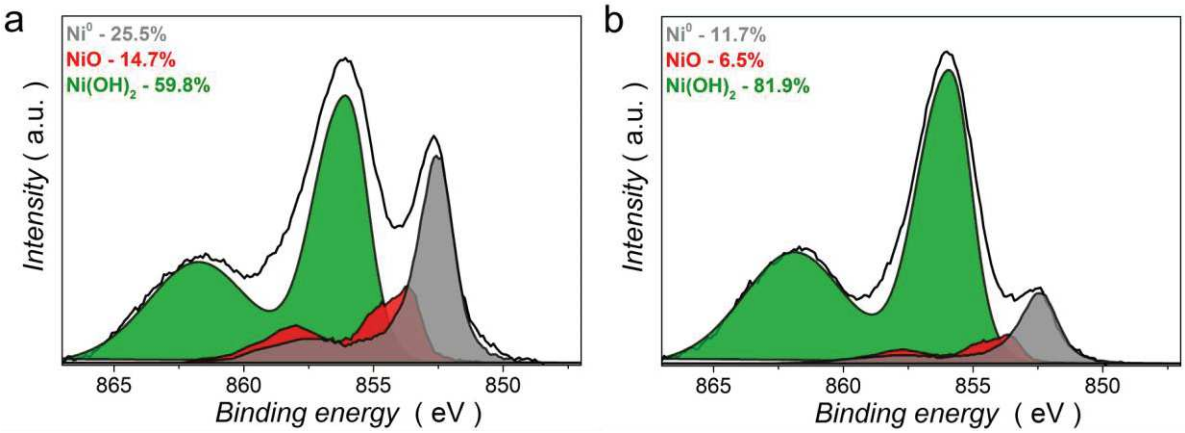

Fig. 4.8 *X-Ray photoelectron Ni $2p_{3/2}$ spectra obtained for non-activated Ni_{ED}/XC-72 (a) before and (b) after cycling of the electrode in the potential interval of [-0.06 – 0.40 V] at 0 take-off angle. Spectra were curve-fitted with Ni^0 (gray), NiO (red) and $Ni(OH)_2$ (green) components, their resulting atomic concentrations are indicated in corresponding panels. The curve-fitting procedure is described in Section 2.2.3.*

4.3.2. Electrochemical properties of Ni_{ED}/ XC-72 electrocatalysts

Fig. 4.9a shows CVs registered for freshly prepared non-activated Ni_{ED}/XC-72 sample just after its immersion in N_2-saturated 0.10 M NaOH. Unlike the previously studied samples, only a small cathodic peak was observed in the first scans of the CVs. Besides, much smaller value of the open-circuit potential was obtained for non-activated Ni_{ED}/XC-72 (0.1 – 0.15 V) in comparison with either non-activated Ni_{ED}/GC particles or non-activated polycrystalline Ni rod (0.4 – 0.5 and 0.2 – 0.3 V, respectively). The observed lower degree of oxidation of the surface of Ni_{ED}/XC-72 during the electrode transfer to the electrochemical cell with 0.1 M NaOH (the procedure usually took less than 15 s) might be explained by porous structure of the sample. As a result, only Ni particles located on the outer surface of the carbon support are accessible to the oxygen from air. The apparent contradiction with the results of XPS measurements then may be reconciled by taking into account the small depth of the XPS analysis (< 10 nm), according to which oxidized Ni particles located at the external surface of carbon support mostly contribute to the XP spectra. At the same time, Ni particles within the pores of the XC-72 carbon are also available for electrochemical measurements. On the second scan of the CVs the typical anodic (a_1)

and cathodic (c_1) peaks can be observed (Fig. 4.9a). It should be noted that due to considerable values of the current on Ni_{ED}/XC-72 samples, the potentials of the CVs were corrected by the Ohmic drop, which resulted in a significant change of the limits in comparison with the applied values of [-0.20 – 0.40 V].

Fig. 4.9b shows the comparison of CVs obtained for the non-activated Ni_{ED}/XC-72 and XC-72/GC (electrode before the electrodeposition of Ni), after normalization of the currents to the geometric surface area of the GC electrode. Due to high metal loading on the surface of XC-72 support (42 ± 3 wt.%), the currents originating from the carbon support were found to be insignificant compared to those corresponding to the electrochemical processes on the surface of Ni nanoparticles. Therefore the carbon contribution was not taken into account in further discussions. In addition, comparison of CVs registered for non-activated Ni_{ED}/GC and Ni_{ED}/XC-72 (Fig. 4.9b) confirms deposition of significantly larger amount of Ni on the surface of porous XC-72 support, than on the bare GC surface.

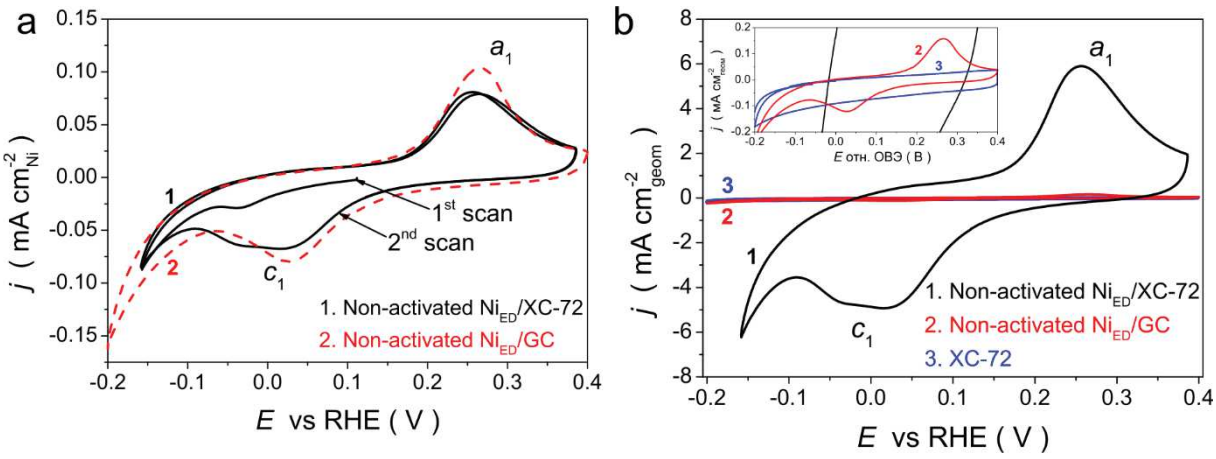

Fig. 4.9 *CVs for non-activated Ni_{ED}/XC-72 (curve 1, black), Ni_{ED}/XC-72 (curve 2, red) and XC-72/GC (curve 3, blue) obtained in N_2-saturated 0.10 M NaOH at $v = 20\ mV \cdot s^{-1}$. The currents are normalized to (a) S_{EC} or (b) S_{geom} of GC electrode.*

In order to inspect the influence of the partial oxidation of the surface of Ni_{ED}/XC-72 nanoparticles on their electrochemical and electrocatalytic properties, a Ch activated Ni_{ED}/XC-72 samples (i. e. measured after chemical oxidation of freshly prepared sample under air for typically ca. 24 h. (*cf.* Section 2.3.4.1)) were studied. Fig. 4.10a shows CVs obtained for the Ni_{ED}/XC-72 sample taken from air. The open-

circuit potential measured for this electrode after its immersion into the electrolyte was found to be between 0.60 and 0.70 V, thus similar to the values measured for Ch activated Ni_{ED}/GC. Cycling of the electrode in the potentials range of [-0.06 – 0.40 V] allows one to observe the typical evolution of CVs (Fig. 4.10a), which was described above. Similarly to Ch activated Ni_{ED}/GC, *partial* reduction of the surface of the Ch activated Ni_{ED}/XC-72 nanoparticles results in a current plateau in the potential region of [0 – 0.20 V], which is absent for non-activated samples (Fig. 4.10b), instead of well-defined single peak a_2. In addition, Fig. 4.10b shows the CV registered for freshly prepared Ni_{ED}/XC-72 electrode after its prolonged cycling in the potential interval of [-0.06 – 0.40 V] in H_2 atmosphere (*cf.* Section 4.3.4). The shape of the CV was found to be essentially similar to that obtained for Ch activated Ni_{ED}/XC-72, which indicates a partial oxidation of the surface of Ni particles after such treatment, being in agreement with the XPS measurements (see Section 4.3.1).

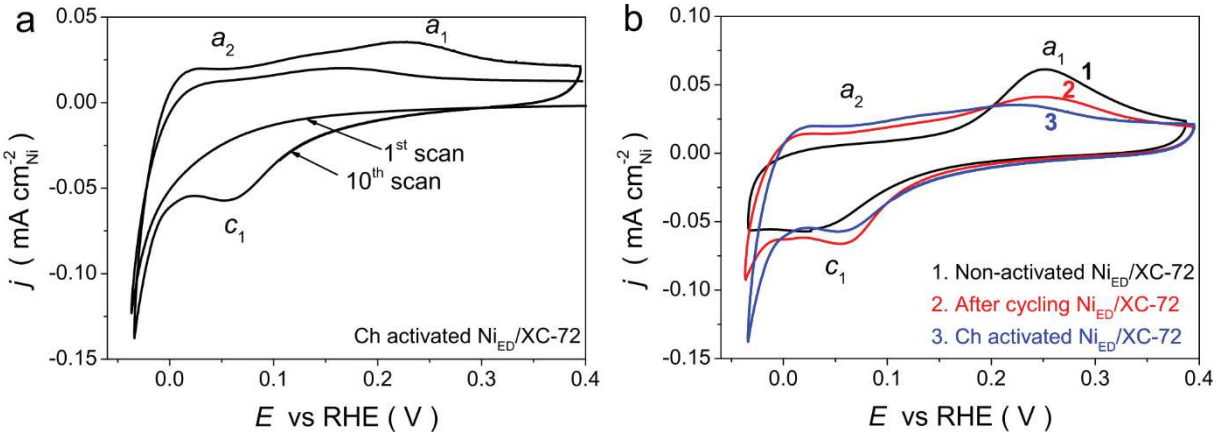

Fig. 4.10 *(a) CVs obtained for Ch activated Ni_{ED}/XC-72 just after an immersion of the electrode in N_2-saturated 0.10 M NaOH at v = 20 mV·s^{-1}; (b) Comparison of the CVs registered for non-activated Ni_{ED}/XC-72 electrode before (curve 1, black) and after (curve 2, red) cycling in the potential interval of [-0.06 – 0.40 V] and Ch activated (curve 3, blue) Ni_{ED}/XC-72 electrode.*

4.3.4. Kinetics of the HOR/HER on Ni_{ED}/XC-72 electrocatalysts

Fig. 4.11a shows CVs obtained for Ni_{ED}/XC-72 electrocatalysts in H_2 atmosphere at v = 5 mV·s^{-1}. Unlike either polycrystalline Ni rod or Ni_{ED}/GC, the currents registered for Ni_{ED}/XC-72 samples were found to depend on the rotation rate of the electrode (Fig. 4.12). The latter indicates the influence of mass transfer of hydrogen to the

electrode surface. This difference in the behavior of Ni rod and Ni_{ED}/GC particles, on the one side, and Ni_{ED}/XC-72 electrode, on the other side, is related to much larger amount of Ni in the latter case. Therefore, the exchange currents were determined by rotating of the electrode at 1600 rpm. The specific electrocatalytic activities of Ni_{ED}/XC-72 samples normalized to either S_{EC} or mass of Ni are listed in Table 4.3.

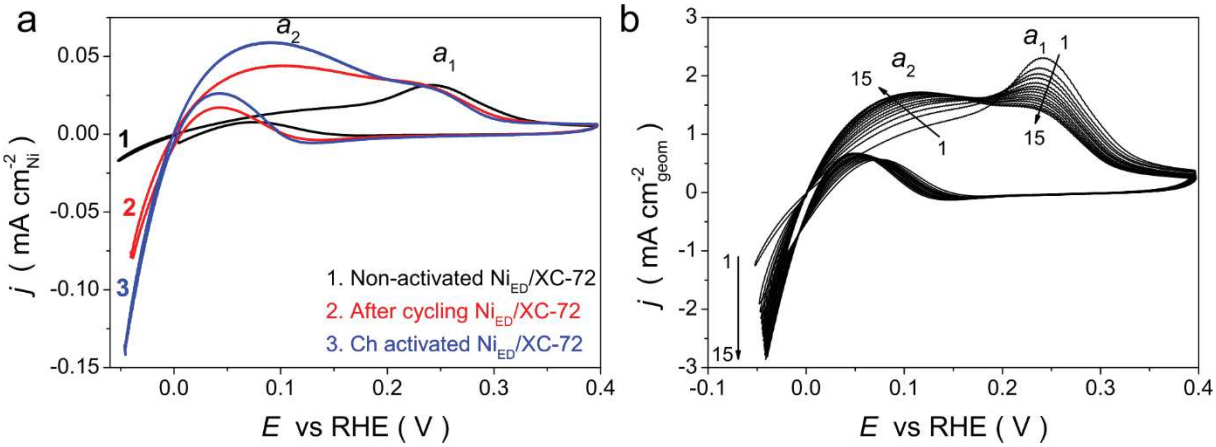

Fig. 4.11 *(a) Cyclic voltammograms for non-activated (curve 1, black), EC activated (curve 2, red) and Ch activated (curve 3, blue) Ni_{ED}/XC-72 registered in H_2-saturated 0.1 M NaOH at v = 5 mV/s and ω = 1600 rpm; (b) evaluation of cyclic voltammograms obtained for non-activated Ni_{ED}/XC-72 during continuous cycling in the potential interval of [-0.06 – 0.40 V] at v = 5 mV s^{-1} and ω = 1600 rpm.*

It was found that specific surface-weighted activity of freshly prepared Ni_{ED}/XC-72 is in line with the values obtained for freshly prepared Ni_{ED}/GC and polished Ni rod (Appendix 1), despite the difference in the size of Ni particles deposited on the surface of GC and XC-72/GC support (25 ± 5 nm and 10 ± 2, respectively). This observation confirms the earlier assumption that the specific activity of Ni catalysts in the HOR/HER does not depend on their morphology in the case of (essentially) reduced surface, at least at a particle size of more than 10 nm. At the same time the size of Ni particles and/or their nanostructure affect the process of oxidation of electrodeposited samples and, probably, stability of formed Ni oxides against reduction. As a result, specific surface-weighted activity of Ch activated Ni_{ED}/XC-72 is 2 times as high as the activity of Ch activated Ni_{ED}/GC (Appendix 1). Furthermore, the tendency of Ni nanoparticles towards oxidation resulted in

continuous change of the CV shape of non-activated Ni_{ED}/XC-72, which is accompanied by an increase of its HOR/HER activity, during cycling in the potential interval of [-0.06 – 0.40 V] (Fig. 4.11b). After ca. 15 scans the CV profile is stabilized, likely suggesting that a steady-state between Ni metal sites and Ni (hydr)oxide sites on the surface of the Ni_{ED}/XC-72 catalyst is reached under these conditions. The resulting electrode was named as "After cycling". The corresponding increase of the activity in the HOR/HER (compared to non-activated Ni_{ED}/XC-72) was found to be ca. 4.7 and ca. 2.5 times, if normalizing by the surface area and mass of Ni, respectively (Table 4.3).

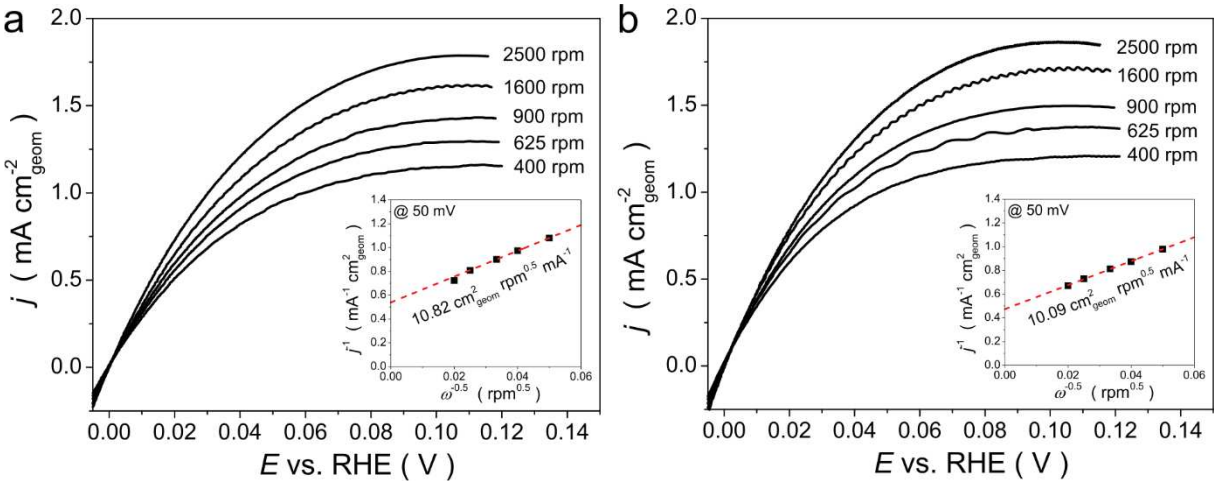

Fig. 4.12 *Polarization curves of the HOR obtained using rotating disk electrode in H_2-saturated 0.10 M NaOH at v = 5 mV·s^{-1} and various rotation speeds for (a) Ch activated Ni_{ED}/XC-72 electrode and (b) Ni_{ED}/XC-72 electrode after prolonged cycling. Insets show the Koutecky-Levich plot at overpotential of 50 mV.*

Finally, it is interesting to compare electrocatalytic activities of Ni_{ED}/XC-72 samples in the HOR with the values reported for PGM-free catalysts as well as finely dispersed Pd/C and Pt/C catalysts (Appendix 1). It was found that the specific surface-weighted activity of the activated Ni_{ED}/XC-72 nanoparticles is either comparable (for the sample obtained after cycling) or exceeds (for the Ch activated sample) the values reported for the best PGM-free catalysts of this process. Besides, the mass-weighted activity of non-activated Ni_{ED}/XC-72 electrocatalyst is more than 1.5 times higher compared to the values reported for state-of-the-art Ni/N-CNT (3.5 A g_{Ni}^{-1}, Appendix 1), which can be attributed to the small size of Ni nanoparticles (10 ± 2 nm) and,

likely, their special nanostructured nature. Moreover, activation of the Ni_{ED}/XC-72 electrocatalyst by *partial* oxidation of its surface allows to further improve its specific mass-weighted activity up to ca. 14 and ca. 22 A g_{Ni}^{-1} for the sample obtained after cycling and Ch activated sample, respectively. The mass-weighted activity of the Ch activated Ni_{ED}/XC-72 is just 1.7 and 16 times lower compared to commercial 20% Pd/C (Premetek Co) and 46% Pt/C (TKK) catalysts, respectively. Finally, kinetic current densities of the HOR were calculated for the activated Ni_{ED}/XC-72 samples at an overpotential of 50 mV in accordance with the eq. 2.5 (see Section 2.3.4.3). The obtained values were found to be about 3.5 times higher than the values reported for the best PGM-free Ni/N-CNT catalyst described in the literature (Appendix 1).

Table 4.3 *The values of the specific electrocatalytic activities in the HOR/HER obtained for Ni_{ED}/XC-72 particles after various pre-treatments of the electrode surface*

Catalysts	S_{EC} / cm^2	Exchange current density		Kinetic current densities	
		j_0 / μA·cm$^{-2}_{Ni}$	i_o / A g_{Ni}^{-1}	i_k^{50mV} / A g_{Ni}^{-1}	j_k^{50mV} / μA cm_{Ni}^{-2}
Non-activated Ni_{ED}/XC-72	13.0 ± 1.1	6.2 ± 0.6	5.7 ± 0.2	-	-
After cycling Ni_{ED}/XC-72	6.1 ± 1.4	29 ± 7	14.2 ± 3.1	27.8 ± 1.4	50 ± 4
Ch activated Ni_{ED}/XC-72	4.9 ± 0.9	56 ± 10	22.4 ± 4.3	32.1 ± 4.8	83 ± 12

4.4. Conclusions of Chapter 4

This work shows that using electrodeposition technique it is possible to synthesize nanostructured Ni particles of small size deposited on the surface of either smooth (glassy carbon) or porous (Vulcan XC-72) support. The main findings, namely the change of the shape of cyclic voltammograms and an increase of the specific activity of Ni in the HOR/HER observed for massive polycrystalline Ni after partial oxidation of its surface, were also detected in the case of electrodeposited Ni particles of different diameters. Hence we conclude that the observed changes are universal and do not depend on the morphology of the Ni catalyst.

Carbon supported 40% Ni_{ED}/XC-72 electrocatalyst prepared by electrodeposition demonstrates mass-weighted activity in the HOR, which is 6 times as high as the activity of the best PGM-free Ni/N-CNT catalyst reported up to now. This high activity might be presumably attributed to the low size of Ni particles, their defective nature as well as the synergistic effect between metal Ni sites and nearby "irreversible" oxide species present on the surface of the Ni_{ED}/XC-72 electrocatalyst. Taking into account an insignificant difference between the mass-weighted activity of the activated Ni_{ED}/XC-72 catalyst and the commercial Pd/C catalyst, the sample obtained in this work can be considered as a promising alternative to noble metals at the anode of AMFC.

Chapter 5: Bimetallic Ni-based electrocatalysts

5.1. Introduction

Analysis of the literature presented in Section 1.3.3 shows that many bi- and polymetallic Ni-based catalysts have been investigated in the HER, demonstrating an increase of the catalytic activity and, importantly, stability in comparison with monometallic Ni electrocatalysts. However only few materials have been studied in the potential interval of the HOR in alkaline media [28,192,195,294]. The rapid development of AMFCs and the need to replace Pt catalysts with inexpensive PGM-free analogues stimulate the interest in the investigation of bimetallic Ni-based catalysts for the anodes of AMFC. Besides, despite a significant progress during the past decades, the question about the optimal composition in bimetallic NiM system still remains open even for the cathodic *hydrogen evolution* process.

In this chapter we analyze the carbon supported NiCu/C and NiMo/C electrocatalysts in alkaline media with the aim to determine the effect of Cu and Mo on the electrochemical properties of Ni, as well as its activity in the HOR. The positive effect of Cu on the activity of Ni in the HER has been already shown in the literature with the use of electrodeposited films of various compositions [201–203]. However the carbon supported metal particles have not been studied in the HOR/HER yet. Besides, the optimum Ni:Cu ratio for the anodic *hydrogen oxidation* has not been known. According to the literature, addition of Mo allows one to significantly increase the activity of Ni in the HER [211,212,214,216,217,220]. However the origin of this catalytic enhancement is still not fully understood. Besides, there is no information concerning the activity of carbon supported NiMo/C electrocatalysts in the HOR.

5.2. Bimetallic NiCu/C electrocatalysts

Monometallic Ni/C and bimetallic $Ni_{1-x}Cu_x$/C catalysts with $0.05 \leq x \leq 0.50$ prepared by traditional wetness impregnation technique (as described in Section 2.1.3) were studied with the aim to inspect the effect of Cu on the activity of Ni in the HOR/HER and define the optimum Ni:Cu ratio. However, as will be shown below, the resulting samples had a high degree of heterogeneity, which impede the estimation of the optimum Ni:Cu ratio. To obtain more homogeneous samples the synthetic procedure was modified by replacing the step of vacuum drying with freeze-drying (lyophilization). For the second series of catalysts (for convenience, denoted as $Ni_{1-x}Cu_x$/C (lyo)), the Cu content was varied in a narrower range ($0.02 \leq x \leq 0.10$) near the maximum activity found for $Ni_{1-x}Cu_x$/C catalysts. As will be shown in this section, the main conclusions are valid for both series of samples.

5.2.1. Investigation of the NiCu/C electrocatalysts by physicochemical techniques

Morphology and dispersion of Ni/C and NiCu/C particles

TEM analysis of the Ni/C and $Ni_{1-x}Cu_x$/C electrocatalysts synthesized using wetness impregnation technique in conventional manner revealed high heterogeneity of the metal particles with the size ranging from 1 to 100 nm in size (Fig. 5.1a). Nevertheless, comparison of the TEM data for monometallic Ni/C and bimetallic $Ni_{1-x}Cu_x$/C samples allowed us to draw several important conclusions. It was found that the surface of "large" particles (d_{TEM} > ca. 20 nm) is covered by NiO layer independent of the catalyst composition. However the thickness of the oxide shell decreases in the presence of Cu (Fig. 5.2). Moreover, while "small' particles (d_{TEM} < 10 nm) in the monometallic Ni/C sample are fully oxidized, in $Ni_{1-x}Cu_x$/C catalysts they remain in the metallic state (Fig. 5.2b).

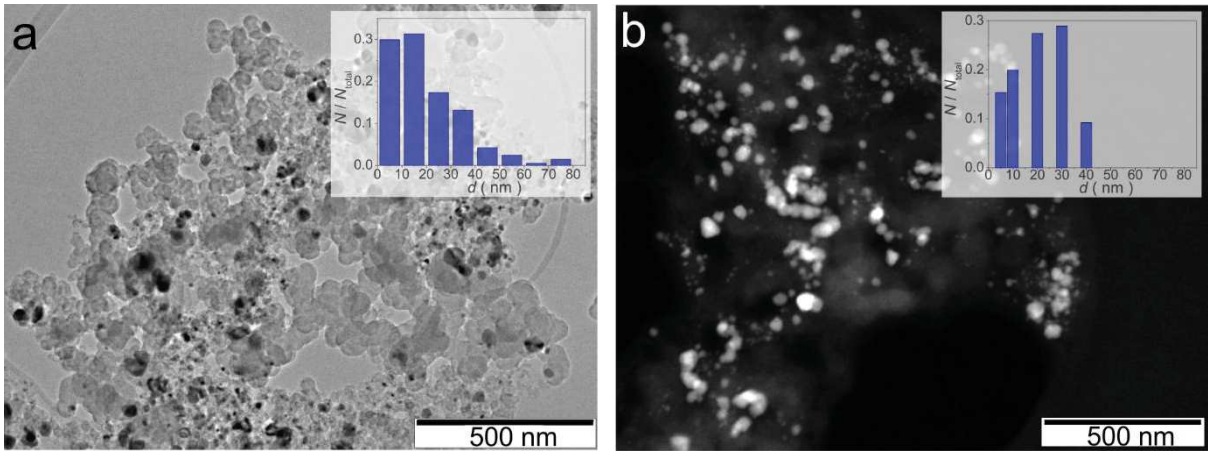

Fig. 5.1 *TEM images of the $Ni_{0.95}Cu_{0.05}$/C catalysts prepared by wetness impregnation technique in either conventional manner (a) or with the use of lyophilization (b). Insets show corresponding particles size distribution.*

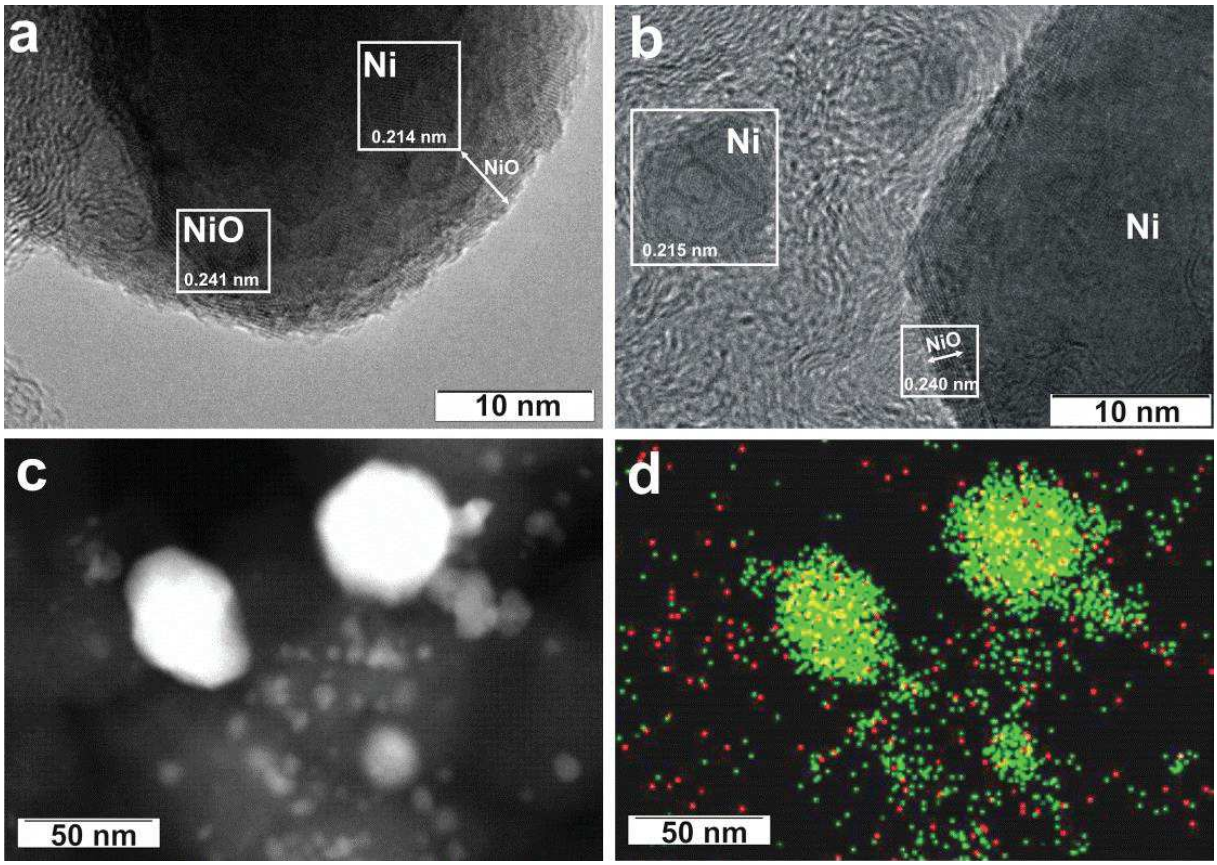

Fig. 5.2 *HRTEM images of the (a) Ni/C and (b) $Ni_{0.95}Cu_{0.05}$/C catalysts; (c) HAADF-STEM image of $Ni_{0.95}Cu_{0.05}$/C catalyst and (d) corresponding to it elemental map (Ni – green and Cu – red).*

Elemental mapping using energy dispersive X-ray spectroscopy revealed that the composition of bimetallic particles is also inhomogeneous and depends on the particle

size (Table 5.1). The highest Cu content was detected in small particles with $d_{TEM} < 5$ nm, while large particles ($d_{TEM} > 20$ nm) mostly consist of Ni. This observation allows one to suppose that the presence of metal particles with $d_{TEM} < 10$ nm in bimetallic $Ni_{1-x}Cu_x/C$ samples is probably due to significant content of Cu in them.

Modification of the synthetic procedure by the use of freeze-drying instead of traditional drying in vacuum allows one to obtain samples with a narrower particle size distribution (Fig. 5.1b) and, in addition, more homogeneous composition (Table 5.1).

Table 5.1 *Approximate fraction of Ni in the particles of different size determined for $Ni_{1-x}Cu_x/C$ on the basis of the analysis of STEM images in dark field*

Catalyst	Ni fraction (at. %) in particles depending on their diameter d_{TEM} (nm)		
	$d_{TEM} < 5$	$5 \le d_{TEM} \le 20$	$d_{TEM} > 20$
$Ni_{0.95}Cu_{0.05}$	14-18	62-99[g]	98-99
$Ni_{0.90}Cu_{0.10}$	-[h]	10-83g	71-89
$Ni_{0.70}Cu_{0.30}$	-h	2-6	83-89
$Ni_{0.50}Cu_{0.50}$	-h	2-14	75-83
$Ni_{0.95}Cu_{0.05}$ (lyo)	92	93	94

Crystalline structure of Ni/C and NiCu/C particles

XRD patterns obtained for selected $Ni_{1-x}Cu_x/C$ catalysts and for the monometallic Ni/C reference are displayed in Fig. 5.3. It was found that despite oxidation of the samples under ambient conditions (as it is evidenced by TEM and XPS measurements), no diffraction peaks of nickel oxide/hydroxide phases were detected. This observation suggests that Ni (hydr)oxide phase is amorphous or consists of either very small or highly distorted crystallites. Analysis of the XRD patterns also revealed some differences in the structure of bimetallic $Ni_{1-x}Cu_x/C$ and $Ni_{1-x}Cu_x/C$ (lyo) catalysts. While the cell parameter of metallic Ni phase in the first series of samples (Ni/C and $Ni_{1-x}Cu_x/C$) was $a = 3.524$ Å, which agrees well with the tabulated data [ICDD PDF-2 #00-004-0850], in the second series of the samples (Ni_{1-}

[g] Ni fraction strongly increases with the particle size in the interval from 5 to 20 nm
[h] Ni fraction below the detection limit

$_x$Cu$_x$/C (lyo)) it slightly exceeded the tabulated values (a = 3.527(2) Å). This increase of the lattice parameter of Ni is manifested in a small but measurable shift of the 220 reflection (see inset in Fig. 5.3b). Consequently, an enlarged cell parameter suggests formation of Ni-Cu alloy particles and according to the Vegard's law corresponds to ca. 5 at.% Cu content for Ni$_{0.95}$Cu$_{0.05}$/C (lyo) and Ni$_{0.90}$Cu$_{0.10}$/C (lyo) samples. The lower Cu content than the nominal composition of the Ni$_{0.90}$Cu$_{0.10}$/C (lyo) could be tentatively attributed to the Cu segregation on the surface of the particles due to its smaller surface energy, as it was found in a number of experimental and computational studies [295–297].

Based on the XRD analysis we conclude that drying of the catalyst precursors in vacuum favors Ni and Cu phase separation (Fig. 5.3a), while the use of freeze-drying results in formation of more homogeneous NiCu alloy particles. The average size of Ni crystallites estimated from the (111) peak broadening using the Scherrer equation varies between 11 and 17 nm depending on the catalyst composition.

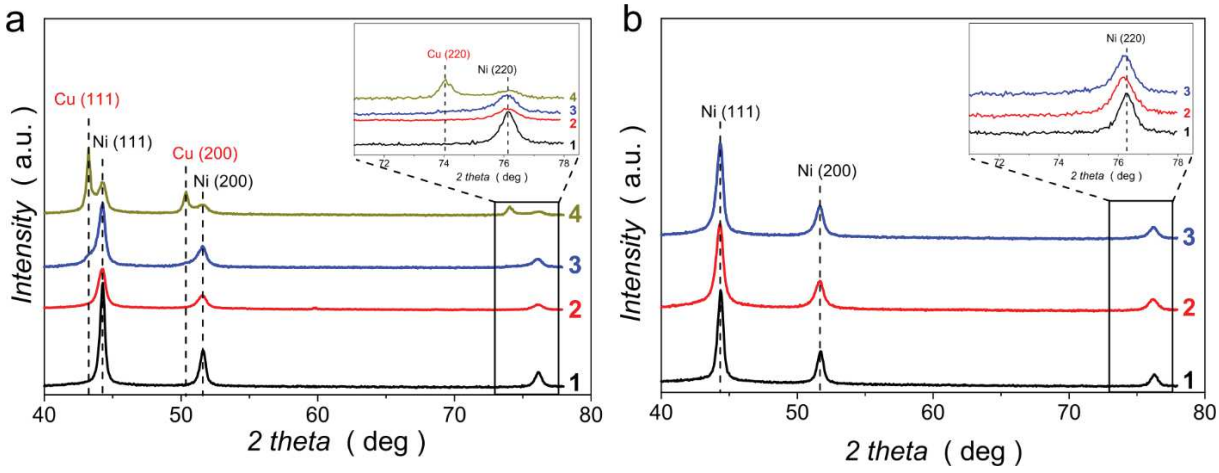

Fig. 5.3 *XRD patterns for (a) Ni/C (1), Ni$_{0.95}$Cu$_{0.05}$/C (2), Ni$_{0.80}$Cu$_{0.20}$/C (3), Ni$_{0.50}$Cu$_{0.50}$/C (4) and (b) Ni/C (lyo) (1), Ni$_{0.95}$Cu$_{0.05}$/C (lyo) (2), Ni$_{0.90}$Cu$_{0.10}$/C (lyo) (3). Insets on the panels zoom into selected areas corresponding to the Cu (220) and Ni (220) diffraction peaks.*

Surface state of Ni/C and NiCu/C particles

As it has been shown in previous chapters, the surface state of Ni electrocatalysts might significantly affect their electrochemical and electrocatalytic properties. XPS analysis of selected Ni$_{1-x}$Cu$_x$/C catalysts showed that copper is always present in

metallic state (Fig. 5.4). Meanwhile, the Ni 2p spectra exhibit several overlapping peaks corresponding to Ni^0, NiO and $Ni(OH)_2$ components (Fig. 5.5). XP spectra deconvolution clearly demonstrates that increase of the nominal Cu fraction in the catalysts prevents their oxidation, thereby enhancing the metallic Ni^0, and reducing the NiO and $Ni(OH)_2$ contribution in the near-surface region of the particles. This observation confirms conclusions derived from the TEM analysis.

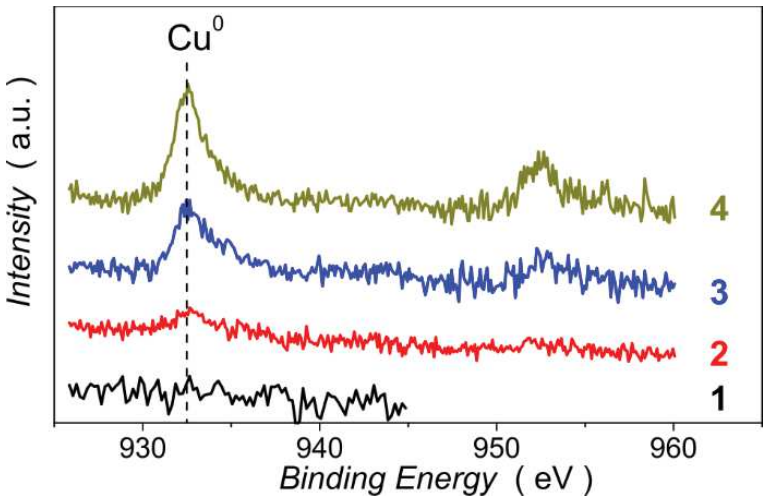

Fig. 5.4 *X-Ray photoelectron Cu 2p spectra for the Ni/C (1, black), $Ni_{0.95}Cu_{0.05}$/C (2, red), $Ni_{0.90}Cu_{0.10}$/C (3, blue) and $Ni_{0.80}Cu_{0.20}$/C (4, dark yellow) catalysts at 0 take-off angle.*

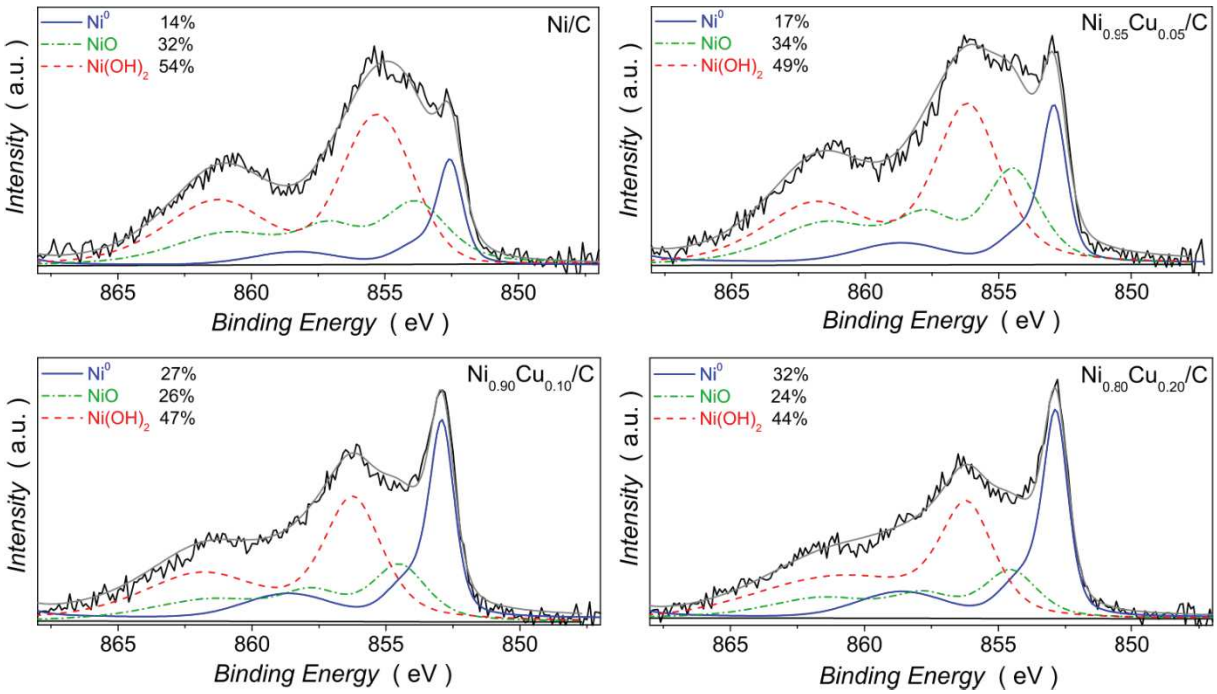

Fig. 5.5 *X-Ray photoelectron Ni $2p_{3/2}$ spectra for the Ni/C, $Ni_{0.95}Cu_{0.05}$/C, $Ni_{0.90}Cu_{0.10}$/C and $Ni_{0.80}Cu_{0.20}$/C catalysts at 0 take-off angle. Spectra were curve-fitted with Ni^0 (solid line, blue), NiO (dash-dotted line, green) and $Ni(OH)_2$ (dashed line, red) components, their resulting atomic concentrations are indicated in the panels. The curve-fitting procedure is described in Section 2.2.3.*

5.2.2. Electrochemical properties of NiCu/C electrocatalysts

Despite the fact that utilization of freeze-drying allows one to prepare more homogeneous catalysts, the electrochemical behavior of the $Ni_{1-x}Cu_x$/C and $Ni_{1-x}Cu_x$/C (lyo) samples was found to be essentially similar. Therefore in this section we preferentially discuss the first series of samples, in which the Cu content varied over a wider range.

In accordance with the results of TEM and XPS studies, electrochemical measurements also showed that the surface of Ni/C and $Ni_{1-x}Cu_x$/C catalysts is largely oxidized. The latter is evidenced in particular by the value of the open-circuit potential (0.75 – 0.85 V), measured just after the immersion of the electrode in the electrolyte. That is why, prior to the main measurements, the electrode surface was subjected to electrochemical reduction as described in Section 2.3.4.1. However, the presence of some amount of unreduced β-$Ni(OH)_2$ on the surface of Ni/C and $Ni_{1-x}Cu_x$/C catalysts after such treatment cannot be excluded.

CVs of the Ni/C and $Ni_{1-x}Cu_x$/C catalysts obtained in Ar-saturated 0.10 M NaOH after electrochemical reduction (Fig. 5.6a) exhibit anodic (a_1) and cathodic (c_1) peaks typical of Ni, which have been already described in previous chapters. For the $Ni_{0.50}Cu_{0.50}$/C sample CVs in inert atmosphere exhibited small currents, only slightly exceeding those of the carbon support. We tentatively explain this by blocking of the Ni active sites by Cu atoms, which have a tendency to segregate to the surface of NiCu particles [295–297]. In the case of monometallic Ni/C sample, low currents (compared to bimetallic samples (Fig. 5.6b)) are likely due to, first, smaller specific surface area of Ni (see below) and, second, its stronger oxidation (see Fig. 5.5). It is worth to note, that the anodic currents in the potential region of the peak a_2 described above for partially oxidized Ni samples (see Chapters 3 and 4) were observed in the CVs of some $Ni_{1-x}Cu_x$/C catalysts along with the peak a_1. Their relative contribution to the overall anodic currents is the highest for the $Ni_{0.95}Cu_{0.05}$/C catalyst.

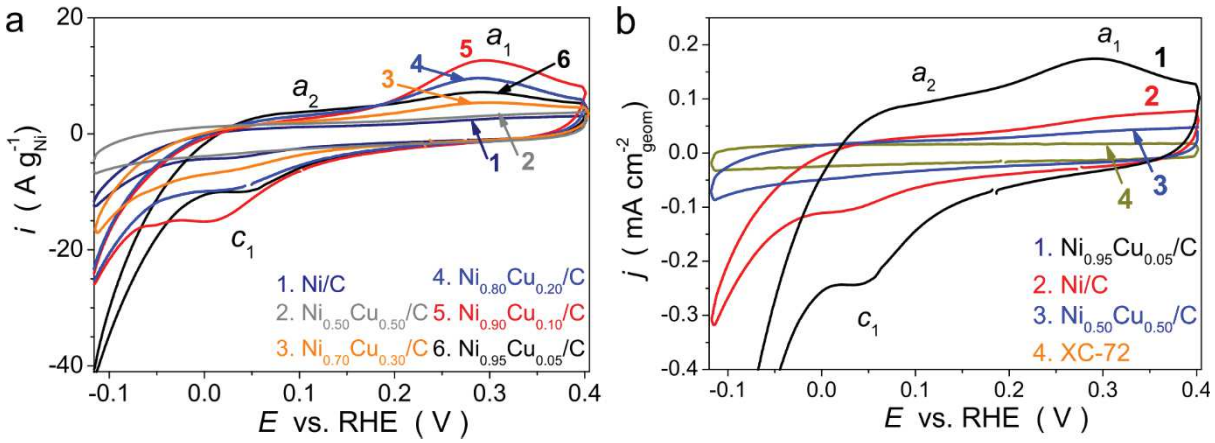

Fig. 5.6 *CVs for Ni/C and $Ni_{1-x}Cu_x$/C obtained in Ar-saturated 0.10 M NaOH at $v = 20\ mV \cdot s^{-1}$ and $T = 298$ K. For comparison, the panel (b) shows the CV of the XC-72 support, the amount of which on the surface of GC electrode was similar to that in the supported catalysts. The currents on the CVs are normalized by either (a) the mass of Ni or (b) geometric surface area of the GC electrode.*

Estimation of the Ni surface area

The surface area of Ni in monometallic Ni/C and bimetallic $Ni_{1-x}Cu_x$/C catalysts was determined using two approaches: (i) by gas-phase CO chemisorption performed just after (before their passivation) the preparation of the samples (S_{CO}, the procedure is described in Section 2.2.5) and (ii) by measuring of the anodic charge of the CVs

(S_{EC}) obtained in the potential range of [-0.02 – 0.40 V] or [-0.12 – 0.40 V] at a sweep rate of 20 $mV \cdot s^{-1}$ after subtraction of the charge related to the XC-72 carbon support. Comparison of the obtained values is shown on the Fig. 5.7. First, we note that all methods essentially provide similar values for the specific surface area of Ni. However, depending on the negative potential limit, the values of S_{EC} are either slightly inferior (for E_C = - 0.02 V) or slightly superior (for E_C = - 0.12 V) to those of S_{CO}. We believe that this discrepancy is caused by an underestimation of the S_{EC} values in the first case (due to an incomplete reduction of formed Ni (hydr)oxide) or their overestimation in the second case (due to a contribution of currents corresponding to the oxidation of formed Ni hydrides), as was shown in Section 3.2.1. Nevertheless, regardless the method of the determination, the comparison of the data in Fig. 5.7 allows to make several conclusions. First, addition of Cu in a small fraction allows one to increase specific surface area of Ni, while it decreases at high Cu content. Second, higher values of S_{CO} were obtained for the samples prepared using freeze-drying. Considering the uncertainties in the values of S_{EC} obtained at different potential limits, in what follows we use S_{CO} values, when discussing the kinetics of the HOR/HER on NiCu/C catalysts.

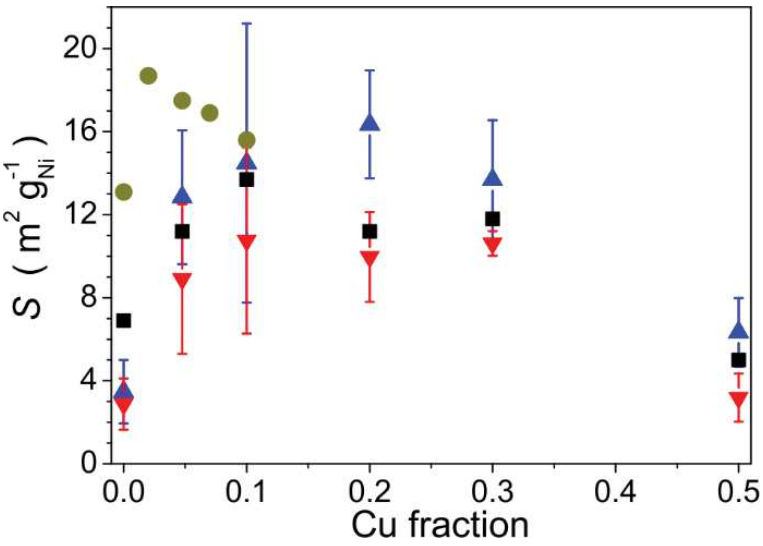

Fig. 5.7 *Comparison of specific surface areas of Ni in $Ni_{1-x}Cu_x/C$ samples, derived from the CO-chemisorption measurements, S_{CO} (black squares) and from the electrochemical measurements, S_{EC}, based on the CVs registered in the potential interval of [-0.02 – 0.40 V] (down triangles, red) and [-0.12 – 0.40 V] (up triangles, blue) at v = 20 mV·s^{-1}. Dark yellow circles refer to $Ni_{1-x}Cu_x/C$ (lyo) as measured using CO-chemisorption.*

5.2.3. Kinetics of the HOR/HER on NiCu/C electrocatalysts

Electrocatalytic activity in the HOR/HER as a function of the catalyst composition

To measure the catalytic activity of the Ni/C and $Ni_{1-x}Cu_x/C$ catalysts in the HOR/HER, CVs were registered in H_2-purged 0.10 M NaOH at $v = 2$ mV·s^{-1} (Fig. 5.8a). The catalytic activities were compared in terms of exchange currents, which, considering low activity of Cu in the HOR/HER [23,203], were normalized either to the mass (i_0) or to the surface (j_0) of Ni (Figs. 5.8b and c).

Inspection of the Fig. 5.8 allows us to conclude that an addition of small amount of Cu ($0.05 \leq x \leq 0.30$) leads to a notable increase of the mass-weighted activity of Ni in the HOR/HER. There are two factors leading to the enhancement, namely (i) an increase of the specific surface area of Ni (Figs. 5.7), and (ii) an increase of the specific (surface-weighted) electrocatalytic activity (Fig. 5.8b). Besides, we note that preparation of more homogeneous $Ni_{1-x}Cu_x/C$ (lyo) catalysts allowed us, first, to confirm that the maximum activity in the HOR/HER is achieved at 5 at% of Cu

fraction in the catalyst and, second, enhance the mass-weighted activity due to an increase of the dispersion of the active component.

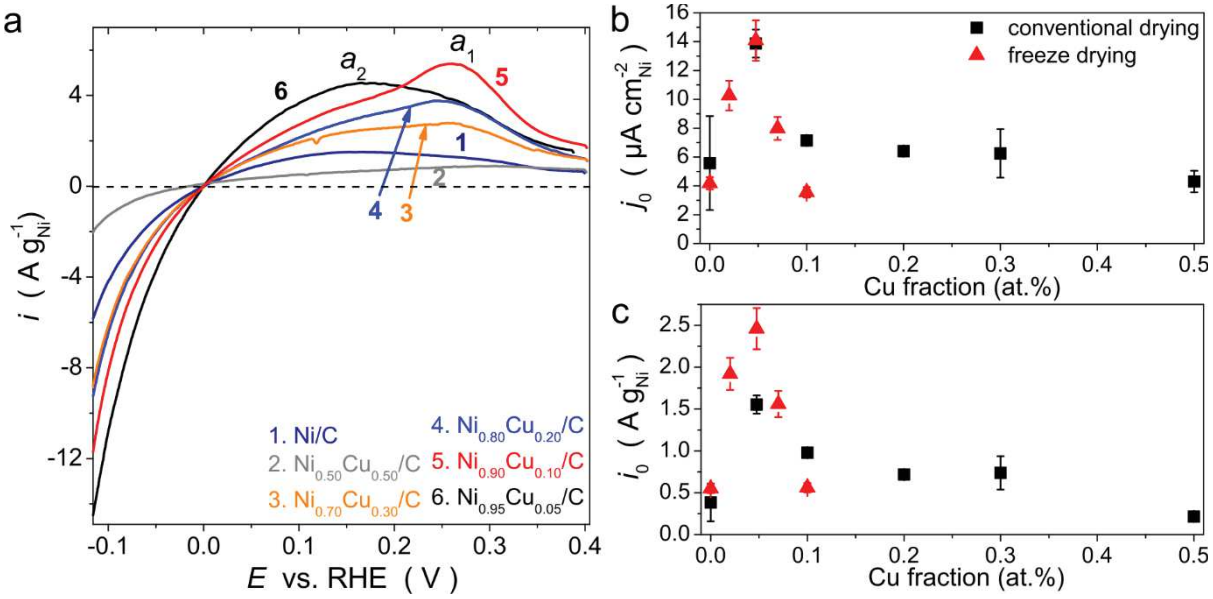

Fig. 5.8 *(a) Anodic sweep of CVs for Ni/C and $Ni_{1-x}Cu_x$/C samples obtained in H_2-saturated 0.10 M NaOH at v = 2 mV·s^{-1}. Specific (b) mass- and (c) surface-weighted activity as a function of the Cu fraction in the catalyst.*

Influence of Cu on the activity of Ni in the HOR/HER

On the basis of XPS and TEM data we conclude that addition of Cu to Ni catalysts improves their tolerance to oxidation and facilitates electrochemical reduction of surface oxides, as suggested by electrochemical measurements. Our experimental results are in line with the surface science study of Domnick et al. who found that subsurface Cu hinders oxidation of the top-most nickel layers [298].

Inspection of the electrochemical behavior of $Ni_{1-x}Cu_x$/C samples showed that an increase of the Ni activity at a small Cu fraction correlates with the change of the shape of CVs obtained in inert atmosphere (Fig. 5.6a). The largest relative contribution of the peak a_2 to anodic currents in inert atmosphere was observed for the $Ni_{0.95}Cu_{0.05}$/C sample, which also demonstrates the highest activity in the HOR/HER. As discussed in Section 3.3.3, the appearance of an additional anodic peak at lower potentials might be associated with a decrease of the Ni-H_{ad} binding energy. The latter could be one of the reasons for the increase of the HOR/HER activity of Ni. However,

the kinetic modeling study has to be performed for $Ni_{1-x}Cu_x$/C samples for drawing unambiguous conclusions. The change in the Ni-H_{ad} binding energy after addition of Cu to the catalyst composition can be caused by two factors: (i) 'electronic effect' leading to the change of the electronic properties of Ni and/or 'ensemble effect', according to which the presence of Cu on the surface affects the ratio between the metallic Ni and the oxidized NiO sites. Unambiguous differentiation between these factors requires additional *in situ* spectroscopic measurements and determination of the surface state of $Ni_{1-x}Cu_x$/C electrocatalysts as a function of applied potential.

5.3. Bimetallic NiMo/C electrocatalyst

Analysis of the literature showed (see Section 1.2.2.3) that among studied NiMo catalysts the highest activity in the HER was achieved at about 10 at.% of Mo fraction [212]. In order to answer the question about the prospects of using NiMo electrocatalysts in AMFCs, we investigated $Ni_{0.9}Mo_{0.1}$/KB sample with a total metal content of 50 wt.% (the synthesis is described in Section 2.1.4).

5.3.1. Investigation of the NiMo/C electrocatalyst by physicochemical techniques

Morphology and dispersion of NiMo/C particles

TEM analysis of synthesized $Ni_{0.90}Mo_{0.10}$/C electrocatalyst revealed that notwithstanding the high (50 wt.%) loading of the active component, the metal particles are quite uniformly distributed on the surface of the support with no sign of particle agglomeration (Fig. 5.9). This can be attributed to the high specific surface area of the KB support utilized for the NiMo catalyst preparation. The surface mean diameter of the NiMo particles was estimated to be 22 ± 6 nm (under the assumption of the spherical particle shape).

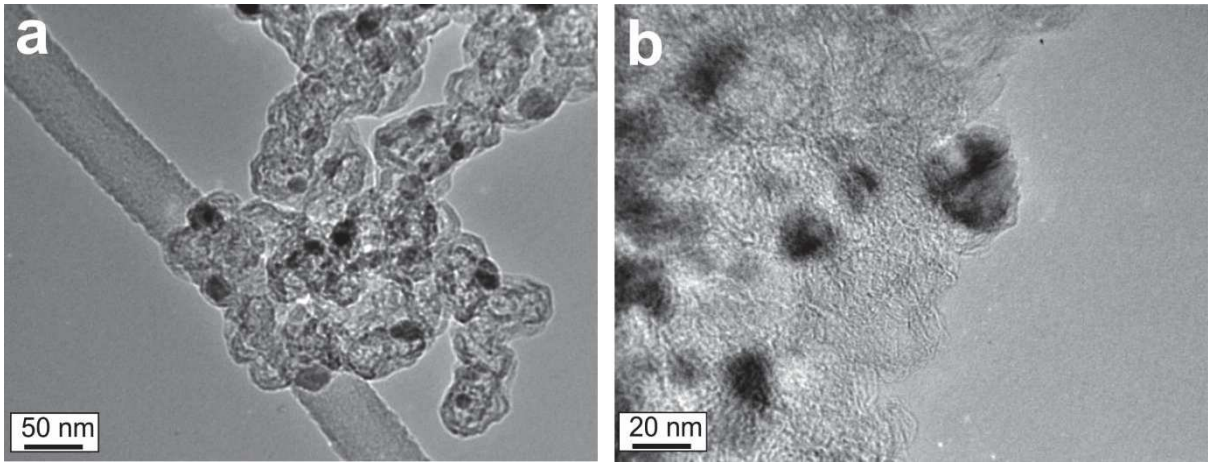

Fig. 5.9 *TEM images of the $Ni_{0.90}Mo_{0.10}$/C electrocatalyst at different magnifications.*

Crystalline structure of NiMo/C particles

The XRD pattern obtained for the $Ni_{0.90}Mo_{0.10}$/C catalyst suggests that it comprises three phases: Ni metal (FCC), MoO_2 (monoclinic) and $NiMo_4$ (FCC) traces with the content of ca. 80, 18 and 2 wt.%, respectively (Fig. 5.10). Similarly to NiCu/C samples, no diffraction peaks of crystalline nickel oxide/hydroxide phases were detected for the $Ni_{0.90}Mo_{0.10}$/C sample. The cell parameter of the Ni metal phase was calculated to be a = 3.529 Å, which slightly exceeds the tabulated data for pure Ni (FCC), 3.524 Å [ICDD PDF-2 #00-004-0850]. The average size of Ni crystallites estimated from the (111) peak broadening using Scherrer equation is ca. 19 nm. Poor angular resolution of the peaks corresponding to $NiMo_4$ and MoO_2 phases indicates that they are not highly crystalline and the presence of amorphous mixed oxides ($NiMoO_4$) cannot be excluded.

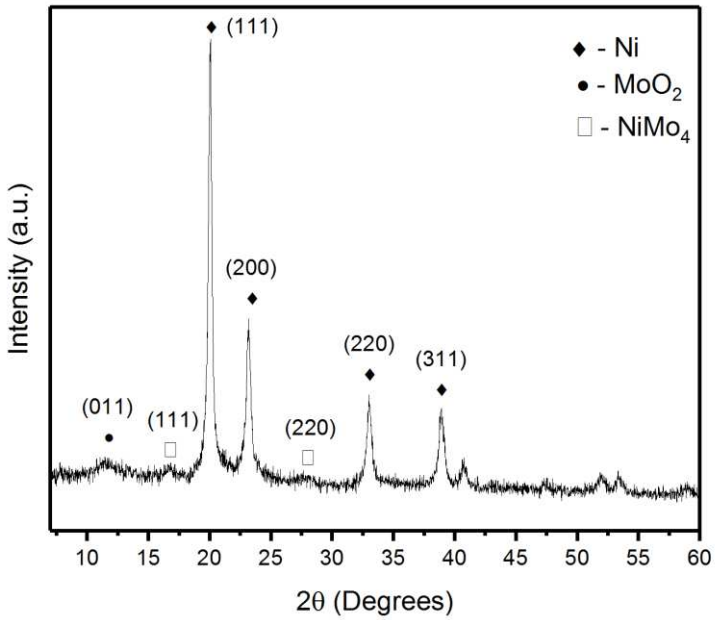

Fig. 5.10 *XRD patterns for $Ni_{0.90}Mo_{0.10}$/C electrocatalyst. Specific reflections of the indexed phases used in the pattern refinement are shown in the right corner.*

Surface state of NiMo/C particles

XPS analysis of $Ni_{0.90}Mo_{0.10}$/C sample shows surface (compared to the bulk) enrichment in molybdenum. Indeed, after adjusting the signals to the difference in the sampling depth of Mo3d (~5 nm) and Ni2p (~2.4 nm), the Ni:Mo ratio on the top surface is calculated to be 1.5:1, which is much lower than the atomic ratio (Ni:Mo = 9:1). Fig. 5.11 shows $Ni2p_{3/2}$ and Mo3d XP spectra, which were curve-fitted under the following assumptions: (i) oxidation of Ni results in the formation of surface NiO and $Ni(OH)_2$ [64,89,110,263]; (ii) oxidation of Mo results in the formation of a mixture of Mo (IV), Mo (V) and Mo (VI) oxides [270,271]. In addition, a possible formation of the $NiMoO_4$ phase observed in some studies [268,269] was considered. Results of the XP spectra deconvolution are presented in Fig. 5.11 and in Table 5.2. It was found that Ni is present on the catalyst surface mainly in an oxidized state with about 19% of metallic component and 11% of $NiMoO_4$. The main contribution of Mo is assigned with MoO_3 and $NiMoO_4$ compounds with small contributions of Mo(IV) and Mo(V) phases.

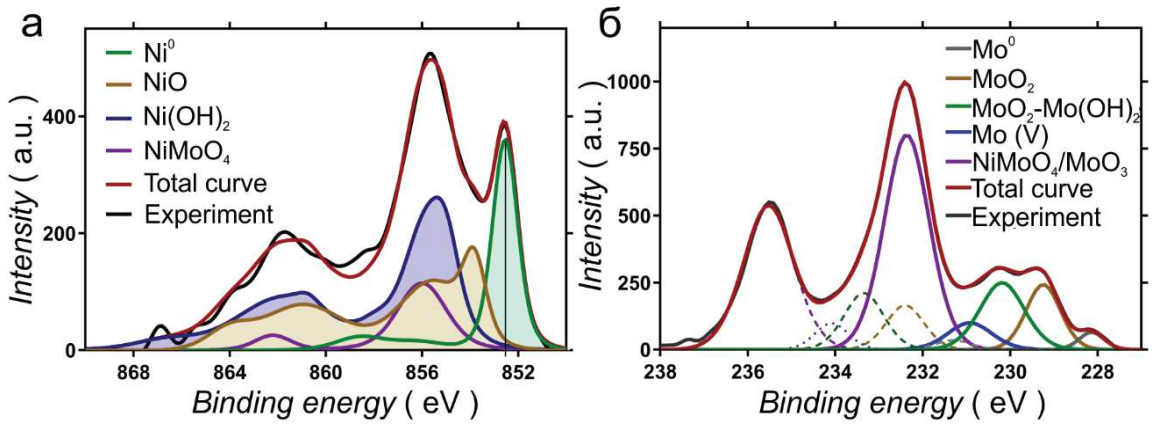

Fig. 5.11 *X-Ray photoelectron $Ni2p_{3/2}$ (a) and Mo3d (b) spectra for the $Ni_{0.90}Mo_{0.10}$/C electrocatalyst at 0 take-off angle. Spectra were curve-fitted with the components listed in the graphs, according to the procedure described in Section 2.2.3.*

Table 5.2 *The concentrations (in at.%) of different types of Ni and Mo species present on the surface of $Ni_{0.90}Mo_{0.10}$/C as revealed by XPS*

$Ni2p_{3/2}$	**Ni^0**	**NiO**	**$Ni(OH)_2$**	**$NiMoO_4$**	
	19.0	30.2	39.4	11.4	
Mo3d	**Mo^0**	**MoO_2**	**MoO_2 / $Mo(OH)_2$**	**Mo (V)**	**$NiMoO_4$ / MoO_3**
	2.7	13.6	18.1	7.2	58.4

5.3.2. Electrochemical properties of NiMo/C electrocatalyst

Fig. 5.12 shows CVs of the $Ni_{0.90}Mo_{0.10}$/KB electrocatalyst in N_2-saturated 0.10 M NaOH. In agreement with the XPS data, electrochemical measurements showed that the surface of the electrode taken from air is covered by metal oxide species, as it is evidenced by the value of the open-circuit potential (0.50 – 0.60 V) measured after immersion of the electrode in the electrolyte. Besides, no peaks were observed in CVs registered in the potential interval of [-0.06 – 0.40 V] (Fig. 5.12a). That is why the $Ni_{0.90}Mo_{0.10}$/C electrocatalyst was subjected to electrochemical reduction as described in Section 2.3.4.1. Fig. 5.12 shows that this procedure results in considerable increase of measured currents and an emergence of typical a_1 and c_1 peaks as well as a shoulder in the potential interval of the peak a_2. It was also found that, despite the high (50 wt.%) metal content on the KB support, the contribution of the currents arising from the carbon support is significant, as evidenced by the comparison of the CVs

presented in Fig. 5.12b. This is consistent with the high specific surface area of the used support. Therefore, the estimation of the S_{EC} was done after subtraction of the charge corresponding to carbon (Table 5.3). A mean diameter of the Ni particles estimated from the S_{EC} value (under the assumption that the metal particles have spherical shape) was found to be 36 ± 2 nm. The obtained value is reasonably close to the one calculated from TEM (22 ± 6 nm), which suggests that under the applied electrochemical conditions Ni surface is essentially reduced.

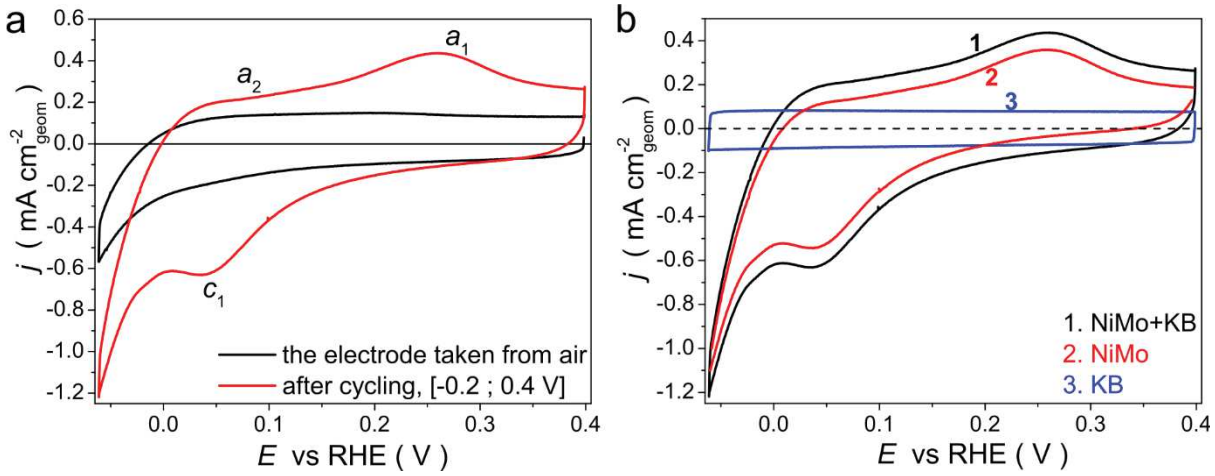

Fig. 5.12 *(a) CVs obtained in N_2-saturated 0.10 M NaOH at v = 20 mV·s^{-1} for $Ni_{0.90}Mo_{0.10}$/C sample after its immersion in the electrolyte (black curve) and after electrochemical reduction of its surface (red curve); (b) Comparison of CVs obtained for $Ni_{0.9}Mo_{0.1}$/C (100 μg cm$^{-2}_{geom}$, curve 1, black) and KB carbon support (50 μg cm$^{-2}_{geom}$, curve 3, blue); in addition, the CV obtained after subtraction of the currents corresponding to the KB support (curve 2, red) is presented.*

5.3.3. Kinetics of the HOR/HER on NiMo/C electrocatalyst

Electrocatalytic activity as a function of the catalyst loading

To measure the catalytic activity of $Ni_{0.90}Mo_{0.10}$/C in the HOR/HER, CVs were registered in H_2-purged 0.10 M NaOH in the potential region of [-0.06 – 0.40 V] at v = 5 mV·s^{-1} and rotating rate of 1600 rpm (Fig. 5.13a). The values of the exchange currents referred to S_{EC} (j_0) or to the mass of metals (Ni+Mo, i_0) are listed in the Table 5.3. It was found that both specific and mass-weighted activities of the $Ni_{0.90}Mo_{0.10}$/C catalyst exceed the values obtained for the $Ni_{0.95}Cu_{0.05}$/C catalyst, as well as those reported in the literature for Ni/N-CNT (Appendix 1).

However, at a small (100 μg cm^{-2}) catalyst loading on the surface of the GC electrode, the measured currents were found to be essentially independent on the rotating rate. Meanwhile, increase of the catalyst loading from 100 to 500 μg cm^{-2} allowed us to significantly increase the measured currents (Fig. 5.13a) and observe their rotating rate dependence (Fig. 5.13b). However, as can be seen from the Fig. 5.13a and Table 5.3, currents do not increase proportionally to the catalyst loading. The latter could be likely attributed to the inaccessibility of a part of the catalyst surface for the electrolyte at increasing thickness of the catalyst layer. This assumption is supported by the lack of proportionality between the catalyst loading and the electrochemical surface area of Ni (see Table 5.3). Considering this fact, determination of the kinetic current density from the rotation rate dependence obtained for the electrode with high catalyst loading is incorrect and therefore was not performed.

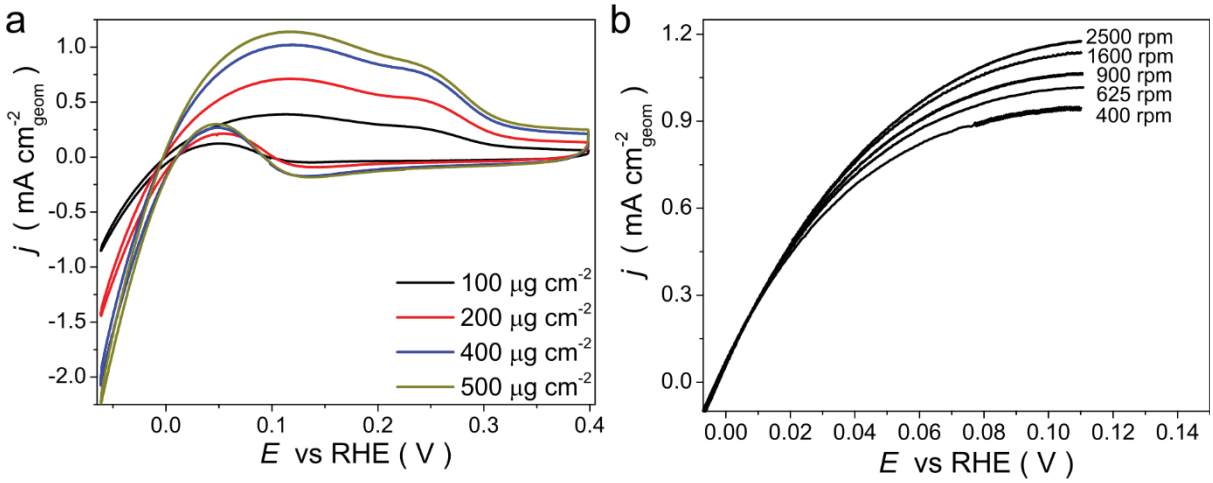

Fig. 5.13 *(a) CVs for $Ni_{0.90}Mo_{0.10}$/C obtained at various loadings of the catalyst on the surface of GC electrode in H_2-saturated 0.10 M NaOH at $v = 5\ mV \cdot s^{-1}$ and $\omega = 1600$ rpm; (b) Polarization curves of the HOR registered for $Ni_{0.90}Mo_{0.10}$/C (with a loading of 500 μg cm^{-2}) in H_2-saturated 0.10 M NaOH at $v = 5\ mV \cdot s^{-1}$ and various rotating rates of the electrode.*

Table 5.3 *The values of the exchange current densities in the HOR/HER obtained for $Ni_{0.9}Mo_{0.1}$/C electrocatalyst at various loadings on the surface of GC electrode*

m_{Me+C} / μr cm^{-2}_{geom}	S_{EC} / cm^2_{Ni}	Exchange current density	
		j_0 / μA cm^{-2}_{Ni}	i_o / A g_{Me}^{-1}
100	1.6 ± 0.2	27 ± 2	4.5 ± 0.2
200	2.4	26	3.1
400	4.7	25	2.9
500	4.8	27	2.6

Influence of Mo on the activity of Ni in the HOR/HER

In order to better understand the origin of high HOR/HER activity of $Ni_{0.90}Mo_{0.10}$/C electrocatalyst, experimental CVs were analyzed with the help of microkinetic modeling (see Section 2.4). The employed parameters are shown in Appendix 2.

Fig. 5.14 compares experimental and simulated CVs obtained in both N_2 and H_2 atmosphere. Good agreement was obtained in the potential interval of [-0.06 – 0.15 V], while at higher potentials simulated currents are much inferior of the experimental ones. This difference is likely related to a possible diversity of the Ni active sites on the catalyst surface, while in the mean-field approximation the surface is considered to be homogeneous. Despite some discrepancies with the experimental data, kinetic modeling predicts a significant increase of the Gibbs energy of adsorption of the hydrogen intermediate ($\Delta_{ad}G^0_H$) from -0.15 eV for non-activated polycrystalline Ni to 0.04 eV for the $Ni_{0.90}Mo_{0.10}$/C catalyst (Appendixes 2 and 3). Therefore the high activity of the $Ni_{0.90}Mo_{0.10}$/C catalyst in the HOR/HER may be attributed to a decrease of the Ni-H_{ad} binding energy. Modification of the hydrogen adsorption energy is in agreement with the work of Paloukis et al. [213], who concluded that the shift of the metal Ni^0 peak on Ni $2p_{3/2}$ XP spectrum from 852.4 eV to 852.6 eV is caused by an influence of Mo on the electronic properties of Ni. In addition, the presence of Mo oxides on the surface of $Ni_{0.90}Mo_{0.10}$/C catalyst might also contribute to the enhanced HOR activity by facilitating the Volmer step [44,132].

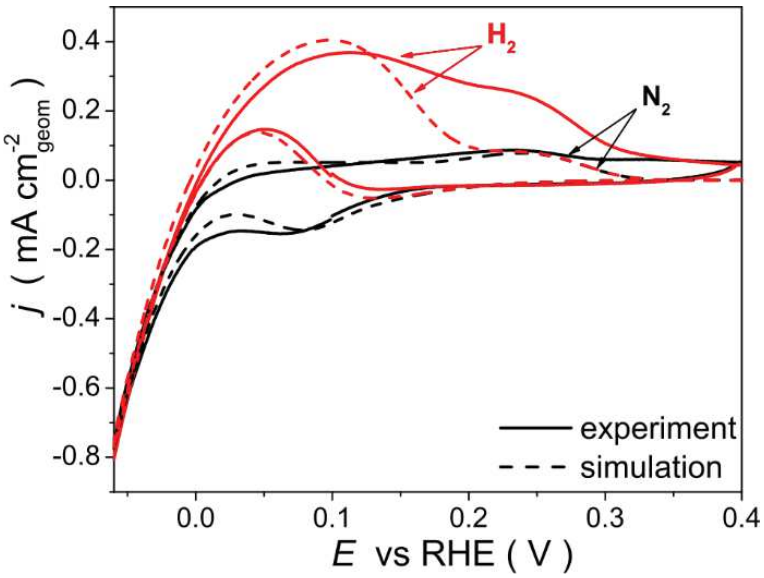

Fig. 5.14 *Comparison of the experimental (solid line) and simulated (dashed line) CVs for $Ni_{0.90}Mo_{0.10}$/C catalyst (with a loading of 100 μg cm^{-2}) in N_2- (black curve) or H_2-saturated (red curve) 0.10 M NaOH at v = 5 $mV \cdot s^{-1}$ and T = 298 K. All the curves are presented after the subtraction of the KB carbon contribution*

Influence of Mo on the stability of Ni-based catalysts in the HOR/HER

As shown in the literature review (see Section 1.3.4), along with an increase of the activity of Ni-based catalysts in the HOR/HER, addition of a second metal in some cases also allows one to improve their stability. To inspect this statement, the HOR/HER activity decay during potential cycling in H_2 atmosphere in the potential interval of [-0.06-0.40 V] at v = 5 $mV \cdot s^{-1}$ (first 10 scans were explored) was studied for three types of catalysts, namely: EC activated Ni rod, Ch activated Ni_{ED}/GC nanoparticles and supported $Ni_{0.9}Mo_{0.1}$/C. As can be seen from Fig. 5.15, the highest decrease of the activity was detected for Ch activated electrodeposited Ni_{ED}/GC nanoparticles, while for $Ni_{0.9}Mo_{0.1}$/C sample the drop of activity was considerably lower and amounted to ca. 12% after 10 scans. Therefore bimetallic Ni-based electrocatalysts can be considered as more promising system in terms of prolonged use at the anode of an AMFC. Nevertheless, the question about their long-term stability in the HOR depending on the polarization regime requires additional studies.

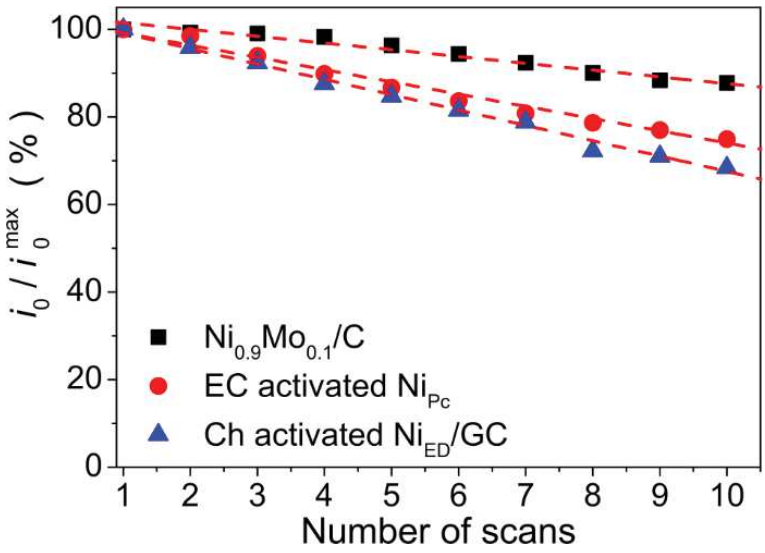

Fig. 5.15 *The change of the specific mass-weighted activity referred to the maximum obtained for $Ni_{0.9}Mo_{0.1}$/C (black squares), EC activated polycrystalline Ni rod (red circles) and Ch activated Ni_{ED}/GC particles (blue triangles) during cycling of the electrodes in H_2-saturated 0.10 M NaOH in the potential interval of [-0.06 – 0.4 V] at $v = 5\ mV \cdot s^{-1}$.*

5.4. Conclusions of Chapter 5

In this chapter we studied carbon supported monometallic Ni/C and bimetallic NiCu/C (with varied amounts of Cu) as well as NiMo/C electrocatalysts. It was found that adding of a small Cu fraction to Ni has a number of consequences, namely (i) increase of the tolerance of the Ni component towards oxidation under ambient conditions; (ii) increase of the specific surface area of Ni particles during the synthesis; and (iii) increase of the mass-weighted catalytic activity of Ni in the HOR/HER. This catalytic activity enhancement was linked to two factors: first, increase of the specific surface area of Ni and second, growth of the specific electrocatalytic activity attributed to an electronic and/or ensemble effect of Cu, which are the most pronounced in the case of $Ni_{0.95}Cu_{0.05}$/C catalyst.

Investigation of the $Ni_{0.90}Mo_{0.10}$/C catalyst showed that, similarly to Cu, adding Mo facilitates an electrochemical reduction of Ni oxide species present on the surface of the electrode taken from air. Besides, the specific activity of $Ni_{0.90}Mo_{0.10}$/C electrocatalyst was found to be ca. 2 times as high as the activity of $Ni_{0.95}Cu_{0.05}$/C (the

best among studied NiCu/C samples). By combining the experimental observations with microkinetic modeling the high activity of $Ni_{0.90}Mo_{0.10}$/C catalyst in the HOR/HER was attributed to a decrease of the adsorption energy of the hydrogen atoms, being intermediate of the HOR/HER, in comparison with non-activated polycrystalline Ni. Furthermore, it was observed that addition of Mo to Ni catalyst allows one to reduce the HOR/HER activity decay during potential cycling.

General conclusions and Outlook

1. It was found that *partial* oxidation of the surface of Ni electrocatalysts significantly affects their electrochemical properties in an alkaline electrolyte. Specific activity of metallic Ni in the HOR/HER does not depend on the morphology of the catalyst, but increases up to 10 times after *partial* oxidation of its surface. On the contrary, *full* oxidation of the electrode surface results in suppression of the activity of Ni in the HOR/HER.

2. The developed kinetic model allows one to describe the kinetics of both *the hydrogen evolution* and *the hydrogen oxidation* reactions taking into account the process of Ni surface oxidation with the formation of Ni hydroxide with the same set of parameters. Based on the data of mathematical modeling we conclude that:

    - the enhancement of the electrocatalytic activity of Ni in the presence of surface Ni oxides is related to a decrease of the adsorption energy of the hydrogen atoms on Ni, along with an increase of the rate constant of the Volmer step;

    - the mechanism of the HOR/HER on Ni is mainly described by the Heyrovsky and the Volmer steps, while the contribution of the Tafel step becomes noticeable only after *partial* oxidation of the electrode surface. The rate of the HOR is controlled by the Volmer step independently on the extent of oxidation of the surface of a Ni electrode.

3. For the first time a highly dispersed 40 wt.% Ni_{ED}/XC-72 electrocatalyst was prepared using electrodeposition technique and Vulcan XC-72 carbon as a support. Its mass-weighted electrocatalytic activity in the HOR significantly exceeds the values reported in the literature for non-noble metal catalysts and approaches the activity of commercial 20% Pd/C electrocatalyst.

4. Investigation of the series of carbon supported NiCu/C electrocatalysts showed that addition of Cu to the active component leads to:

- an increase of specific activity of Ni in the HOR/HER compared to monometallic Ni/C sample, which was prepared by the same method. The highest activity was observed at ca. 5 at.% fraction of Cu in the sample;
- an enhancement of the tolerance of Ni towards oxidation.

5. Investigation of carbon supported $Ni_{0.9}Mo_{0.1}$/C electrocatalyst showed that adding Mo to the active component allows one to increase the specific activity of the catalyst in the HOR/HER. With the help of kinetic modeling this enhancement was attributed to a decrease of the adsorption energy of the hydrogen atoms on Ni as well as an increase of the rate constant of the Volmer step.

The present work has clarified a number of important questions regarding the electrochemical properties of Ni electrodes and their electrocatalytic activity in the HOR/HER. However several aspects could be further improved.

First of all, *in situ* studies of Ni electrodes by physicochemical methods are highly desirable and could allow one to better understand the surface state of Ni depending on the applied potential and unambiguously answer the question about its influence on the mechanism and the kinetics of the HOR/HER on Ni. These might be performed using *in situ* X-ray absorption spectroscopy and X-ray photoelectron spectroscopy if one would be able to deposit Ni particles directly on the polymer membrane, assemble the electrochemical cell and conduct an experiment avoiding influence of oxygen-containing atmosphere at each of the preparation steps. This would allow one to overcome the difficulties encountered in the current study, when the surface of the Ni electrodes prepared for NAP-XPS measurements was oxidized in air, its reduction under applied potential being prevented by the low water pressure in the measurement chamber.

It would be also interesting to prepare carbon supported bimetallic Ni-based electrocatalysts using the method of electrodeposition. This will require development of the synthetic protocol and adjusting a number of parameters, among which are the

composition of the deposition bath, the value of the applied potential and time, etc. These materials are expected to have a number of advantages, such as high metal loading, high dispersion and the possibility to avoid a passivation step (necessary for chemical methods of preparation), which could make them promising candidates for the application in practical AMFCs. Another interesting task in this instance is to design a cell allowing one to scale up the synthesis of electrocatalysts by the method of electrodeposition.

In order to validate the application of Ni-based systems as AMFC anode materials, fuel cell tests are required. Besides, the stability tests are also of great importance. For these, optimization of several parameters such as the thickness of the catalytic layer, the type of the polymer membrane, the quantity of an ionomer and the water management have to be optimized. Furthermore, it would be necessary to optimize the procedure of the preparation of the membrane electrode assembly. Finally, the test protocol for the catalytic activity and stability measurements in alkaline environment should be developed. It will allow one to compare different electrode materials providing guidelines for the development of systems with activities comparable to or even exceeding those of Pt-based electrocatalysts.

References

1. Damaskin B.B., Petrii O.A. Introduction to electrochemical kinetics. 2nd edition – Moscow-Vysshaya Shkola Publishers. – 1983. – 400 p.
2. Krischer K., Savinova E.R. Fundamentals of Electrocatalysis // Handbook of Heterogeneous Catalysis / ed. Ertl G., Knözinger H., Schüth F., Weitkamp J. – V. 1 – Wiley-VCH Verlag GmbH & Co. KGaA. – 2008. – P. 1873–1958.
3. Tafel J. Über die Polarisation bei kathodischer Wasserstoffentwicklung // Z. Phys. Chem. Z phys Chem. – 1905. – V. 50. – P. 641–712.
4. Erdey-Gruz T., Volmer M. The theory of hydrogen overvoltage // Z. Phys. Chem. – 1930. – V. 150. – P. 203–213.
5. Erdey-Gruz T., Volmer M. Zur Frage der Wasserstoffüberspannung // Zeitschrift fur Phys. Chemie A. – 1932. – V. 162. – P. 53.
6. Kobosew N., Nekrassow N.I. Bildung freier wasserstoffatome bei kathodenpolarisation der metalle // Z. Electrochem. – 1930. – V. 36. – P. 529–544.
7. Heyrovský J. Researches with the dropping mercury cathode: Part I. General introduction // Recl. des Trav. Chim. des Pays-Bas. – 1925. – V. 44. – I. 6. – P. 488–495.
8. Heyrovský J., Shikata M. Researches with the dropping mercury cathode: Part II. The Polarograph // Recl. des Trav. Chim. des Pays-Bas. – 1925. – V. 44. – I. 6. – P. 496–498.
9. Heyrovský J. Researches with the dropping mercury cathode: Part III. A Theory of Over-potential // Recl. des Trav. Chim. des Pays-Bas. – 1925. – V. 44. – I. 6. – P. 499–502.
10. Frumkin A.N. Comments to the Theory of Hydrogen Overpotential // Z. Phys. Chem. – 1932. – V. 160. – P. 116–118.
11. Frumkin A.N. Hydrogen Overpotential and the Double Layer Structure // Z. Phys. Chem. – 1933. – V. 164. – P. 121–123.
12. Frumkin A.N., Bagotsky V.S., Ioffe Z.A., Kabanov B.N. // Kinetics of electrode processes. MSU Publishers. – 1952.
13. Conway B.E., Salomonl M. Electrochemical reaction orders: Applications to the hydrogen- and oxygen-evolution reactions // Electrochim. Acta. – 1964. – V. 9. – I. 12. – P. 1599–1615.
14. Trasatti S. Electrocatalysis of Hydrogen Evolution: Progress in Cathode Activation // Advances in Electrochemical Science and Engineering. Wiley-VCH Verlag GmbH. – 2008. – V. 2. – P. 1–85.
15. Notoya R., Matsuda A. Determination of the rate of the discharge step of hydrogen ion on a hydrogen-platinum electrode in aqueous solutions by the galvanostatic transient method // J. Phys. Chem. – 1989. – V. 93. – I. 14. – P. 5521–5523.
16. Saraby-Reintjes A. The hydrogen evolution reaction under mixed kinetic

control // J. Chem. Soc. Faraday Trans. 1 Phys. Chem. Condens. Phases. – 1986. – V. 82. – I. 11. – P. 3343–3355.

17. Divisek J. Determination of the kinetics of hydrogen evolution by analysis of the potential current and potential coverage curves // J. Electroanal. Chem. – 1986. – V. 214. – I. 1–2. – P. 615–632.

18. Trasatti S. Work function, electronegativity, and electrochemical behaviour of metals III. Electrolytic hydrogen evolution in acid solutions // J. Electroanal. Chem. – 1972. – V. 39. – P. 163–184.

19. Sabatier P. Hydrogénations et déshydrogénations par catalyse // Berichte der Dtsch. Chem. Gesellschaft. – 1911. – V. 44. – I. 3. – P. 1984–2001.

20. Boreskov G.K. Heterogeneous catalysis. Moscow: Nauka. – 1986. – 304 p.

21. Parsons R. The rate of electrolytic hydrogen evolution and the heat of adsorption of hydrogen // Trans. Faraday Soc. – 1958. – V. 54. – P. 1053–1063.

22. Nørskov J.K. Bligaard T., Logadottir A., Kitchin J.R., Chen J.G., Pandelov S., Stimming U. Trends in the Exchange Current for Hydrogen Evolution // J. Electrochem. Soc. – 2005. – V. 152. – I. 3. – P. J23–J26.

23. Sheng W., Myint M.N.Z., Chen J.G., Yan Y. Correlating the hydrogen evolution reaction activity in alkaline electrolytes with the hydrogen binding energy on monometallic surfaces // Energy Environ. Sci. – 2013. – V. 6. – I. 5. – P. 1509–1512.

24. Santos E., Hindelang P., Quaino P., Schulz E.N., Soldano G., Schmickler W. Hydrogen electrocatalysis on single crystals and on nanostructured electrodes. // ChemPhysChem. – 2011. – V. 12. – I. 12. – P. 2274–2279.

25. Petrii O.A., Tsirlina G.A. Electrocatalytic activity prediction for hydrogen electrode reaction: intuition, art, science // Electrochim. Acta. – 1994. – V. 39. – I. 11–12. – P. 1739–1747.

26. Quaino P., Juarez F., Santos E., Schmickler W. Volcano plots in hydrogen electrocatalysis - uses and abuses. // Beilstein J. Nanotechnol. – 2014. – V. 5. – P. 846–854.

27. Greeley J., Jaramillo T.F., Bonde J., Chorkendorff, I.B., Nørskov J.K. Computational high-throughput screening of electrocatalytic materials for hydrogen evolution. // Nat. Mater. – 2006. – V. 5. – I. 11. – P. 909–913.

28. Sheng W., Bivens A.P., Myint M.N.Z., Zhuang Z., Forest R.V., Fang Q., Chen J.G., Yan Y. Non-precious metal electrocatalysts with high activity for hydrogen oxidation reaction in alkaline electrolytes // Energy Environ. Sci. – 2014. – V. 7. – I. 5. – P. 1719–1724.

29. Jakšić M.M. Advances in electrocatalysis for hydrogen evolution in the light of the Brewer-Engel valence-bond theory // Int. J. Hydrogen Energy. – 1987. – V. 12. – I. 11. – P. 727–752.

30. Leonard K.C., Bard A.J. Pattern Recognition Correlating Materials Properties of the Elements to Their Kinetics for the Hydrogen Evolution Reaction // J. Am.

Chem. Soc. – 2013. – V. 135. – I. 42. – P. 15885–15889.

31. Kita H., Kurisu T. Electrocatalysis by d- and sp-metals // J. Res. Inst. Catalysis. – 1974. – P. – 200–246. 32. Sheng W., Gasteiger H.A., Shao-Horn Y. Hydrogen Oxidation and Evolution Reaction Kinetics on Platinum: Acid vs Alkaline Electrolytes // J. Electrochem. Soc. – 2010. – V. 157. – I. 11. – P. B1529.
33. Durst J., Siebel A., Simon C., Hasché F., Herranz J., Gasteiger H.A. New insights into the electrochemical hydrogen oxidation and evolution reaction mechanism // Energy Environ. Sci. – 2014. – V. 7. – I. 7. – P. 2255–2260.
34. Marković N.M., Grgur B.N., Ross P.N. Temperature-Dependent Hydrogen Electrochemistry on Platinum Low-Index Single-Crystal Surfaces in Acid Solutions // J. Phys. Chem. B. – 1997. – V. 101. – I. 27. – P. 5405–5413.
35. Rheinlander P.J., Herranz J., Durst J., Gasteiger H.A. Kinetics of the Hydrogen Oxidation/Evolution Reaction on Polycrystalline Platinum in Alkaline Electrolyte Reaction Order with Respect to Hydrogen Pressure // J. Electrochem. Soc. – 2014. – V. 161. – I. 14. – P. F1448–F1457.
36. Zheng J., Sheng W., Zhuang Z., Xu B., Yan Y. Universal dependence of hydrogen oxidation and evolution reaction activity of platinum-group metals on pH and hydrogen binding energy // Sci. Adv. – 2016. – V. 2. – I. 3. – P. e1501602.
37. Sheng W., Zhuang Z., Gao M., Zheng J., Chen J.G., Yan Y. Correlating hydrogen oxidation and evolution activity on platinum at different pH with measured hydrogen binding energy // Nat. Commun. – 2015. – V. 6. – P. 5848.
38. Van Der Niet M.J.T.C., Garcia-Araez N., Hernandez J., Feliu J.M., Koper M.T M. Water dissociation on well-defined platinum surfaces: The electrochemical perspective // Catal. Today. – 2013. – V. 202. – I. 1. – P. 105–113.
39. Strmcnik D., Lopes P.P., Genorio B., Stamenkovic V.R., Markovic N.M. Design principles for hydrogen evolution reaction catalyst materials // Nano Energy. – 2016. – V. 29. – P. 29–36.
40. Strmcnik D., Uchimura M., Wang C., Subbaraman R., Danilovic N., van der Vliet D., Paulikas A.P., Stamenkovic V.R., Markovic N.M. Improving the hydrogen oxidation reaction rate by promotion of hydroxyl adsorption. // Nat. Chem. – 2013. – V. 5. – I. 4. – P. 300–306.
41. Wang Y., Wang G., Li G., Huang B., Pan J., Liu Q., Han J., Xiao Li, Lu J., Zhuang L. Pt–Ru catalyzed hydrogen oxidation in alkaline media: oxophilic effect or electronic effect? // Energy Environ. Sci. – 2015. – V. 8. – I. 1. – P. 177–181.
42. Rizo R., Sitta E., Herrero E., Climent V., Feliu J.M. Towards the understanding of the interfacial pH scale at Pt(111) electrodes // Electrochim. Acta. – 2015. – V. 162. – P. 138–145.

43. Martínez-Hincapié R., Sebastián-Pascual P., Climent V., Feliu J.M. Exploring the interfacial neutral pH region of Pt(111) electrodes // Electrochem. Commun.. – 2015. – V. 58. – P. 62–64.

44. Subbaraman R., Tripkovic D., Chang K.-C., Strmcnik D., Paulikas A.P., Hirunsit P., Chan M., Greeley J., Stamenkovic V., Markovic N.M. Trends in activity for the water electrolyser reactions on 3d M(Ni,Co,Fe,Mn) hydr(oxy)oxide catalysts. // Nat. Mater. – 2012. – V. 11. – I. 6. – P. 550–557.

45. Subbaraman R., Tripkovic D., Strmcnik D., Chang K.-C., Uchimura M., Paulikas A.P., Stamenkovic V., Markovic N.M. Enhancing hydrogen evolution activity in water splitting by tailoring Li^+-$Ni(OH)_2$-Pt interfaces. // Science. – 2011. – V. 334. – I. 6060. – P. 1256–1260.

46. Zeng Z., Chang K.-C., Kubal J., Markovic N.M., Greeley J. Stabilization of ultrathin (hydroxy)oxide films on transition metal substrates for electrochemical energy conversion // Nat. Energy. – 2017. – V. 2. – I. May. – P. 17070.

47. Ledezma-Yanez I., Wallace W.D.Z., Sebastián-Pascual P., Climent V., Feliu J.M., Koper M.T.M. Interfacial water reorganization as a pH-dependent descriptor of the hydrogen evolution rate on platinum electrodes // Nat. Energy. – 2017. – V. 2. – I. 4. – P. 17031.

48. Pletcher D., Li X. Prospects for alkaline zero gap water electrolysers for hydrogen production // Int. J. Hydrogen Energy.– 2011. – V. 36. – I. 23. – P. 15089–15104.

49. Emelianova N. V. Researches with the dropping mercury cathode: Part VII. Nickel and Cobalt // Recl. des Trav. Chim. des Pays-Bas. – 1925. – V. 44. – I. 6. – P. 528–548.

50. Lukovtsev P., Levina S., Frumkin A. Hydrogen Overpotential on Nickel // Acta Physicochim. U.S.S.R. – 1939. – V. 11. – P. 21.

51. Frumkin A. Hydrogen overvoltage // Discuss. Faraday Soc. – 1947. – V. 1. – P. 57–67.

52. Legran A., Levina S. Hydrogen overvoltage on Ni in acid solutions // Z. Phys. Chem. – 1940. – V. 15. – I. 2. P. 211–216.

53. Conway B.E., Bourgault P.L. The electrochemical behavior of the nickel – nickel oxide electrode: part i. kinetics of self-discharge // Can. J. Chem. – 1959. – V. 37. – I. 1. – P. 292–307.

54. Bourgault P.L., Conway B.E. The electrochemical behavior of the nickel oxide electrode: part ii. quasi-equilibrium behavior // Can. J. Chem. – 1960. – V. 38. – I. 9. – P. 1557–1575.

55. Conway B.E., Bourgault P.L. Electrochemistry of the nickel oxide electrode: part iii. anodic polarization and self-discharge behavior // Can. J. Chem. – 1962. – V. 40. – I. 8. – P. 1690–1707.

56. Conway B.E., Gileadi E. Electrochemistry of the nickel oxide electrode: part iv. electrochemical kinetic studies of reversible potentials as a function of degree of oxidation // Can. J. Chem. – 1962. – V. 40. – I. 10. – P. 1933–1942.

57. Conway B.E., Sattar M.A. Electrochemistry of the nickel oxide electrode // J. Electroanal. Chem. Interfacial Electrochem. – 1968. – V. 19. – I. 4. – P. 351–364.

58. Conway B.E., Sattar M.A., Gilroy D. Electrochemistry of the nickel-oxide electrode—V. Self-passivation effects in oxygen-evolution kinetics // Electrochim. Acta. – 1969. – V. 14. – I. 8. – P. 677–694.

59. Sattar M.A., Conway B.E. Electrochemistry of the nickel-oxide electrode—VI. Surface oxidation of nickel anodes in alkaline solution // Electrochim. Acta. – 1969. – V. 14. – I. 8. – P. 695–710.

60. Conway B.E., Sattar M.A., Gilroy D. Electrochemistry of the nickel-oxide electrode—VII. Potentiostatic step method for study of adsorbed intermediates // Electrochim. Acta. – 1969. – V. 14. – I. 8. – P. 711–724.

61. Weininger J.L., Breiter M.W. Effect of Crystal Structure on the Anodic Oxidation of Nickel // J. Electrochem. Soc. – 1963. – V. 110. – I. 6. – P. 484.

62. Weininger J.L., Breiter M.W. Hydrogen Evolution and Surface Oxidation of Nickel Electrodes in Alkaline Solution // J. Electrochem. Soc. – 1964. – V. 111. – I. 6. – P. 707–712.

63. Bockris J.O., Potter E.C. The Mechanism of Hydrogen Evolution at Nickel Cathodes in Aqueous Solutions // J. Chem. Phys. – 1952. – V. 20. – I. 4. – P. 614–628.

64. Hall D.S., Bock C., MacDougall B.R. The Electrochemistry of Metallic Nickel: Oxides, Hydroxides, Hydrides and Alkaline Hydrogen Evolution // J. Electrochem. Soc. – 2013. – V. 160. – I. 3. – P. F235–F243.

65. Hall D.S., Lockwood D.J., Bock C., MacDougall B.R. Nickel hydroxides and related materials: a review of their structures, synthesis and properties // Proc. R. Soc. A Math. Phys. Eng. Sci. – 2014. – V. 471. – I. 2174. – P. 20140792.

66. Alsabet M., Grden M., Jerkiewicz G. Electrochemical Growth of Surface Oxides on Nickel. Part 1: Formation of α-Ni(OH)2 in Relation to the Polarization Potential, Polarization Time, and Temperature // Electrocatalysis. – 2011. – V. 2. – I. 4. – P. 317–330.

67. Alsabet M., Grden M., Jerkiewicz G. Electrochemical Growth of Surface Oxides on Nickel. Part 2: Formation of β-Ni(OH)2 and NiO in Relation to the Polarization Potential, Polarization Time, and Temperature // Electrocatalysis. – 2013. – V. 5. – I. 2. – P. 136–147.

68. Alsabet M., Grdeń M., Jerkiewicz G. Electrochemical Growth of Surface Oxides on Nickel. Part 3: Formation of β-NiOOH in Relation to the Polarization Potential, Polarization Time, and Temperature // Electrocatalysis. – 2014. – V. 6. – I. 1. – P. 60–71.

69. Grden M., Klimek K., Czerwinski A. A quartz crystal microbalance study on a metallic nickel electrode // J. Solid State Electrochem. – 2004. – V. 8. – I. 6. – P. 390–397.

70. Melendres C.A., Pankuch M. On the composition of the passive film on nickel: a surface-enhanced Raman spectroelectrochemical study // J. Electroanal. Chem. – 1992. – V. 333. – I. 1–2. – P. 103–113.

71. Simpraga R., Conway B.E. Realization of monolayer levels of surface oxidation of nickel by anodization at low temperatures // J. Electroanal. Chem. – 1990. – V. 280. – P. 341–357.

72. Beverskog B., Puigdomenech I. Revised Pourbaix diagrams for iron at 25-300??C // Corrosion Science. – 1996. – V. 38. – I. 12. – P. 2121–2135.

73. Grdeń M., Klimek K. EQCM studies on oxidation of metallic nickel electrode in basic solutions // J. Electroanal. Chem. – 2005. – V. 581. – I. 1. – P. 122–131.

74. Conway B.E., Barnett B. Angerstein-Kozlowska H., Tilak B.V. A surface-electrochemical basis for the direct logarithmic growth law for initial stages of extension of anodic oxide films formed at noble metals // J. Chem. Phys. – 1990. – V. 93. – I. 11. – P. 8361.

75. D'Alkaine C. V, Santanna M.A. Passivating films on nickel in alkaline solutions I. General aspects of the Ni (II) region // J. Electroanal. Chem. – 1998. – V. 457. – P. 5–12.

76. Šimpraga R., Conway B.E. Realization of monolayer levels of surface oxidation of nickel by anodization at low temperatures // J. Electroanal. Chem. Interfacial Electrochem. – 1990. – V. 280. – I. 2. – P. 341–357.

77. Seyeux A., Maurice V., Klein L.H., Marcus P. In situ scanning tunnelling microscopic study of the initial stages of growth and of the structure of the passive film on Ni(111) in 1 mM NaOH(aq) // J. Solid State Electrochem. – 2005. – V. 9. – I. 5. – P. 337–346.

78. Machado S.A.S., Avaca L.A. The hydrogen evolution reaction on nickel surfaces stabilized by H-absorption // Electrochim. Acta. – 1994. – V. 39. – I. 10. – P. 1385–1391.

79. Nakamura M., Ikemiya N., Iwasaki A., Suzuki Y., Ito M. Surface structures at the initial stages in passive film formation on Ni(111) electrodes in acidic electrolytes // J. Electroanal. Chem. – 2004. – V. 566. – I. 2. – P. 385–391.

80. Seghiouer A., Chevalet J., Barhoun A., Lantelme F. Electrochemical oxidation of nickel in alkaline solutions: a voltammetric study and modelling // J. Electroanal. Chem. – 1998. – V. 442. – I. 1–2. – P. 113–123.

81. Visscher W., Barendrecht E. Anodic oxide films of nickel in alkaline electrolyte // Surf. Sci. – 1983. – V. 135. – I. 1–3. – P. 436–452.

82. Beden B., Bewick A. The anodic layer on nickel in alkaline solution: an investigation using in situ IR spectroscopy // Electrochim. Acta. – 1988. – V. 33. – I. 11. – P. 1695–1698.

83. Hoppe H.-W., Strehblow H.-H. XPS and UPS examinations of the formation of passive layers on Ni in 1 M sodium hydroxide and 0.5 M sulphuric acid // Surf. Interface Anal. – 1989. – V. 14. – I. 3. – P. 121–131.

84. Visscher W., Barendrecht E. Absorption of hydrogen in reduced nickel oxide // J. Appl. Electrochem. – 1980. – V. 10. – P. 269–274.

85. Burke L.D., Twomey T.A.M. Voltammetric behaviour of nickel in base with particular reference to thick oxide growth // J. Electroanal. Chem. Interfacial Electrochem. – 1984. – V. 162. – I. 1–2. – P. 101–119.

86. MacDougall B., Cohen M. Anodic Oxidation of Nickel in Neutral Sulfate Solution // J. Electrochem. Soc. – 1974. – V. 121. – I. 9. – P. 1152.

87. Schrebler Guzmán R.S., Vilche J.R., Arvía A.J. The kinetics and mechanism of the nickel electrode-III. The potentiodynamic response of nickel electrodes in alkaline solutions in the potential region of Ni(OH)2 formation // Corros Sci. – 1978. – V. 18. – I. 8. – P. 765–778.

88. Desilvestro J. Characterization of Redox States of Nickel Hydroxide Film Electrodes by In Situ Surface Raman Spectroscopy // J. Electrochem. Soc. – 1988. – V. 135. – I. 4. – P. 885.

89. Medway S.L., Lucas C.A., Kowal A., Nichols R.J., Johnson D. In situ studies of the oxidation of nickel electrodes in alkaline solution // J. Electroanal. Chem. – 2006. – V. 587. – I. 1. – P. 172–181.

90. Samoilov G.P., Khrushcheva E.I., Shumilova N.A., Bagotzky V.S. The study of oxygen adsorption on Ni by electrochemical method // Kinetika i Kataliz. – 1973. – V. 15. – I. 5. P. 1235–1238.

91. Visscher W., Barendrecht E. The anodic oxidation of nickel in alkaline solution // Electrochim. Acta. – 1980. – V. 25. – I. 5. – P. 651–655.

92. Shumilova N.A., Bagotzky V.S. Oxygen ionization on nickel in alkaline solutions // Electrochim. Acta. – 1968. – V. 13. – I. 3. – P. 285–293.

93. Bode H., Dehmelt K., Witte J. Zur kenntnis der nickelhydroxidelektrode—I.Über das nickel (II)-hydroxidhydrat // Electrochim. Acta. – 1966. – V. 11. – I. 8. – P. 1079–1087.

94. Oliva P., Leonardi J., Laurent J.F., Delmas C., Braconnier, J.J., Figlarz M., Fievet F., de Guibert A. Review of the structure and the electrochemistry of nickel hydroxides and oxy-hydroxides // J. Power Sources. – 1982. – V. 8. – P. 229–255.

95. de Souza L.M.M., Kong F.P. McLarnon F.R., Muller R.H. Spectroscopic ellipsometry study of nickel oxidation in alkaline solution // Electrochim. Acta. – 1997. – V. 42. – I. 8. – P. 1253–1267.

96. Guzmán R.S.S., Vilche J.R., Arvía A.J. Non-equilibrium effects in the nickel hydroxide electrode // J. Appl. Electrochem. – 1979. – V. 9. – I. 2. – P. 183–189.

97. Kim M.-S. A Study on the Phase Transformation of Electrochemically Precipitated Nickel Hydroxides Using an Electrochemical Quartz Crystal Microbalance // J. Electrochem. Soc. – 1998. – V. 145. – I. 2. – P. 507.

98. Gomez Meier H., Vilche J.R., Arvia A.J. The influence of temperature on the current peak multiplicity related to the nickel hydroxide electrode // J. Appl. Electrochem. – 1980. – V. 10. – I. 5. – P. 611–621.

99. Trzesniewski B.J. et al. In Situ Observation of Active Oxygen Species in Fe-Containing Ni-Based Oxygen Evolution Catalysts: The Effect of pH on Electrochemical Activity // J. Am. Chem. Soc. – 2015. – V. 137. – I. 48. – P. 15112–15121.

100. Johnston C., Graves P.R. In situ Raman spectroscopy study of the nickel oxyhydroxide electrode (NOE) system // Appl. Spectrosc. – 1990. – V. 44. – I. 1. – P. 105–115.

101. Oblonsky L.J., Devine T.M. Surface Enhanced Raman Spectra from the Films Formed on Nickel in the Passive and Transpassive Regions // J. Electrochem. Soc. – 1995. – V. 142. – I. 11.

102. Yeo B.S., Bell A.T. In Situ Raman Study of Nickel Oxide and Gold-Supported Nickel Oxide Catalysts for the Electrochemical Evolution of Oxygen // J. Phys. Chem. C. – 2012. – V. 116. – I. 15. – P. 8394–8400.

103. El Gabaly F., McCarty K.F., Bluhm H., McDaniel A.H. Oxidation stages of Ni electrodes in solid oxide fuel cell environments // Phys. Chem. Chem. Phys. – 2013. – V. 15. – I. 21. – P. 8334–8341.

104. Hall D.S., Lockwood D.J., Poirier S., Bock C., MacDougall B.R. Applications of in situ Raman spectroscopy for identifying nickel hydroxide materials and surface layers during chemical aging. // ACS Appl. Mater. Interfaces. – 2014. – V. 6. – I. 5. – P. 3141–3149.

105. Flanagan T.B., Lewis F.A. Hydrogen absorption by palladium in aqueous solution // J. Chem. Soc., Faraday Trans. – 1959. – V. 55. – P. 1400.

106. Wollan E., Cable J., Koehler W. The hydrogen atom positions in face centered cubic nickel hydride // J. Phys. Chem. Solids. – 1963. – V. 24. – I. 9. – P. 1141–1143.

107. Baranowski B., Majchrzak S., Flanagan T.B. The volume increase of fcc metals and alloys due to interstitial hydrogen over a wide range of hydrogen contents // J. Phys. F Met. Phys. – 1971. – V. 1. – I. 3. – P. 307.

108. Boniszewski T., Smith G.C. A note on nickel hydride // J. Phys. Chem. Solids. – 1961. – V. 21. – I. 1–2. – P. 115–118.

109. Soares D.M., Teschke O., Torriani I. Hydride Effect on the Kinetics of the Hydrogen Evolution Reaction on Nickel Cathodes in Alkaline Media // J. Electrochem. Soc. – 1992. – V. 139. – I. 1. – P. 98–105.

110. Holloway P.H. Chemisorption and oxide formation on metals: Oxygen–nickel reaction // J. Vac. Sci. Technol. – 1981. – V. 18. – I. 2. – P. 653–659.

111. Maurice V., Talah H., Marcus P. A scanning tunneling microscopy study of the structure of thin oxide films grown on Ni (111) single crystal surfaces by anodic polarization in acid electrolyte // Surf. Sci. – 1994. – V. 6028. – I. 93.

112. Lambers E.S., Dykstal C.N., Seo J.M., Rowe J.E., Holloway P.H. Room-temerature oxidation of Ni(110) at low and atmospheric oxygen pressures // Oxid. Met. – 1996. – V. 45. – I. 3–4. – P. 301–321.

113. Katić J., Metikoš-Huković M., Peter R., Petravić M. The electronic structure of the α–Ni(OH)2 films: Influence on the production of the high–performance Ni–catalyst surface // J. Power Sources. – 2015. – V. 282. – P. 421–428.

114. MacDougall B., Mitchell D.F., Graham M.J. Changes in Oxide Films on Nickel during Long-Term Passivation // J. Electrochem. Soc. – 1985. – V. 132. – I. 12. – P. 2895.

115. Floner D., Lamy C., Leger J.-M. Electrocatalytic oxidation of hydrogen on polycrystal and single-crystal nickel electrodes // Surf. Sci. – 1990. – V. 234. – I. 1–2. – P. 87–97.

116. Hu C.-C., Wen T.-C. Effects of the nickel oxide on the hydrogen evolution and para-nitroaniline reduction at Ni-deposited graphite electrodes in NaOH // Electrochim. Acta. – 1998. – V. 43. – I. 12–13. – P. 1747–1756.

117. Pshenichnikov A.G. Electrocatalytic properties of nickel and nickel-based alloys // Mater. Chem. Phys. – 1989. – V. 22. – I. 1–2. – P. 121–148.

118. Karimi Shervedani R., Lasia A. Evaluation of the surface roughness of microporous Ni-Zn-P electrodes by in situ methods // J. Appl. Electrochem. – 1999. – V. 29. – I. 8. – P. 979–986.

119. Keddam M. Transpassive Dissolution of Ni in Acidic Sulfate Media: A Kinetic Model // J. Electrochem. Soc. – 1985. – V. 132. – I. 11. – P. 2561.

120. Beden B., Floner D., Léger J.M., Lamy C. A voltammetric study of the formation on hydroxides and oxyhydroxides on nickel single crystal electrodes in contact with an alkaline solution // Surf. Sci. – 1985. – V. 162. – I. 1–3. – P. 822–829.

121. Zoltowski P. The capacity of monocrystalline nickel electrode in potassium hydroxide solution at low hydrogen overpotentials // Electrochim. Acta. – 1993. – V. 38. – I. 14. – P. 2129–2133.

122. Trasatti S., Petrii O.A. Real surface area measurements in electrochemistry // J. Electroanal. Chem. – 1992. – V. 327. – I. 1–2. – P. 353–376.

123. Zhuang Z., Giles S.A., Zheng J., Jenness G.R., Caratzoulas S., Vlachos D.G., Yan Y. Nickel supported on nitrogen-doped carbon nanotubes as hydrogen oxidation reaction catalyst in alkaline electrolyte // Nat. Commun. – 2016. – V. 7. – P. 10141.

124. Grdeń M., Alsabet M., Jerkiewicz G. Surface science and electrochemical analysis of nickel foams. // ACS Appl. Mater. Interfaces. – 2012. – V. 4. – I. 6. – P. 3012–3021.

125. Bai L., Harrington D.A., Conway B.E. Behavior of overpotential-deposited species in Faradaic reactions-II. ac Impedance measurements on H2 evolution kinetics at activated and unactivated Pt cathodes // Electrochim. Acta. – 1987. – V. 32. – I. 12. – P. 1713–1731.

126. Lasia A., Rami A. Kinetics of hydrogen evolution on nickel electrodes // J. Electroanal. Chem. Interfacial Electrochem. – 1990. – V. 294. – I. 1–2. – P. 123–141.

127. Navarro-Flores E., Chong Z., Omanovic S. Characterization of Ni, NiMo, NiW and NiFe electroactive coatings as electrocatalysts for hydrogen evolution in an acidic medium // J. Mol. Catal. A Chem. – 2005. – V. 226. – I. 2. – P. 179–197.

128. Herraiz-Cardona I., Ortega E., Antón J.G., Pérez-Herranz V. Assessment of the roughness factor effect and the intrinsic catalytic activity for hydrogen evolution reaction on Ni-based electrodeposits // Int. J. Hydrogen Energy. – 2011. – V. 36. – I. 16. – P. 9428–9438.

129. Chen L., Lasia A. Study of the Kinetics of Hydrogen Evolution Reaction on Nickel-Zinc Alloy Electrodes // J. Electrochem. Soc. – 1991. – V. 138. – I. 11. – P. 3321–3328.

130. Ho J.C.K., Piron D.L. Active surface area in oxide electrodes by overpotential deposited oxygen species for the oxygen evolution reaction // J. Appl. Electrochem. – 1996. – V. 26. – I. 5. – P. 515–521.

131. McCrory C.C.L., Jung S., Ferrer I.M., Chatman S.M., Peters J.C., Jaramillo T.F. Benchmarking Hydrogen Evolving Reaction and Oxygen Evolving Reaction Electrocatalysts for Solar Water Splitting Devices // J. Am. Chem. Soc. – 2015. – V. 137. – I. 13. – P. 4347–4357.

132. Li X., Liu P.F., Zhang Le, Zu M.Y., Yang Y.X., Yang H.G. Enhancing alkaline hydrogen evolution reaction activity through Ni–Mn_3O_4 nanocomposites // Chem. Commun. – 2016. – V. 52. – I. 69. – P. 10566–10569.

133. Lyons M.E.G., Brandon M.P. The oxygen evolution reaction on passive oxide covered transition metal electrodes in aqueous alkaline solution. Part 1-Nickel // Int. J. Electrochem. Sci. – 2008. – V. 3. – I. 12. – P. 1386–1424.

134. Hall D.S., Bock C., MacDougall B.R. An Oxalate Method for Measuring the Surface Area of Nickel Electrodes // J. Electrochem. Soc. – 2014. – V. 161. – I. 12. – P. H787–H795.

135. Mohsenzadeh A., Richards T., Bolton K. DFT study of the water gas shift reaction on Ni(111), Ni(100) and Ni(110) surfaces // Surf. Sci. – 2016. – V. 644. – P. 53–63.

136. Greeley J., Mavrikakis M. A first-principles study of surface and subsurface H on and in Ni(111): Diffusional properties and coverage-dependent behavior // Surf. Sci. – 2003. – V. 540. – P. 215–229.

137. Panczyk T., Szabelski P., Rudzinski W. Hydrogen adsorption on nickel (100) single-crystal face. A Monte Carlo study of the equilibrium and kinetics. // J. Phys. Chem. B. 2005. – V. 109. – I. 21. – P. 10986–10994.

138. Reddy A.K.N. Preferred orientations in nickel electro-deposits: I. The mechanism of development of textures in nickel electrodeposits // J. Electroanal. Chem. – 1963. – V. 6. – I. 2. – P. 141–152.

139. Kresse G. Dissociation and sticking of H_2 on the Ni(111), (100), and (110) substrate // Phys. Rev. B. – 2000. – V. 62. – I. 12. – P. 8295.

140. Christmann K. Adsorption of hydrogen on nickel single crystal surfaces // J. Chem. Phys. – 1974. – V. 60. – I. 11. – P. 4528.

141. Bhatia B., Sholl D.S. Chemisorption and diffusion of hydrogen on surface and subsurface sites of flat and stepped nickel surfaces // J. Chem. Phys. – 2005. – V. 122. – I. 20. – P. 1–8.

142. Winkler A., Rendulic K.D. Adsorption kinetics for hydrogen adsorption on nickel and coadsorption of hydrogen and oxygen // Surf. Sci. – 1982. – V. 118. – P. 19–31.

143. Taylor C., Kelly R.G., Neurock M. First-Principles Calculations of the Electrochemical Reactions of Water at an Immersed Ni(111)/H_2O Interface // J. Electrochem. Soc. – 2006. – V. 153. – I. 12. – P. E207.

144. Mohsenzadeh A., Bolton K., Richards T. DFT study of the adsorption and dissociation of water on Ni(111), Ni(110) and Ni(100) surfaces // Surf. Sci. – 2014. – V. 627. – P. 1–10.

145. Seenivasan H., Tiwari A.K. Water adsorption and dissociation on Ni(110): How is it different from its close packed counterparts? // J. Chem. Phys. – 2014. – V. 140. – I. 17. – P. 174704.

146. Fajín J.L.C., Cordeiro M.N.D.S., Illas F., Gomes J.R.B. Descriptors controlling the catalytic activity of metallic surfaces toward water splitting // J. Catal. – 2010. – V. 276. – I. 1. – P. 92–100.

147. Herron A., Scaranto J., Ferrin P., Li S., Mavrikakis M. Trends in Formic Acid Decomposition on Model Transition Metal Surfaces : A Density Functional Theory study // ACS Catalysis. – 2014. – V. 4. – I. 1. – P. 4434–4445.

148. Hammer B., Hansen L., Nørskov J. Improved adsorption energetics within density-functional theory using revised Perdew-Burke-Ernzerhof functionals // Phys. Rev. B. – 1999. – V. 59. – I. 11. – P. 7413–7421.

149. Kresse G., Hafner J. First-principles study of the adsorption of atomic H on Ni (111), (100) and (110) // Surf. Sci. – 2000. – V. 459. – I. 3. – P. 287–302.

150. Che F., Gray J.T., Ha Su, McEwen J.-S. Catalytic water dehydrogenation and formation on nickel: Dual path mechanism in high electric fields // J. Catal. – 2015. – V. 332. – P. 187–200.

151. Shan J., Aarts J.F.M., Kleyn A.W., Juurlink L.B.F. The interaction of water with Ni(111) and H/Ni(111) studied by TPD and HREELS. // Phys. Chem. Chem. Phys. – 2008. – V. 10. – I. 16. – P. 2227–2232.

152. Yang H., Whitten J. The adsorption of water and hydroxyl on Ni(111) // Surf. Sci. – 1989. – V. 223. – I. 1–2. – P. 131–150.

153. Huang Y., Ling C., Jin M., Du J., Zhou T., Wang S. Water adsorption and dissociation on Ni surface: effects of steps, dopants, coverage and self-aggregation. // Phys. Chem. Chem. Phys. – 2013. – V. 15. – I. 41. – P. 17804–17817.

154. Shan J., Aarts J.F.M., Kleyn A.W., Juurlink L.B.F. Co-adsorption of water and hydrogen on Ni(111) // Phys. Chem. Chem. Phys. – 2008. – V. 10. – I. 32. – P. 4994–5003.

155. Liu S., Ishimoto T., Koyama M. First-principles study of Oxygen Coverage Effect on Hydrogen Oxidation on Ni(111) Surface // Appl. Surf. Sci. – 2015. – V. 333. – P. 86–91.

156. Schulze M., Reißner R., Bolwin K., Kuch W. Interaction of water with clean and oxygen precovered nickel surfaces // Fresenius. J. Anal. Chem. – 1995. – V. 353. – I. 5. – P. 661–665.

157. Yang H., Whitten J.L. Adsorption of SH and OH and coadsorption of S, O and H on Ni(111) // Surf. Sci. – 1997. – V. 370. – I. 2–3. – P. 136–154.

158. Xing B., Wang G.-C. Insight into the general rule for the activation of the X-H bonds (X = C, N, O, S) induced by chemisorbed oxygen atoms. // Phys. Chem. Chem. Phys. – 2014. – V. 16. – I. 6. – P. 2621–2629.

159. Yang H., Whitten J. Energetics of hydroxyl and influence of coadsorbed oxygen on metal surfaces // J. Phys. Chem. B. – 1997. – V. 5647. – I. 100. – P. 4090–4096.

160. Safizadeh F., Ghali E., Houlachi G. Electrocatalysis developments for hydrogen evolution reaction in alkaline solutions – A Review // Int. J. Hydrogen Energy. – 2015. – V. 40. – I. 1. – P. 256–274.

161. Kiros Y., Majari M., Nissinen T.A. Effect and characterization of dopants to Raney nickel for hydrogen oxidation // J. Alloys Compd. – 2003. – V. 360. – P. 279–285.

162. Birry L., Lasia A. Studies of the Hydrogen Evolution Reaction on Raney Nickel–Molybdenum Electrodes // J. Appl. Electrochem. – 2004. – V. 34. – I. 7. – P. 735–749.

163. Endoh E., Otouma H., Morimoto T., Oda Y. New Raney nickel composite-coated electrode for hydrogen evolution // Int. J. Hydrogen Energy. – 1987. – V. 12. – I. 7. – P. 473–479.

164. Bates M.K., Jia Q., Ramaswamy N., Allen R.J., Mukerjee S. Composite Ni/NiO-Cr_2O_3 catalyst for alkaline hydrogen evolution reaction // J. Phys. Chem. C. – 2015. – V. 119. – I. 10. – P. 5467–5477.

165. Raj I.A., Vasu K.I. Transition metal-based hydrogen electrodes in alkaline solution - electrocatalysis on nickel based binary alloy coatings // J. Appl. Electrochem. – 1990. – V. 20. – I. 1. – P. 32–38.

166. Makrides A.C. Hydrogen Overpotential on Nickel in Alkaline Solution // J. Electrochem. Soc. – 1962. – V. 109. – I. 10. – P. 977–984.

167. Doyle D.M., Palumbo G., Aust K.T., El-Sherik A.M., Erb U. The influence of intercrystalline defects on hydrogen activity and transport in nickel // Acta Metall. Mater. – 1995. – V. 43. – I. 8. – P. 3027–3033.

168. Ahn S.H., Hwang S.J., Yoo S.J., Choi I., Kim H.-J., Jang J.H., Nam S.W., Lim T.-H., Lim T., Kim S.-K., Kim J.J. Electrodeposited Ni dendrites with high activity and durability for hydrogen evolution reaction in alkaline water electrolysis // J. Mater. Chem. – 2012. – V. 22. – I. 30. – P. 15153–15159.

169. Maximovitch S., Durand R. Role of nickel oxidation in the electrocatalytic properties of nickel electrodes versus hydrogen reactions in KOH solutions // J. Electroanal. Chem. Interfacial Electrochem. – 1983. – V. 149. – I. 1–2. – P. 273–277.

170. Hall D.E. Plasma-sprayed nickel cathode coatings for hydrogen evolution in alkaline electrolytes // J. Appl. Electrochem. – 1984. – V. 14. – I. 1. – P. 107–115.

171. Marozzi C.A., Chialvo A.C. Development of electrode morphologies of interest in electrocatalysis. Part 2: Hydrogen evolution reaction on macroporous nickel electrodes // Electrochim. Acta. – 2001. – V. 46. – I. 6. – P. 861–866.

172. Gabler A., Müller C.I., Rauscher T., Köhring M., Kieback B., Röntzsch L., Schade W. Ultrashort pulse laser-structured nickel surfaces as hydrogen evolution electrodes for alkaline water electrolysis // Int. J. Hydrogen Energy. – 2017. – V. 42. – I. 16. – P. 10826–10833.

173. Lee J.K., Yi Y., Lee H.J., Uhm S., Lee J. Electrocatalytic activity of Ni nanowires prepared by galvanic electrodeposition for hydrogen evolution reaction // Catal. Today. – 2009. – V. 146. – I. 1–2. – P. 188–191.

174. Chen P.C., Chang Y.M., Wu P.W., Chiu Y.F. Fabrication of Ni nanowires for hydrogen evolution reaction in a neutral electrolyte // Int. J. Hydrogen Energy. – 2009. – V. 34. – I. 16. – P. 6596–6602.

175. Ewing S.J., Lan R., Xu X.X., Tao S.W. Synthesis of dendritic nano-sized nickel for use as anodematerial in an alkaline membrane fuel cell // Fuel Cells. – 2010. – V. 10. – I. 1. – P. 72–76.

176. Kuang Y., Feng G., Li P., Bi Y., Li Y., Sun X. Single-Crystalline Ultrathin Nickel Nanosheets Array from in Situ Topotactic Reduction for Active and Stable Electrocatalysis // Angew. Chem. Int. Ed. – 2016. – V. 55. – I. 2. – P. 693–697.

177. Ogihara H., Fujii M., Saji T. Hydrogen evolution reaction (HER) over electroless-deposited nickel nanospike arrays // RSC Adv. – 2014. – V. 4. – I. 102. – P. 58660–58663.

178. Choquette Y., Brossard L., Ménard H. In situ activation of the Raney-Ni composite-coated electrode for the hydrogen evolution reaction // Int. J. Hydrogen Energy. – 1980. – V. 15. – I. 8. – P. 551–555.

179. Dyer C. Improved cathodes for industrial electrolytic hydrogen production // Int. J. Hydrogen Energy. – 1984. – V. 9. – I. 12. – P. 993–995.

180. Beeck O. Catalysis and the Adsorption of Hydrogen on Metal Catalysts // Adv. Catal. – 1950. – V. 2. – P. 151–195.

181. Wang J., Mao S., Liu Z., Wei Z., Wang H., Chen Y., Wang Y. Dominating Role of Ni0 on the Interface of Ni/NiO for Enhanced Hydrogen Evolution Reaction // ACS Appl. Mater. Interfaces. – 2017. – V. 9. – I. 8. – P. 7139–7147.

182. Danilovic N., Subbaraman R., Strmcnik D., Chang K.-C., Paulikas A.P., Stamenkovic V.R., Markovic N.M. Enhancing the alkaline hydrogen evolution reaction activity through the bifunctionality of Ni(OH)2/metal catalysts. // Angew. Chem. Int. Ed. Engl. – 2012. – V. 51. – I. 50. – P. 12495–12498.

183. Gong M., Zhou Wu, Tsai M.-C., Zhou J., Guan M., Lin M.-C., Zhang Bo, Hu Y., Wang D.-Y., Yang, J., Pennycook S.J., Hwang B.-J., Dai H. Nanoscale nickel oxide/nickel heterostructures for active hydrogen evolution electrocatalysis // Nat. Commun. – 2014. – V. 5. – P. 4695.

184. Gong M., Zhou Wu, Kenney M.J., Kapusta R., Cowley S., Wu Y., Lu B., Lin M.-C., Wang D.-Y., Yang J., Hwang B.-J., Dai H. Blending Cr_2O_3 into a NiO-Ni Electrocatalyst for Sustained Water Splitting // Angew. Chemie. – 2015. – V. 127. – I. 41. – P. 12157–12161.

185. Gong M., Wang D.-Y., Chen C.-C., Hwang B.-J., Dai H. A mini review on nickel-based electrocatalysts for alkaline hydrogen evolution reaction // Nano Res. – 2016. – V. 9. – I. 1. – P. 28–46.

186. Xu Y.F., Gao M.R., Zheng Y.R., Jiang J., Yu S.H. Nickel/nickel(II) oxide nanoparticles anchored onto cobalt(IV) diselenide nanobelts for the electrochemical production of hydrogen // Angew. Chem. Int. Ed. – 2013. – V. 52. – I. 33. – P. 8546–8550.

187. Yan X., Tian L., Chen X. Crystalline/amorphous Ni/NiO core/shell nanosheets as highly active electrocatalysts for hydrogen evolution reaction // J. Power Sources. – 2015. – V. 300. – P. 336–343.

188. Zeng K., Zhang D. Recent progress in alkaline water electrolysis for hydrogen production and applications // Prog. Energy Combust. Sci. – 2010. – V. 36. – I. 3. – P. 307–326.

189. Bodner M., Hofer A., Hacker V. H_2 generation from alkaline electrolyzer // Wiley Interdiscip. Rev. Energy Environ. – 2015. – V. 4. – I. 4. – P. 365–381.

190. Zou X., Zhang Y. Noble metal-free hydrogen evolution catalysts for water splitting // Chem. Soc. Rev. – 2015. – V. 44. – P. 5148–5180.

191. Lu S., Zhuang Z. Electrocatalysts for hydrogen oxidation and evolution reactions // Sci. China Mater. – 2016. – V. 59. – I. 3. – P. 217–238.

192. Jenseit W., Khalil A., Wendt H. Material properties and processing in the production of fuel cell components: I. Hydrogen anodes from Raney nickel for lightweight alkaline fuel cells // J. Appl. Electrochem. – 1990. – V. 20. – I. 6. – P. 893–900.

193. Tanaka S., Hirose N., Tanaki T., Ogata Y.H. Effect of Ni-Al Precursor Alloy on the Catalytic Activity for a Raney-Ni Cathode // J. Electrochem. Soc. – 2000. – V. 147. – I. 6. – P. 2242–2245.

194. De Giz M.J., Machado S.A.S., Avaca L.A., Gonzalez E.R. High area Ni-Zn and Ni-Co-Zn codeposits as hydrogen electrodes in alkaline solutions // J. Appl. Electrochem. – 1992. – V. 22. – I. 10. – P. 973–977.

195. Kenjo T. Chromium-Doped Raney Nickel Catalyst for Hydrogen Electrodes in Alkaline Fuel Cells // J. Electrochem. Soc. – 1985. – V. 132. – I. 2. – P. 383–386.

196. Tang M.H., Hahn C., Klobuchar A.J., Ng J.W.D., Wellendorff J., Bligaard T., Jaramillo T.F. Nickel-silver alloy electrocatalysts for hydrogen evolution and oxidation in an alkaline electrolyte. // Phys. Chem. Chem. Phys. – 2014. – V. 16. – I. 36. – P. 19250–19257.

197. Mert M.E., Kardaş G. Electrocatalytic behaviour of NiBi coatings for hydrogen evolution reaction in alkaline medium // J. Alloys Compd. – 2011. – V. 509. – I. 37. – P. 9190–9194.

198. Kaninski M.P.M., Nikolic V.M., Tasic G.S., Rakocevic Z.L. Electrocatalytic activation of Ni electrode for hydrogen production by electrodeposition of Co and V species // Int. J. Hydrogen Energy. – 2009. – V. 34. – I. 2. – P. 703–709.

199. Lupi C., Dell'Era A., Pasquali M. Nickel–cobalt electrodeposited alloys for hydrogen evolution in alkaline media // Int. J. Hydrogen Energy. – 2009. – V. 34. – I. 5. – P. 2101–2106.

200. Zeng K., Zhang D. Evaluating the effect of surface modifications on Ni based electrodes for alkaline water electrolysis // Fuel. – 2014. – V. 116. – P. 692–698.

201. Solmaz R., Döner A., Kardaş G. Electrochemical deposition and characterization of NiCu coatings as cathode materials for hydrogen evolution reaction // Electrochem. commun. – 2008. – V. 10. – I. 12. – P. 1909–1911.

202. Ahn S.H., Park H.H.-Y., Choi I., Yoo S.J., Hwang S.J., Kim H.-J., Cho E., Yoon C.W., Son H., Hernandez J.M., Nam S.W., Lim T.-H., Kim S.-K., Jang J.H. Electrochemically fabricated NiCu alloy catalysts for hydrogen production in alkaline water electrolysis // Int. J. Hydrogen Energy.– 2013. – V. 38. – I. 31. – P. 13493–13501.

203. Ngamlerdpokin K., Tantavichet N. Electrodeposition of nickel–copper alloys to use as a cathode for hydrogen evolution in an alkaline media // Int. J. Hydrogen Energy. – 2014. – V. 39. – I. 6. – P. 2505–2515.

204. Mauer A.E., Kirk D.W., Thorpe S.J. The role of iron in the prevention of nickel electrode deactivation in alkaline electrolysis // Electrochim. Acta. – 2007. – V. 52. – I. 11. – P. 3505–3509.

205. Simpraga R. et al. In situ determination of the “real area factox” in H2 evolution electrocatalysis at porous Ni - Fe composite electrodes // J. Electroanal. Chem. – 1997. – V. 424. – P. 141–151.

206. Brown D.E., Mahmood M.N., Turner A.K., Hall S.M., Fogarty – P.O. Low overvoltage electrocatalysts for hydrogen evolving electrodes // Int. J. Hydrogen Energy. – 1982. – V. 7. – I. 5. – P. 405–410.

207. Conway B.E., Bai L. H_2 evolution kinetics at high activity Ni-Mo-Cd electrocoated cathodes and its relation to potential dependence of sorption of H // Int. J. Hydrogen Energy. – 1986. – V. 11. – I. 8. – P. 533–540.

208. Huot J.Y., Trudeau M.L., Schulz R. Low Hydrogen Overpotential Nanocrystalline Ni-Mo Cathodes for Alkaline Water Electrolysis // J. Electrochem. Soc. – 1991. – V. 138. – I. 5. – P. 1316–1321.

209. Albertini L.B., Angelo A.C.D., Gonzalez E.R. A nickel molybdenite cathode for the hydrogen evolution reaction in alkaline media // J. Appl. Electrochem. – 1992. – V. 22. – I. 9. – P. 888–892.

210. Gennero de Chialvo M.R., Chialvo A.C. Hydrogen evolution reaction on smooth Ni(1−x)+Mo(x) alloys ($0 \leq x \leq 0.25$) // J. Electroanal. Chem. – 1998. – V. 448. – I. 1. – P. 87–93.

211. Jakšić J., Vojnović M., Krstajić N. Kinetic analysis of hydrogen evolution at Ni–Mo alloy electrodes // Electrochim. Acta. – 2000. – V. 45. – I. 25–26. – P. 4151–4158.

212. Kawashima A., Akiyama E., Habazaki H., Hashimoto K. Characterization of sputter-deposited Ni-Mo and Ni-W alloy electrocatalysts for hydrogen evolution in alkaline solution // Mater. Sci. Eng., A – 1997. – V. 226–228. – P. 905–909.

213. Paloukis F., Zafeiratos S., Drakopoulos V., Neophytides S.G. Electronic structure modifications and HER of annealed electrodeposited Ni overlayers on Mo polycrystalline surface // Electrochim. Acta. 2008. – V. 53. – I. 27. – P. 8015–8025.

214. Krstajic N., Jovic V., Gajickrstajic L., Jovic B., Antozzi A., Martelli G. Electrodeposition of Ni–Mo alloy coatings and their characterization as cathodes for hydrogen evolution in sodium hydroxide solution // Int. J. Hydrogen Energy. – 2008. – V. 33. – I. 14. – P. 3676–3687.

215. Chen W.-F., Sasaki K., Ma C., Frenkel A.I., Marinkovic N., Muckerman J.T., Zhu Y., Adzic R.R. Hydrogen-evolution catalysts based on non-noble metal

nickel-molybdenum nitride nanosheets. // Angew. Chem. Int. Ed. Engl. 2012. – V. 51. – I. 25. – P. 6131–6135.

216. McKone J.R., Sadtler B.F., Werlang C.A., Lewis N.S., Gray H.B. Ni-Mo nanopowders for efficient electrochemical hydrogen evolution // ACS Catal. – 2013. – V. 3. – I. 2. – P. 166–169.

217. Tang X., Xiao Li, Yang C., Lu J., Zhuang L. Noble fabrication of Ni–Mo cathode for alkaline water electrolysis and alkaline polymer electrolyte water electrolysis // Int. J. Hydrogen Energy. – 2014. – V. 39. – I. 7. – P. 3055–3060.

218. Zhang L., Xiong K., Nie Y., Wang X., Liao J., Wei Z. Sputtering nickel-molybdenum nanorods as an excellent hydrogen evolution reaction catalyst // J. Power Sources. – 2015. – V. 297. – P. 413–418.

219. Fang M., Gao W., Dong G., Xia Z., Yip S.P., Qin Y., Qu Y., Ho J.C. Hierarchical NiMo-based 3D electrocatalysts for highly-efficient hydrogen evolution in alkaline conditions // Nano Energy. – 2016. – V. 27. – P. 247–254.

220. Fan C., Piron D., Rojas M. Polarization of cobalt-molybdenum and nickel-molybdenum hydrogen electrodes for alkaline fuel cells // Int. J. Hydrogen Energy. – 1994. – V. 19. – I. 6. – P. 529–533.

221. Danaee I., Noori S. Kinetics of the hydrogen evolution reaction on NiMn graphite modified electrode // Int. J. Hydrogen Energy. – 2011. – V. 36. – I. 19. – P. 12102–12111.

222. Aaboubi O., Ali-Omar A.-Y., Dzoyem E., Marthe J., Boudifa M. Ni–Mn based alloys as versatile catalyst for different electrochemical reactions // J. Power Sources. – 2014. – V. 269. – P. 597–607.

223. Franceschini E.A., Lacconi G.I., Corti H.R. Kinetics of hydrogen evolution reaction on nickel modified by spontaneous Ru deposition: A rotating disk electrode and impedance spectroscopy approach // Int. J. Hydrogen Energy. – 2016. – V. 41. – I. 5. – P. 3326–3338.

224. Jović B.M., Lačnjevac, U.Č., Krstajić, N.V., Jović, V.D. Ni–Sn coatings as cathodes for hydrogen evolution in alkaline solutions // Electrochim. Acta. – 2013. – V. 114. – P. 813–818.

225. Machida K., Enyo M., Adachi G., Shiokawa J. The hydrogen electrode reaction characteristics of thin film electrodes of Ni-based hydrogen storage alloys // Electrochim. Acta. – 1984. – V. 29. – I. 6. – P. 807–815.

226. Panek J., Serek A., Budniok A. Rówinski E., Łagiewka E. Ni + Ti composite layers as cathode materials for electrolytic hydrogen evolution // Int. J. Hydrogen Energy. – 2002. – V. 28. – I. 2. – P. 169–175.

227. Kellenberger A., Vaszilcsin N., Brandl W., Duteanu N. Kinetics of hydrogen evolution reaction on skeleton nickel and nickel–titanium electrodes obtained by thermal arc spraying technique // Int. J. Hydrogen Energy. – 2007. – V. 32. – I. 15. – P. 3258–3265.

228. Brown D.E., Mahmood M.N., Man M.C.M., Turner A.K. Preparation and characterization of low overvoltage transition metal alloy electrocatalysts for hydrogen evolution in alkaline solutions // Electrochim. Acta. – 1984. – V. 29. – I. 11. – P. 1551–1556.

229. Abouatallah R.M., Kirk D.W., Thorpe S.J., Graydon J.W. Reactivation of nickel cathodes by dissolved vanadium species during hydrogen evolution in alkaline media // Electrochim. Acta. – 2001. – V. 47. – I. 4. – P. 613–621.

230. Lu S.F., Pan J., Huang A.B., Zhuang L., Lu J.T. Alkaline polymer electrolyte fuel cells completely free from noble metal catalysts // Proc. Natl. Acad. Sci. U. S. A. – 2008. – V. 105. – I. 52. – P. 20611–20614.

231. Oliver-Tolentino M.A., Arce-Estrada E.M., Cortés-Escobedo C.A., Bolarín-Miro A.M., Sánchez-De Jesús F., González-Huerta R.de G., Manzo-Robledo A. Electrochemical behavior of Ni_xW_{1-x} materials as catalyst for hydrogen evolution reaction in alkaline media // J. Alloys Compd. – 2012. – V. 536. – P. S245–S249.

232. Hu Q., Li G., Pan J., Tan L., Lu J., Zhuang L. Alkaline polymer electrolyte fuel cell with Ni-based anode and Co-based cathode // Int. J. Hydrogen Energy. – 2013. – V. 38. – I. 36. – P. 16264–16268.

233. Marini S., Salvi P., Nelli P., Pesenti R., Villa M., Kiros Y. Stable and inexpensive electrodes for the hydrogen evolution reaction // Int. J. Hydrogen Energy. – 2013. – V. 38. – I. 26. – P. 11484–11495.

234. Salvi P., Nelli P., Villa M., Kiros Y., Zangari G., Bruni G., Marini A., Milanese C. Hydrogen evolution reaction in PTFE bonded Raney-Ni electrodes // Int. J. Hydrogen Energy. – 2011. – V. 36. – I. 13. – P. 7816–7821.

235. Choquette Y. Study of the Kinetics of Hydrogen Evolution Reaction on Raney Nickel Composite-Coated Electrode by AC Impedance Technique // J. Electrochem. Soc. – 1990. – V. 137. – I. 6. – P. 1723–1730.

236. Lupi C., Dell'Era A., Pasquali M. In situ activation with Mo of Ni-Co alloys for hydrogen evolution reaction // Int. J. Hydrogen Energy. – 2014. – V. 39. – I. 5. – P. 1932–1940.

237. Tasic G.S., Maslovara S.P. Zugic D.L., Maksic A.D., Marceta Kaninski M.P. Characterization of the Ni–Mo catalyst formed in situ during hydrogen generation from alkaline water electrolysis // Int. J. Hydrogen Energy. – 2011. – V. 36. – I. 18. – P. 11588–11595.

238. Huot J., Brossard L. Time dependence of the hydrogen discharge at 70°C on nickel cathodes // Int. J. Hydrogen Energy. – 1987. – V. 12. – I. 12. – P. 821–830.

239. Wang X., Su R., Aslan H., Kibsgaard J., Wendt S., Meng L., Dong M., Huang Y., Besenbacher F. Tweaking the composition of NiMoZn alloy electrocatalyst for enhanced hydrogen evolution reaction performance // Nano Energy. – 2015. – V. 12. – P. 9–18.

240. Jaksic M.M. Hypo-hyper-d-electronic interactive nature of interionic synergism in catalysis and electrocatalysis for hydrogen reactions // Int. J. Hydrogen Energy. – 2001. – V. 26. – I. 6. – P. 559–578.

241. Franceschini E.A., Lacconi G.I., Corti H.R. Kinetics of the hydrogen evolution on nickel in alkaline solution: new insight from rotating disk electrode and impedance spectroscopy analysis // Electrochim. Acta. – 2015. – V. 159. – P. 210–218.

242. Bernardini M., Comisso N. Davolio G., Mengoli G., Sinico L. Formation of nickel hydrides by hydrogen evolution in alkaline media: effect of temperature // J. Electroanal. Chem. – 1998. – V. 457. – I. 1–2. – P. 205–219.

243. Rommal H.E.G., Morgan P.J. The Role of Absorbed Hydrogen on the Voltage-Time Behavior of Nickel Cathodes in Hydrogen Evolution // J. Electrochem. Soc. – 1988. – V. 135. – I. 2. – P. 343.

244. Huot J.-Y. Hydrogen Evolution and Interface Phenomena on a Nickel Cathode in 30 w/o KOH // J. Electrochem. Soc. – 1989. – V. 136. – I. 7. – P. 1933.

245. Rommal H.E.G. Time-Dependent Energy Efficiency Losses at Nickel Cathodes in Alkaline Water Electrolysis Systems // J. Electrochem. Soc. – 1985. – V. 132. – I. 2. – P. 325–329.

246. Conway B.E. Study of a Decomposing Hydride Phase at Nickel Cathodes by Measurement of Open-Circuit Potential Decay // J. Electrochem. Soc. – 1983. – V. 130. – I. 9. – P. 1825–1836.

247. Szklarska-Smialowska Z., Smialowski M. Electrochemical Study of the Nickel-Hydrogen System // J. Electrochem. Soc. – 1963. – V. 110. – I. 5. – P. 444.

248. Solmaz R., Döner A., Kardaş G. The stability of hydrogen evolution activity and corrosion behavior of NiCu coatings with long-term electrolysis in alkaline solution // Int. J. Hydrogen Energy. – 2009. – V. 34. – I. 5. – P. 2089–2094.

249. Hu W., Lee J.-Y. Electrocatalytic properties of Ti2Ni/Ni-Mo composite electrodes for hydrogen evolution reaction // Int. J. Hydrogen Energy. – 1998. – V. 23. – I. 4. – P. 253–257.

250. Bockris J.O., Conway B.E. Preparation and Maintenance of Electrodes in a Hydrogen Atmosphere // J. Sci. Instrum. – 1948. – V. 25. – I. 8. – P. 283–283.

251. Devanathan M.A. V., Selvaratnam M. Mechanism of the hydrogen-evolution reaction on nickel in alkaline solutions by the determination of the degree of coverage // Trans. Faraday Soc. – 1960. – V. 56. – P. 1820–1831.

252. Kreysa G., Håkansson B. Electrocatalysis by amorphous metals of hydrogen and oxygen evolution in alkaline solution // J. Electroanal. Chem. Interfacial Electrochem. – 1986. – V. 201. – I. 1. – P. 61–83.

253. Kreysa G., Hakansson B., Ekdunge P. Kinetic and Thermodynamic Analysis of Hydrogen Evolution At Nickel Electrodes // Electrochim. Acta. – 1988. – V. 33. – I. 10. – P. 1351–1357.

254. Kibria M. Electrochemical studies of a nickel electrode for the hydrogen evolution reaction // Int. J. Hydrogen Energy. – 1995. – V. 20. – I. 6. – P. 435–440.

255. Diard J.P., LeGorrec B., Maximovitch S. Etude de l'activation du degagement d'hydrogene sur electrode d'oxyde de nickel par spectroscopie d'impedance // Electrochim. Acta. – 1990. – V. 35. – I. 6. – P. 1099–1108.

256. Conway B.E., Bai L. Determination of the adsorption behaviour of "overpotential-deposited" hydrogen-atom species in the cathodic hydrogen-evolution reaction by analysis of potential-relaxation transients // J. Chem. Soc. Faraday Trans. 1 Phys. Chem. Condens. Phases. – 1985. – V. 81. – I. 8. – P. 1841–1862.

257. Krstajić N., Popović M., Grgur B., Vojnović M., Šepa D. On the kinetics of the hydrogen evolution reaction on nickel in alkaline solution - Part I. The mechanism // J. Electroanal. Chem. – 2001. – V. 512. – I. 1–2. – P. 16–26.

258. Angely L., Bronoel G., Peslerbe G. Relation between nickel crystalline structures and their electrocatalytic properties: Part III. Steady-state oxidoreduction characteristics of hydrogen on Ni // J. Electroanal. Chem. Interfacial Electrochem. – 1979. – V. 96. – I. 2. – P. 203–208.

259. Conway B.E., Jerkiewicz G. Thermodynamic and electrode kinetic factors in cathodic hydrogen sorption into metals and its relationship to hydrogen adsorption and poisoning // J. Electroanal. Chem. – 1993. – V. 357. – I. 1–2. – P. 47–66.

260. Ekdunge P., Jiittner K., Kreyso G. Electrochemical Impedance Study on the Kinetics of Hydrogen Evolution at Amorphous Metals in Alkaline Solution. – 1991. – V. 138. – I. 9. – P. 2660–2668.

261. Krstajić N., Popović M., Grgur B., Vojnović M., Šepa D. On the kinetics of the hydrogen evolution reaction on nickel in alkaline solution Part II. Effect of temperature // J. Electroanal. Chem. – 2001. – V. 512. – I. 1–2. – P. 27–35.

262. Yeh J.-J. Atomic calculation of photoionization cross-sections and asymmetry parameters. Gordon & Breach Science Publ.; AT&T Bell Laboratories. – 1993.

263. Scherer J., Ocko B., Magnussen O. Structure, dissolution, and passivation of Ni(111) electrodes in sulfuric acid solution: an in situ STM, X-ray scattering, and electrochemical study // Electrochim. Acta. – 2003. – V. 48. – I. 9. – P. 1169–1191.

264. Biesinger M.C., Payne B.P., Lau L.W.M., Gerson A., Smart R.St.C. X-ray photoelectron spectroscopic chemical state quantification of mixed nickel metal, oxide and hydroxide systems // Surf. Interface Anal. – 2009. – V. 41. – I. 4. – P. 324–332.

265. Peck M.A., Langell M.A. Comparison of Nanoscaled and Bulk NiO Structural and Environmental Characteristics by XRD, XAFS, and XPS // Chem. Mater. – 2012. – V. 24. – I. 23. – P. 4483–4490.

266. Payne B.P., Biesinger M.C., McIntyre N.S. The study of polycrystalline nickel metal oxidation by water vapour // J. Electron Spectros. Relat. Phenomena. – 2009. – V. 175. – I. 1–3. – P. 55–65.

267. Barr T.L., Sudipta S. Nature of the use of adventitious carbon as a binding energy standard // J. Vac. Sci. Technol. A Vacuum, Surfaces, Film. – 1995. – V. 13. – I. 3. – P. 1239–1246.

268. Zhang Z., Liu Y., Huang Z., Ren L., Qi X., Wei X., Zhong J. Facile hydrothermal synthesis of $NiMoO_4$ @$CoMoO_4$ hierarchical nanospheres for supercapacitor applications // Phys. Chem. Chem. Phys. – 2015. – V. 17. – I. 32. – P. 20795–20804.

269. Haetge J., Djerdj I., Brezesinski T. Nanocrystalline NiMoO4 with an ordered mesoporous morphology as potential material for rechargeable thin film lithium batteries // Chem. Commun. – 2012. – V. 48. – I. 53. – P. 6726–6728.

270. Scanlon D.O., Watson G.W., Payne D.J., Atkinson G.R., Egdell R.G., Law D.S.L. Theoretical and Experimental Study of the Electronic Structures of MoO_3 and MoO_2 // J. Phys. Chem. C. – 2010. – V. 114. – I. 10. – P. 4636–4645.

271. Baltrusaitis J., Mendoza-Sanchez B., Fernandez V., Veenstra R., Dukstiene N., Roberts A., Fairley N. Generalized molybdenum oxide surface chemical state XPS determination via informed amorphous sample model // Appl. Surf. Sci. – 2015. – V. 326. – P. 151–161.

272. Sarkany J. On the use of the dynamic pulse method to measure metal surface areas // J. Catal. – 1982. – V. 76. – I. 1. – P. 75–83.

273. Bard A.J., Faulkner L.R. Electrochemical Methods: Fundamentals and Applications. 2nd ed. JOHN WILEY & SONS, INC.. – 2001. 856 p.

274. Damaskin B.B., Petrii O.A., Tsirlina G.A. Electrochemistry, 2nd ed. Moscow: Chemistry, KolosS. – 2006. – 672 p.

275. Lide D.R. CRC Handbook of chemistry and physics. 84th ed. CRC Press. – 2003. 2475 p.

276. Bonnefont A. et al. Hydrogen electrooxidation on PdAu supported nanoparticles: An experimental RDE and kinetic modeling study // Catal. Today. – 2013. – V. 202. – P. 70–78.

277. Salmeron M., Schlogl R. Ambient pressure photoelectron spectroscopy: A new tool for surface science and nanotechnology // Surf. Sci. Rep. – 2008. – V. 63. – I. 4. – P. 169–199.

278. Saveleva V.A., Wang Li, Luo W., Zafeiratos S., Ulhaq-Bouillet C., Gago A.S., Friedrich K. A., Savinova E.R. Uncovering the Stabilization Mechanism in Bimetallic Ruthenium-Iridium Anodes for Proton Exchange Membrane Electrolyzers // J. Phys. Chem. Lett. – 2016. – V. 7. – I. 16. – P. 3240–3245.

279. Diaz-Morales O., Calle-Vallejo F., de Munck C., Koper M.T.M. Electrochemical water splitting by gold: evidence for an oxide decomposition mechanism // Chem. Sci. – 2013. – V. 4. – I. 6. – P. 2334.

280. Kitakatsu N., Maurice V., Hinnen C., Marcus P. Surface hydroxylation and local structure of NiO thin films formed on Ni(111) // Surf. Sci. – 1998. – V. 407. – I. 1–3. – P. 36–58.

281. Medford J.A, Johnston-Peck A.C., Tracy J.B. Nanostructural transformations during the reduction of hollow and porous nickel oxide nanoparticles. // Nanoscale. – 2013. – V. 5. – I. 1. – P. 155–159.

282. Sadykov V.A., Tikhov S.F., Tsybulya S.V., Kryukova G.N., Veniaminov S.A., Kolomiichuk V.N., Bulgakov N.N., Paukshtis E.A., Ivanov V.P., Koshcheev S.V., Zaikovskii V.I., Isupova L.A., Burgina L.B. Role of defect structure in structural sensitivity of the oxidation reactions catalyzed by dispersed transition metal oxides // J. Mol. Catal. A Chem. – 2000. – V. 158. – I. 1. – P. 361–365.

283. Tsybulya S.V., Kryukova G.N., Goncharova S.N., Shmakov A.N., Balzhinimaev B.S. Study of the Real Structure of Silver Supported Catalysts of Different Dispersity // J. Catal. – 1995. – V. 154. – I. 2. – P. 194–200.

284. Oshchepkov A.G., Simonov A.N., Simonov P.A., Shmakov A.N., Rudina N.A., Ishchenko A.V., Cherstiouk O.V., Parmon V.N. Interrelation between catalytic activity for oxygen electroreduction and structure of supported platinum // J. Electroanal. Chem. – 2014. – V. 729. – P. 34–42.

285. Lebedeva N.P., Koper M.T.M., Feliu J.M., van Santen R.A. Role of Crystalline Defects in Electrocatalysis: Mechanism and Kinetics of CO Adlayer Oxidation on Stepped Platinum Electrodes // J. Phys. Chem. B. – 2002. – V. 106. – I. 50. – P. 12938–12947.

286. Sieben J.M. Controlled size formation of electrodeposited Pt–Ru nanostructured catalysts using chelating compounds // Mater. Chem. Phys. – 2011. – V. 128. – I. 1–2. – P. 243–249.

287. Cherstiouk O.V., Gavrilov A.N., Plyasova L.M., Molina I.Yu., Tsirlina G.A., Savinova E.R. Influence of structural defects on the electrocatalytic activity of platinum // J. Solid State Electrochem. – 2008. – V. 12. – I. 5. – P. 497–509.

288. Napolskii K.S., Barczuk P.J., Vassiliev S.Yu., Veresov A.G., Tsirlina G.A., Kulesza P.J. Templating of electrodeposited platinum group metals as a tool to control catalytic activity // Electrochim. Acta. – 2007. – V. 52. – I. 28. – P. 7910–7919.

289. Simonov A.N., Cherstiouk O.V., Vassiliev S.Yu., Zaikovskii V.I., Filatov A.Yu., Rudina N.A., Savinova E.R., Tsirlina G.A. Potentiostatic electrodeposition of Pt on GC and on HOPG at low loadings: Analysis of the deposition transients and the structure of Pt deposits // Electrochim. Acta. – 2014. – V. 150. – P. 279–289.

290. Scharifker B., Hills G. Theoretical and experimental studies of multiple nucleation // Electrochim. Acta. – 1983. – V. 28. – I. 7. – P. 879–889.

291. Plyasova L.M., Molina I.Yu., Gavrilov A.N., Cherepanova S.V., Cherstiouk O.V., Rudina N.A., Savinova E.R., Tsirlina G.A. Electrodeposited platinum revisited: Tuning nanostructure via the deposition potential // Electrochim. Acta.

– 2006. – V. 51. – I. 21. – P. 4477–4488.

292. Plyasova L.M., Molina I.Yu., Cherepanova S.V., Rudina N.A., Sherstyuk O.V., Savinova E.R., Pron'kin S.N., Tsirlina G.A. Disperse Electrolytic Platinum and Palladium Deposits of Submicron Thickness on Polycrystalline Supports: An X-ray Diffractometry and Microscopy Study // Russ. J. Electrochem. – 2002. – V. 38. – I. 10. – P. 1116–1131.

293. Hammer B., Nørskov J. Theoretical surface science and catalysis—calculations and concepts // Adv. Catal. – 2000. – V. 45. – P. 71–129.

294. Linnekoski J.A., Krause A.O.I., Keskinen J., Lamminen J., Anttila T. Processing of Raney-Nickel Catalysts for Alkaline Fuel Cell Applications // J. Fuel Cell Sci. Technol. – 2007. – V. 4. – I. 1. – P. 45–48.

295. Santos E., Quaino P., Hindelang P.F., Schmickler W. Hydrogen evolution on a pseudomorphic Cu-layer on Ni(111) – A theoretical study // J. Electroanal. Chem. – 2010. – V. 649. – I. 1–2. – P. 149–152.

296. Medvedev I.G. To a theory of electrocatalysis for the hydrogen evolution reaction: The hydrogen chemisorption energy on the transition metal alloys within the Anderson-Newns model // Russ. J. Electrochem. – 2004. – V. 40. – I. 11. – P. 1123–1131.

297. Kelley M.J., Ponec V. Surface composition of alloys // Prog. Surf. Sci. – 1981. – V. 11. – I. 3. – P. 139–244.

298. Domnick R., Held G., Witte P., Steinrück H.-P. The transition from oxygen chemisorption to oxidation of ultra-thin Ni layers on Cu(111) // J. Chem. Phys. – 2001. – V. 115. – I. 4. – P. – 1902.

299. Zheng J., Zhou S., Gu S., Xu B., Yan Y. Size-Dependent Hydrogen Oxidation and Evolution Activities on Supported Palladium Nanoparticles in Acid and Base // J. Electrochem. Soc. – 2016. – V. 163. – I. 6. – P. F499–F506.

Appendices

Appendix 1 Summarized data regarding the electrocatalytic activity of various catalysts used in the thesis, as well as from the literature (values obtained at pH = 13)

Catalyst	S_M / cm^2	j_0 / µA cm$^{-2}{}_M$	i_o / A g_M^{-1}	i_k^{50mV} / A g_{Ni}^{-1}	j_k^{50mV} / µA cm_{Ni}^{-2}
Non-activated Ni rod	0.52 ± 0.03	2.3 ± 0.1	-	-	-
Ch activated Ni rod	0.35 ± 0.03	20 ± 2			
EC activated Ni rod	0.42 ± 0.04	14 ± 2	-	-	-
Polished Ni rod	0.52 ± 0.03	6.0 ± 0.8			
Non-activated Ni_{ED}/GC	0.20 ± 0.09	6.4 ± 0.6			
Ch activated Ni_{ED}/GC	0.17 ± 0.04	25 ± 3			
Non-activated Ni_{ED}/XC-72	13.0 ± 1.1	6.2 ± 0.6	5.7 ± 0.2	-	-
After cycling Ni_{ED}/XC-72	6.1 ± 1.4	29 ± 7	14.2 ± 3.1	27.8 ± 1.4	50 ± 4
Ch activated Ni_{ED}/XC-72	4.9 ± 0.9	56 ± 10	22.4 ± 4.3	32.1 ± 4.8	83 ± 12
$Ni_{0.95}Cu_{0.05}$/XC-72	-	14 ±1 (S_{CO})	2.5 ± 0.2		
$Ni_{0.9}Mo_{0.1}$/KB	1.6 ± 0.2	27 ± 2	4.5 ± 0.2		
Ni/CNT [123]	5.2	9	1.0	1.9	18
Ni/N-CNT [123]	6.2	28	3.5	9.3	75
CoNiMo [28]		15			44 ± 5
20% Pd/C Premetek Co [299]	2.9±0.2	52 ± 2	38 ± 4		
46% Pt/C (d=2.0±0.6 nm) TKK [32]	0.32±0.4	570±70	350±50		

Appendix 2. Parameters used for the kinetic modeling at T = 298 K

Parameter	Meaning	Dimension	Value		
			Non-activated Ni rod	Ch activated Ni rod	Bimetallic $Ni_{0.90}Mo_{0.10}/C$
C_{H2}	H_2 concentration	M	$7\ 10^{-4}$	$7\ 10^{-4}$	$7\ 10^{-4}$
C_{OH-}	OH^- concentration	M	0.1	0.1	0.1
S_t	Density of Ni surface active sites	$mol \cdot cm^{-2}$	$2.2\ 10^{-9}$	$2.2\ 10^{-9}$	$2.0\ 10^{-8}$
α_2	Charge transfer coefficient of the Heyrovsky step	-	0.4	0.4	0.4
α_3	Charge transfer coefficient of the Volmer step	-	0.5	0.5	0.5
k_1^0	H_2 adsorption rate constant by the Tafel step	$cm^3 \cdot s^{-1} \cdot mol^{-1}$	$3.94\ 10^7$	$1.53\ 10^6$	$6.3\ 10^4$
k_{-1}^0	H_2 formation rate constant by the Tafel step	s^{-1}	0.010	0.220	1
k_2^0	H_2 adsorption rate constant by the Heyrovsky step	$cm^6 \cdot s^{-1} \cdot mol^{-2}$	$8.7\ 10^9$	$2.5\ 10^9$	$1.1\ 10^9$
k_{-2}^0	H_2 desorption rate constant by the Heyrovsky step	s^{-1}	0.016	0.1	0.3
k_{-3}^0	H_{ad} formation rate constant by the Volmer step	s^{-1}	0.21 [i]	0.44[j]	0.11[k]
k_3^0	H_{ad} oxidation rate constant by the Volmer step	$cm^3 \cdot s^{-1} \cdot mol^{-1}$	$4.3\ 10^1$ [i]	$2.0\ 10^3$ [j]	$5.4\ 10^3$ [k]
k_4^0	Ni-OH_{ad} formation rate constant	$cm^3 \cdot s^{-1} \cdot mol^{-1}$	$1.9\ 10^4$	$1.9\ 10^4$	10^5
k_{-4}^0	Ni-OH_{ad} reduction rate constant	s^{-1}	19.3	19.3	10
E_4^0	Ni-OH_{ad} formation potential	V	0.06	0.06	0.0
k_5^0	Ni-$(OH)_{2,ad}$ formation rate constant	$cm^3 \cdot s^{-1} \cdot mol^{-1}$	30	30	11
k_{-5}^0	Ni-$(OH)_{2,ad}$ reduction rate constant	s^{-1}	3.3	3.3	0.82
E_5^0	Ni-$(OH)_{2,ad}$ formation potential	V	0.18	0.18	0.17
T	Temperature	K	298	298	298
γ	Frumkin parameter		0	0	4

[i] These values of k_3^0 and k_{-3}^0 correspond to $\Delta_{ad}G^0_H$=-RT ln(10000*k_{-3}^0 /k_3^0)=-0.1 eV.
[j] These values of k_3^0 and k_{-3}^0 correspond to $\Delta_{ad}G^0_H$ =-RT ln(10000*k_{-3}^0 /k_3^0)=-0.02 eV.
[k] These values of k_3^0 and k_{-3}^0 correspond to $\Delta_{ad}G^0_H$ =-RT ln(10000*k_{-3}^0 /k_3^0)=0.04 eV.

Appendix 3. Parameters used for the kinetic modeling of CVs obtained for polycrystalline Ni rod at various temperatures

Parameter	Non-activated Ni rod					EC activated Ni rod				
	298 K	**308 K**	**318 K**	**328 K**	**338 K**	**298 K**	**308 K**	**318 K**	**328 K**	**338 K**
k_1^0, cm^3 s^{-1} mol^{-1}	$4.74\cdot10^{8}$	$3.24\cdot10^{8}$	$2.27\cdot10^{8}$	$1.63\cdot10^{8}$	$1.19\cdot10^{8}$	$4.42\cdot10^{6}$	$4.95\cdot10^{6}$	$5.16\cdot10^{6}$	$5.11\cdot10^{6}$	$5.31\cdot10^{6}$
k_{-1}^0, s^{-1}	$2.8\cdot10^{-3}$	$2.8\cdot10^{-3}$	$2.8\cdot10^{-3}$	$2.8\cdot10^{-3}$	$2.8\cdot10^{-3}$	$6.3\cdot10^{-2}$	$8.0\cdot10^{-2}$	$9.4\cdot10^{-2}$	$1.0\cdot10^{-1}$	$1.2\cdot10^{-1}$
k_2^0, cm^6 s^{-1} mol^{-2}	$3.33\cdot10^{10}$	$4.38\cdot10^{10}$	$5.37\cdot10^{10}$	$6.37\cdot10^{10}$	$7.72\cdot10^{10}$	$3.51\cdot10^{9}$	$5.15\cdot10^{9}$	$7.29\cdot10^{9}$	$9.90\cdot10^{9}$	$1.17\cdot10^{10}$
k_{-2}^0, s^{-1}	$6.76\cdot10^{-3}$	$1.08\cdot10^{-2}$	$1.58\cdot10^{-2}$	$2.21\cdot10^{-2}$	$3.13\cdot10^{-2}$	$3.51\cdot10^{-2}$	$5.48\cdot10^{-2}$	$8.23\cdot10^{-2}$	$1.18\cdot10^{-1}$	$1.47\cdot10^{-1}$
k_3^0, cm^3 s^{-1} mol^{-1}	$1.71\cdot10^{1}$	$2.98\cdot10^{1}$	$5.18\cdot10^{1}$	$7.74\cdot10^{1}$	$1.26\cdot10^{2}$	$9.44\cdot10^{1}$	$1.60\cdot10^{2}$	$2.49\cdot10^{2}$	$3.34\cdot10^{2}$	$3.95\cdot10^{2}$
k_{-3}^0, s^{-1}	0.56	0.85	1.24	1.56	2.17	$6.62\cdot10^{-2}$	$1.05\cdot10^{-1}$	$1.54\cdot10^{-1}$	$1.96\cdot10^{-1}$	$2.20\cdot10^{-1}$
k_4^0, cm^3 s^{-1} mol^{-1}	$6.22\cdot10^{4}$	$6.46\cdot10^{4}$	$6.69\cdot10^{4}$	$6.92\cdot10^{4}$	$7.14\cdot10^{4}$	$6.22\cdot10^{4}$	$6.46\cdot10^{4}$	$6.69\cdot10^{4}$	$6.92\cdot10^{4}$	$7.14\cdot10^{4}$
k_{-4}^0, s^{-1}	$6.43\cdot10^{1}$	$6.19\cdot10^{1}$	$5.98\cdot10^{1}$	$5.78\cdot10^{1}$	$5.60\cdot10^{1}$	$6.43\cdot10^{1}$	$6.19\cdot10^{1}$	$5.98\cdot10^{1}$	$5.78\cdot10^{1}$	$5.60\cdot10^{1}$
E_4^0, V	0.06	0.06	0.06	0.06	0.06	0.06	0.06	0.06	0.06	0.06
k_5^0, cm^3 s^{-1} mol^{-1}	$5.39\cdot10^{1}$	$5.93\cdot10^{1}$	$6.48\cdot10^{1}$	$7.04\cdot10^{1}$	$7.62\cdot10^{1}$	$5.39\cdot10^{1}$	$5.93\cdot10^{1}$	$6.48\cdot10^{1}$	$7.04\cdot10^{1}$	$7.62\cdot10^{1}$
k_{-5}^0, s^{-1}	1.86	1.69	1.54	1.42	1.31	1.86	1.69	1.54	1.42	1.31
E_5^0, V	0.15	0.15	0.15	0.15	0.15	0.15	0.15	0.15	0.15	0.15

Résumé de la thèse

I. Introduction

L'augmentation de la demande en énergie et la diminution des ressources en combustibles fossiles ont largement stimulé l'utilisation de sources d'énergie renouvelable au cours des dernières décennies. L'hydrogène est considéré comme l'un des meilleurs candidats pour stocker et produire l'énergie. La conversion de l'énergie peut être réalisée en utilisant la technologie des piles à combustible, dans laquelle la réaction d'électrooxydation de l'hydrogène (HOR) produit de l'électricité. Cependant, la commercialisation des piles à combustible à membrane à échange de protons, la technologie la plus développée actuellement, est entravée par le prix élevé et la pénurie de catalyseurs à base de métaux nobles utilisés à leurs anode et cathode [1]. L'une des approches prometteuses pour réduire le coût des piles à combustible est basée sur le remplacement de la membrane échangeuse de protons par une membrane échangeuse d'anions compatible avec des catalyseurs métalliques non nobles.

Le nickel, Ni, est perçu comme l'un des électrocatalyseurs les plus prometteurs à l'anode de la pile à combustible à membrane alcaline (AMFC), en raison de sa stabilité vis à vis de la corrosion en milieu alcalin et de son activité relativement élevée pour les réactions d'oxydation/évolution de l'hydrogène (HOR/HER) par rapport à d'autres métaux non nobles. Cependant, l'activité du Ni pour l'HOR/HER est beaucoup plus faible que celle du Pt. L'addition d'un deuxième métal de transition (par exemple, Zn, Fe, Cu, Mo, etc.) permet d'améliorer la performance catalytique du Ni pour l'HER. Mais il n'y a pratiquement pas d'études consacrées à l'étude de l'HOR sur des électrodes à base de Ni. En outre, les raisons pour lesquelles une augmentation de l'activité catalytique est observée après l'ajout d'un second métal ne sont toujours pas entièrement comprises, et font encore l'objet de discussions. De plus, les valeurs de l'activité spécifique des électrodes monométalliques de Ni vis à vis de l'HOR/HER publiées dans la littérature peuvent différer jusqu'à deux ordres de grandeur (Fig. 1). Par conséquent, les principaux objectifs de cette thèse étaient d'obtenir des données reproductibles pour l'activité spécifique (par rapport à la surface réelle) de Ni dans le

HOR/HER et de comprendre comment le prétraitement de la surface de l'électrode ainsi que l'addition d'un second métal (Cu ou Mo) influencent l'activité électrocatalytique du Ni pour l'HOR.

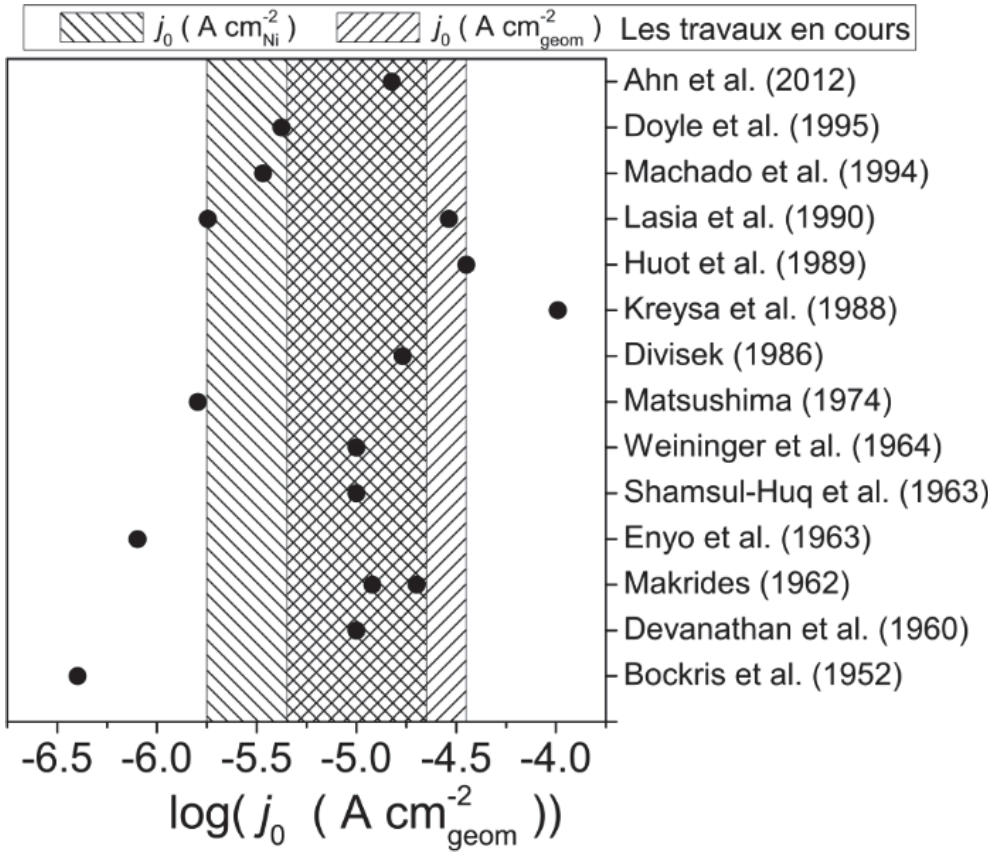

Fig. 1 *Les symboles sur le graphique correspondent aux valeurs des activités de l'HER rapportées pour le Ni polycristallin dans la littérature. La zone hachurée correspond aux données obtenues dans la thèse et montre la dispersion des valeurs des activités spécifiques du Ni pour l'HOR/HER en fonction de l'état de surface de l'électrode de Ni.*

II. Résultats et discussion

II.1. Ni polycristallin

Malgré le fait qu'un changement notable de l'activité électrocatalytique des électrodes de Ni pour l'HER ait été déjà reporté après l'oxydation de leur surface [2,3], il n'y a pas encore eu d'étude systématique de cet effet. Pour mieux comprendre ce phénomène, la première partie de la thèse a été consacrée à l'étude de l'influence de l'état de surface de l'électrode polycristalline de Ni (Ni_{PC}) sur son activité vis à vis de l'HOR/HER. Deux états de surface, (préférentiellement) métallique et partiellement oxydé, ont été considérés. Les électrodes du premier type ont été appelées "non activées". Les électrodes du second type ont été appelées "Ch activé" ou "EC activé", en fonction de la manière d'oxyder leur surface (chimiquement au contact de l'air ou électrochimiquement par des cycles de potentiels jusqu'à des potentiels positifs élevés, respectivement). Il faut mentionner que l'oxydation totale de la surface de l'électrode de Ni entraîne un blocage des sites actifs libres à la surface du Ni, qui sont nécessaires à la formation de H_{ad} et donc la suppression de l'activité pour l'HOR.

On a constaté que l'activité spécifique[1] de Ni_{PC} vis à vis de l'HOR/HER, normalisée par la surface de l'électrode électrochimiquement active ($\mu A\ cm^{-2}_{Ni}$), augmente jusqu'à dix fois après une oxydation partielle de sa surface (Tableau 1). En outre, l'activité normalisée par la surface géométrique ($\mu A\ cm^{-2}_{geom}$) augmente aussi (environ 5 fois). La comparaison des données obtenues avec les valeurs d'activité de Ni_{PC} pour l'HOR/HER (Fig. 1) publiées dans la littérature nous a permis de suggérer que les variations des valeurs d'activité du Ni existant dans la littérature résultent vraisemblablement de deux raisons principales. La première raison est liée aux différences dans les méthodologies utilisées pour le préconditionnement de la surface de l'électrode de Ni avant les mesures. Par conséquent, la cinétique de l'HOR/HER est étudiée pour différents états de la surface de Ni. La deuxième raison est liée à la

[1] En électrocatalyse, l'activité est mesurée en terme de densité de courant d'échange normalisée soit par la surface (j_0), soit sur la masse (i_0) du composé actif.

normalisation de l'activité par la surface géométrique de l'électrode qui peut différer significativement de la surface réelle de catalyseur accessible électrochimiquement.

Tableau 1. *Activités électrocatalytiques de diverses électrodes de Ni pour l'HOR/HER en fonction du prétraitement de surface.*

Catalyseurs	**Densité de courant d'échange**		
	j_0, **µA·cm$^{-2}_{Ni}$**	j_0 **/ µA cm$^{-2}_{geom}$**	i_o **/ A g$_{Ni}^{-1}$**
Ni_{PC} non activées	2.3 ± 0.1	6.0 ± 0.6	-
Ni_{PC} poli[m]	6.0 ± 0.8	15.9 ± 0.8	-
Ni_{PC} Ch activé	20 ± 2	33 ± 5	-
Ni_{PC} EC activated	14 ± 2	29 ± 3	-
Ni_{ED}/GC non activées	6.4 ± 0.6		-
Ni_{ED}/GC Ch activé	25 ± 3		-
Ni_{ED}/XC-72 non activées	6.2 ± 0.6		5.7 ± 0.2
Ni_{ED}/XC-72 Ch activé	56 ± 10		22.4 ± 4.3

Le changement de l'activité du Ni vis à vis de l'HOR/HER après l'oxydation partielle de sa surface s'accompagne de changements dans les cycles voltampérométriques (CV) enregistrés dans 0.1 M NaOH (Figs. 2a,b). Étant donné que les pics observés sur CV sont dus à certains processus électrochimiques survenant à la surface de l'électrode, les changements de la forme du CV révèlent la modification de l'état de surface de l'électrode. La paire de pics anodique (a_1) et cathodique (c_1) observés sur le CV du Ni non activé sous atmosphère inerte (Fig. 2a) correspond à la formation et à la réduction de l'oxyde α-$Ni(OH)_2$ superficiel, respectivement [4,5]. En plus, sur les CV du Ni activé, un deuxième pic anodique (a_2) apparaît à des potentiels inférieurs (Fig. 2b) et son apparition est probablement liée à des processus

[m] Contrairement à la barre de Ni non activée, dont l'activité a été mesurée immédiatement après le polissage, les données pour la barre de Ni polie ont été obtenues après l'enregistrement de CV dans une atmosphère inerte, c'est-à-dire de la même manière que pour Ni_{ED}/GC et Ni_{ED}/XC-72 électrodes.

électrochimiques se produisant sur des sites de Ni libres à proximité de sites de Ni oxydé (Fig. 3).

Afin d'étudier le mécanisme du HOR / HER sur des électrodes de Ni métalliques et partiellement oxydées et pour comprendre les raisons de l'augmentation de la cinétique de l'HOR/HER en présence d'oxydes de Ni de surface, les courbes expérimentales de voltampérométrie cyclique ont été analysées à l'aide d'un modèle cinétique champ moyen. Le modèle est basé sur le mécanisme Tafel-Heyrovsky-Volmer pour l'HOR/HER en milieu alcalin (eq. 1 – 3, respectivement):

$$\mathrm{H_2} + 2\mathrm{Ni} \underset{k_{-1}}{\overset{k_1}{\rightleftarrows}} 2\mathrm{Ni} - \mathrm{H_{ad}} \qquad \text{(eq. 1)}$$

$$\mathrm{H_2} + \mathrm{OH^-} + \mathrm{Ni} \underset{k_{-2}}{\overset{k_2}{\rightleftarrows}} \mathrm{Ni} - \mathrm{H_{ad}} + \mathrm{H_2O} + \mathrm{e^-} \qquad \text{(eq. 2)}$$

$$\mathrm{Ni} - \mathrm{H_{ad}} + \mathrm{OH^-} \underset{k_{-3}}{\overset{k_3}{\rightleftarrows}} \mathrm{Ni} + \mathrm{H_2O} + \mathrm{e^-} \qquad \text{(eq. 3)}$$

Étant donné que l'HOR se produit dans la même gamme de potentiel que l'oxydation de la surface du Ni, la formation en deux étapes de $Ni(OH)_2$ superficiel a également été considérée dans le modèle (selon les Réfs. [2,5,6]):

$$\mathrm{Ni} + \mathrm{OH^-} \underset{k_{-4}}{\overset{k_4}{\rightleftarrows}} \mathrm{Ni} - \mathrm{OH_{ad}} + \mathrm{e^-} \qquad \text{(eq. 4)}$$

$$\mathrm{Ni} - \mathrm{OH_{ad}} + \mathrm{OH^-} \underset{k_{-5}}{\overset{k_5}{\rightleftarrows}} \mathrm{Ni} - (\mathrm{OH})_{2,\,ad} + \mathrm{e^-} \qquad \text{(eq. 5)}$$

où 'Ni' désigne des sites métallique à la surface de l'électrode. La dépendance en potentiel des constantes de vitesse des étapes impliquant un transfert d'électron est décrite par l'équation de Butler-Volmer (eq. 2 – 5). Les étapes d'adsorption/désorption à la surface sont modélisées par des isothermes d'adsorption de Langmuir.

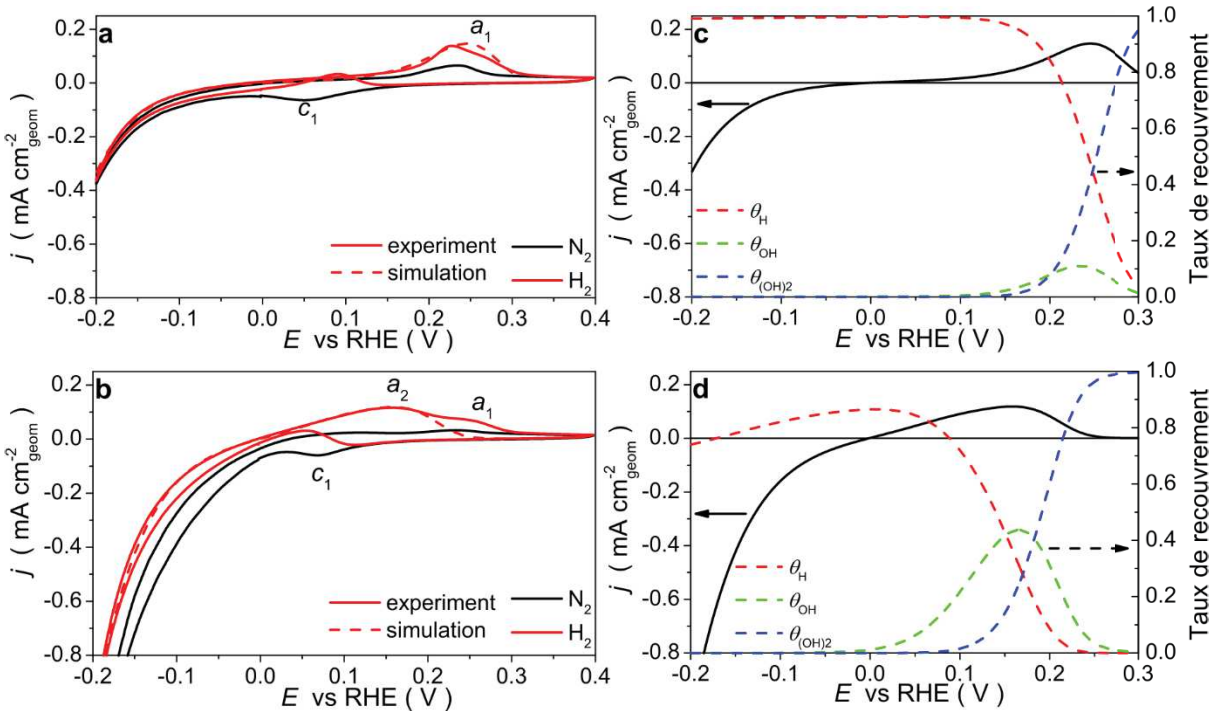

Fig. 2 *Comparaison des CVs expérimentaux (courbes solides) et simulés (courbes pointillées) obtenues pour un disque de Ni non actif (a) et EC activé (b) dans 0.1 M NaOH saturé en N_2 (courbes noires) ou H_2 (courbes rouges) à une vitesse de balayage de 5 mV s^{-1} et T = 298 K. Les courbes en pointillé sur les panneaux (c) et (d) représentent les taux de recouvrement simulés pour la surface du Ni par H_{ad} (θ_H), OH_{ad} (θ_{OH}) et $(OH)_{2,ad}$ ($\theta_{(OH)2}$) adsorbées pour les électrodes de Ni non activées et EC activées, respectivement. Les courbes solides correspondent aux balayages de potentiel anodiques des CV simulés. L'électrode d'hydrogène réversible (RHE) est utilise comme référence.*

Le modèle cinétique développé permet de reproduire les principales caractéristiques des CVs expérimentaux des électrodes Ni (Fig. 2a, b). On a constaté que la faible activité du Ni non activé vis à vis de l'HOR est causée par, premièrement, une forte énergie d'adsorption de H_{ad} à la surface du Ni (en accord avec les calculs DFT [7,8]) et, deuxièmement, un vitesse de l'oxydation de H_{ad} relativement faible par l'étape de Volmer (k_3^0). A partir de la Fig. 2c, les résultats du modèle cinétique suggèrent que le pic a_1 résulte de la contribution à la fois de la

désorption électrochimique de H_{ad} et de la formation de $Ni(OH)_{2,ad}$, en accord avec les conclusions de Hall et al. [4].

Dans le cas de l'électrode de Ni *partiellement* oxydée, le modèle cinétique prédit que les changements observés expérimentalement dans le CV (l'apparition du pic a_2) et l'amélioration de l'activité du HOR/HER sont dus à l'affaiblissement de la force de liaison de Ni-H_{ad} dû à la présence de NiO_x superficielle. Ce dernier correspond à une augmentation de l'énergie de Gibbs de l'adsorption H_{ad} d'environ 0.1 eV. En outre, la constante de vitesse k_3^0 de l'étape de Volmer augmente d'un ordre de grandeur pour les électrodes de Ni activées. Ceci est probablement causé par des changements dans la structure à double couche sur l'interface électrode/électrolyte (en raison du changement de la force de liaison de Ni-H_2O_{ad}) en présence d'oxydes de Ni superficiels [9,10] et aussi du point de charge nulle de l'électrode. Selon le modèle, le pic a_2 sur le CV de l'électrode de Ni activée a été attribué à l'oxydation de H_{ad} et à la formation de Ni-OH_{ad} (Fig. 2d), tandis qu'une seconde étape d'oxydation de la surface de Ni avec la formation de $Ni(OH)_2$, se produit ensuite au potentiel du pic a_1.

Comme on peut le voir à partir de la Fig. 2b, il existe quelques différences entre CV expérimental et modèle à $E > 0.2$ V. Cela est probablement dû à l'approximation du champ moyen utilisée dans le modèle cinétique, selon laquelle la surface de l'électrode est supposée pour être homogène. Cependant, en réalité, il existe probablement plusieurs types de sites réactifs avec une activité différente dans l'HOR/HER à la surface de l'électrode de Ni activée (Fig. 3). En conséquence, sur les sites de Ni libres isolés, le HOR se produit dans l'intervalle de potentiel du pic a_1, alors qu'il se déroule aux potentiels du pic a_2 sur les sites Ni libres situés à proximité de sites de Ni oxydés.

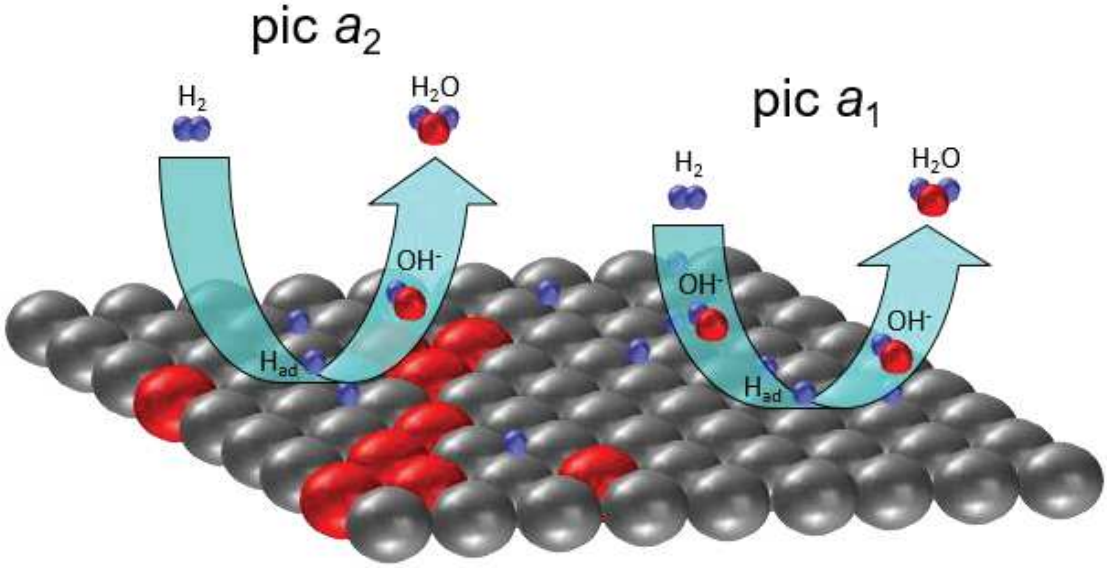

Fig. 3 *Illustration schématique de la structure de l'électrode Ni activée in situ et un mécanisme d'activation HOR provisoire. Codes de couleurs: gris – Ni^0, rouge – NiO_x.*

Sur la base des mesures effectuées à différentes températures, l'énergie d'activation apparente (E_a) a été calculée et vaut 30 ± 1 et 26 ± 1 kJ mol^{-1} pour l'état de surface non activé et activé de l'électrode de Ni_{PC}, respectivement. Dans le même temps, l'utilisation de la modélisation cinétique a permis d'estimer les constantes de vitesse et valeurs de E_a, correspondant aux étapes élémentaires du mécanisme de l'HOR/HER. Il a été constaté qu'à la surface des électrodes de Ni non activées, le HOR/HER suit le mécanisme de Heyrovsky-Volmer, l'étape de Volmer directe (k_3^0) étant l'étape déterminant la vitesse de l'HOR, tandis que la vitesse de l'HER est contrôlée par l'étape de Heyrovsky inverse (k_{-2}^0). A la surface des électrodes de Ni activées, l'étape de Tafel doit également être prise en compte. Dans ce cas, les vitesses des étapes inverses de Volmer (k_{-3}^0) et Heyrovsky (k_{-2}^0), participant au processus d'évolution de l'hydrogène, sont comparables. Cela entraîne une diminution du taux de couverture de la surface du Ni par H_{ad} adsorbé par rapport à l'électrode de Ni non activée (Fig. 2c, d). Pendant ce temps, l'HOR est toujours contrôlé par l'étape lente de Volmer (k_3^0).

II.2. Électrocatalyseurs de Ni nanostructurés

La deuxième partie de la thèse a été consacrée à la synthèse et à l'étude des nanoparticules de Ni supportées sur carbone vitreux (GC) ou carbone poreux Vulcan XC-72. Ces catalyseurs ont été préparés par électrodéposition (ED) à partir de l'électrolyte contenant 0.01 M $NiSO_4$ et 0.10 M $(NH_4)_2SO_4$. Le support GC a été utilisé pour le développement de la procédure d'électrodéposition et la synthèse des échantillons modèles Ni_{ED}/GC. Ensuite, une série de catalyseurs Ni_{ED}/XC-72 qui peuvent être potentiellement utilisés aux anodes de l'AMFC a été obtenue. La caractérisation des échantillons électrodéposés par microscopie électronique (SEM, TEM, STEM) a montré que les particules de Ni sont réparties de manière homogène sur la surface du support, tandis que leur diamètre moyen en surface (sous l'hypothèse que la forme des particules est sphérique) est estimé à 25 ± 5 et 10 ± 2 nm pour NiED/GC et NiED/XC-72 respectivement. En outre, les images STEM haute résolution (figures 4b, c) montrent clairement la nature nanostructurée des nanoparticules de Ni : les particules sont constituées de cristallites de la taille d'environ. 3 nm, connectées par des joints de grain. De plus, par l'utilisation de la technique ICP-AES (spectrométrie d'émission atomique à plasma à couplage inductif), la charge typique de métal dans le catalyseur Ni_{ED}/XC-72 a été estimée à 42 ± 3 % en poids.

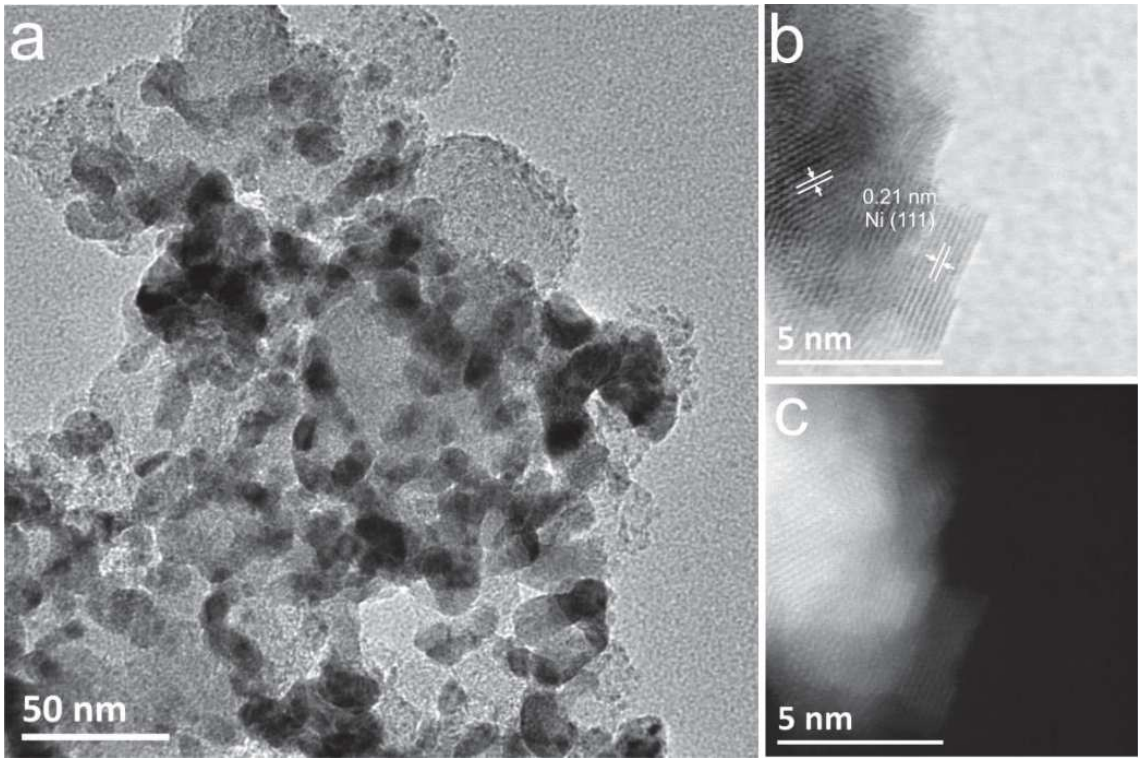

Fig. 4 *Images haute résolution de TEM (a) et STEM (champ clair (b) et sombre (c)) de l'électrocatalyseur* Ni_{ED}*/XC-72*

Afin de savoir comment la présence d'oxydes de Ni de surface influence les propriétés électrochimiques et électrocatalytiques des électrocatalyseurs Ni_{ED}/GC et Ni_{ED}/XC-72 nanostructurés, des mesures ont été réalisées soit immédiatement après leur préparation par électrodéposition (ces électrodes ont été appelées “non activées”) soit après une oxydation préliminaire de la surface de l'électrode sous son contact avec l'air et une réduction électrochimique partielle dans NaOH 0,1 M (ces électrodes ont été appelées “Ch activé”).

La comparaison des données obtenues pour le cylindre de Ni poli et les électrodes Ni_{ED}/GC et Ni_{ED}/XC-72 non activées (Tableau 1) montre que l'activité spécifique de la surface de Ni métallique pour l’HOR/HER ne dépend pas de sa morphologie. En même temps, la taille des particules de Ni et/ou de leur nanostructure affectent le processus d'oxydation des échantillons électrodéposés et, vraisemblablement, la stabilité des oxydes de Ni formés retardant leur réduction. Par conséquent, l'activité spécifique surfacique de Ni_{ED}/XC-72 Ch activée est 2 fois plus

élevée que l'activité de Ni_{ED}/GC Ch activée. De plus, son activité pondérée en masse vis à vis de l'HOR est significativement plus élevée par rapport aux meilleures valeurs des électrocatalyseurs actuels publiés à base de métaux non nobles et seulement 1.7 fois plus faible que l'activité du catalyseur commercial 20% Pd/C (Premetek Co).

II.3. Électrocatalyseurs bimétalliques à base de Ni

Afin de mieux comprendre comment l'ajout d'un second métal au catalyseur Ni affecte ses propriétés électrochimiques dans les milieux alcalins ainsi que l'activité électrocatalytique pour l'HOR/HER, la partie finale de la thèse a été consacrée à l'étude de catalyseurs 25 wt.% $Ni_{1-x}Cu_x$/C et 50 wt.% $Ni_{0.9}Mo_{0.1}$/C.

Les catalyseurs Ni/C monométalliques et $Ni_{1-x}Cu_x$/C bimétalliques ont été préparés par une technique d'imprégnation par voie humide en utilisant du carbone XC-72 comme support suis un séchage conventionnel sous vide ($0{,}05 \leq x \leq 0{,}50$) soit une lyophilisation ($0{,}02 \leq x \leq 0{,}10$) pendant la synthèse. Cette dernière a permis (démontré par par XRD et TEM) de produire des particules métalliques avec une distribution de taille plus étroite et une composition plus uniforme. L'analyse des échantillons par XPS a révélé que le Cu est toujours présent dans un état métallique, tandis que le Ni est présent principalement sous forme oxydée. Cependant, l'augmentation de la fraction nominale de Cu renforce notablement le Ni^0 métallique.

L'étude des propriétés électrocatalytiques des catalyseurs $Ni_{1-x}Cu_x$/C en milieu alcalin a montré qu'une addition d'une petite fraction de Cu ($0.02 \leq x \leq 0.10$) entraîne une augmentation de l'activité pondérée en masse spécifique de Ni pour l'HOR/HER (Fig. 5). Cette amélioration a été attribuée à deux facteurs : (i) une augmentation de la surface spécifique du Ni (selon les mesures de chimisorption de CO) et (ii) une augmentation de l'activité spécifique pondérée en surface de Ni vis à vis de l'HOR/HER en raison d'un effet électronique et/ou d'ensemble de Cu, qui est le plus visible dans le cas du catalyseur $Ni_{0.95}Cu_{0.05}$/C. En outre, l'utilisation de la lyophilisation pendant la synthèse a entraîné une augmentation supplémentaire de l'activité massique de Ni dans le HOR/HER en raison de la préparation de catalyseurs plus homogènes en taille.

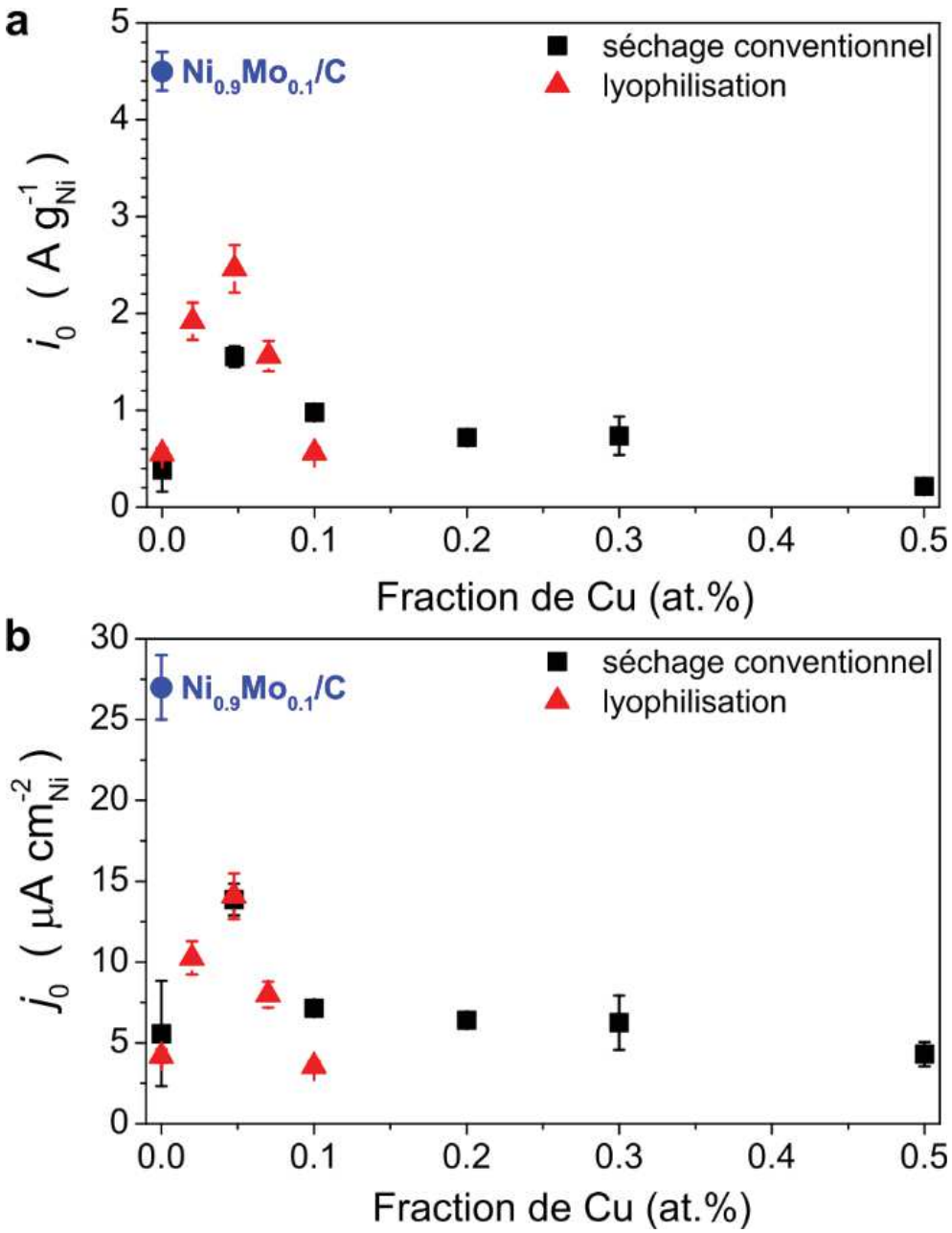

Fig. 5 *Activités pondérées en masse (a) et en surface (b) obtenues pour les catalyseurs Ni/C et $Ni_{1-x}Cu_x$/C en fonction de la fraction de Cu. Les échantillons ont été préparés par séchage conventionnel (carrés noirs) soit par lyophilisation (triangles rouges) pendant la synthèse. De plus, les valeurs d'activité obtenues pour le catalyseur $Ni_{0.9}Mo_{0.1}$/C sont indiquées par des cercles bleus.*

Un catalyseur bimétallique $Ni_{0.9}Mo_{0.1}/C$ (le rapport atomique Ni:Mo a été choisi en fonction des études des propriétés d'échantillons de NiMo pour l'HER [11]) a été préparé par technique d'imprégnation d'humidité en utilisant du carbone KetjenBlack-600 comme support.

L'utilisation du carbone, dont la surface spécifique est environ 6 fois plus grande par rapport à XC-72, a permis d'obtenir un catalyseur avec une teneur élevée en Ni et une dispersion relativement élevée des particules métalliques. L'étude de l'échantillon par diverses méthodes physicochimiques (TEM, XRD, XPS) a montré que les particules métalliques sont réparties de manière assez homogène sur la surface du carbone et leur diamètre de Sauter est estimé à 22 ± 6 nm. On a constaté que le Ni est principalement présent sous forme oxydée avec une fraction Ni^0 métallique proche de 19%, tandis que Mo est présent principalement dans le degré d'oxydation le plus élevé avec une faible teneur en Mo (IV) et Mo (V).

Il a été constaté que l'activité électrocatalytique spécifique de $Ni_{0.9}Mo_{0.1}/C$ pour l'HOR/HER est environ 2 fois plus élevée que l'activité de catalyseurs $Ni_{0.95}Cu_{0.05}/C$ et environ 6 fois plus élevée que l'activité de catalyseurs Ni/C synthétisés chimiquement (Fig. 5). Sur la base de la modélisation cinétique, l'activité catalytique élevée de l'électrocatalyseur $Ni_{0.9}Mo_{0.1}/C$ dans le HOR/HER a été attribuée à une diminution (par rapport au Ni_{PC} non activé) de l'énergie d'adsorption de H_{ad}, qui est une espèce intermédiaire de l'HOR/HER, avec une augmentation de la constante de vitesse de l'étape de Volmer. De plus, il a été observé que l'addition de Mo à Ni permet de ralentir la perte d'activité vis à vis de l'HOR/HER lors d'un cyclage en potentiel prolongé.

III. Conclusions générales

1. On a constaté que l'oxydation partielle de la surface des électrocatalyseurs de Ni affectait de manière significative leurs propriétés électrochimiques dans un électrolyte alcalin. L'activité spécifique du Ni dans le HOR/HER ne dépend pas de la morphologie du catalyseur, mais augmente jusqu'à 10 fois après une oxydation partielle de leur surface. Au contraire, l'oxydation totale de la surface entraîne une suppression de l'activité de Ni pour l'HOR/HER.
2. Un modèle cinétique a été développé qui permet de décrire la cinétique des réactions de l'oxydation et de dégagement de l'hydrogène en tenant compte du processus d'oxydation de la surface du Ni avec la formation d'hydroxydes de Ni. Sur la base des données de la modélisation mathématique, nous avons conclu que:
    - l'amélioration de l'activité électrocatalytique du Ni en présence d'oxydes de Ni superficiel est liée à une diminution de l'énergie d'adsorption de l'hydrogène intermédiaire sur Ni et à une augmentation de la constante de vitesse de l'étape de Volmer
    - le mécanisme de l'HOR/HER sur Ni est principalement décrit par les étapes de Heyrovsky et de Volmer, alors que la contribution de l'étape de Tafel ne devient perceptible qu'après une oxydation partielle de la surface de l'électrode. La vitesse de l'HOR est limitée par l'étape de Volmer indépendamment du degré d'oxydation de la surface de l'électrode Ni.
3. Pour la première fois, un électrocatalyseur hautement dispersé 40 wt.% Ni_{ED}/XC-72 a été préparé en utilisant une technique d'électrodéposition et du Vulcan XC-72 comme support. Son activité électrocatalytique pondérée en masse pour l'HOR dépasse de manière significative les valeurs indiquées dans la littérature pour les catalyseurs de métaux non nobles et s'approche de l'activité de l'électrocatalyseur commercial 20% Pd/C
4. L'étude de la série d'électrocatalyseurs NiCu/C supportés sur carbone a montré que l'ajout de Cu au composant actif conduit à:

- une augmentation de l'activité spécifique du Ni vis à vis de l'HOR/HER par rapport à l'échantillon de Ni/C monométallique, qui a été préparé selon la même méthode. L'activité la plus élevée a été observée pour 5 at.% de teneur en Cu dans l'échantillon
- une amélioration de la tolérance du Ni à l'oxydation.

5. L'étude de l'électrocatalyseur $Ni_{0.9}Mo_{0.1}$/C supporté sur carbone a montré que l'ajout de Mo au composant actif permet d'augmenter l'activité spécifique du catalyseur pour l'HOR/HER. Avec l'aide de la modélisation cinétique, cette amélioration de l'activité catalytique a été attribuée à une diminution de l'énergie d'adsorption de l'hydrogène sur Ni ainsi qu'à une augmentation de la constante de vitesse de l'étape de Volmer.

Références

[1] Watanabe M., Tryk D. A. Fuel Cells: An Overview with Emphasis on Polymer Electrolyte Fuel Cells // Electrochemical Science for a Sustainable Society. – Springer International Publishing, 2017. – P. 51-94.

[2] A. Lasia, A. Rami, Kinetics of Hydrogen Evolution on Nickel Electrodes, J. Electroanal. Chem. Interfacial Electrochem. 294 (1990) 123–141.

[3] J.L. Weininger, M.W. Breiter, Hydrogen Evolution and Surface Oxidation of Nickel Electrodes in Alkaline Solution, J. Electrochem. Soc. 111 (1964) 707–712.

[4] D.S. Hall, C. Bock, B.R. MacDougall, The Electrochemistry of Metallic Nickel: Oxides, Hydroxides, Hydrides and Alkaline Hydrogen Evolution, J. Electrochem. Soc. 160 (2013).

[5] M. Alsabet, M. Grden, G. Jerkiewicz, Electrochemical Growth of Surface Oxides on Nickel. Part 1: Formation of α-Ni(OH)2 in Relation to the Polarization Potential, Polarization Time, and Temperature, Electrocatalysis. 2 (2011) 317–330.

[6] D. Floner, C. Lamy, J.-M. Leger, Electrocatalytic Oxidation of Hydrogen on

Polycrystal and Single-crystal Nickel Electrodes, Surf. Sci. 234 (1990) 87–97.

[7] A. Mohsenzadeh, T. Richards, K. Bolton, DFT Study of the Water Gas Shift Reaction on Ni(111), Ni(100) and Ni(110) Surfaces, Surf. Sci. 644 (2016) 53–63.

[8] W. Sheng, M. Myint, J.G. Chen, Y. Yan, Correlating the Hydrogen Evolution Reaction Activity in Alkaline Electrolytes with the Hydrogen Binding Energy on Monometallic Surfaces, Energy Environ. Sci. 6 (2013) 1509–1512.

[9] S. Liu, T. Ishimoto, M. Koyama, First-principles Study of Oxygen Coverage Effect on Hydrogen Oxidation on Ni(111) Surface, Appl. Surf. Sci. 333 (2015) 86–91.

[10] F. Che, J.T. Gray, S. Ha, J.-S. McEwen, Catalytic Water Dehydrogenation and Formation on Nickel: Dual Path Mechanism in High Electric Fields, J. Catal. 332 (2015) 187–200.

[11] A. Kawashima, E. Akiyama, H. Habazaki, K. Hashimoto, Characterization of Sputter-deposited Ni-Mo and Ni-W Alloy Electrocatalysts for Hydrogen Evolution in Alkaline Solution, Mater. Sci. Eng. A. 226–228 (1997) 905–909.